The Palaeoecological and Industrial Significance of Inertinite (Charcoal) in Late Permian Coals from the Kuznetsk Basin, Russia

Victoria Anne Hudspith

Royal Holloway University of London

A thesis submitted for the degree of Doctor of Philosophy

2012

DECLARATION OF AUTHORSHIP

I, Victoria Hudspith, hereby declare that this thesis and the work presented in it is entirely my own. Where I have consulted the work of others, this is always clearly stated.

Signed: …….

Date: …….

ABSTRACT

Thirteen Late Permian subbituminous coal seams (numbered 68-94) were sampled from the Kuznetsk Basin, Russia. The coals formed in extensive long-lived peat-forming (mire) environments on floodplains as part of a fluvial system (Davies et al., 2010). Fossil plants (permineralised, charcoalified or impressions) show characteristics consistent with cordaitaleans, which were the dominant peat-forming plants in Angara during the Permian.

Crushed coal samples show temporal variation in inertinite (charcoal content) from 7.1% - 50.2%, with a high overall mean of 28.3%. More detailed petrographic work was carried out on five *in situ* coal pillars (seams 78, 88 and 91) where inertinite distribution was used to interpret palaeowildfire occurrence and type as well as providing an approach to calculating fire return intervals (FRI) in deep time. *In situ* pillars are essential for this type of research as they retain the original spatial and temporal variation in inertinite distribution. Inertinite is present in all lithotype units (up to 61% mineral matter free basis). The coal pillars show comparable wildfire histories despite differences in environments of deposition. In addition, FRI may have been more frequent in the Permian than in modern peat-forming environments.

Quantitative reflectance of macroscopic and microscopic (inertodetrinite) charcoal in coal pillars has revealed that both size fractions are within the temperature range of modern low temperature surface fires. However, a small amount of the charcoal reflectance values are >4%Ro and may in fact represent charcoal derived from high temperature crown fires. This demonstrates the importance of reflectance measurements of both macro- and microscopic charcoal in interpretation of palaeowildfire type.

Despite inertinite contents of up to 61% in these Permian coals, neither inertinite content nor distribution strongly affects the characterisation (proximate and ultimate) properties of the coal as a whole. However, coals with high inertinite contents (>30%) do produce denser chars and show poorer burnout during pilot-scale Drop Tube Furnace (DTF) combustion experiments.

TABLE OF CONTENTS

FIGURES

Chapter 4

Chapter 5

Chapter 6

Chapter 7

Chapter 8

TABLES

Chapter 2

ACKNOWLEDGEMENTS

This research could not have been possible without the NERC and CASE Studentship (NE/F013698/1) which is gratefully acknowledged. I am also indebted to my supervisors, Andrew Scott, Margaret Collinson and Gerry Riley for giving me this opportunity and for their valuable assistance, guidance, feedback and advice throughout this process. I would also like to thank my advisors Nathalie Grassineau and Trudy Beeley for their continual helpful support.

I would also like to express my gratitude to all those at RWE Npower involved in the logistics and organisation of the Russian fieldwork and the staff at the Siberian mines who were extremely hospitable and helpful during sampling. The fieldwork could not have been possible without the help of Natalia Pronina for translating at the mines, assisting during sampling and later for helping with maceral identification. I would like to thank Tracy Hoar, John Eckersley and Kimberley Stewart from RWE Npower for sparing their time to train me in the various coal characterisation techniques and for letting me use the labs. Thanks to Jason Powis for Drop Tube Furnace training at RWE Npower and to Abdul Nuamah and Ed Lester for collaboration. I am also grateful to James Hower for characterisation analysis at CAER and for help with maceral identification. I would also like to thank Dave Waltham and James France for help with statistics, as well as James Howard and those at CASP for use of your archives on the Kuznetsk Basin. And to David Alderton for XRD analysis, to Sharon Gibbons for SEM training, maceration and technical support, Neil Holloway for his patience and help with sample preparation, Patricia Goggin for SEM preparation, Kevin d'Souza for photography of polished blocks and Art Cohen for providing peat samples.

I would like to dedicate this thesis to my parents, I couldn't have done this without your continual encouragement, support and belief in me and I hope I have made you proud. I would also like to thank my brother for his long distance support. I would also like to thank all of my friends for being so understanding during this process and for providing some much needed distraction at times. Finally, to John whose love, support and patience have helped me through this, I couldn't have done it without you.

CHAPTER 1

INTRODUCTION

1.1 PERMIAN COALS AS ARCHIVES OF PAST WILDFIRE OCCURRENCE

The presence of charcoal in the fossil record provides unequivocal evidence for ancient wildfires (Scott, 1989a; Scott, 2010). Charcoal has a high preservation potential due to its relatively inert nature (Ascough et al., 2010, 2011). Occurrences of charcoal in various sedimentary environments have been reported from the Silurian onwards (e.g. Demchuk, 1993; Glasspool et al., 2004; Glasspool and Scott 2010; Scott, 2010; Brown et al 2012; Hamad et al., 2012) and therefore, wildfires have always been an important part of terrestrial ecosystems. When found in coal, wildfire derived fossil charcoal is termed inertinite (Scott, 1989a; Teichmüller, 1989; Sander and Gee, 1990; Diessel, 1992; Bustin and Guo, 1999; Scott and Jones 1994; Falcon-Lang 2000; Crosdale et al., 2002; Glasspool 2003a,b; Uhl and Kerp, 2003; Uhl et al., 2007; Glasspool and Scott, 2010). Inertinite is studied by coal petrologists using petrographic analysis, and is subdivided into different macerals (e.g. fusinite, inertodetrinite) according to the International Committee for Coal and Organic Petrology (ICCP) classification (ICCP, 2001; Table 2.3).

The occurrence of long-lived peat-forming temperate mire environments during the Permian in the Kuznetsk Basin, Russia have resulted in laterally extensive, economic coal deposits. High inertinite contents have been documented in industrial analyses of Permian coals from the Kuznetsk Basin (Pakh and Artser, 2003). However, evidence of inertinite distribution within the coal was lost because crushing is part of the industry standard method of analysis. By contrast, coal pillars with undisturbed stratigraphy provide an intact archive of past peat-forming environments. Therefore, the distribution of inertinite within pillars from coal seams is used in this thesis to obtain palaeoenvironmental information on wildfire occurrence, fire type and fire return intervals during deposition of these Permian peats.

Inertinite contents are higher in Southern Hemisphere Permian coals than in other geological Periods (Stach et al., 1982; Hunt, 1989; Glasspool, 2000; Glasspool, 2003a,b; Choudhury et al., 2007) with a mean of 38.9% for the Late Permian Changhsingian stage (253 – 251Ma), suggesting that wildfires may have been more widespread than at other times in Earth history (Glasspool and Scott, 2010). It has been suggested that these high Permian inertinite contents (compared to modern peats, mean 4.3%) may be related to modelled high Permian atmospheric oxygen levels (Glasspool and Scott, 2010).

Phanerozoic mass-balance palaeoatmospheric models all suggest atmospheric oxygen levels were above PAL (21%) during the Permian Period (Berner et al., 2000; Berner et al., 2003) with a suggested upper limit of 25% (Lenton, 2001) which may have even reached 30% (Berner, 2006, 2009). During the Permian, organic carbon burial rates were high (Berner, 2005) and this is thought to be the major cause of variation in atmospheric oxygen levels over geological time (Lenton, 2001). The models are independently corroborated by geological evidence including, a rise and fall of insect gigantism at 300Ma (Lenton, 2001; Harrison et al., 2010). Also, experimental data suggests high atmospheric oxygen causes increased isotopic fractionation ($\delta^{13}C$) during plant growth and a 5‰ $\delta^{13}C$ anomaly is observed between 300-150Ma consistent with modelled elevated atmospheric oxygen during this time (Beerling et al., 2002).

Oxygen is required for ignition and a record of charcoal since 423Ma (Glasspool et al., 2004) provides evidence for high enough atmospheric oxygen to sustain natural fires (>18.5% O_2) (Lenton, 2001; Belcher et al., 2010). Furthermore, experimental combustion of dry *Sphagnum* peat by Belcher et al. (2010) has demonstrated that atmospheric oxygen levels of 19% - 22% can lead to enhanced combustion. Charcoal is a relatively recalcitrant material that shows reduced breakdown and slow turnover in ecosystems. Higher charcoal contents in coal may have attributed to enhanced carbon sequestration and provided a positive feedback loop between increased charcoal production and burial causing further atmospheric oxygen increase during the Permian (Scott and Glasspool, 2006).

If elevated atmospheric oxygen led to increased global wildfire activity then Permian coals from all areas of the world should show consistently high inertinite contents. However, the data compilation by Glasspool and Scott (2010) does not include any Late Permian Russian coals. Therefore, inertinite contents obtained from intact coal pillars and crushed coals, from the Kuznetsk Basin, Russia, are used in this thesis as a comparison to previously published Permian petrographic data from other areas.

Inertinite macerals show variable visual reflectance (from grey to white) which has implications for interpretations of palaeowildfires from coal. Experimental charcoalification on a plethora of plant material has repeatedly demonstrated that there is a positive relationship between increasing reflectance with increasing charring temperature (e.g. Bustin and Guo, 1999; McParland et al., 2007, 2009b; Scott and Glasspool, 2007; McParland, 2010). When the charring duration is unknown, charcoal reflectance can be used to infer minimum charring temperatures (Scott and Glasspool, 2006; Hudspith et al., 2010). Modern wildfires occur over a range of temperatures and surface fires occur at lower temperatures than crown fires (Hartford and Frandsen, 1992). Therefore, by measuring the reflectance of inertinite macerals in the Late Permian coal pillars it may be possible to infer original charring temperatures as a means to interpret ancient palaeowildfire types.

1.2 INERTINITE AND ECONOMIC UTILISATION OF PERMIAN KUZNETSK BASIN COALS

Russia has the second highest global recoverable coal reserves (157 billion tonnes) (Malyshev, 2000) in 22 basins (Fig. 3.1 A). There are 240 operational mines with current annual production of 320 million tonnes (Mt) (Moore, 2010), 90.7Mt of which is exported (EIA, 2010). The largest volume of coal from Siberian mines is extracted from the Kuznetsk and Kansk-Achinsk Basins (Kurlenya and Cheskidov, 2001; Anshits et al., 2010; Patzek and Croft, 2010; Rutledge, 2011) and production from these basins is expected to continue until 2101 (Rutledge, 2011). The large volume of minable resources in this basin, suggests that this coal is likely to continue to be a globally important energy resource in the future. Furthermore, Permian Kuznetsk Basin coal is currently utilised in the United Kingdom.

High inertinite content in a coal may ultimately affect its characterisation properties, and the amount of carbon, or unburned coal, in ash (burnout behaviour). Large amounts of unburned carbon in ash can render the pulverised fuel ash unsalable (Beeley et al., 1995; Cloke et al., 1997a). Previous work has focussed on the effect of variation in proportions of individual maceral groups on characterisation properties (e.g. Dyrkacz et al., 1984; Borrego et al., 2000; Ward et al., 2005) but within seam variation in inertinite distribution and the effect this may have on coal characterisation properties has not previously been investigated. The way the macerals are distributed in a coal may be significant, as interactions between macerals occur during combustion (Milligan et al., 1997). Furthermore, inertinite macerals are typically less reactive than vitrinite macerals in the same coal (Méndez et al., 2003) and often do not release sufficient volatiles to maintain flame temperature or stability (Cai et al., 1998). Understanding these parameters is important for boiler design and combustion control (Chi et al., 2010). Therefore, in addition to the palaeowildfire aspects, coal characterisation properties and coal combustion are studied in this thesis to determine if variation in inertinite distribution might affect the industrial utilisation of Kuznetsk Basin coals.

1.3 THESIS STRUCTURE

Field collecting procedures, sample preparation, and reflectance microscopy techniques for petrographic analysis of *in situ* coal pillars are described in **chapter 2**. The macroscopic appearance of the seams studied, their associated interseam sediments and plant fossils are used to interpret the depositional setting and peat-forming vegetation in the Late Permian peat-forming environment of the Kuznetsk Basin (**chapter 3**). Detailed petrographic analysis of three *in situ* coal pillars and their inertinite distribution is used to interpret palaeowildfire occurrence and fire type as well as to develop a novel approach to calculating fire return intervals (**chapter 4**). Petrographic analysis of two additional coal pillars is undertaken to document within seam spatial and temporal variability in inertinite distribution and hence fire occurrence (**chapter 5**). Reflectance measurements are used to infer minimum charring temperatures to aid understanding of palaeowildfire types (**chapter 6**). The effect of inertinite content and distribution on the characterisation properties of the coal for commercial use is also assessed (**chapter 7**). Methodologies used in the thesis, problems with the ICCP inertinite classification

scheme, and the extent to which fire types can be recognised in the fossil record are critically evaluated in **chapter 8**. Overall conclusions are presented in **chapter 9**. Appendices contain numerical data (**Appendix 1**; **Appendix 2**; **Appendix 7**), additional figures documenting maceral relationships and characterisation properties for chapter 7 are presented in **Appendix 4** and summary tables of characterisation data (**Appendix 5**; **Appendix 6**). Then a published extended abstract completed as part of a collaborative coal combustion project (**Appendix 8**) and a published paper, based on chapter 4, (**Appendix 9**) on the extent to which inertinite distribution from *in situ* coal pillars can be used to interpret palaeowildfire occurrence and fire frequency is included.

CHAPTER 2

METHODOLOGY

In this chapter the field sampling, sample preparation, petrographic and coal maceration methodologies are explained. Methods applied in only a single chapter are given in those chapters, including petrographic recognition of charcoal horizons (chapter 4), reflectance methodology (chapter 6; chapter 7), characterisation (chapter 7; Appendix 3) and burnout behaviour methodologies (chapter 7; Appendix 8).

2.1 FIELD SAMPLING

Thirteen coal seams (numbered 68 to 94) were sampled from two open cast coal mines in the Kuznetsk Basin of Siberia, Russia (chapter 3). Both mines exploit coal seams from the Late Permian Kolchuginskaya Series (Fig. 3.2). The mines were visited during a four day field season in September 2009.

2.1.1 Sampling *in situ* orientated coal pillars which retain intact stratigraphy

Seams were commonly >10m thick (as shown in, Fig. 3.2; Fig. 3.5 A; Fig. 3.7; Fig. 3.9 A; Fig. 4.1). Coal pillars were randomly sampled from accessible locations at the coal face. Pillars were sampled along natural fractures in the coal to enable ease of extraction using a geological hammer (examples of *in situ* pillar size relative to seam thickness are illustrated in Fig. 4.1 and Fig. 5.1). In this study the term 'coal pillar' refers to an orientated piece of coal sampled from a known location in the seam. This pillar can be of variable size, and as a result, can produce either single or multiple polished blocks for petrographic analysis. Orientated pillars were sampled from seams 78, 88 and 91. In order to document within seam variation (chapter 5), additional coal pillars were taken from seam 88 (1m distant) and seam 78 (5 km distant). The pillars were wrapped in foil (marked with orientation arrows) and bubblewrap then sealed in a sampling bag to prevent breakage during transport.

2.1.2 General coal samples

Due to the inaccessibility of many seams, and the limited sampling time at each seam, it was essential to collect a bag of loose pieces from each seam, termed a

‘general sample’ (chapter 3). General coal samples were randomly sampled from loose piles of coal pieces immediately in front of that seam in order to ensure they were derived from that seam.

2.1.3 Sampling coal mine stockpiles

During mining the coal is processed into stockpiles of two size fractions, both of which consist of coal from all worked seams (excluding seams 68, 92 and 94) from both mines. The first stockpile is composed of a small size fraction with pieces ranging from 1mm - 5cm (termed ‘stockpile fine’ in this thesis; Fig. 2.1 A). This coal is exported. The second stockpile consists of larger pieces up to 10cm in size (‘stockpile pieces’ in this thesis; Fig. 2.1 B) and is utilised locally. There are also small privately owned mines operating in this area, it is therefore feasible that coal from these mines could also be incorporated into the stockpiles however, this has not been confirmed.

Samples were taken from stockpiles in order to provide a comparison with general samples from individual seams (chapter 7). Coal pieces from the coarser stockpile were taken from the base of the pile at regular intervals as the track hopper was in use at the time and it was unsafe to climb the stockpile. This introduces bias to the sampling as all samples collected could be from one seam from one mine. The finer size fraction stockpile should incorporate a blend of more than one seam in the sample, thus reducing the sampling bias compared to the coarse stockpile.

FIG. 2.1 Field photographs of stockpile size fractions, incorporating seams 73 to 91, from both open cast mines (images courtesy of A. C. Scott, 2009). **A –** Fine stockpile fraction. Scale bar = 1m. **B -** Coarser stockpile fraction and V. Hudspith (for scale) sampling the base of the stockpile.

2.2 PREPARING CRUSHED AND PULVERISED COAL FOR CHARACTERISATION ANALYSES

General samples, stockpile samples and lithotype units from *in situ* coal pillars were all separately crushed to a <1mm size fraction (industry standard for petrographic analysis) using a pestle and mortar. A subsample of the crushed coal was retained for petrographic analysis. The remainder was pulverised through a 0.2mm screen (now termed pulverised fuel or pf) using a Retsch ZM200 mill, with a grinding speed of 14,000rpm (BS 1017-1:1989).

2.3 PRODUCING POLISHED BLOCKS

Polished block methodology varies depending on whether the sample is whole (*in situ* pillars, section 2.3.1) or crushed (section 2.3.2) but the same grinding and polishing technique was applied to all blocks (section 2.3.3).

2.3.1 *In situ* coal pillars

The coal pillars were unwrapped and embedded in plaster of Paris to retain integrity of the sample. The coal in the plaster jacket was then sawn into two halves perpendicular to bedding. One half was retained for lithotype unit sampling and characterisation analysis. The second half was embedded in Tiranti multi-purpose polyester resin (1% hardener to 99% resin) while in the plaster jacket, to retain integrity during cutting. When the resin had set, a thin slice (perpendicular to bedding) of the coal pillar was cut, while still in the plaster jacket. The pillar was then cut parallel to bedding into blocks of a manageable size that could fit on the reflectance microscope stage. Cardboard moulds were made to fit each block then Tiranti multi-purpose polyester resin filled the mould. When set, the blocks were labelled, marked with an orientation arrow, and individually ground and polished (section 2.3.3).

2.3.2 Crushed coal

Some coal lithotypes (defined in Table 2.1), in particular fusain (fossil charcoal), produce a fine powder when crushed using a pestle and mortar. In the British standard procedure, the <75μm size fraction is typically discarded before producing polished blocks of crushed coal (ISO 7404-2: 1985). In this study, in order to prevent sample loss (particularly of fusain) no material was removed after crushing. Once samples were crushed (section 2.2) the crushed coal was stored in labelled airtight containers to prevent oxidation of the sample. In order to reduce sampling bias prior to producing the polished blocks, the sample container was rotated mechanically for one minute to ensure thorough mixing of the sample (BS 1016-104.1:1999). A 1cm thick layer of the crushed coal was placed in a 30mm circular mould using a spatula. Due to the fine size of the crushed coal particulates the Tiranti multi-purpose polyester resin (used to make coal pillar polished blocks) would not set, and therefore Struers Epofix resin (15:2, resin: Epofix hardener) was used. Resin was

poured over the coal in the circular mould until the resin covered the coal. The mixture was then mixed with a spatula to ensure the resin coated all of the coal particles, left to set and more resin was added to fill the mould. The sample was then ground and polished (as in section 2.3.3).

2.3.3 Grinding and polishing resin blocks

All polished blocks were milled on a Knoth Rotor using sandpaper discs of progressively decreasing grain size (80 – 2500 grit) to produce a flat surface and the resulting scratches were then removed by polishing by hand on a napped cloth coated with a 0.3µm aluminium oxide solution. The blocks were then polished again using a 0.05µm aluminium oxide solution (Glasspool, 2000). During each stage of polishing the blocks were pressed firmly to the surface to reduce topography (Jones, 1999). During the final cleaning stage, to remove all aluminium oxide residue from the coal, the polished block was placed in a sonic bath. This can cause fragments of coal to be plucked from the face (Falkner, 1987; Hower et al., 2008) although this was not observed for any samples.

2.4 PETROGRAPHIC METHODOLOGY FOR *IN SITU* PILLARS AND CRUSHED COALS

2.4.1 Previous approaches

Approaches to developing a petrographic methodology for *in situ* coal pillars has been attempted by several workers (e.g. Glasspool, 2000, 2003a,b; Belcher et al., 2003; Collinson et al., 2007) but there is currently no standardised methodology (Stach et al., 1982). For further comparative discussion on the advantages and disadvantages of the various methodologies see chapter 8.

2.4.2 Macroscopic subdivisions in coal pillar polished blocks

Once the coal pillars were embedded in polished blocks, visually distinct subdivisions could be observed (Figs. 4.4, 4.9, 4.14, 5.4, 5.7, 6.3, 7.5, 7.6). Stopes (1919) first visually subdivided coal into four groupings or ‘ingredients’ (vitrain, clarain, durain and fusain). These were later expanded and referred to as coal lithotypes (ICCP, 1963; Table 2.1). Visually distinct subdivisions of the coal pillars in this study, have been termed lithotype units (LU), and have been subdivided according to the descriptive brightness scheme by Diessel (1965) into, bright, bright

banded, banded, dull banded, dull and fibrous coal (fusain) lithotype categories (defined in Table 2.1). This scheme is considered to be appropriate as Diessel mainly studied Permian coals, as in this study, whereas Stopes mainly worked on Carboniferous coals.

The pillars were then divided into three equally spaced vertical transects (perpendicular to bedding) for petrographic analysis. Lithotype logs are used in the field, to describe lithotype variation throughout the whole coal seam (Diessel, 1992) therefore, this term was not appropriate for describing lithotype variation at polished block scale. The term microlithotype could also not be used as it is a coal petrography term used to describe microscopic constituents (macerals) in the coal. Therefore, logs constructed of small (millimetre scale) variation in polished blocks, in hand specimen, are referred to as macrolithotype logs (own term used in this thesis, Figs. 4.5, 4.10, 4.15, 5.5, 5.8). These were produced to illustrate spatial variation in coal lithotypes between petrographic transects. In addition, the size, morphology, colour and distribution of vitrain and fusain were documented and illustrated on the macrolithotype log diagrams.

Lithotype	**Description**
Bright coal (vitrain)	Vitreous lustre; may contain up to 10% dull coal in bands <5mm thick
Banded bright coal (clarain)	Mainly bright coal containing thin (<5mm) dull coal bands ranging in proportion between 10-40%
Banded coal (duroclarain)	Contains bright and dull bands (all <5mm) ranging in proportion between 40-60% each
Banded dull coal (clarodurain)	Mainly dull coal containing thin (<5mm) bright bands ranging in proportion between 10-40%
Dull coal (durain)	Matt lustre; may contain 10% bright bands <5mm thick
Fibrous coal (fusain)	Dull with satin sheen; friable; may contain up to 10% of other coal lithotypes less than 5mm thick

TABLE 2.1 The classification of black coal lithotypes (after Diessel, 1965, 1992). Also refer to macrolithotype logs, Figs. 4.5, 4.10, 4.15, 5.5 and 5.8.

2.4.3 Petrographic methodology for *in situ* pillars

2.4.3.1 Dividing each pillar into transects

Three equally spaced transects (left, centre and right sides of each polished block) were used for petrographic analysis of each coal pillar. The spacing of these transects accounts for any lateral variation in inertinite clast size, content, and distribution. Systematic analysis along transects is considered to be statistically preferable to random analysis as the resulting data is more reproducible (Hilliard and Cahn, 1961).

2.4.3.2 Microscope and graticule for petrographic analysis

The polished blocks were studied under oil (immersion oil, RI = 1.514 at 23°C) using a Leica DM 2500 P reflectance microscope with ×10, ×20 and ×50 objectives (with ×10 eyepiece magnification). Petrographic analysis was carried out using the same lamp setting to ensure consistency. The British standard for petrographic analysis of bituminous coal and anthracite (BS 6127-4, 1990) is a point counting strategy. The industry standard graticule used for point counting (Kötter graticule, illustrated in Fig. 2.2 A, B) was mounted in the reflectance microscope eyepiece. This graticule was used in order to compare results from this thesis to previously published coal petrographic data (that has also used the British standard procedure). Other workers have used different graticules, such as the Whipple grid (e.g. Belcher et al., 2003; Collinson et al., 2007) and the implications of this variation in methodology will be discussed in chapter 8.

The British standard for petrographic analysis (BS 6127-4: 1990) states that maximum Kötter graticule dimensions in any field of view have to be 50μm on the specimen (Fig. 2.2 B) which requires a ×25 magnification reflectance objective. A ×25 objective is not available on the Royal Holloway, University of London reflectance microscope. Therefore, to provide closely comparable data, the point counting petrographic analysis of *in situ* pillars and crushed coal was undertaken using a ×20 objective with a ×10 eyepiece magnification. Refer to Table 2.2 for field of view and respective graticule dimensions using a given objective with ×10 eyepiece magnification.

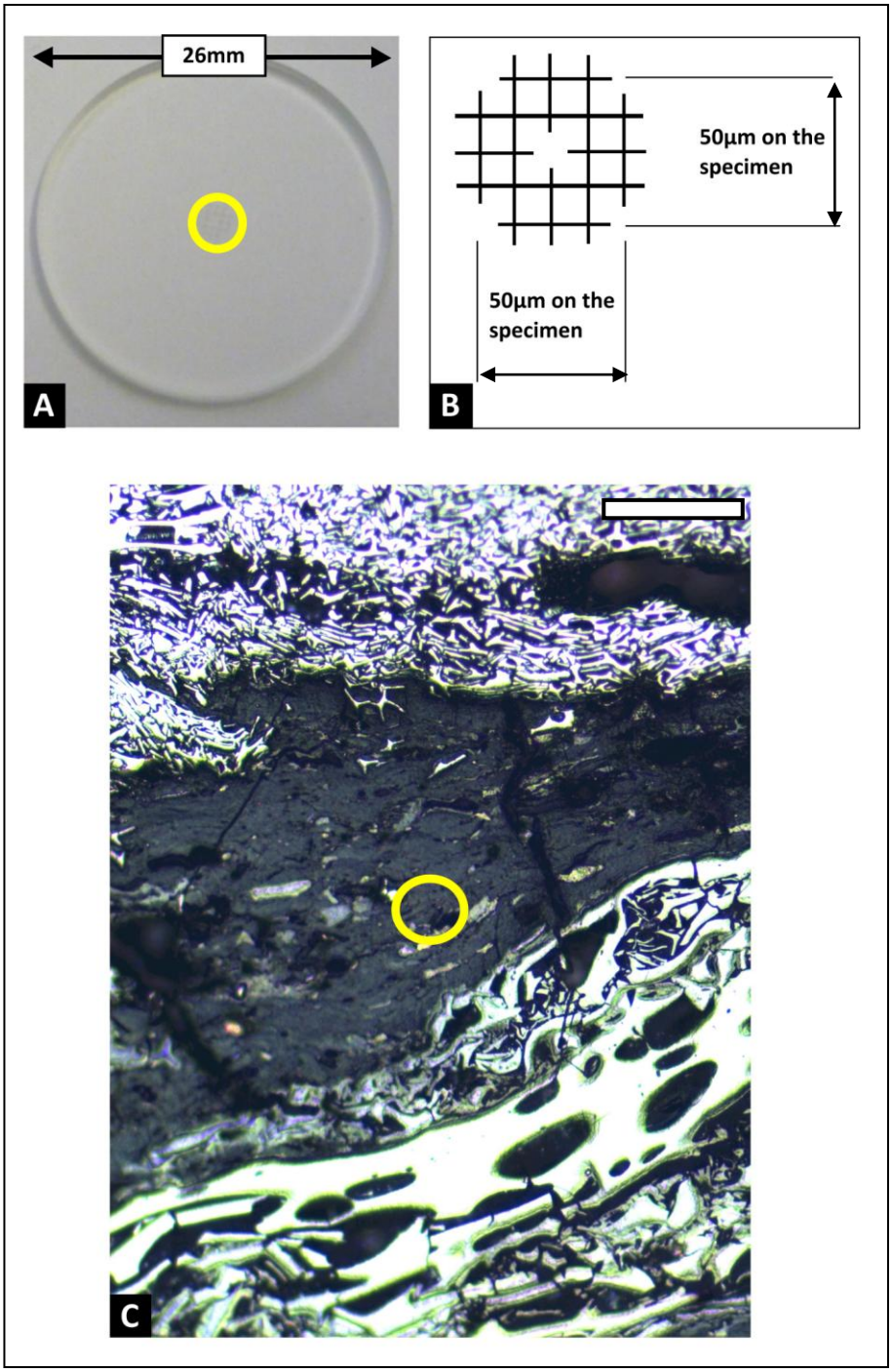

FIG. 2.2 Kötter graticule (yellow circle in **A** and schematically enlarged in **B**) used for coal petrographic point counting (this study; BS 6127-4: 1990). **A** – Photograph illustrating the actual size of the Kötter graticule (yellow circle). **B** – Schematic enlarged drawing of the Kötter graticule (yellow circle in **A**) (image from BS 6127-4: 1990). During petrographic point counting analysis, all crosshairs on the graticule were counted (n = 20 per field of view). **C** – Representative reflectance microscopy image of one of the coal pillar samples (×20 objective, ×10 eyepiece magnification) illustrating the size of the Kötter graticule (yellow circle) in relation to the field of view. Scale bar corresponds to 100µm.

Objective	Maximum breadth of field of view (FOV)	Graticule size	
		Individual small square	***Entire graticule (maximum length)***
×10	850µm	25µm	125µm
×20	425µm	12.5µm	62.5µm
×50	175µm	5µm	25µm

TABLE 2.2 Field of view and graticule size dimensions under each magnification. The ×20 objective was used in this study (grey highlight).

2.4.3.3 Coal petrographic classification schemes

Organic constituents within coal are termed maceral groups (vitrinite, liptinite and inertinite) each of which is subdivided into macerals (e.g. fusinite, semifusinite in the latter). The word maceral was proposed by Stopes in 1935 and originates from the Latin, 'to macerate'. The maceral names all terminate in –inite as a parallel to mineral descriptive terminology (Scott, 2002). The International Committee for Coal and Organic Petrology (ICCP) have devised visual classification schemes (ICCP, 1998, 2001) for identifying these macerals in coal (Table 2.3). The ICCP classification schemes are internationally recognised, which is the rationale for using these schemes for the petrographic analysis of the Late Permian coals in this study. The advantages and disadvantages of the ICCP classification scheme for inertinite macerals will be discussed further in chapter 8.

The focus of this thesis is on the inertinite macerals which are therefore defined in Table 2.3. Multiple subdivisions of vitrinite and liptinite maceral groups were not considered necessary during petrographic analysis and only the macerals referred to in the thesis have been defined in Table 2.3. All maceral groups are illustrated in chapters 4 and 5.

MACERAL GROUP	MACERAL	DEFINITION
Vitrinite Vitrinite designates a group of macerals whose colour is grey and whose reflectance is generally between that of the associated darker liptinites and lighter inertinites over the rank range in which the three maceral groups can be readily recognized.	Telovitrinite	Telovitrinite is a subgroup of the maceral group vitrinite, comprising vitrinites with well preserved botanical cell structures which may or may not be visible.
	Detrovitrinite	Detrovitrinite is a subgroup of the maceral group vitrinite consisting of finely fragmented vitrinitized plant remains occurring either isolated or cemented by amorphous vitrinitic matter.
	Collodetrinite	Collodetrinite is a maceral of the maceral subgroup detrovitrinite within the maceral group vitrinite occurring as a mottled vitrinitic groundmass binding other coal components.
	Corpogelinite	Corpogelinite is a maceral of the maceral subgroup gelovitrinite within the maceral group vitrinite, consisting of homogeneous and discrete bodies representing cell infillings.
Liptinite A maceral group formed of the chemically resistant polymers that include spore exines, plant and arthropod cuticles, resins, waxes, fats and oils.		
Inertinite Inertinite is a maceral group that comprises macerals whose reflectance in low- and medium-rank coals and in sedimentary rocks of corresponding rank is higher in comparison to the macerals of the vitrinite and liptinite groups.	Fusinite	Fusinite is a maceral of the inertinite maceral group, showing highly reflecting, well preserved cellular structure of at least one complete cell of parenchyma, collenchyma, or sclerenchyma.
	Semifusinite	Semifusinite is a maceral of the inertinite maceral group that shows intermediate reflectance and structure between humotelinite/vitrinite and fusinite in the same coal or sedimentary rock.
	Inertodetrinite	Discrete small inertinite fragments of varying shape.
	Funginite	Funginite is a maceral of the inertinite maceral group, consisting of mainly high reflecting single or multi-celled fungal spores, sclerotia, hyphae and mycelia (stromata, mycorrhiza), and other fungal remains.
	Secretinite	Secretinite is a maceral of the inertinite maceral group which is commonly composed of round, vesicled to non-vesicled, and equant to elongate bodies without obvious plant structure.
	Macrinite	Macrinite is a maceral of the inertinite maceral group that occurs either as an amorphous matrix or as discrete, structureless bodies of variable shapes, which are commonly elongated when viewed perpendicular to bedding.
	Micrinite	Micrinite is a maceral of the inertinite maceral group which occurs in very small rounded grains (2µm).

TABLE 2.3 ICCP coal petrographic definitions of all coal macerals petrographically point counted or referred to in this thesis (after ICCP 1998, 2001; Glasspool, 2000). All coal macerals are illustrated in chapters 4 and 5. See text for further explanation. Micrinite (inertinite maceral group) was not observed using the ×20 objective during petrographic analysis due to its small size (2µm).

2.4.3.4 Microscopy procedure for petrographic analysis

For details of the reflectance microscope see section 2.4.3.2. Each polished block was too large to be mounted on the reflectance microscope stage using a glass slide, and was therefore mounted using Blu-tack putty. The block was pressed carefully onto the stage to ensure the surface was level prior to optical petrographic analysis. Immersion oil (RI = 1.514 at 23°C) was put onto the polished block at the base of the first petrographic transect line (T1, transect positions illustrated in Figs. 4.4, 4.9, 4.14, 5.4, 5.7, 6.3). In the first field of view (FOV) at the base of T1, all intersections of the Kötter graticule (n = 20, illustrated in Fig. 2.2 B) were manually counted according to the maceral groups that intersected the cross hairs on the graticule. Macerals were identified according to internationally recognised coal petrographic classification schemes (ICCP 1998, 2001; Table. 2.3). Any intersections on mineral grains were counted as 'mineral matter' and any intersections on embedding resin were not counted. The block was then moved manually, using a joystick control, with a vertical step distance of 425µm (1 FOV). This step distance was chosen as it is used in the British Standard (BS 6127-3: 1995) for crushed coals and is judged to account for the natural banding in the coal (Taylor et al., 1998). This method was repeated for all three transects. Transect data were subdivided according to individual lithotype units, and all three transects were combined to give maceral percentages for each lithotype unit. Maceral data are reported to a mineral included basis (Fig. 4.3; Fig. 5.3; chapter 7) and inertinite is also reported to a mineral free basis (mmf) (Fig. 4.4; Fig. 4.9; Fig. 4.14; Fig. 5.4; Fig. 5.7; chapter 7). Whole pillar maceral data (all three transects) was also combined in order to calculate whole pillar inertinite averages (Table 4.2; Table 5.1).

2.4.4 Petrographic methodology for crushed coal

The small circular blocks were mounted on a glass slide using Blu-tack putty. The sample was then pressed, using a press, before being placed on the reflectance microscope stage. Petrographic analysis of crushed coals was undertaken using the same method as in section 2.4.3.4. The British standard for petrographic analysis of crushed coal requires a minimum of 500 points to be counted (BS 6127-4:1990; BS 6127-3:1995). In this study, three equally spaced parallel traverses of the block were point counted as a comparable methodology to coal pillars. Intersections of the

graticule on embedding resin were not counted so counts vary from 715 (general sample seam 92) to 1,274 (general sample seam 78 S2) (Table A.4.1).

2.4.5 Photography of crushed coals and pillars

Representative colour photographs were taken using a 5 megapixel camera attached to the reflectance microscope, using Prog-Res Capture Pro 2.7 software. Images have 2560 × 1920 pixel resolution. However, images used for montages were taken at lower pixel resolution (1290 × 972) and saved as .jpegs (3.5Mb per image, compared to 13Mb per .tiff image) to enable multiple images to be stitched together using i-solution software (up to n = 95; Fig. 4.8; Fig. 4.13; Fig. 5.12). Images were taken using the same lamp setting to ensure consistency.

Images used in chapters 4 and 5 were initially too dark to clearly observe the different macerals and have all been brightened by the same amount. The brightness of all macerals has been raised by the same amount so all images remain comparable. Images in chapter 5 have also been rotated, as the large size of the polished blocks meant they were placed on the stage lengthways, to ensure a complete petrographic transect could be taken without re-positioning the block. In addition, the colour of the digital photographs did not reflect the colour of the coal observed down the eyepiece. The colour balance of the images was therefore altered, using GIMP software, to magenta = 37, yellow = 33, red = 8.

2.5 FLUORESCENCE MICROSCOPY

Polished blocks were examined under oil (immersion oil of RI 1.514 at 23°C) using a Leica DM 2500 P reflectance microscope attached to a Leica EL6000 external fluorescence light source. The filter set used was a bp450/490 dichroic 510, with lp515 as barrier, Leica size k filter system 13 for blue excitation (part No. 11513878). Samples were examined with ×20 and ×50 objectives and an eyepiece magnification of ×10. Fluorescence microscopy was used principally to distinguish liptinite from mineral matter in pillar 88(a) (chapter 4) during petrographic point count analysis, and to identify internal structure of unidentifiable entities of liptinite colouration observed in coal pillars (see chapters 4 and 5).

2.6 MACERATION OF CHARCOAL FROM FRAGMENTAL BANDS

Fragmental bands observed in the field (chapter 3) blackened the hands to touch and were therefore likely to contain fusain (fossil charcoal; Scott, 1989a). Two fragmental bands were sampled from seam 78, in different areas of the same mine (chapter 3).

For maceration, the fragmental bands were broken into pieces (0.5-1cm in size) and placed in separate 500ml conical flasks until the bottom of the flask was completely covered in sample. 200ml of 68% nitric acid was added to each sample and left until swelling occurred. The exothermic reaction for both samples was violent (but no sample loss). The samples were left for seven days and topped up with distilled water to dilute the acid. The solution was then decanted and passed through a 180µm sieve. The >180µm fraction was put into another 500ml conical flask and 200ml of 20% ammonium nitrate solution added (equivalent to the amount of acid), which was then diluted with distilled water and left overnight. The solution was washed through a 180µm sieve with distilled water until neutral (Pearson and Scott, 1999). The >180µm size fraction (consisting of charcoal, cuticle and spores) was then studied in a petri dish under distilled water using a low power binocular microscope. Pieces of charcoal were randomly sampled, using a fine paintbrush (Pearson and Scott, 1999), air dried and mounted onto stubs for SEM analysis (see section 2.7).

2.7 LOW VOLTAGE SCANNING ELECTRON MICROSCOPY (LVSEM)

Randomly sampled pieces of macerated charcoal from fragmental bands (>180µm size fraction) were studied by SEM to document the types of plants that were charred (see 3.6.3). A carbon tab was used to adhere the pieces of charcoal to the aluminium SEM stub. Samples were mounted onto stubs using a fine paintbrush; however, due to the delicate nature of the material, many pieces broke on mounting. Samples were coated at Southampton University Hospital courtesy of P. Goggin. The samples were given a single coating using a Gold/Palladium target for 75s (50nm thick coating). Scanning electron microscopy was undertaken at the Royal Holloway Electron Microscopy Unit using a Hitachi S-3000. Due to the single coating, the samples started charging immediately (e.g. Fig. 3.17 D) so the images were taken using the backscatter detector under low vacuum to reduce further charging. Operating

conditions were 20.0kV, with a working distance of 17.4-19.8mm. Resulting images had a 1280 × 960 pixel resolution.

2.8 X-RAY DIFFRACTION (XRD)

XRD was undertaken on ten samples [pillar 78(a) LU5; pillar 78(b) LU1-LU3; pillar 88(a) LU2, LU4, LU6; pillar 88(b) LU3, LU12; general samples from seams 78, 91(1) and 92], in order to determine any variation in inorganic content within (chapters 4 and 5) or between seams (chapter 7). This could aid the palaeoenvironmental interpretation as well as confirming the composition of 'mineral matter' identified by petrographic analysis (chapters 4 and 5).

The samples were prepared and analysed by D. Alderton at Royal Holloway, University of London. The pulverised coal samples were ground manually using an agate pestle and mortar with a small amount of water. A thin film of ground coal was then smeared onto a glass slide and dried in an oven at 40°C. X-Ray Diffraction was undertaken on a Philips PW1710/1830 X-ray spectrometer using Cu K α radiation. The samples were run from 4° to 60° (2 θ°) at a rate of 1° per minute. Diffraction traces were produced using GBC Scientific equip. Pty. Ltd Traces (v.6) software. Intensity peaks on the resulting traces (Fig. 4.2; Fig. 5.2; Fig. 7.1) were identified and allocated to different minerals using the ICDD (International Centre Diffraction Data) mineral powder diffraction file by D. Alderton.

2.9 TIME TAKEN FOR EACH METHODOLOGICAL APPROACH

Coal petrography is a very time consuming technique. In this project a total of 184,358 points were counted manually on *in situ* pillars, and crushed coal polished blocks. In total, forty one samples were analysed using characterisation techniques (see chapter 7; Appendix 7) which took around 3 months. The experimental combustion (Appendix 8) was also time consuming, as these coals have a high %volatile matter content (chapter 7; Appendices 5 - 7) and therefore little char was produced during combustion, and the samples had to be run multiple times.

CHAPTER 3

THE SEDIMENTOLOGICAL SETTING AND FOSSIL PLANTS OF THE PERMIAN COAL-BEARING SEQUENCE FROM THE KUZNETSK BASIN

This chapter introduces the geological and sedimentological background of the Kuznetsk Basin. This is followed by macroscopic descriptions of the thirteen Late Permian coal seams sampled and the associated interseam sediments. Examples of plants are then discussed, both from interseam sediments (impressions and permineralised plant axes) and from the coal itself (fusain).

3.1 THE KUZNETSK BASIN

The Kuznetsk Basin (Fig. 3.1) is located in South Western Siberia and has an area of 26,000 km^2 (Davies et al., 2010). Basin infill consists of 9 – 11 km (Polyansky et al., 2004) of Devonian to Triassic sediments with Carboniferous and Permian coal-bearing strata (Evtushenko et al., 1975).

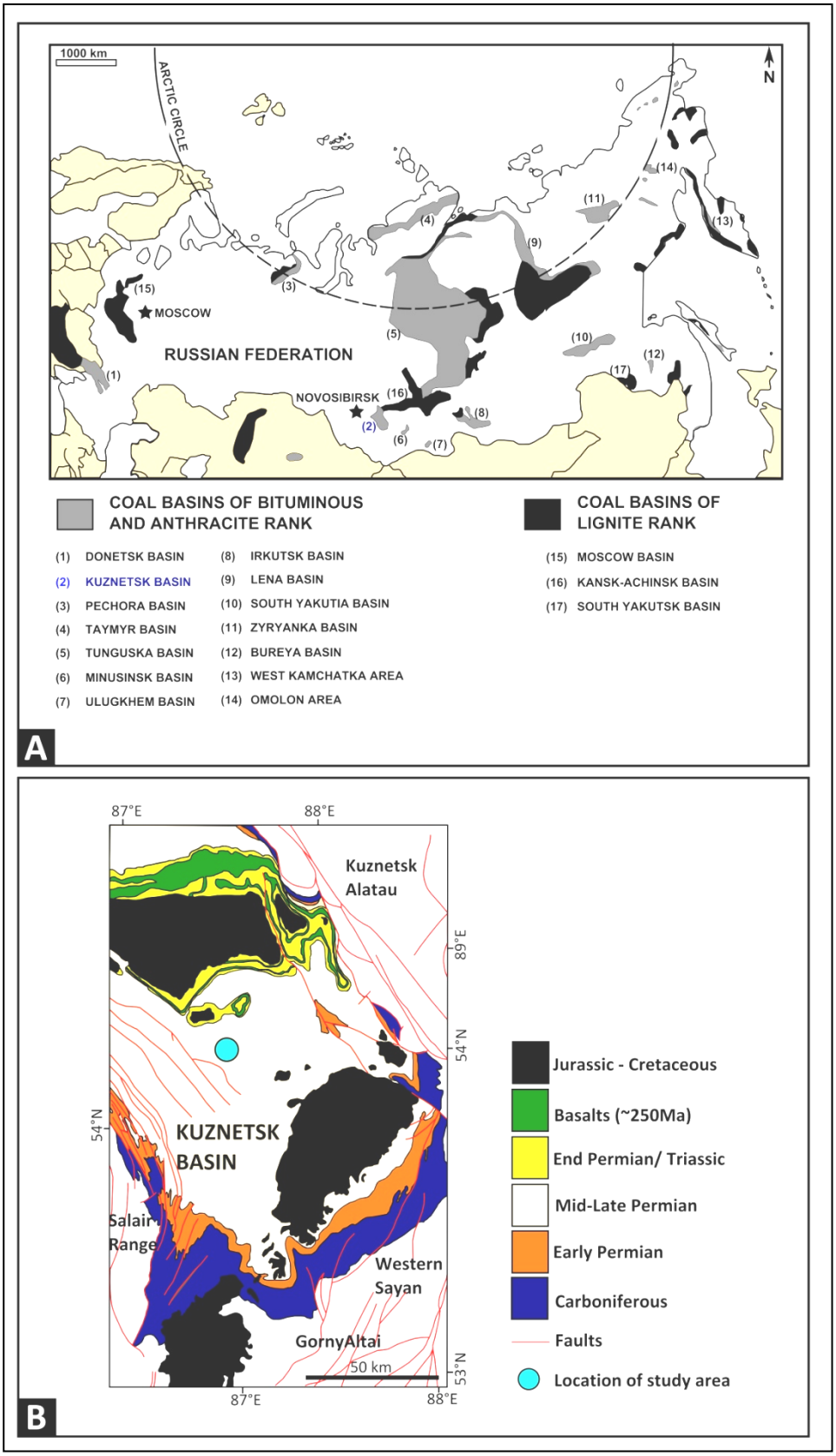

FIG. 3.1 Maps showing the study area, the Kuznetsk Basin. **A** – The size and location of the Kuznetsk Basin (highlighted in blue) in relation to other coal basins in Russia (base map after Walker, 2000; Coal basins labelled from Thomas, 1992; Bibler et al., 1998). **B** - Geological map of the Southern Kuznetsk Basin showing the study area (after Davies et al., 2010).

3.1.1 Geological and sedimentological background

During the Permian Russia made up part of the supercontinent Pangaea which formed during the Late Palaeozoic due to the closure of the Rheic Ocean between Gondwana and Laurussia (McElhinny and McFadden, 2000). At the same time the Siberian Craton and Kazakhstan microcontinent joined Laurussia as the Uralian Ocean closed (Pisarevsky et al., 2006). The palaeolatitude of Siberia was thought to be ~56°N during the Late Permian (Changhsinginan Stage) (Cocks and Torsvik, 2007; Domeier et al., 2012). A small Northern polar ice cap combined with extensive precipitation at higher latitudes enabled a wide range of temperate peat-forming environments to develop (Ziegler, 1990; Wagner, 2003). The Kuznetsk Basin was located within the Angaran floral belt in the Permian and peat-forming vegetation was dominated by cordaites (Oshurkova, 1996; Krassilov, 2000).

The Kuznetsk Basin is a closed intramontane depression (Evtushenko et al., 1975) consisting of folded outliers of Mesozoic and Permian strata and is bordered by four fold thrust belts (labelled in Fig. 3.1 B) that verge towards the Basin interior (Davies et al., 2004; Davies et al., 2010). These fold-thrust belts form part of the Altaid collage which is the orogenic belt that constructed most of the basement of central Asia during the Palaeozoic. No distinct Kuznetsk Basin existed during the Devonian to Carboniferous (Davies et al., 2010). By the Permian the underlying accreted Palaeozoic basement was consolidated. This stability enabled the formation of vast Permian coal basins (Morton et al., 2005). The Permian-Triassic collision of Kazakhstan and Siberia caused sinistral shearing along the West Sayan fault and juxtaposed the Gorny Altai and West Sayan (Fig. 3.1 B) to their present position (De Grave et al., 2009; Glorie et al., 2012). Provenance studies on zircons suggest Permian sediment fill in the Kuznetsk Basin was sourced from the West (Salair range) and South (Gorny Altai and West Sayan) (Fig. 3.1 B) (Davies et al., 2004; Morton et al., 2005; Morton et al., 2007).

The majority of sedimentary deposition in the Kuznetsk Basin occurred in the Late Palaeozoic (Polyansky et al., 2004). The Carboniferous sequence is dominated by carbonates, followed by an Upper Carboniferous to Permian non-marine clastic succession (Davies et al., 2010). The Upper Carboniferous coal-bearing Balakhonskaya Series contains coal seams ranging from 2 - 28m in thickness

(Evtushenko et al., 1975). The Balakhonskaya Series extends into the Early Permian where it consists of thick sandstones and siltstones with several coal seams which are occasionally thick (1.5 – 20m) (Evtushenko et al., 1975). This is directly overlain by the coal-bearing Kolchuginskaya Series (Fig. 3.2), the focus of this study.

For this research, thirteen coal seams (numbered 68-94) were sampled from the Late Permian Kolchuginskaya Series which consists of siliciclastics and coal seams (Evtushenko et al., 1975). In the study area, this Series is 2800m in thickness with 74 worked coal seams (>0.7m thick) (Pronina personal communication, 2010). The seams sampled are from the Gramoteinskaya Formation (seams 68-73; Fig. 3.2), which consists of sandstones, siltstones, mudstones, minor conglomerates and coal seams (15-30m thick, and up to 50m) and the Tailuganskaya Formation (seams 78-94; Fig. 3.2) which consists of the same sediments but coal seam thickness varies greatly. The majority of coal production in the Kuznetsk Basin is from the Tailuganskaya Formation (Evtushenko et al., 1975).

The Permian sequence is overlain by coal barren Triassic volcanic rocks (Evtushenko et al., 1975). A Triassic-Jurassic boundary deformation event folded Permian and Triassic sediments causing uplift of the Altai and renewed sediment input to the basin from fluvial systems (Davies et al., 2004). The Jurassic strata is unconformable on either Permian or Triassic units and is no more than 1 km thick. Lower Cretaceous units are only in the South-West of the basin, with no lower Cretaceous or Palaeogene strata elsewhere as most of central Asia was a peneplain at this time. The Kuznetsk Basin is currently active and being incised as a long distance effect of the India-Asia collision (Davies et al., 2010).

3.1.2 Burial history of the Kuznetsk Basin

Lithospheric models suggest rapid basin subsidence occurred in the Kuznetsk Basin in two main phases. The first episode is postulated to have occurred from the Mid-Upper Devonian (370 – 380 Ma), this episode covered three quarters of the current basin and reached maximum burial temperatures of >300°C (Polyansky et al., 2004). The second episode occurred from 280 – 290 Ma (Early Permian) and from 260 – 270 Ma (Upper Permian) both are thought to have consisted of 10 Ma periods of rapid subsidence during which sedimentation rates are estimated to have been 90 –

130m/Ma (Polyansky et al., 2004). The thermal history of the basin suggests that maximum temperatures may have reached >400°C, in the centre of the Kuznetsk Basin, after the rapid subsidence events in the Permian (Polyansky et al., 2004). The model is independently corroborated by vitrinite reflectance, which is both a coal rank parameter and temperature proxy. Coals and coaly sandstones suggest maximum temperatures were reached during the final stages of sedimentation and range from 90 – 190°C, in agreement with vitrinite reflectance (0.56%Ro = 90 – 110°C) which may correspond to subsidence of 2-3 km (Polyansky et al., 2004). Mean random vitrinite reflectance measurements from the thirteen Late Permian coal seams in this study are also consistent with this observation, with an overall mean of 0.53%Ro (2sd = 0.08) (Chapter 7.3.1; Appendix 7). Vitrinite reflectance measurements from other Permian, Triassic and Jurassic Kuznetsk Basin coals by Davies et al. (2007) range from 0.41 - 0.52%Ro. They show no trend of decreasing vitrinite reflectance with decreasing stratigraphic age and no jumps in vitrinite reflectance across unconformities which suggests denudation prior to further burial (Davies et al., 2007). This range of values is consistent with the removal of 2 km of the sedimentary sequence during the Triassic – Jurassic (Davies et al., 2007).

3.2 DATING RUSSIAN COAL BEARING SEQUENCES

The Permian sequence is dated by traditional Russian correlation using a biostratigraphic framework which incorporates floral, ostracode, conchostracan, bivalve and charophyte assemblages (Mogutcheva and Krugovykh, 2009). The latest Permian has been dated by Ar-Ar age determination of two basalt flows (250.3 ± 0.7 Ma and 250.7 ± 0.6 Ma), which are slightly younger than the Meishan P-T boundary stratotype, between 249.25 ± 0.14 Ma and 249.83 ± 0.15 Ma (Reichow et al., 2009; Davies et al., 2010). The basalt flows occur in the coal barren succession above the latest coal seams (Davies et al., 2010) therefore the seams in this study must be older than 250.3 ± 0.7 Ma.

3.3 FIELD SAMPLING

Thirteen Late Permian coal seams from the Kolchuginskaya Series (numbered 68 to 94) were sampled from two open cast Mines that are 8km × 8km in size and 5km apart (the study area is shown in Fig. 3.1 B). Seams 78, 84, 84-86 and 91 were sampled at multiple locations in both Mines. Mine information has been removed at

the Mine owners' request therefore the first Mine visited will be referred to as Mine 1 and the second Mine 2. See chapter 2.1 for sampling techniques. The sampling strategy was based on seam access and availability. For each coal seam a bag of randomly sampled loose pieces, termed 'general sample' was taken (chapter 2.1.2). Two stockpile size fractions incorporating all worked seams (seams 73 to 91) were sampled (chapter 2.1.3; Fig. 2.1). Five orientated pillars from three seams (78, 88 and 91) were also sampled (chapter 2.1.1; chapter 4; chapter 5).

3.4 FIELD DESCRIPTION OF SEAMS AND INTERSEAM SEDIMENTS

The seams will be systematically described from oldest (64) to youngest (94) including information on the interseam sediments. No sedimentary logs were made of the interseam sediments due to very limited sampling time and access to each seam. Information regarding interseam sediments was therefore taken both from general field observations and field photographs.

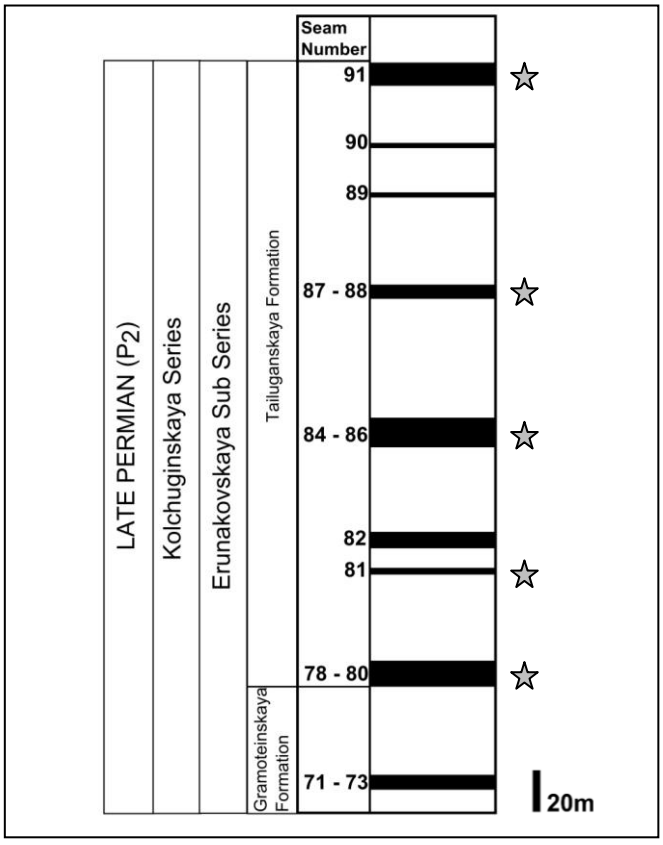

FIG. 3.2 Schematic representation of relative coal seam and interseam sediment thicknesses obtained from borehole data from Mine 1 in the Kuznetsk Basin (redrawn from Siberian Mine company copy). Seams 68 and 92-94 were only observed in Mine 2. Grey stars next to each seam represent the seams sampled in Mine 1.

Seam 68: This seam was only sampled in Mine 2. Seam 68 was vertically dipping with no access to the coal face. The seam was five metres thick and contained three siltstone-mudstone sediment interlayers (0.5-1m thick).

Seam 73: This seam was only sampled in Mine 2. Seam 73 was twelve metres thick and contained abundant dull coal. Some pieces in the general sample contained thin fragmental bands (field term for a layer with sufficient fusain to blacken hands). The overlying interseam sediments consist of fine-grained cross-stratified sandstone and mudstone (Fig. 3.3).

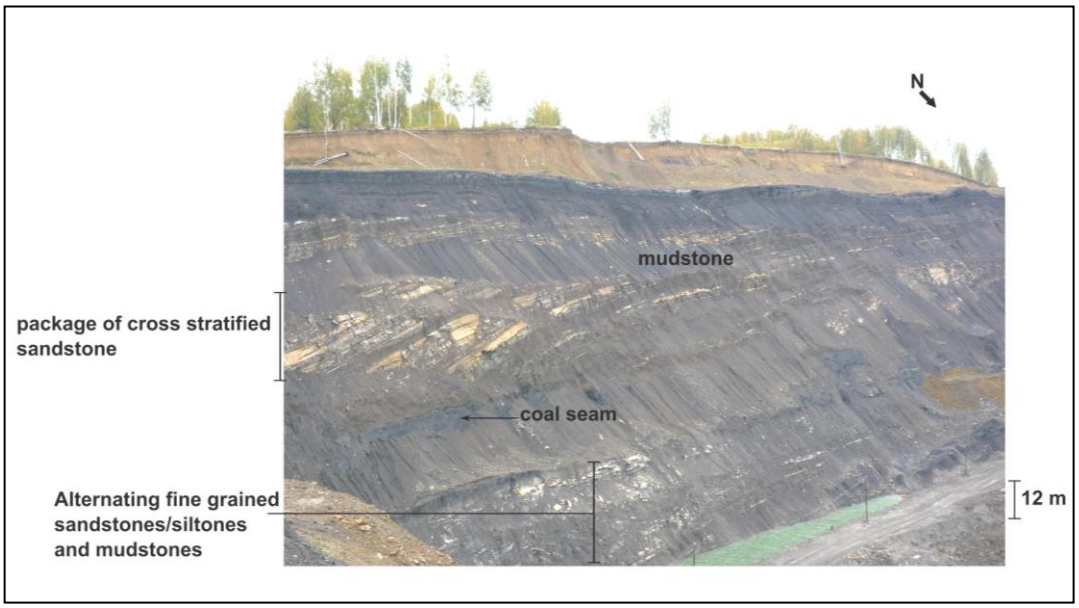

FIG. 3.3 Annotated representative field photograph of interseam sediments overlying seam 73 (Mine 2). The seam itself is below this image.

Seam 78: The seam was sampled from both Mines 1 and 2, and ranged from 8-11m in thickness. In Mine 1 an orientated coal pillar was sampled near the base of the seam [pillar 78(b) chapter 5; Fig 5.1 B]. In one area of Mine 2 (5 km from Mine 1), only general samples from intervals throughout the seam could be obtained. Fragmental bands occurring in the middle of the seam were sampled and macerated (see 3.6.3). In another area of Mine 2, the seam was 8m thick. One orientated pillar was sampled [pillar 78(a) chapter 4; Fig. 4.1 A(i); Fig. 4.1 A(ii)]. Fragmental bands were abundant in this area (Fig. 3.4), two were sampled, and fragmental band 2 was macerated (see section 3.6.3).

Fusain is fossil charcoal (Scott, 1989a), and can be distinguished in the field by its brittle appearance and the black residue it leaves on the hands when touched. The fragmental bands observed in the field (Fig. 3.4; observed in seams 73, 78, 82, 84) were brittle and left a black residue on the hands. However, when the fragmental bands were macerated, only a small proportion was charcoal and the remainder was vitrain.

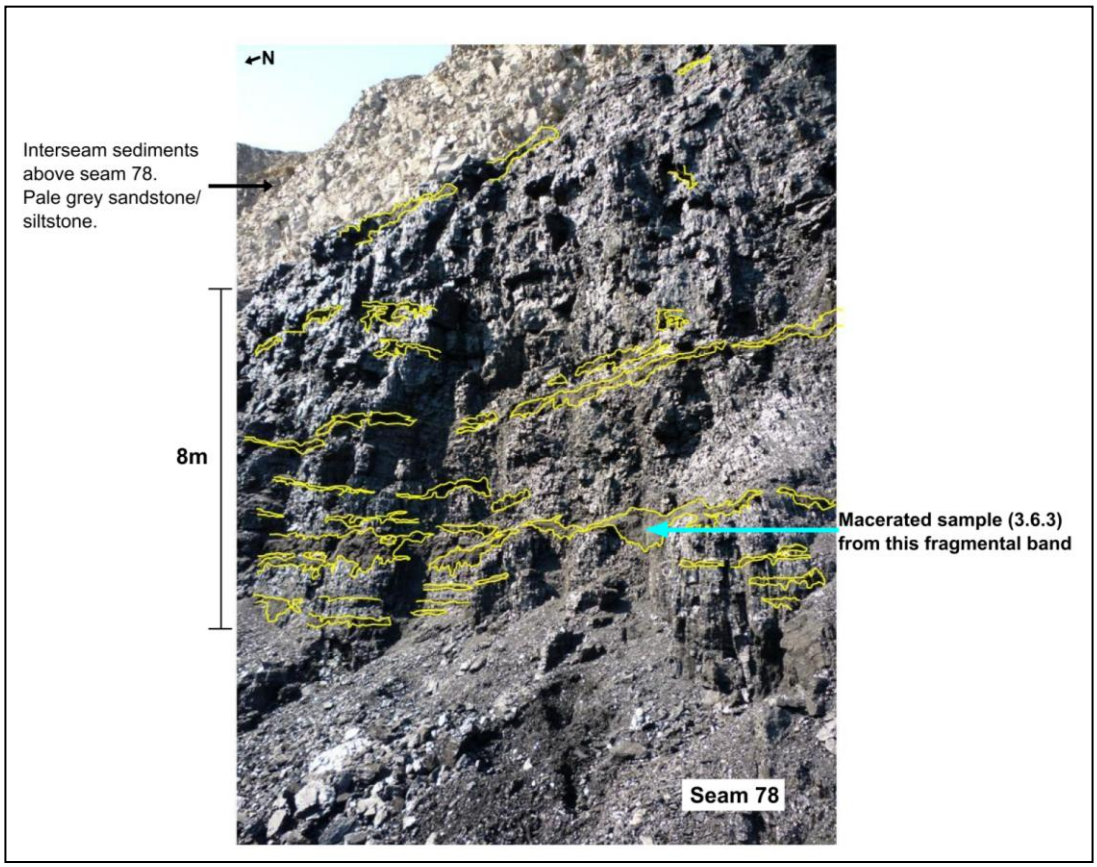

FIG. 3.4 Annotated field photograph of seam 78, Mine 2 [the same seam where pillar 78(a); chapter 4 was sampled] with fragmental bands highlighted in yellow. Despite outcrop erosion (discontinuities in yellow highlight) some of the fragmental bands could be traced laterally along the seam for several tens of metres.

In Mine 2 the lithologies of the interseam sediments overlying seam 78 were thinly bedded pale yellow to grey sandstone/ siltstone (Fig. 3.4) becoming more mudstone dominated to the top of the sequence (Fig. 3.5 B). However, in Mine 1 the interseam sediments consist of large scale cross-stratified sandstone (Fig. 3.5 A).

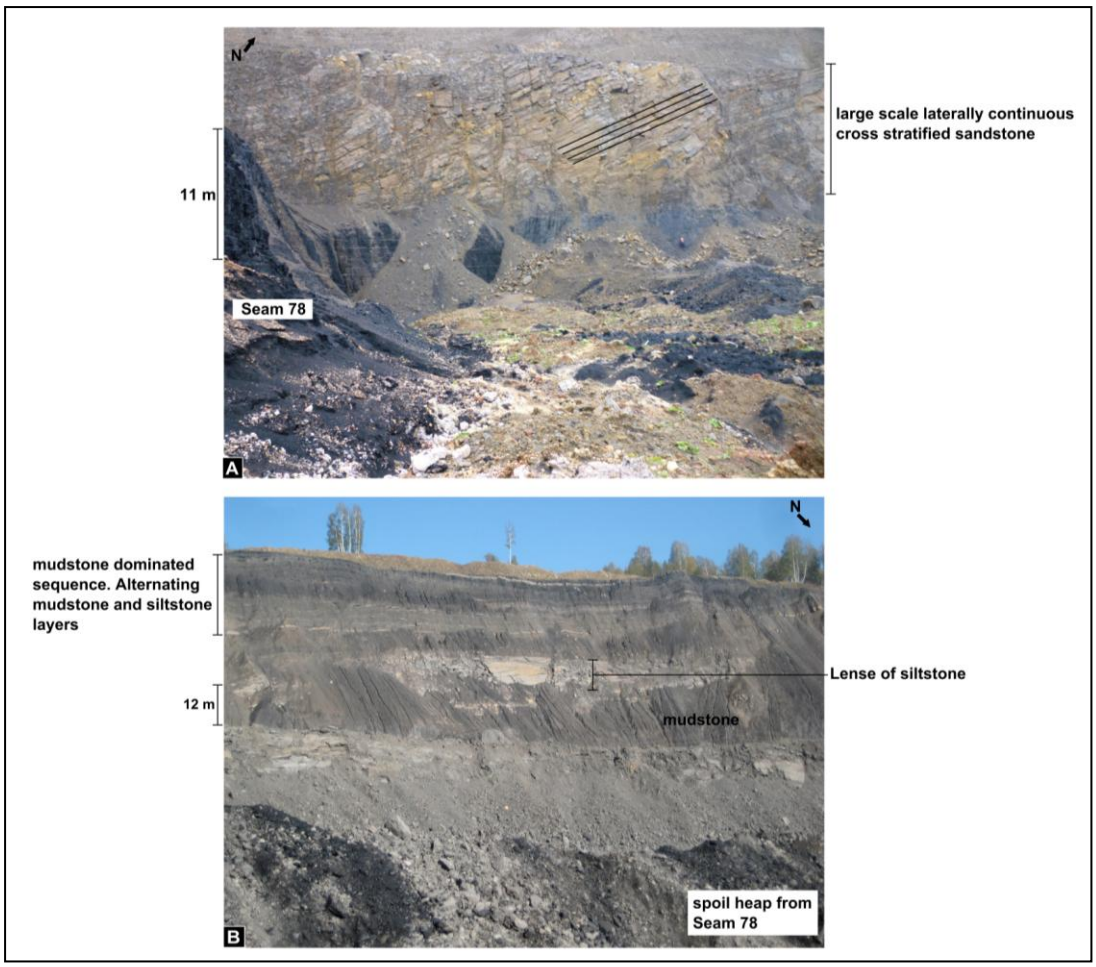

FIG. 3.5 Annotated field photographs of seam 78 and overlying interseam sediments. **A -** Mine 1 [the locality used to sample pillar 78(b)] sampled 5 km from **B** showing cross-stratified sandstone with black lines highlighting the scale and dip angle of the cross-stratification. **B –** Mine 2. Mudstone dominated sequence containing an elongate lense of cross-stratified siltstone.

Seams 80-81 combined: A general sample was collected from one area in Mine 2. These seams were poorly exposed and the interseam sediments (overburden) had been removed.

Seam 81: A general sample was collected from this seam in another area of Mine 2. The interseam sediments overlying seam 81 were dominated by mudstone with a few well spaced alternating fine-grained siltstone and sandstone beds**.**

Seam 82: This seam was sampled in Mine 2 and is steeply dipping. The only example of macroscopic *in situ* pieces of fusain seen during the entire fieldwork, were observed on a bedding plane of seam 82 (Fig. 3.6).

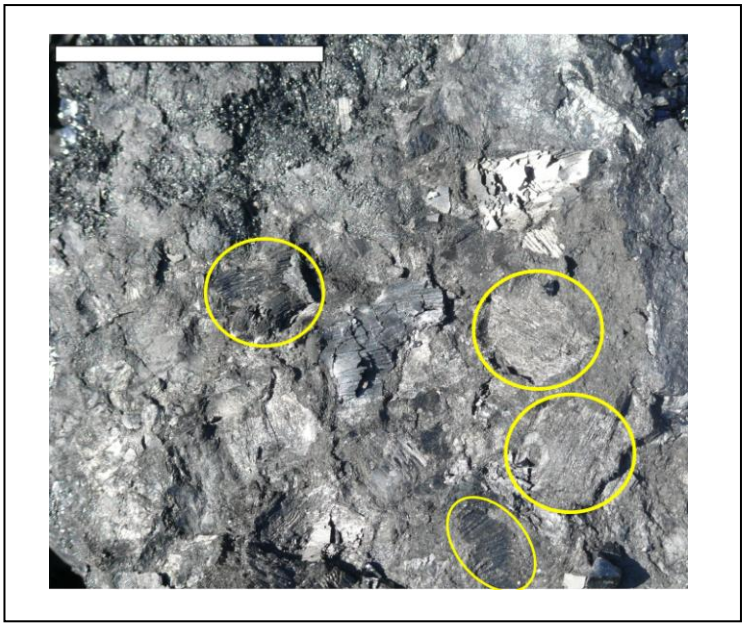

FIG. 3.6 Field photograph showing *in situ* macroscopic pieces of charcoal on a bedding plane within seam 82. Some of the whole fusain pieces are highlighted in yellow but many more can be observed. Scale bar = 50mm.

Seams 84-86 combined: Seams 84-86 coalesce in one area of Mine 1 (Fig. 3.7) and the combined thickness reached 18m. Regularly spaced vitrain bands are observed throughout, which are associated with sedimentary interlayers within the seams. Overlying interseam sediments consist of massive cross-stratified sandstone with a large channel (Fig. 3.7).

FIG. 3.7 Annotated field photograph of seams 84-86 (Mine 1) showing the overlying interseam sediments and the location of seam 88. The dip of the cross-stratified sandstones is highlighted using black lines.

Seam 84: The single seam was sampled in Mines 1 and 2. Seam thickness remained relatively constant at both Mines at around five metres. In Mine 2 (not illustrated), seam 84 was weathered and steeply dipping, composed of thin leaves that break easily making sampling difficult. In Mine 1 the majority of the seam was submerged (Fig. 3.8) but was observed to contain frequent sedimentary interlayers and the general sample contained a fragmental band.

Plant impressions were observed on bedding planes within interseam sediments at both Mines (Fig. 3.15 C, D). The interseam sediments overlying seam 84 (Mine 1; Fig. 3.8) consist of large scale laterally continuous cross-stratified sandstones which change dip angle locally (Fig. 3.8). This is the only seam where an erosive contact was observed between the coal seam and overlying sedimentary sequence.

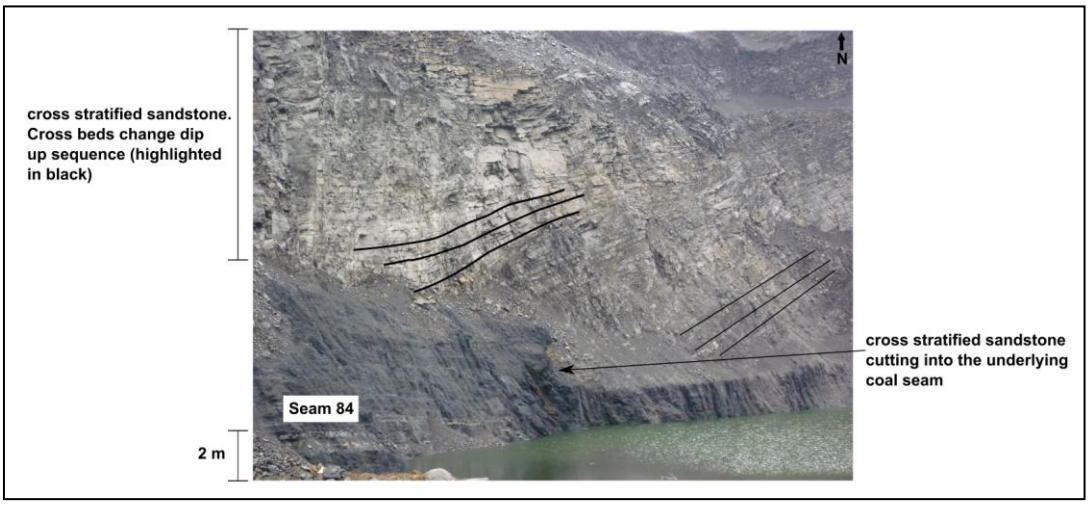

FIG. 3.8 Annotated field photograph of the interseam sediments overlying seam 84 (Mine 1). Black lines highlight dip of cross-stratified sandstone.

Seam 88: Seam 88 was only sampled in Mine 1 (Fig. 3.7) and is one of the thinnest seams in the sequence at 3m. Two orientated pillars were sampled [pillars 88(a) chapter 4 and 88(b) chapter 5; Fig. 5.1 A]. One contained thick dull layers (durain) which are grey in colour, amorphous in appearance and not fragmental [also seen in general samples from seams 84-86 and 91(1)] and are likely to be inertinite-rich (Diessel, 1992). The overlying interseam sediments range from thinly bedded fine-grained sandstones and siltstones grading up to laminated mudstone at the top of the sequence.

Seam 91: Sampled from Mines 1 and 2. At Mine 1 seam 91 is one of the thickest seams in the sequence (14m; Fig. 3.2) containing at least five mudstone interlayers within the seam. An orientated pillar was sampled at the base of the seam (chapter 4; Fig. 4.1 C; pillar 91).

The overlying interseam sediments (Mine 1; Fig. 3.9 A; Fig. 4.1 C) consist of massive cross-stratified sandstones which change dip angle throughout the sequence and downlap onto seam 91 (Fig. 3.9 A). In Mine 2 (5 km distant) the interseam sediments consist of alternating, laterally extensive, fine-grained sandstone, siltstone and mudstone (Fig. 3.9 B) containing climbing ripples (Fig. 3.10) and plant impressions (Fig. 3.15 A).

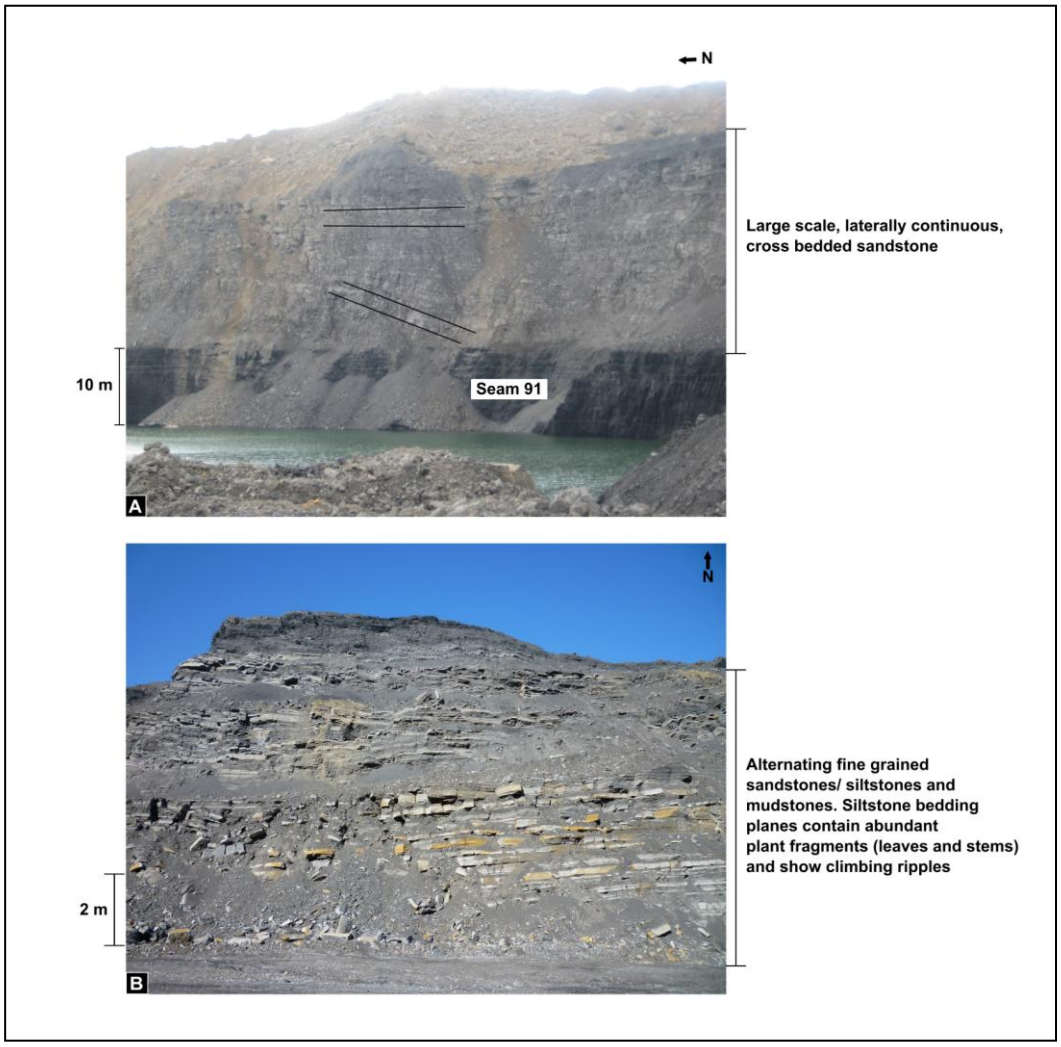

FIG. 3.9 Annotated field photographs of interseam sediments overlying seam 91. **A** - Mine 1. Cross-stratified sandstone (image courtesy of A.C. Scott, 2009). The dip angles of cross-stratification appear to change throughout the sequence (highlighted with black lines)**. B -** Mine 2. Alternating fine-grained sandstones/ siltstones and mudstones, seam 91 is immediately below this image.

FIG. 3.10 Field photograph of climbing ripples on a loose block of fine-grained sandstone/ siltstone from the interseam sediments overlying seam 91 (Mine 2). The surface of the block (with ripples) is perpendicular to bedding. Scale bar = 15cm.

Seam 92: This seam was sampled at Mine 2. It was weathered, poorly exposed and the coal is bright but fragments easily and flakes into thin laminae (shale like). The interseam sediments (overburden) had been removed at this locality but a loose block of siltstone from the overlying interseam sediments was observed (Fig. 3.11), which contained a microchannel structure and climbing ripples.

FIG. 3.11 Field photograph of climbing ripples on a loose block of siltstone from the interseam sediments overlying seam 92. The surface of the block is perpendicular to bedding and a microchannel and different types of ripples including climbing ripples are observed. Scale bar = 15cm.

Seam 94: The youngest seam in the sequence was only sampled in Mine 2. The outcrop is heavily weathered and the coal is friable and light in colour. The interseam sediments consist of alternating mudstone and siltstone beds in a mudstone dominated sequence (Fig. 3.12).

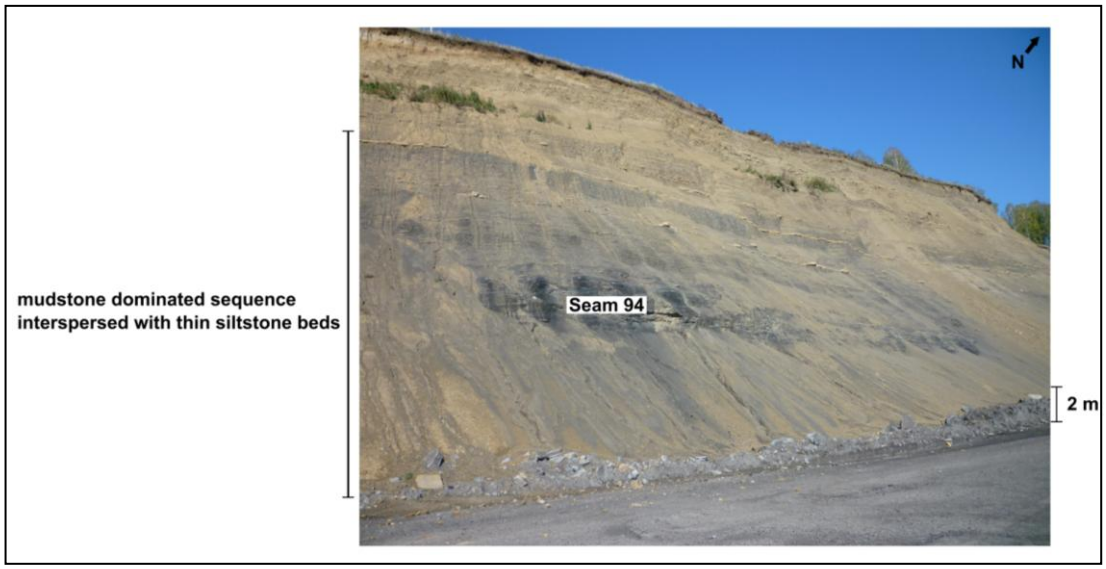

FIG. 3.12 Annotated field photograph showing the mudstone dominated interseam sediments both beneath and overlying seam 94. The seam is weathered and difficult to observe in the field.

3.5 INTERPRETATION OF INTERSEAM SEDIMENTS

Previous work on the Permian sedimentary sequence from the Kuznetsk Basin (outside the area studied in this work) by Davies et al. (2010) has grouped the sediments into three facies associations: fluvial channel-belt, overbank and floodplain/floodplain pond with palaeoflow indicators showing a N/NE flow into the West Siberian Basin. Sandstone foresets from the fluvial channel-belt facies are generally 0.5-1m in height suggesting channel depths of 18-50m. 6-10m high sandstone sets are indicative of lateral bar migration or mid channel bars in high energy braided or meandering rivers across a large floodplain (Davies et al., 2010). Overbank facies include crevasse splays and crevasse channels (up to 30m wide) (Davies et al., 2010) which are followed by floodplain mudstone and/or coal facies (Davies et al., 2010). The peats were formed in extensive mire systems (Gore, 1983) that existed for considerable periods of time, producing coals often in excess of 10 metres thick (Fig. 3.2; Fig. 3.5 A; Fig. 3.7; Fig. 3.9 A; Fig. 4.1 C; Fig. 5.1 B).

The facies associations observed by Davies et al. (2010) can also be observed in interseam sediments studied here. Large fluvial channels can be observed above seam 78 (Fig. 3.13 A) and seams 84-86 (Fig. 3.14). The channel geometry suggests that they represent a single channel body that is mobile (avulsing), forming extensive lateral accretion (point bar) deposits (Gibling, 2006). As represented by large scale cross-stratified sandstones (e.g. Fig. 3.5 A; Fig. 3.7; Fig. 3.8; Fig. 3.9 A). The presence of lateral accretion surfaces within the fining up succession of a channel fill deposit is also an indication that the river was meandering (Nichols, 2009). Divergent accretion dips of point bars (as seen in Fig. 3.8; Fig. 3.9 A) may also indicate channel migration and avulsion (Gibling, 2006). Dips of point bar deposits are inclined towards the deepest part of the channel and are perpendicular to flow direction (Nichols, 2009) overall the orientation of the large bedforms, suggest an E-W (Fig. 3.13) to NE-SW (Fig. 3.14) flow trend.

The fine-grained sandstone, siltstone and mudstone sequences (e.g. Fig. 3.3; Fig. 3.5 B; Fig. 3.9 B; Fig. 3.13 B) are interpreted to represent the overbank/ floodplain facies as reported by Davies et al. (2010). Small bedforms may be observed in proximal floodplain sediments (Fig. 3.3; Fig. 3.5 B; Fig. 3.13 B) thus providing evidence for small channels or crevasse splay deposits. Climbing ripples (Fig. 3.10; Fig. 3.11) represent rapid deposition (Allen, 1970, 1971, 1973; Ashley et al., 1982; Nichols, 2009) in low energy flow regimes, either during the waning period of a flood, on the tops of point bars or as overbank deposits (McKee et al., 1967; Diessel, 1992; Brierley et al., 1997).

Peat deposition is abruptly terminated by incursion of fluvial sediments giving a sharp contact with the between the roof of the coal seam and overlying sediments (Fig. 3.5 A; Fig. 3.7; Fig. 3.9 A; Fig. 3.13 A; Fig. 3.14).

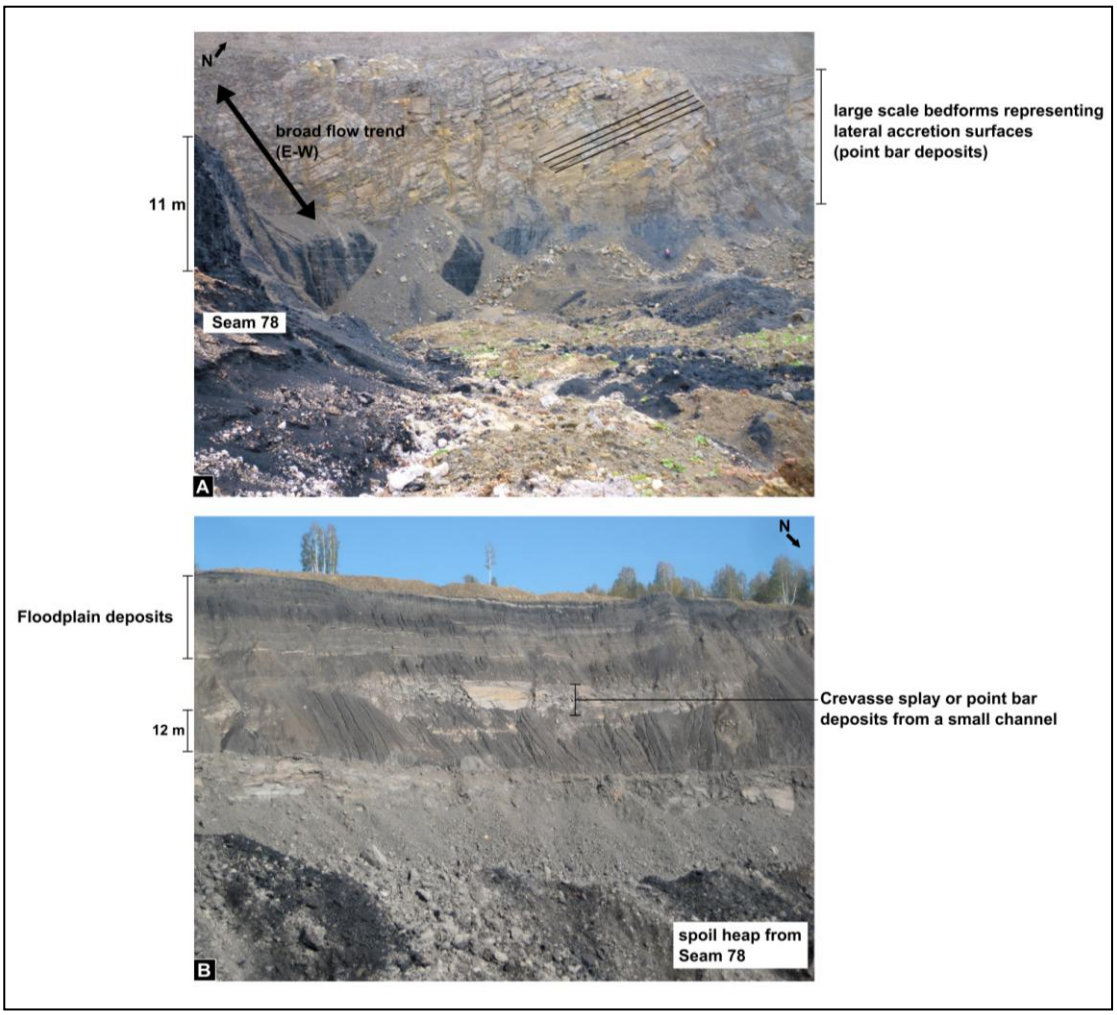

FIG. 3.13 Annotated field photographs of interseam sediments overlying seam 78 and interpreted environment of deposition. **A -** Mine 1 [the locality used to sample pillar 78(b)] sampled 5 km from **B** showing cross-stratified sandstone representing point bar deposits proximal to the fluvial channel and inferred flow trend based on the orientation of the lateral accretion surfaces. **B –** Mine 2. Mudstone dominated floodplain environment of deposition with a crevasse splay deposit, distal to the fluvial channel.

FIG. 3.14 Annotated field photograph of seams 84-86 and the overlying interseam sediments with the interpreted environment of deposition. The presence of lateral accretion surfaces suggest that the river was meandering. The inferred flow trend is based on the orientation of the lateral accretion surfaces

3.6 PLANTS FROM INTERSEAM SEDIMENTS AND COAL MACERATIONS

3.6.1 Plant impressions

Plant impressions and poorly preserved compressions were abundant and observed on loose blocks of fine-grained mudstone/ siltstone interseam sediments on spoil heaps (seams: 73, 78, 81, 84, 84-86, 91, 92 and 94). They are randomly distributed across the bedding planes and range from entire (Fig. 3.15 A, B) to fragmented (Fig. 3.15 D). The majority are narrow, elongate leaves (Fig. 3.15 A, B, D) or stems (Fig. 3.15 C). The leaves range in size but have the same morphology and occur in monotypic assemblages throughout the sequence. The difference in size may be the result of different growth stages being preserved (Meyen, 1984) or different species (Šimůnek and Libertín, 2006). The poor preservation of the material made it seem unlikely that cuticles could be prepared so this was not attempted, however the overall gross morphology of these stem and leaf impressions is consistent with cordaitaleans (Harms and Leisman, 1961; Meyen, 1984; Ignatiev and Meyen, 1989).

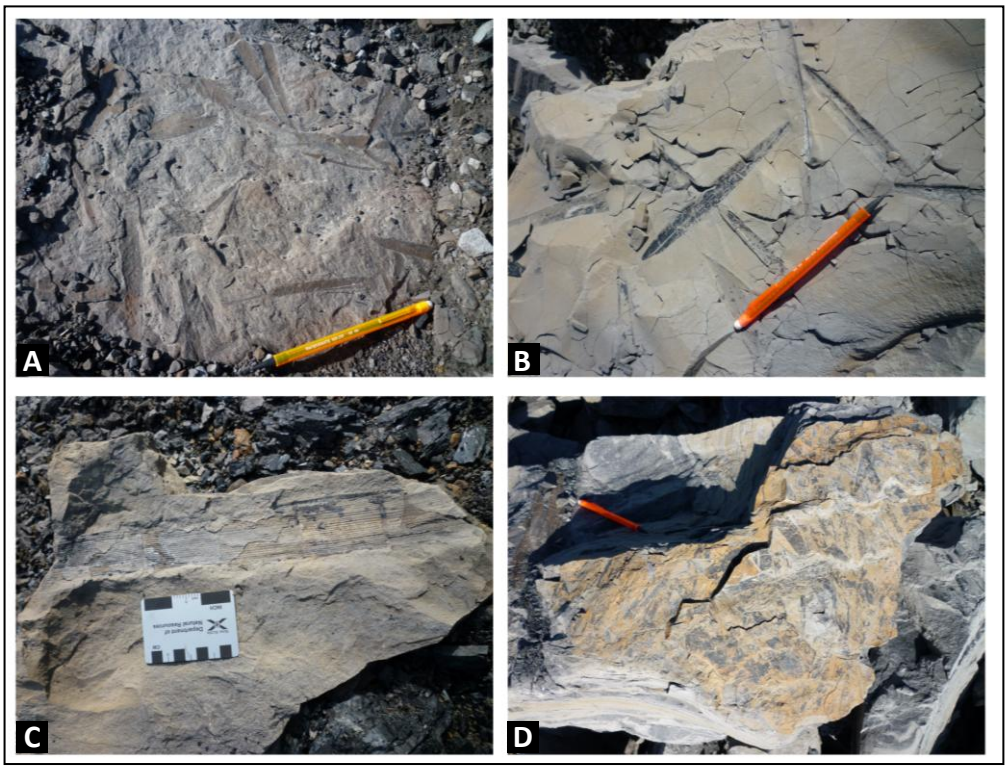

FIG. 3.15 Representative field photographs of plant impressions preserved on bedding planes of interseam sediments. **A** - Randomly distributed thin elongate leaves (seam 91; Mine 2). **B** - Thin elongate leaves that are narrower than those in **A** and may represent a different species or a different stage of growth. **C** – Poorly preserved impression of a stem (seam 84; Mine 1). **D** - Fragments of leaves showing the typical number of impressions on a given block (seam 84; Mine 2). Pencil scale bar = 15cm.

3.6.2 Permineralised plant axis

Permineralised plants were observed amongst loose blocks of interseam sediments overlying seams 81 and 92. A thin section of a representative plant axis from interseam sediments overlying seam 92 was studied using transmitted light microscopy (Fig. 3.16). The plant axis consists of rows of repeating similar sized rectangular cells (pycnoxylic gymnospermous wood) and contains two growth rings (one illustrated in Fig. 3.16 A-C) providing evidence for interruption of growth probably in a seasonal climate (Chaloner and Creber, 1973).

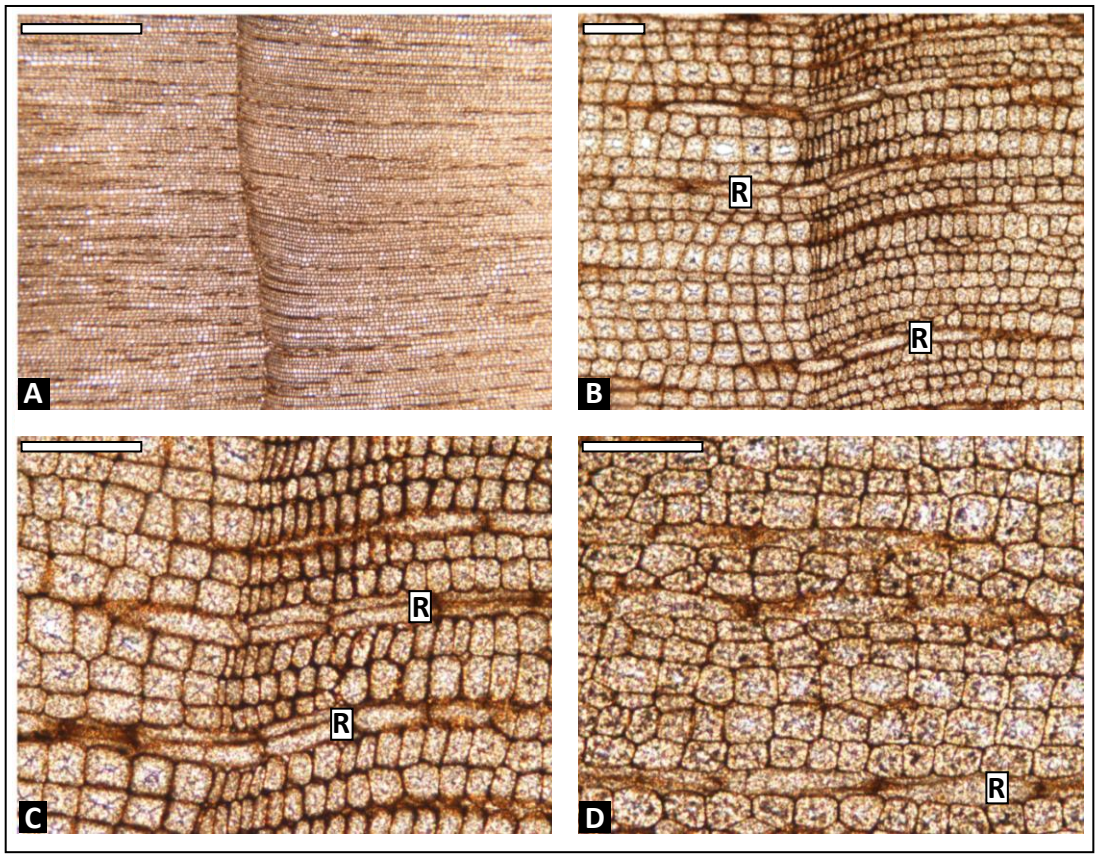

FIG. 3.16 Transmitted light microscope images (TS) of a wood preserved in a small permineralised plant axis sampled from interseam sediments overlying seam 92. **A -** Distinct growth ring, **B -** growth ring junction and radially discontinuous rays, **C -** Rays 1-2 cells wide and variation in tracheids size in different positions in the growth ring, **D -** detail of centre of growth ring showing rays and similarly sized tracheids. R label in white box = rays (**B-D**). Scale bar 1mm in **A**; 100µm in **B-D**.

3.6.3 Fusain (fossil charcoal)

Pieces of charcoal macerated from fragmental bands were studied by SEM to illustrate the types of plants that were charred. The pieces ranged from 200µm – 10mm in size and were usually thin lathes. Detailed taxonomic identification is outside the scope of this project.

The charcoal samples (n = c. 40) are mostly wood and in longitudinal section exhibit uniseriate to biseriate bordered pitting (arrows in Fig. 3.17 C). When biseriate, the pits may fill the entire tracheid wall (Fig. 3.17 C) which is a characteristic of cordaitaleans (Seward, 1919). The bordered pit pairs are either alternating (Fig. 3.17 C) or opposite (not illustrated). Uniseriate rays are observed in Fig. 3.17 B (arrow 1) and ray cells commonly showed splitting (an example illustrated in Fig. 3.17 B, arrow 2) which is a feature characteristic of charring (Harris, 1957). Unfortunately most pieces of charcoal split in to thin flakes or cell walls were crushed (Fig. 3.17 D) so that good transverse sections for comparison with Fig. 3.16 could not be observed. In addition, very few fracture planes passed through even a partial radial longitudinal plane. Overall the morphology of the charcoal specimens is also consistent with cordaitaleans (Wilson and Johnston, 1940; Falcon-Lang and Bashforth, 2005; Falcon-Lang and Scott, 2000).

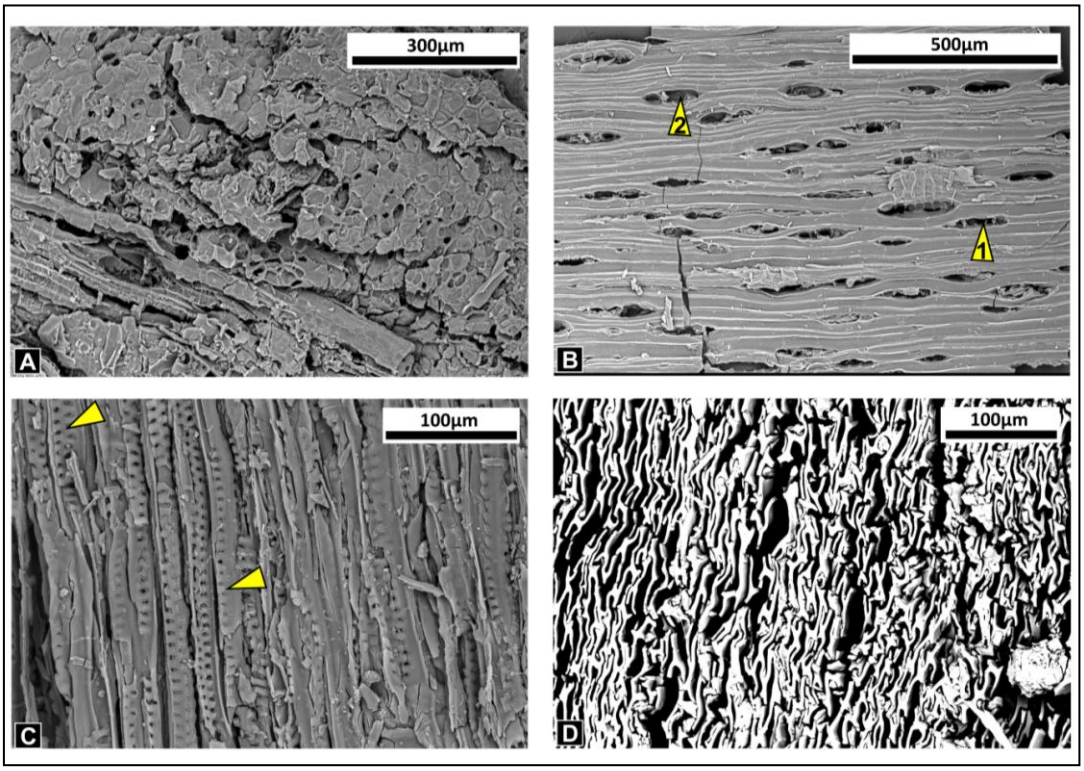

FIG. 3.17 Representative SEM images of charcoal macerated from fragmental band 2 in seam 78 (Fig. 3.4) >180µm size fraction. **A** = rare example of irregular tissue, possibly parenchymatous. **B** = tangential longitudinal section (TLS) of wood showing tracheids and mostly short uniseriate rays (arrow 1) and split rays (arrow 2). **C** = Longitudinal section (probable radial LS) of wood showing uniseriate and biseriate bordered pits (arrows). **D** = Crushed wood with shattered cell walls. The white colouration of the image is due to charging of the specimen.

3.7 SUMMARY

Thirteen Late Permian coal seams were sampled from two open cast Mines in the Kuznetsk Basin. The majority of seams were in excess of 10m thick. General samples were obtained from all 13 coal seams, stockpile fractions (chapter 7) and orientated *in situ* coal pillars from seams 78, 88 and 91 (chapters 4 and 5). Fragmental bands containing fusain (fossil charcoal) were observed in seams 73, 78, 82, 84. Macroscopic pieces of *in situ* fusain were also observed in seam 82. Charcoalified woods were studied from two macerated fragmental bands from seam 78 and abundant plant leaf and stem impressions/ poorly preserved compressions were observed in interseam sediments. Although not studied in detail (outside the scope of this project) these plant fossils are consistent with cordaite dominated vegetation as expected for Angaran Permian peat-forming environments (Meyen 1982; Oshurkova, 1996; Krassilov, 2000; Rees et al., 2002). An example of a permineralised plant axis contained growth rings which suggest a seasonal climate. The peats accumulated in a long-lived mire environment on a floodplain. Observations of floodplain, lateral accretion deposits and fluvial channel bodies from interseam sediments provide evidence for a single channel fluvial depositional system which conforms to facies interpretation from previously published work.

CHAPTER 4

PALAEOECOLOGICAL INTERPRETATION OF INERTINITE DISTRIBUTION FROM *IN SITU* COAL PILLARS

In this chapter three *in situ* coal pillars [78(a), 88(a) and 91] were studied using standard coal petrographic techniques. The study of *in situ* coal pillars is currently the best resource to aid understanding of ancient peat-forming environments (e.g. Belcher et al., 2003; Collinson et al., 2007; Glasspool, 2000, 2003a,b; Jerrett et al., 2011b,c).

4.1 INTRODUCTION

4.1.1 Wildfires: Factors involved in charcoal formation and dispersal

Inertinite is now generally accepted to represent fossil charcoal derived from palaeowildfires (Scott, 1989a; Scott and Jones, 1994; Bustin and Guo, 1999; Glasspool and Scott, 2010; Scott, 2010; Scott and Glasspool, 2007). Abundance and distribution of inertinite can therefore be used to interpret palaeowildfire occurrence and fire type in the peat-forming environment, during the time interval of coal pillar formation. Horizons of macroscopic fusinite and semifusinite are likely to represent water transported charcoal from local surface fires (Scott, 2010) within the peat-forming environment (as seen in modern fires e.g. Tolonen, 1983; Clark, 1988; Clark and Royall, 1995; Tinner et al., 1998; Blackford, 2000) whereas scattered microscopic inertinite (<180µm, but often <20µm) may represent a windborne size fraction from regional fire events within 20 - 100km of the fire source (Clark et al., 1998; Pitkänen et al., 1999; Ohlson and Tryterud, 2000; Lynch et al., 2004; Collinson et al., 2007; Peters and Higuera, 2007; Conedara et al., 2009). However, certain conditions, such as severe convection in high intensity crown fires and favourable topography, can sometimes carry centimetre sized charcoal particles several kilometres (Pisaric, 2002; Tinner et al., 2006).

Reconstructing past wildfire regimes requires an understanding of basin, climatic and vegetation factors as well as fire dynamics and dispersal of produced charcoal (Scott, 2010). In order to interpret fire frequency (return interval) the transport of

charcoal needs to be considered (Tinner et al., 2006). Microscopic (windblown) charcoal transport is controlled by a number of variables: fire intensity, height of the fire plume, fire type (ground, surface and crown), wind speed and particle size (Clark, 1988; Clark and Royall, 1995; Tinner et al., 1998; Carcaillet et al., 2001; Lynch et al., 2004). However, most macroscopic charcoal is considered to be water transported (Scott, 2010) and if macroscopic charcoal fragments are rounded in shape this could indicate transport over long distances (Uhl and Kerp 2003; Conedara et al., 2009) but this depends on the degree of charring and other variables (Nichols et al., 2000).

There is a wide variation in the size classification scheme used by charcoal analysts (Table 4.1) which can result in inconsistencies between workers in the literature. For example, the 'macroscopic' charcoal size of >50µm from Peters and Higuera (2007) was referred to in Conedara et al. (2009) in the context of km scale dispersal of macroscopic charcoal (>1cm in size). In this chapter the term microscopic refers to inertinite <180µm in size (but commonly <20µm) and macroscopic represents inertinite clast size >425µm [which equals 1 field of view (FOV) under the reflectance microscope, using the ×20 objective and ×10 eyepiece magnification].

Term for charcoal size fractions	**Published charcoal size classification schemes**					
	Scott (2010)	**Blackford (2000)**	**Peters and Higuera (2007)**	**Conedara et al. (2009)**	**Thevenon et al. (2003)**	**Ohlson and Tryterud (2000)**
Macroscopic	>1mm	>125µm	>50µm	>100-200µm	>150µm (coarse)	>2mm (large)
Mesoscopic	180µm - 1mm					
Microscopic	<180µm	<125µm	<50µm	10-200µm	0.2-1µm (ultra fine)	0.5-2mm (small)

TABLE 4.1 Variations in published descriptive size classification schemes for charcoal.

4.1.2 Aims

Randomly sampled *in situ* coal pillars from three seams [78(a), 88(a) and 91] from the Kuznetsk Basin, Siberia were compared using petrographic techniques to interpret small scale palaeowildfire history in the Late Permian. These coal pillars represent a portion of the overall seam and therefore provide an insight into the peat-

forming environment and local wildfire occurrence during the time interval of coal pillar formation. This chapter also aims to investigate whether seam 91 contains the lowest inertinite content (21%) in the sequence and seam 78 the highest inertinite content (33%) as indicated by previous petrographic work on bulk seam crushed samples by Pakh and Artser (2003). Unlike crushed samples in *situ* coal pillars retain their orientation and original inertinite distribution, and therefore enable interpretation of palaeowildfire history.

4.2 METHODOLOGY

4.2.1 Field sampling

Coal pillars were randomly sampled from accessible locations at the coal face from seams 78, 88 and 91 (Fig. 4.1). Refer to chapter 2.1.1 for sampling methods. Polished blocks were produced using the method outlined in chapter 2.3.1. The resulting coal pillars vary in length (compare Figs. 4.4, 4.9, 4.14), which was taken into consideration when interpreting the petrographic data.

4.2.2 Petrographic methodology

Macrolithotype logs were produced using the method given in chapter 2.4.2. The petrographic methodology devised for *in situ* coal pillars was followed (see chapter 2.4.3) and macerals were identified according to coal petrographic standards (ICCP, 1998; 2001; chapter 2.4.3.3; Table 2.3). Representative colour photographs of maceral distribution in each lithotype unit (LU) were taken using the method given in chapter 2.4.5. In addition, kaolinite has a similar morphology and colouration to liptinite group macerals under reflected light using the ×20 objective (illustrated in Fig. 4.11 C, G; Fig. 4.12 C; Fig. 4.13). To avoid incorrect representation of liptinite counts, fluorescence microscopy (see chapter 2.5) was used to highlight the liptinite macerals.

Petrographic data are reported to a mineral included basis (e.g. Fig. 4.3) and inertinite is also reported to a mineral matter free (mmf) basis (e.g. Fig. 4.4; Fig. 4.9; Fig. 4.14). Some lithotype units contain a large amount of inertinite but make up a small proportion of the total coal pillar [e.g. 78(a) LU2 in Fig. 4.4]. Thin lithotype units will be represented by a small number of petrographic counts as they cover few of fields of view (FOV). Therefore, in order to calculate a representative mean

inertinite content for the entire coal pillar, the petrographic data for each field of view, per transect, for the whole coal pillar were combined (Table 4.2). A whole pillar mean inertinite content was then calculated by combining the total inertinite point counts for each petrographic transect (Table 4.2). The standard deviation represents the variation in total inertinite content between transects (Table 4.2).

Pillar	Transect	Total inertinite (%)	Standard deviation of transect means of inertinite (2 sd)	Whole pillar mean inertinite value (%)
78(a)	1	26.26	2.5	27.6
	2	28.75		
	3	27.69		
88(a)	1	45.88	4.68	48
	2	47.66		
	3	50.52		
91	1	34.01	1.84	34.9
	2	34.89		
	3	35.85		

TABLE 4.2 Pillar averages of inertinite point count data for each transect (using all points for that transect). The whole pillar mean inertinite content for each pillar is an average of the three total inertinite contents for each petrographic transect. The standard deviation for all transect means is also presented. All inertinite values are reported to a mineral matter free basis.

4.2.2.1 Recognising and classifying charcoal horizons

In this thesis the term charcoal horizon refers to a layer of 'macroscopic' [>425µm, 1 field of view (FOV)] clasts of semifusinite and fusinite that can be traced laterally (under the microscope) along the entire width of a polished block. These clasts may have variable morphology and qualitative reflectance. They are observed as a layer of individual pieces and not a continual band formed by a single clast (illustrated in Fig. 4.8; Fig. 4.13). In order to enable the charcoal horizon to be traced laterally across the block the individual clasts have to be close together (but they do not necessarily have to be adjoining pieces). The clasts making up the horizon may also be associated with other maceral groups. These charcoal horizons can be of variable thickness (ranging from 0.5 - 3mm; this study) but if the pieces making up the horizon are separated vertically by a single (several millimetres thick), or multiple, detrovitrinite or telovitrinite layers then these would be classified as separate horizons. Macroscopic clasts of fusinite and semifusinite that do not occur in layers that can be traced along the width of the block are not referred to as charcoal horizons due to their limited lateral extent. Recognition of charcoal horizons is significant for palaeoecological interpretation.

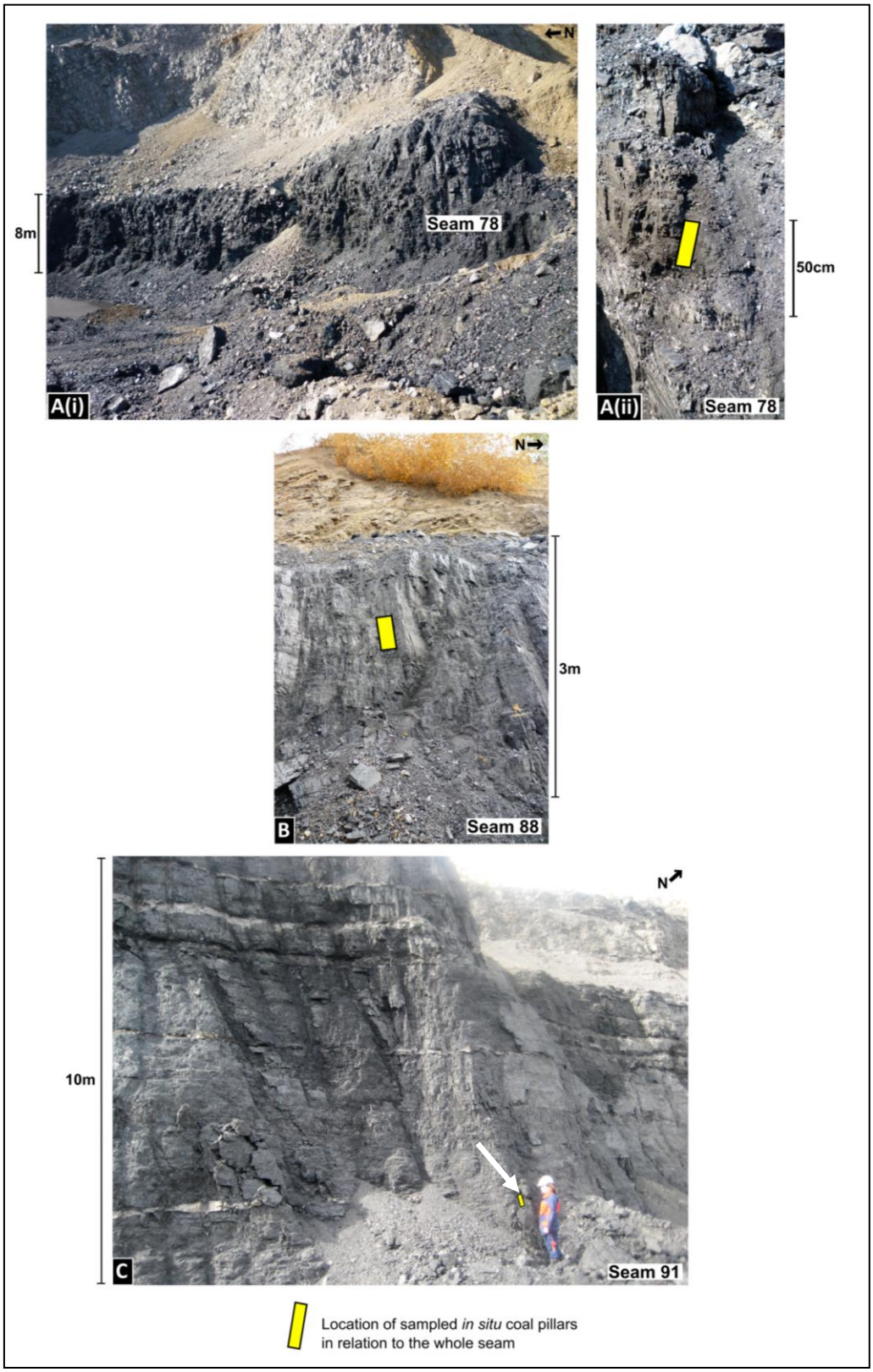

FIG. 4.1 Field photographs illustrating the position and size of sampled *in situ* coal pillars in relation to total seam thickness (compare to Fig. 5.1). **A(i)** - seam 78 (mine 2) illustrating seam thickness, **A(ii) –** part of seam 78 in **A(i)** with the position of coal pillar 78(a) highlighted. **B –** Seam 88 (mine 1) with the position of pillar 88(a). **C** - Seam 91 (mine 1) with the position of pillar 91 (emphasised with a white arrow), image **C** courtesy of A.C. Scott (2009).

4.2.3 XRD

Procedure outlined in chapter 2.8.

4.2.4 Coal characterisation

The sample weight of the individual lithotype units was too small to enable analysis of %ash content at the RWE Npower facility so samples were sent to the Kentucky Center for Applied Energy Research and analysed according to standard ASTM techniques (ASTM Standard D5142-04, 2004). %total Sulphur data are reported to a dry ash free (daf) basis and %ash data are reported to a dry (d) basis.

4.3 RESULTS

4.3.1 Characterisation and mineral content of pillars 78(a), 88(a) and 91

All lithotype units in the three coal pillars have low %total Sulphur contents (<1.3% dry ash free basis) (Appendix 5). Pillar 78(a) has <7.5% ash content (dry basis) for all lithotype units (<7.3% mineral matter). Pillar 91 shows a small range in %ash from 3.3% (91 LU3-5; <3.5% mineral matter) to 9.4% (91 LU1; 10.7% mineral matter) whereas pillar 88(a) shows a wider range from 7% ash (LU3; 1% mineral matter) to 21% (LU4; 22% mineral matter). The majority of the mineral matter in these pillars is either quartz or kaolinite (determined by XRD; Fig. 4.2). Quartz is inert during high temperature ashing (Gluskoter, 1975) which may explain why the %ash and point count mineral matter values are comparable.

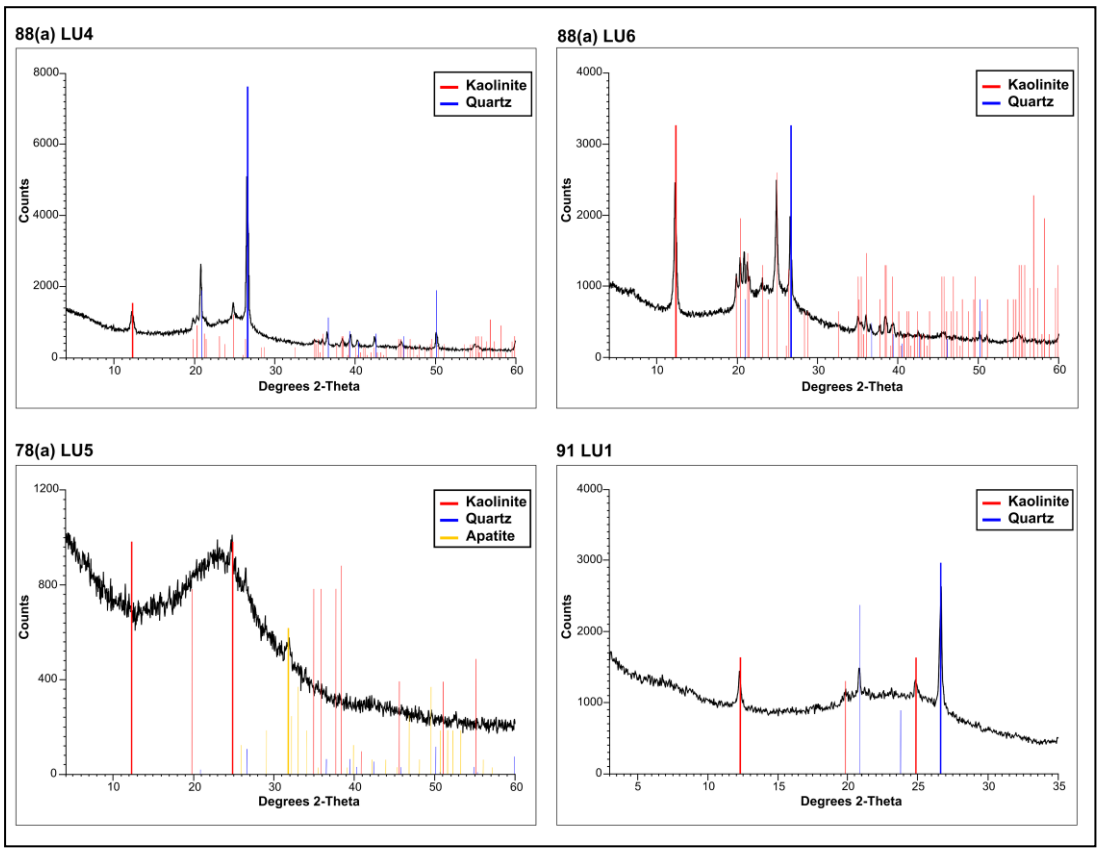

FIG. 4.2 XRD traces showing differences in mineral content both between coal pillars and between lithotype units in the same coal pillar. The area of elevated counts between 20-27 degrees 2-Theta on the background trace (black zig-zagged line) represents the organic matter content of the coal and the flatter the background trace, the higher the mineral content of the coal. The thickness of each coloured line represents the general abundance of that mineral scaled to the peak on the background trace. Red lines = kaolinite, blue = quartz, yellow = apatite.

4.3.2 Petrographic results for coal pillars 78(a), 88(a) and 91

Comparable stacked bar charts of petrographic data for all lithotype units in pillars 78(a), 88(a) and 91 are presented in Fig. 4.3. For raw petrographic point count data refer to Appendix 1.

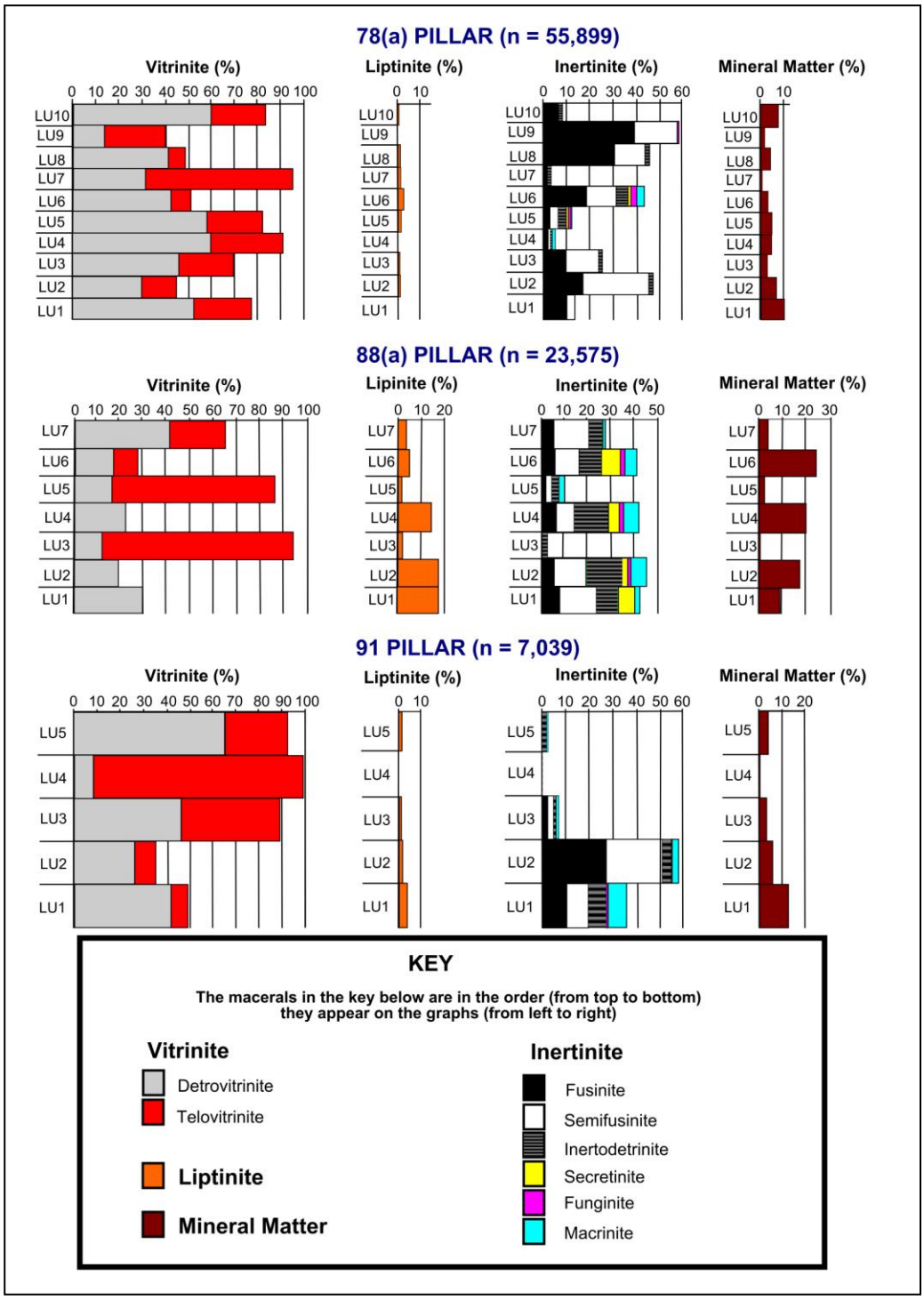

FIG. 4.3 Comparative stacked bar charts showing the petrographic point count results for the three coal pillars to a mineral included basis. Macerals were identified using ICCP schemes (1998, 2001) (defined in Table 2.3). The value next to the seam name corresponds to the total number of points counted for that pillar.

4.3.3 Inertinite distribution and abundance in pillar 78(a)

The 78(a) pillar can be divided macroscopically into ten visually distinct lithotype units, hereafter LU (Fig. 4.4; Fig. 4.5). These are, bright (LU1, LU4, LU7 and LU9),

dull banded (LU2, LU3, LU5, LU6, LU8) or bright banded (LU10). In addition, macroscopic variation in fusain and vitrain distribution was observed, both between transects and lithotype units, as illustrated in the macrolithotype log (Fig. 4.5). Variation in fusain distribution in dull units has also been observed in Permian Australian coal (Glasspool, 2003a).

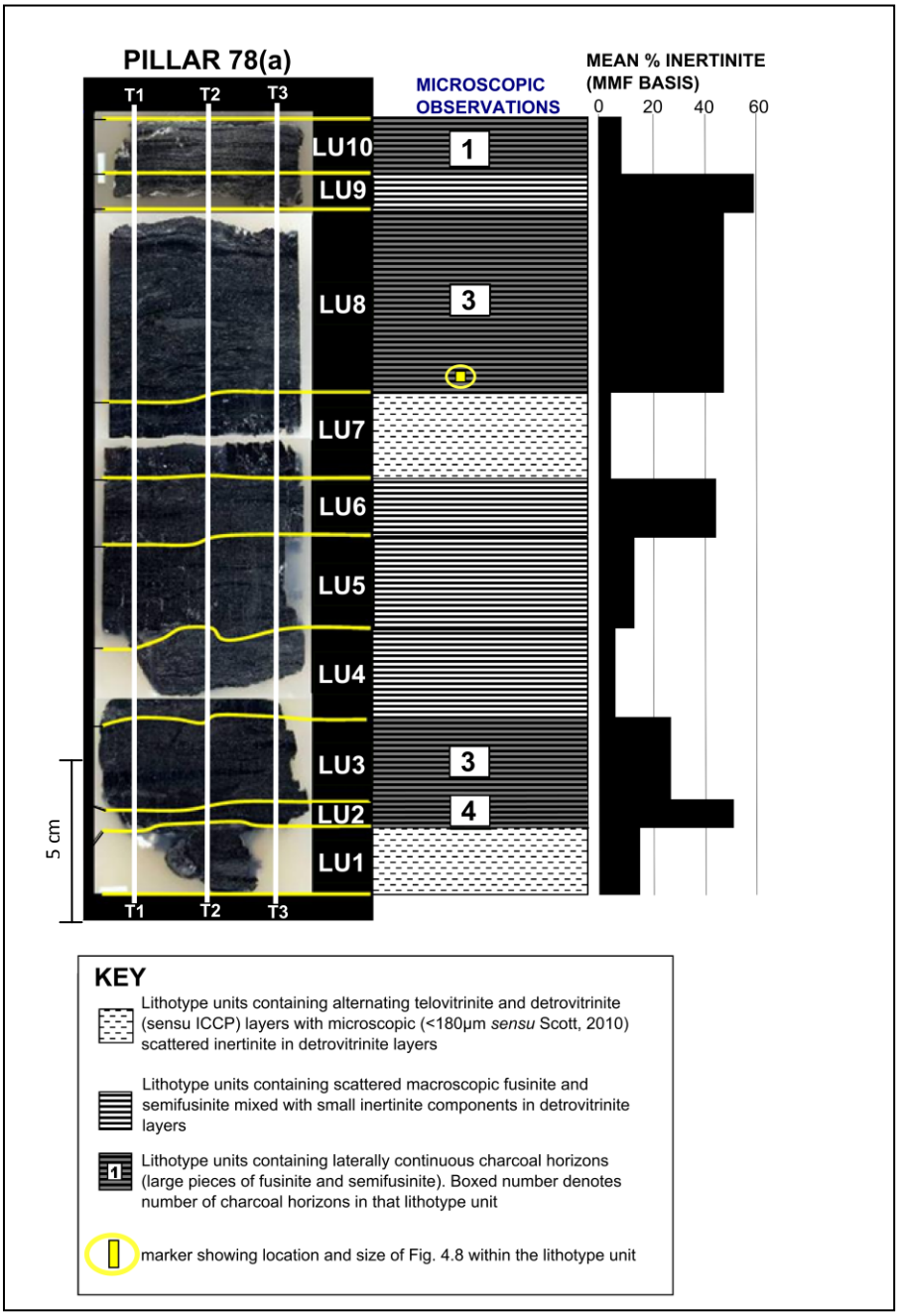

FIG. 4.4 Photograph of pillar 78(a) polished blocks highlighting the location and lateral variability of lithotype units (horizontal yellow lines across the block) as well as transect positions (white vertical lines) for petrographic analysis. The central column is a visual representation of the variation in inertinite distributions between lithotype units in 78(a) and the bar chart on the right is the total inertinite content (mineral matter free = mmf basis) for each lithotype unit.

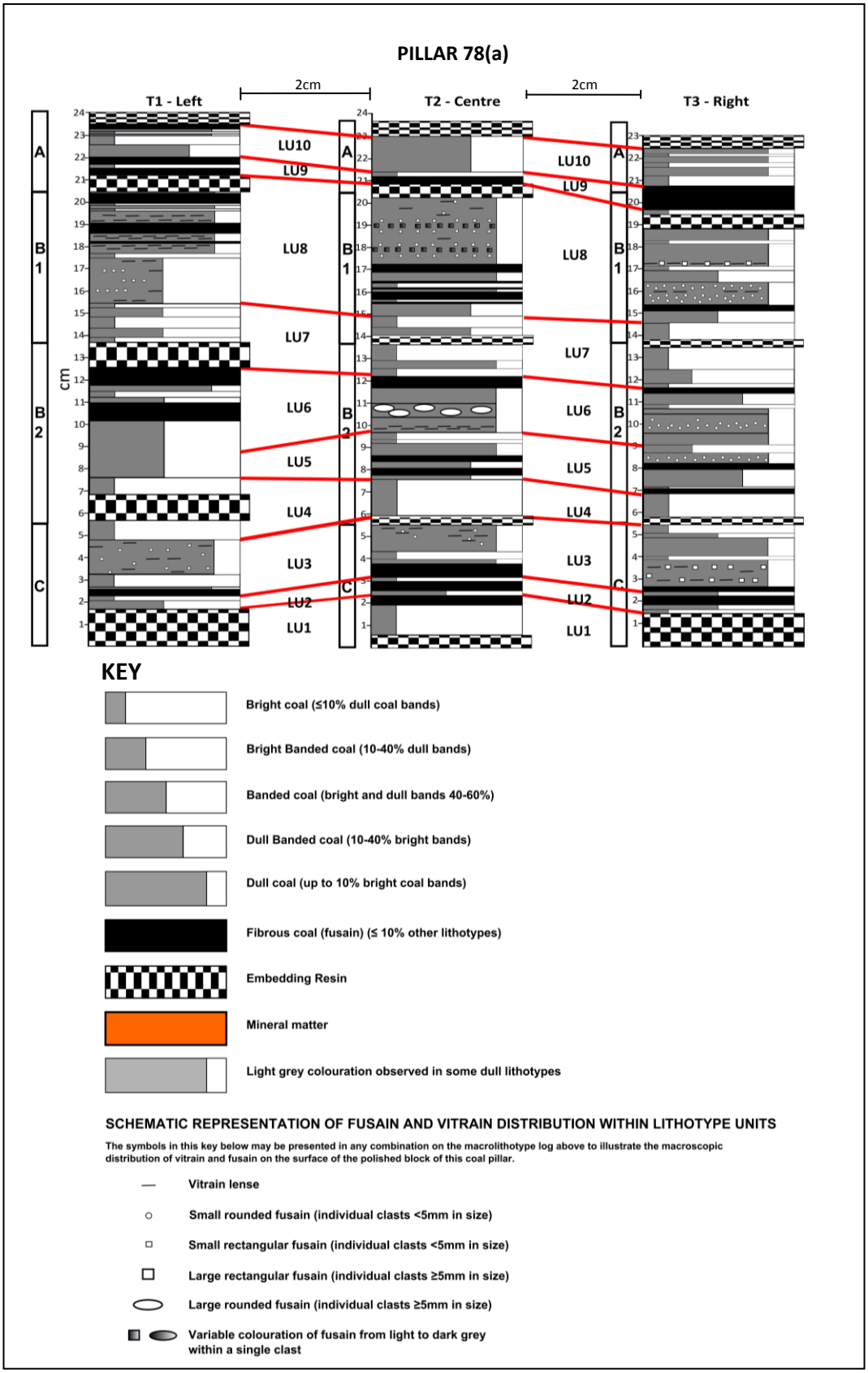

FIG. 4.5 Macrolithotype logs of pillar 78(a) showing location of lithotype unit divisions through the three transects studied (red lines), lateral variation in both lithotype unit thickness and position and fusain distribution in hand specimen. Lithotype units are described using Diessel's (1965) brightness scheme and patterns of vitrain and fusain distribution are own terms, this study. The vertical scale is in cm. Transect positions are shown on a photograph of the polished blocks in Fig. 4.4.

Petrographic results for individual lithotype units are illustrated in Fig. 4.3. Inertinite is present in varying amounts throughout the coal pillar, ranging from 3% to 59% (mineral matter free basis) in different lithotype units (Fig. 4.4), with a pillar average of 27.6% (2 sd = 2.5; Table 4.2). All lithotype units contain alternating telovitrinite and detrovitrinite layers (from single to multiple fields of view in thickness) (Fig. 4.6 E, G; Fig. 4.7 A, C, E, G, I). The microscopic variations in inertinite distribution between lithotype units show repetition and can be subdivided into three categories illustrated in Fig. 4.4 and expanded below.

(i) Detrovitrinite layers containing scattered liptinite, mineral matter and qualitatively high reflecting microscopic (<180µm) inertinite (LU1 and LU7) (Fig. 4.6 A; Fig. 4.7 C, D). Scattered macroscopic (>425µm) clasts of fusinite, semifusinite and macrinite are rare and where observed in LU1 have been crushed, due to the fragmentary nature of this lithotype unit (e.g. Fig. 4.6 B).

(ii) Detrovitrinite layers with liptinite, mineral matter, scattered clasts of macroscopic fusinite and semifusinite (Fig. 4.6 H, J; Fig. 4.7 B, H) and/or scattered microscopic (<180µm) inertinite macerals (Fig 4.6 G, I; Fig. 4.7 A, G) (e.g. LU4-LU6, LU9). The macroscopic fusinite and semifusinite clasts do not occur in a layer that can be traced across the width of the block and are therefore not part of a charcoal horizon.

(iii) Charcoal horizons with laterally continuous layers of macroscopic clasts of fusinite and semifusinite [LU2 (Fig. 4.6 D), LU3 (Fig. 4.6 F), LU8 (Fig. 4.7 F; Fig. 4.8), LU10 (Fig. 4.7 J)] as opposed to a single continuous band of charcoal. The detrovitrinite layers between those containing charcoal horizons contain scattered liptinite, mineral matter, macroscopic and/or microscopic inertinite (Fig. 4.6 C, E; Fig. 4.7 E, I). There are 11 charcoal horizons in total, in four lithotype units, with 1-4 horizons per lithotype unit (Fig. 4.4). Fusinite and semifusinite clast sizes range from >0.5mm to 14mm. Lithotype units LU2 and LU3 contain more semifusinite than fusinite (Fig. 4.3), whereas LU8 and LU10 contain more fusinite than semifusinite (Fig. 4.3). Some macroscopic inertinite clasts in horizons can also grade from qualitative vitrinite reflectance to semifusinite within a single clast (Fig. 4.6 D).

See overleaf for Fig. 4.6

FIG. 4.6

Representative images showing the range of inertinite distribution both within, and between lithotype units, from pillar 78(a) LU1-LU5. Scale bar in **A** corresponds to 100µm and is the same for all images. FOV = field of view (given where known), T = transect number.

Labels in white boxes represent inertinite, vitrinite and liptinite maceral groups, *sensu* ICCP (1998, 2001) (defined in Table 2.3): F = fusinite, SF = semifusinite, In = inertodetrinite, M = macrinite, S = secretinite, TV = telovitrinite, DV = detrovitrinite, L = liptinite and mineral matter = MM.

A, B = 78(a) LU1. **A -** (T2) Scattered well spaced qualitatively high reflecting microscopic inertinite and mineral matter. **B –** (T2) Rare scattered macroscopic pieces of macrinite.

C, D = 78(a) LU2. **C -** (T2) Detrovitrinite layer with well spaced, scattered inertinite macerals (fusinite, inertodetrinite, macrinite) liptinite and mineral matter. **D -** (T1) Macroscopic clasts of semifusinite that grade from vitrinite qualitative reflectance to semifusinite. These clasts occur in a layer that can be traced across the width of the block and therefore represent part of a charcoal horizon.

E, F = 78(a) LU3. **E -** (T2) Alternating telovitrinite and detrovitrinite layers with inertinite, liptinite and mineral matter in detrovitrinite layers. **F -** (T2) Macroscopic clasts of fusinite and semifusinite. These clasts occur in a layer that can be traced across the width of the block and therefore represent part of a charcoal horizon.

G, H = 78(a) LU4. **G** - (T2) Alternating telovitrinite and detrovitrinite layers with well spaced, scattered, microscopic inertinite macerals (<180µm) and mineral matter. **H** - (T2) Clasts of macroscopic fusinite that do not occur in a layer that is traceable across the block and are therefore not part of a charcoal horizon. Note how the perimeter of the fusinite clast has fragmented and the smaller pieces are within the vitrinite layer below.

I, J = 78(a) LU5. **I** - (T2) Detrovitrinite layer with well spaced, scattered microscopic (<180µm) inertinite macerals, liptinite and mineral matter. The detrovitrinite at the base of the image is collodetrinite (defined in Table 2.3). **J** - (T2) Clasts of macroscopic fusinite that do not occur in a layer that is traceable across the block and are therefore not part of a charcoal horizon.

FIG. 4.6

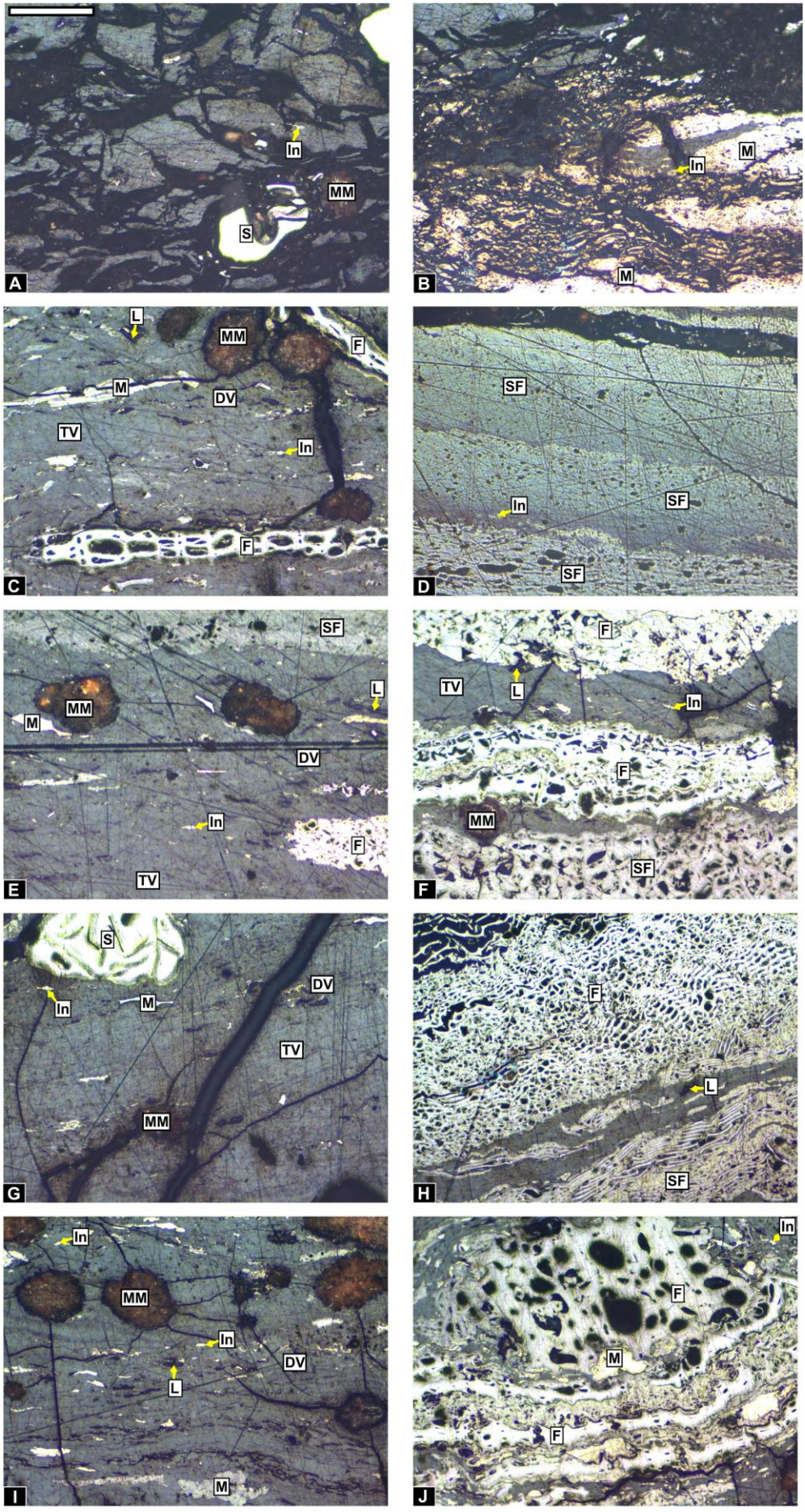
A
In
MM
S
B
In
M
M
C
L
MM
F
M
DV
TV
In
F
D
SF
In
SF
SF
E
SF
L
MM
M
DV
In
F
TV
F
TV
L
In
F
MM
SF
G
S
In
M
DV
TV
MM
H
F
L
SF
I
In
MM
In
DV
L
M
J
In
F
M
F

See overleaf for Fig. 4.7

FIG. 4.7

Representative images showing the range of inertinite distribution both within and between lithotype units from pillar 78(a) LU6-LU10. Scale bar in the top left corner of **A** - corresponds to 100µm and is the same for all images. FOV = field of view (given where known), T = transect number.

Labels in white boxes represent inertinite, vitrinite and liptinite maceral groups, *sensu* ICCP (1998, 2001) (defined in Table 2.3): F = fusinite, SF = semifusinite, In = inertodetrinite, M = macrinite, S = secretinite, TV = telovitrinite, DV = detrovitrinite, L = liptinite and mineral matter = MM.

A, B = 78(a) LU6. **A -** (T2) Alternating telovitrinite and detrovitrinite layers with microscopic inertinite (<180µm), liptinite and mineral matter in detrovitrinite layers. **B -** (T3) Clasts of macroscopic fusinite and semifusinite that do not occur in a layer that is traceable across the block and are therefore not part of a charcoal horizon. Note that the cellular detail of the lowermost semifusinite clast is poor hence why it is not classified as fusinite despite its qualitative high reflectance.

C, D = 78(a) LU7. **C -** (T2) Telovitrinite and detrovitrinite layer with microscopic, scattered inertodetrinite, macrinite, liptinite and mineral matter in the detrovitrinite layer. **D -** (T2) Detrovitrinite layer containing well spaced inertinite, liptinite and mineral matter.

E, F = 78(a) LU8. **E -** (T2) Alternating telovitrinite and detrovitrinite layers with scattered well spaced inertinite, liptinite and mineral matter in detrovitrinite layers. **F -** (T3) Macroscopic clasts of interlocking semifusinite. These clasts occur in a layer that can be traced across the width of the block and therefore represent part of a charcoal horizon (another example of part of two charcoal horizons from LU8 is illustrated in Fig. 4.8).

G, H = 78(a) LU9. **G -** (T2) Alternating telovitrinite and detrovitrinite layers with well spaced inertinite, liptinite and mineral matter in detrovitrinite layers. **H -** (T1) Macroscopic clasts of fusinite and semifusinite that do not occur in a layer that is traceable across the block and are therefore not part of a charcoal horizon.

I, J = 78(a) LU10. **I -** (T2) Alternating telovitrinite and detrovitrinite layers with well spaced scattered inertinite, liptinite and mineral matter. **J -** (T2) Clasts of macroscopic fusinite. These clasts occur in a layer that can be traced across the width of the block and therefore represent part of a charcoal horizon. Note that vitrinite can be present between clasts of fusinite.

FIG. 4.7

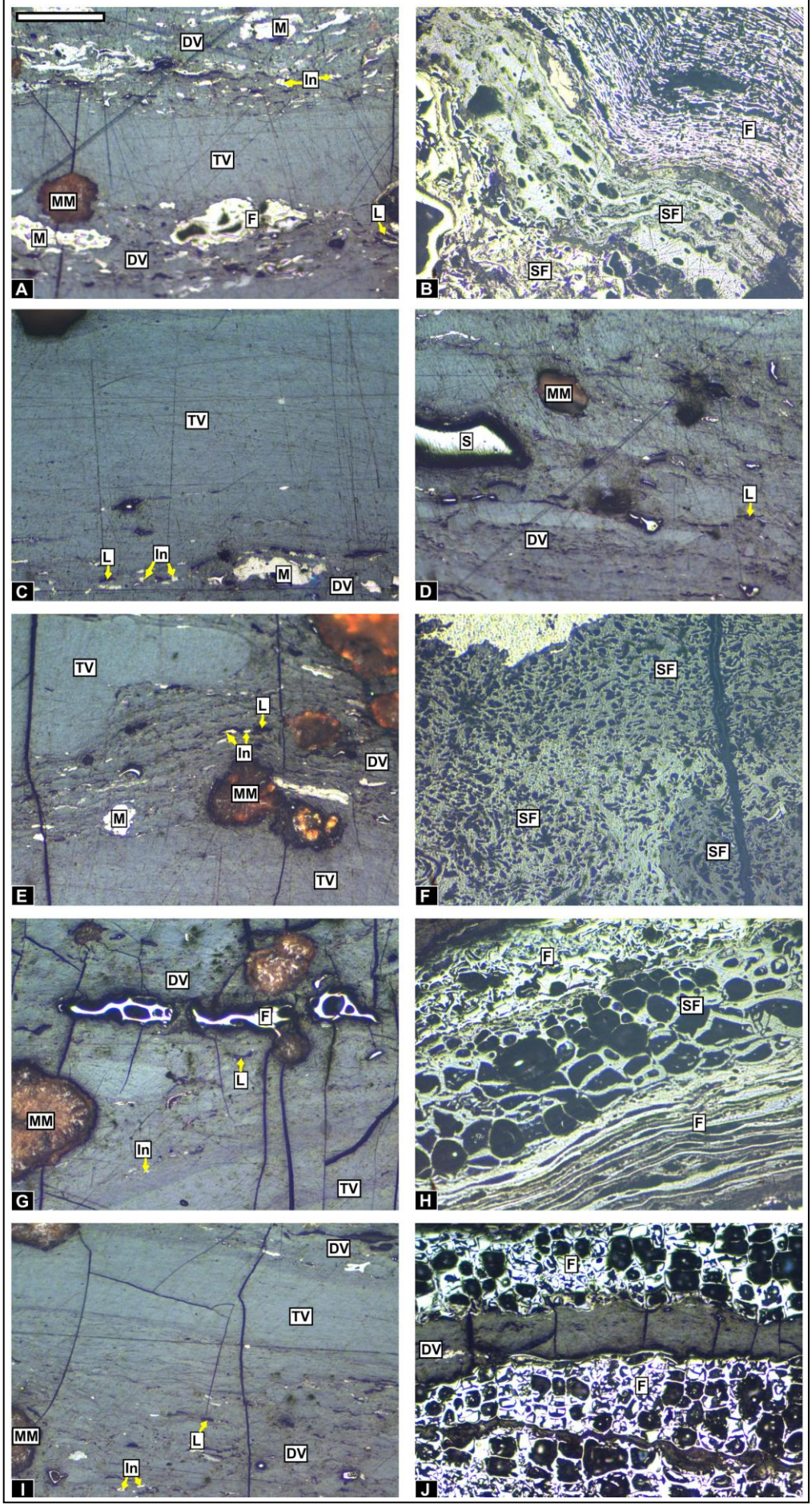
A
DV
M
In
TV
MM
F
L
M
DV
B
F
SF
SF
C
TV
L
In
M
DV
D
MM
S
L
DV
E
TV
L
In
DV
MM
M
TV
F
SF
SF
SF
G
DV
F
L
MM
In
TV
H
F
SF
F
I
DV
TV
MM
L
In
DV
J
F
DV
F

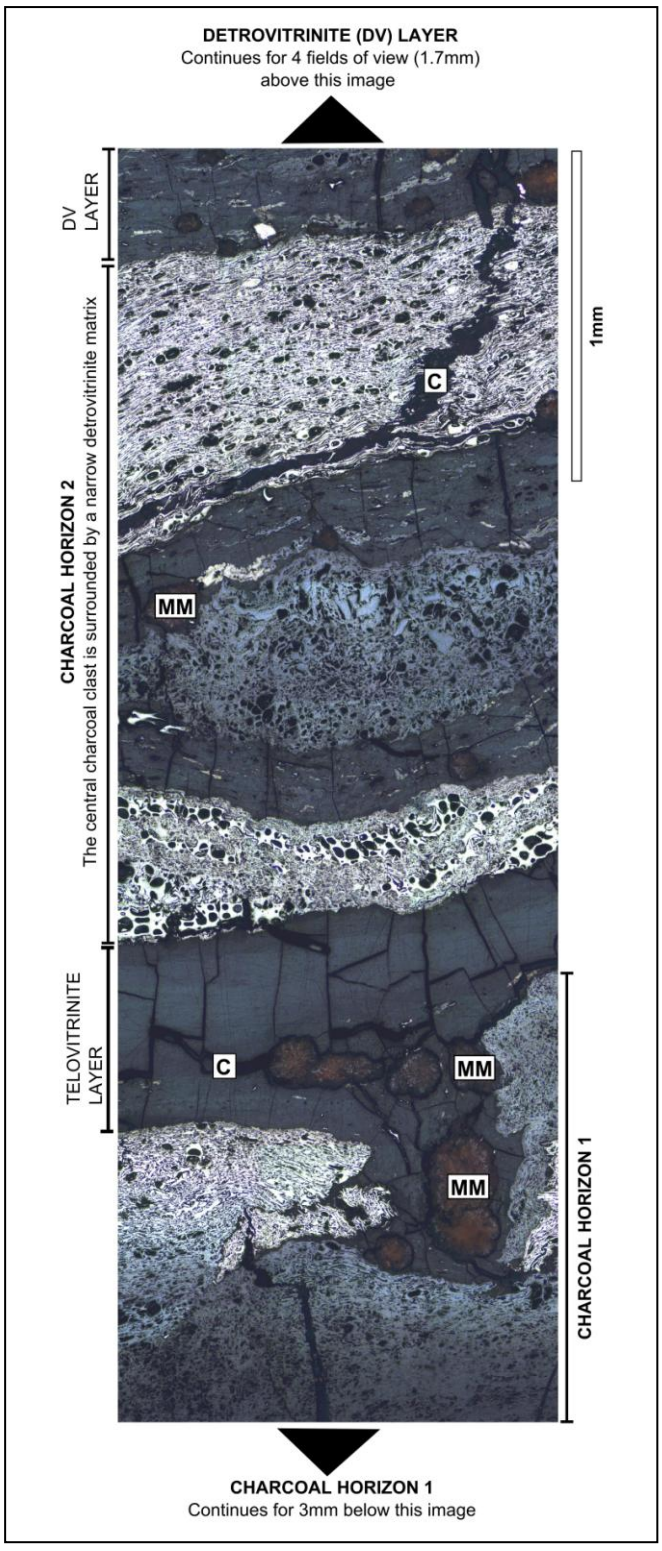

FIG. 4.8 Montaged images (n = 36) showing a representative 1.5mm by 3.75mm section of coal pillar 78(a) LU8 (Fig. 4.4) which contains two charcoal horizons (labelled 1 and 2). These charcoal horizons persist laterally across the block. The central semifusinite clast in charcoal horizon 1 is surrounded by a matrix of detrovitrinite as is typical for the clasts in the charcoal horizons. The detrovitrinite matrix is always less than one FOV in thickness (often much less) in striking contrast to detrovitrinite layers such as that which extends for 1.7mm at the top of the image shown. Labels in white boxes correspond to: MM = mineral matter; C=crack.

4.3.4 Inertinite distribution and abundance in pillar 88(a)

The 88(a) pillar can be divided macroscopically into seven visually distinct lithotype units (Fig. 4.9; Fig. 4.10). These are bright (LU3, LU5), dull (LU2, LU4, LU6) and bright banded (LU1 and LU7).

Petrographic results for individual lithotype units are illustrated in Fig. 4.3. Inertinite is present in varying amounts throughout the coal pillar, ranging from 3% to 56% to a mineral matter free basis (Fig. 4.9) with a whole pillar average of 48% (2 sd = 4.7; Table 4.2). The microscopic variation in inertinite distribution can be divided into four categories (Fig. 4.9). The first three are the same as the inertinite distribution patterns seen in pillar 78(a) i.e. detrovitrinite layers with either, microscopic scattered inertinite [88(a) LU3, LU5; Fig. 4.11 E, F; Fig. 4.12 A, B], scattered macroscopic and/or microscopic inertinite [88(a) LU1; Fig. 4.11 A, B] and charcoal horizons [88(a) LU7; Fig. 4.12 F; Fig. 4.13]. The fourth category is different (i.e. LU2, LU4, LU6; Fig. 4.11 C, D, G, H; Fig. 4.12 C, D; Fig. 4.13). Lithotype units in this fourth category contain no alternating telovitrinite and detrovitrinite layers, are generally vitrinite poor (20 - 28%; Fig. 4.3) and contain scattered inertinite macerals (41 – 45%) in every field of view (Fig. 4.11 C, D, G, H; Fig. 4.12 C, D). The most abundant inertinite macerals in LU2, LU4 and LU6 are semifusinite (8 - 14%) and inertodetrinite (9 - 15%) with minor fusinite (2 - 8%), and high reflecting secretinite (3 - 8%). These lithotype units are also rich in mineral matter (19 – 26%, kaolinite and quartz, confirmed by XRD; Fig. 4.2) and macerals are commonly rounded.

There are 26 charcoal horizons in three lithotype units (Fig. 4.9), LU2 (16 horizons; Fig. 4.11 D; Fig. 4.13), LU4 (8 horizons; Fig. 4.11 H) and LU7 (2 horizons; Fig. 4.12 F) with a maximum clast size of 8mm (LU2). Lithotype units containing charcoal horizons in pillar 88(a) contain more semifusinite (7.5 – 15%) than fusinite (5 - 7%; Fig. 4.3).

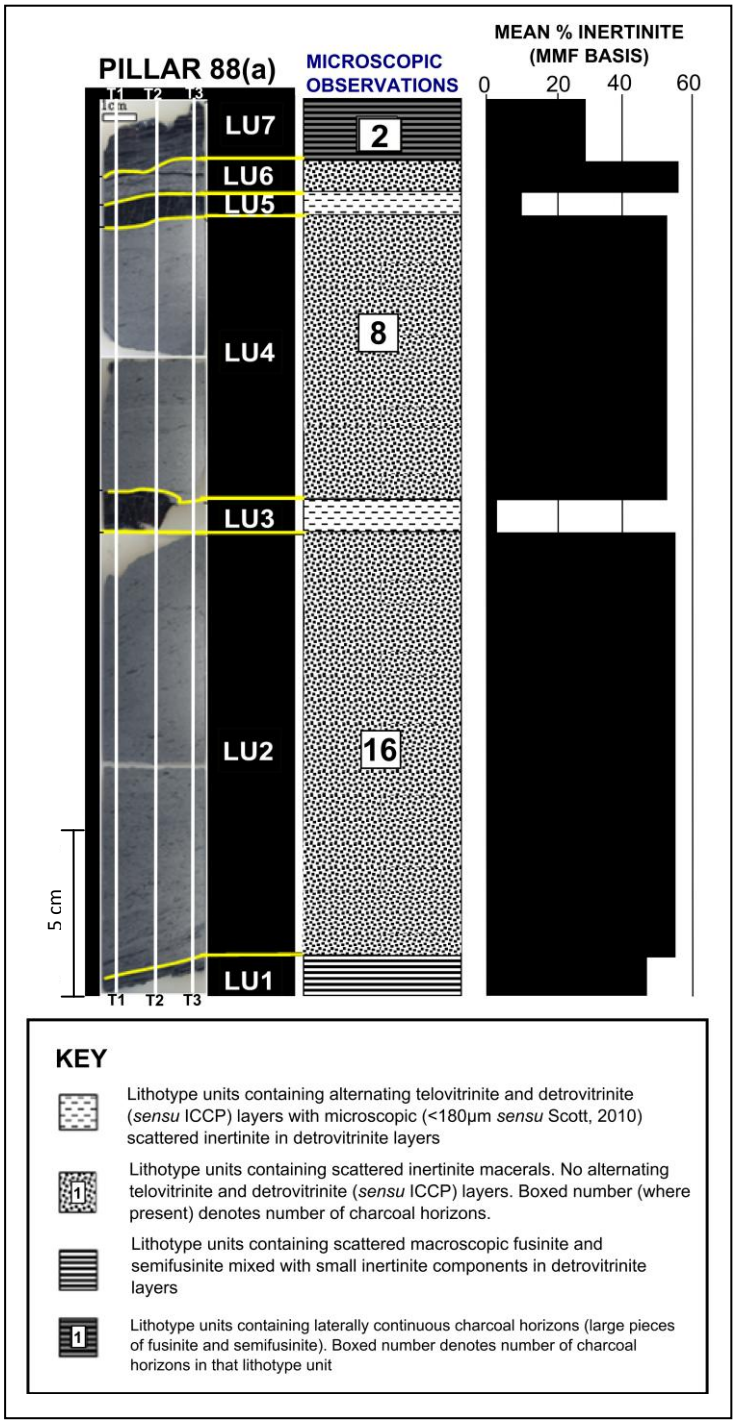

FIG. 4.9 Photograph of pillar 88(a) polished blocks highlighting the location and lateral variability of lithotype units (horizontal yellow lines across the block) as well as transect positions (white vertical lines) for petrographic analysis. The central column is a visual representation of the variation in inertinite distributions between lithotype units in 88(a) and the bar chart on the right is the total inertinite content (mmf basis) for each lithotype unit.

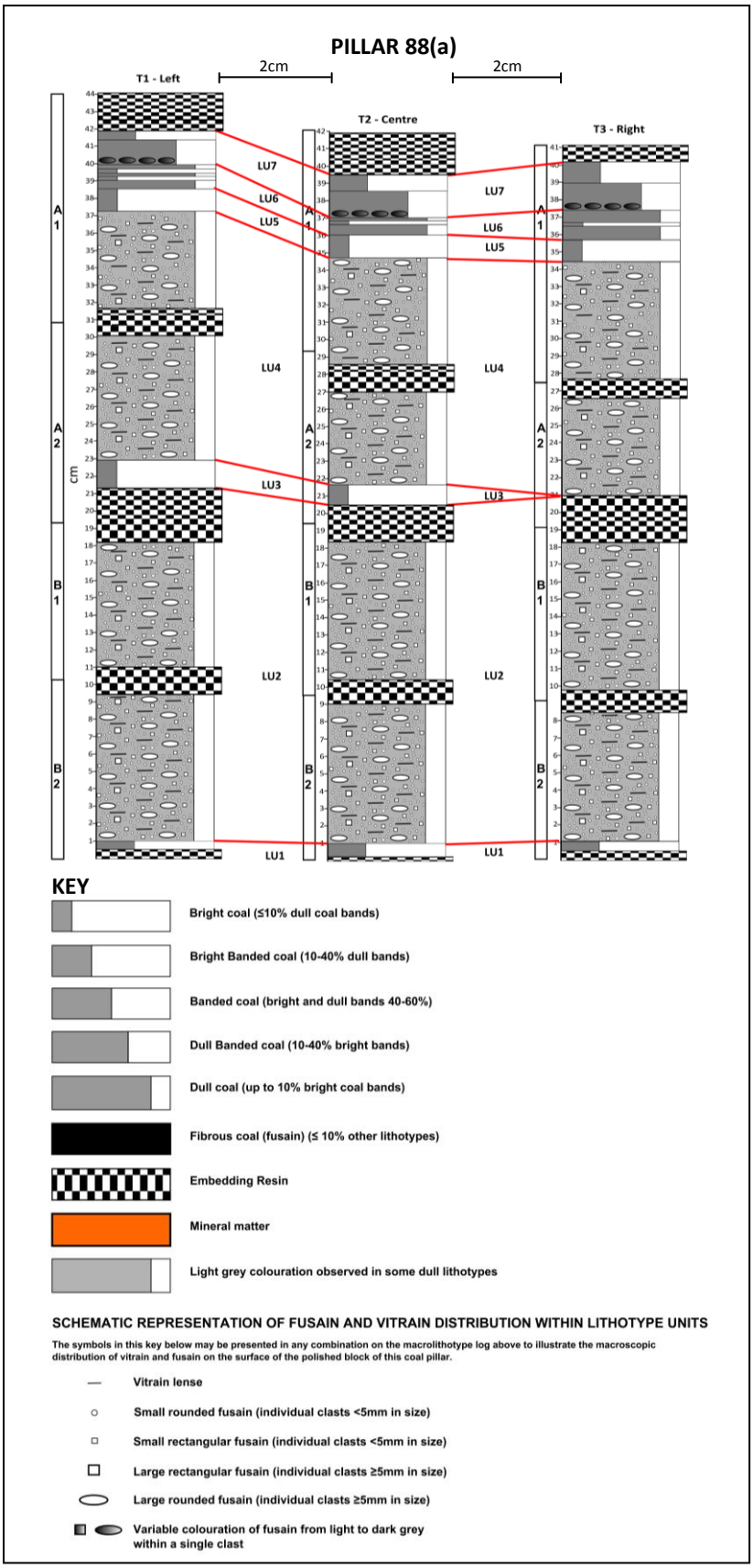

FIG. 4.10 Macrolithotype logs of pillar 88(a) showing location of lithotype unit divisions through the three transects studied (red lines), lateral variation in both lithotype unit thickness and position and fusain distribution in hand specimen. Lithotype units are described using Diessel's (1965) brightness scheme and patterns of vitrain and fusain distribution are own terms, this study. The vertical scale is in cm. Transect positions are shown on a photograph of the polished block in Fig. 4.9.

See overleaf for Fig. 4.11

FIG. 4.11

Representative images showing the range of inertinite distribution both within, and between lithotype units, from pillar 88(a) LU1-LU4. Scale bar in **A** corresponds to 100µm and is the same for all images. FOV = field of view in given T = transect.

Labels in white boxes represent inertinite, vitrinite and liptinite maceral groups, *sensu* ICCP (1998, 2001) (defined in Table 2.3): F = fusinite, SF = semifusinite, In = inertodetrinite, M = macrinite, S= secretinite, TV = telovitrinite, DV = detrovitrinite, L = liptinite and mineral matter = MM.

A, B = 88(a) LU1. **A** – (T1 FOV 3) Alternating telovitrinite and detrovitrinite layers with scattered inertinite, liptinite and mineral matter in detrovitrinite layers. **B –** (T3) Telovitrinite and detrovitrinite layers with more identifiable telovitrinite than **A**.
C, D = 88(a) LU2. **C -** (T1 FOV14) No alternating telovitrinite and detrovitrinite layers, scattered inertinite, liptinite and mineral matter throughout. Note that there is little identifiable vitrinite in this FOV. This pattern of maceral distribution represents the entirety of LU2. **D -** (T3 FOV33) Clasts of macroscopic fusinite and semifusinite. These clasts occur in a layer that can be traced across the width of the block and therefore represent part of a charcoal horizon (another example of a charcoal horizon from LU2 is illustrated in Fig. 4.13).
E, F = 88(a) LU3. **E -** (T1 FOV15) Telovitrinite layer containing scattered inertodetrinite and mineral matter. **F -** (T1 FOV2) Alternating telovitrinite and detrovitrinite layers containing scattered inertinite, liptinite and mineral matter in detrovitrinite layers.
G, H = 88(a) LU4. **G -** (T1) No alternating telovitrinite and detrovitrinite layers, scattered inertinite, liptinite and mineral matter throughout. Note that there is little identifiable vitrinite in this FOV. This pattern of maceral distribution represents the entirety of LU4. **H -** (T3) Macroscopic fusinite clast. This clast occurs in a layer that can be traced across the width of the block and therefore represents part of a charcoal horizon.

FIG. 4.11

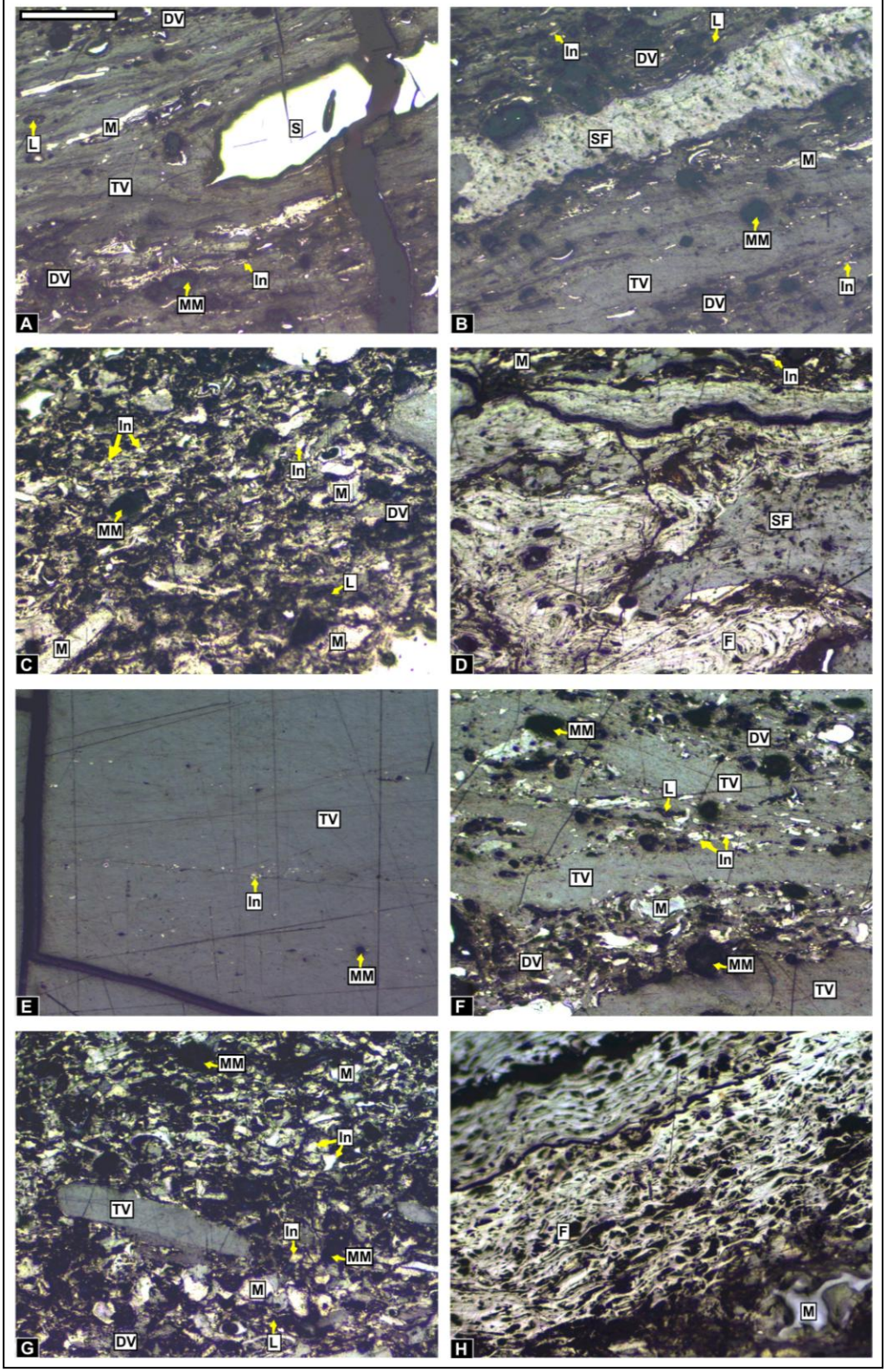
DV
M
S
L
TV
DV
In
MM
A
L
In
DV
SF
M
MM
TV
DV
In
B
In
In
M
DV
MM
L
M
M
C
M
In
SF
F
D
MM
DV
L
TV
In
TV
M
DV
MM
TV
E
TV
In
MM
F
MM
M
In
TV
In
MM
M
DV
L
G
F
M
H

See overleaf for Fig. 4.12

FIG. 4.12

Representative images showing the range of inertinite distribution both within and between lithotype units from pillar 88(a) LU5-LU7. Scale bar in **A** corresponds to 100µm and is the same for all images. FOV = field of view in given T = transect.

Labels in white boxes represent inertinite, vitrinite and liptinite maceral groups, *sensu* ICCP (1998, 2001) (defined in Table 2.3): F = fusinite, SF = semifusinite, In = inertodetrinite, M = macrinite, S = secretinite, Fu = funginite, TV = telovitrinite, DV = detrovitrinite, L = liptinite and mineral matter = MM.

A, B = 88(a) LU5. **A –** (T3) Alternating telovitrinite and detrovitrinite layers with microscopic inertinite, liptinite and mineral matter in detrovitrinite layers**. B -** (T3) Alternating telovitrinite and detrovitrinite layer with scattered inertinite in the detrovitrinite layer.
C, D = 88(a) LU6. **C -** (T3 FOV97) No alternating telovitrinite and detrovitrinite layers, scattered inertinite, liptinite and mineral matter throughout. Note that there is little identifiable vitrinite in this FOV. This pattern of maceral distribution represents the entirety of LU6. **D -** (T3 FOV86) Scattered inertinite and mineral matter in a detrovitrinite layer with more identifiable vitrinite than **C**.
E, F = 88(a) LU7. **E -** (T3) Scattered inertinite, liptinite and mineral matter in a detrovitrinite layer. **F -** (T1 FOV95) Macroscopic clasts of fusinite and semifusinite. These clasts occur in a layer that can be traced across the width of the block and therefore represent part of a charcoal horizon.

FIG. 4.12

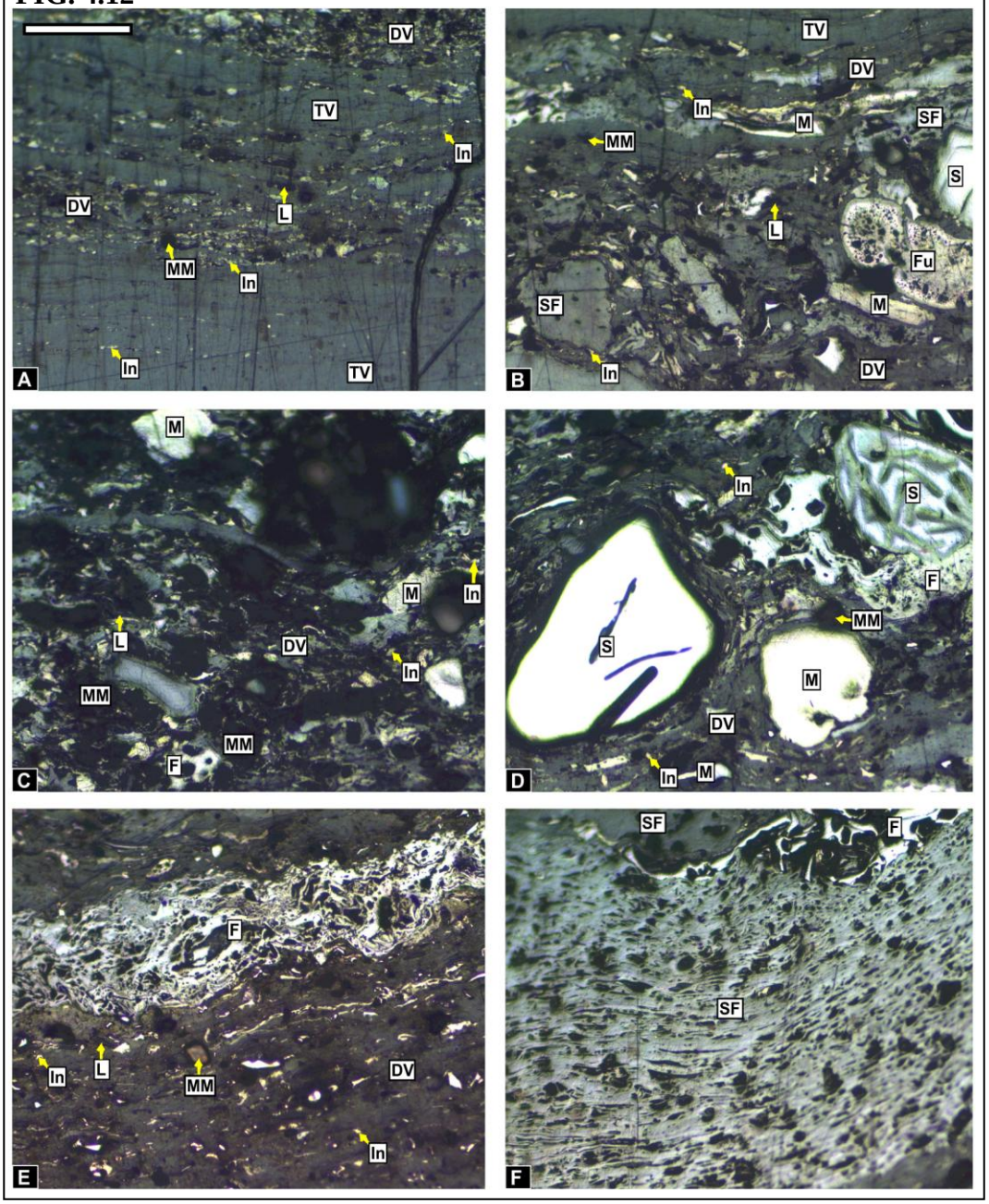
DV
TV
In
DV
L
MM
In
In
TV
A
TV
DV
In
M
SF
MM
S
L
Fu
SF
M
In
DV
B
M
M
In
L
DV
In
MM
MM
F
C
In
S
F
MM
S
M
DV
In
M
D
SF
F
SF
F
In
L
MM
DV
In
E
F

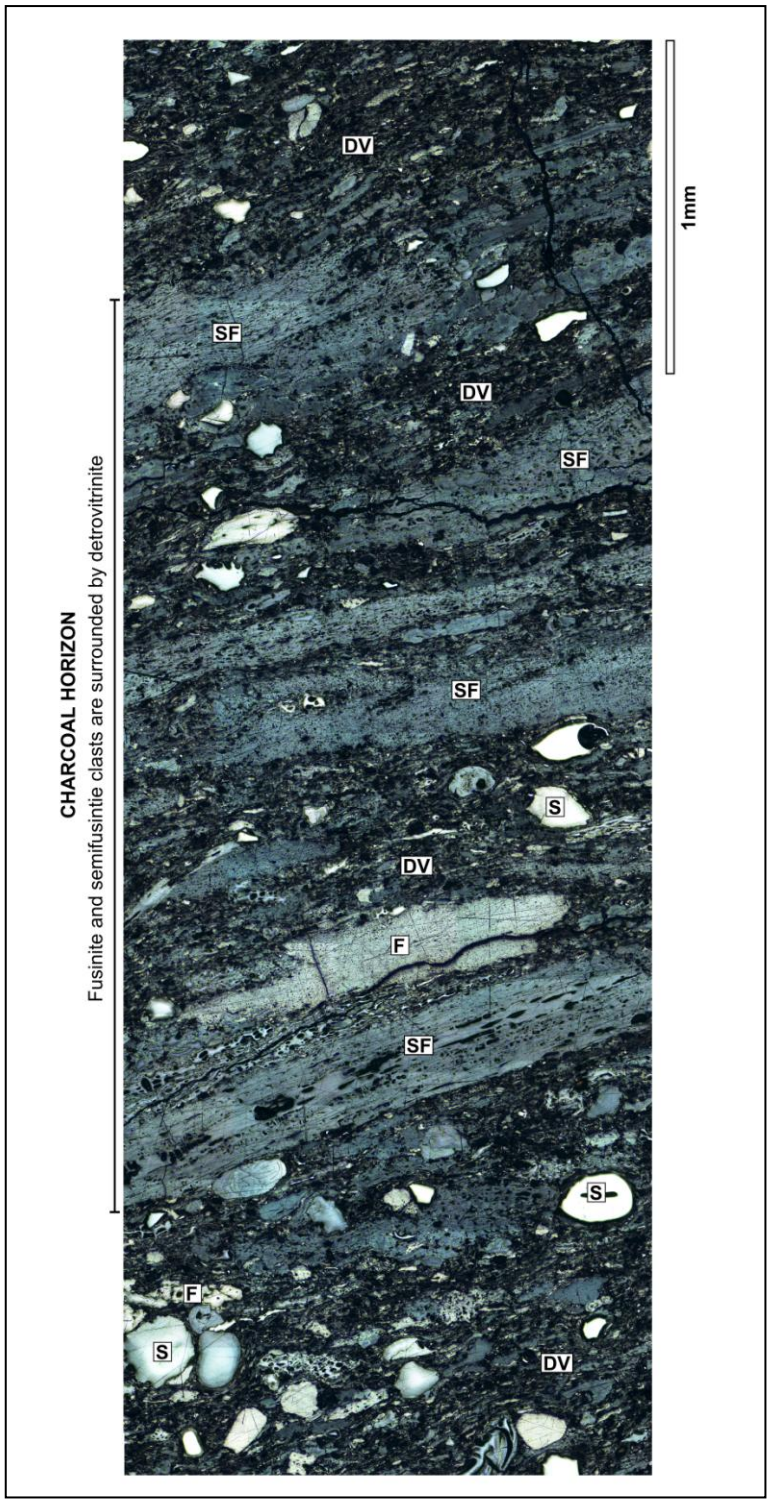

FIG. 4.13 Montaged images (n = 94) showing a representative 1.5mm by 4.5mm section of coal pillar 88(a) LU2 which contains one charcoal horizon (labelled). The charcoal horizon persists laterally across the block. The entirety of LU2 is a single inertinite-rich detrovitrinite layer, containing scattered inertinite (of varying size), liptinite and mineral matter in all fields of view. Therefore a narrow detrovitrinite matrix typically surrounds each macroscopic fusinite and semifusinite clast in the charcoal horizon. This is in contrast to the detrovitrinite both above and below the charcoal horizon which continues for several millimetres above and below this image. Labels in white boxes correspond to: DV = detrovitrinite, F = fusinite, SF = semifusinite, S = secretinite.

4.3.5 Inertinite distribution and abundance in pillar 91

Pillar 91 can be subdivided macroscopically into five visually distinct lithotype units (Fig. 4.14). Two of these are dull (LU1, LU2), and one each is banded (LU3), bright (LU4) and bright banded (LU5) (Fig. 4.15).

Petrographic results for individual lithotype units are illustrated in Fig. 4.3. Inertinite is present in all lithotype units from 0.34% (LU4) to 61.1% (LU2) to a mineral matter free basis (Fig. 4.3). LU1 and LU2 have higher inertinite contents, and are thicker than LU3-LU5 which means the overall pillar average inertinite is high, 34.9% (2 sd = 1.8; Table 4.2; see section 4.4.2).

All lithotype units contain alternating telovitrinite and detrovitrinite layers of varying thickness. Inertinite distribution in pillar 91 (illustrated in Fig. 4.14) can be divided into the same categories as observed in pillars 78(a) and 88(a).

(i) Microscopic (<180µm) scattered qualitatively high reflecting inertinite, liptinite and mineral matter in all detrovitrinite layers and some telovitrinite layers (Fig. 4.16 G, H, I). Rare pieces of fusinite and semifusinite (>0.5mm) are also observed (Fig. 4.16 F). The detrovitrinite layers are principally collodetrinite, which shows poorly preserved cellular structure and contains liptinite and kaolinite (Fig. 4.16 E, H, I).
(ii) Detrovitrinite layers with liptinite, mineral matter, scattered pieces of macroscopic fusinite and semifusinite (up to 1.7mm in size; Fig. 4.16 B) and/or scattered microscopic (<180µm) inertinite macerals (Fig 4.16 A) (e.g. LU1). Inertinite and mineral matter are scattered in every field of view at the base of LU1 (Fig. 4.16 B) comparable to inertinite distribution in 88(a) LU2 and LU4. The macroscopic inertinite clasts do not occur in a layer that can be traced across the width of the block and are not part of a charcoal horizon. Detrovitrinite layers contain progressively smaller and widely spaced scattered inertinite macerals to the top of LU1 (Fig. 4.16 A).
(iii) Charcoal horizons with laterally continuous layers of macroscopic clasts of fusinite and semifusinite (LU2; Fig. 4.16 D) as opposed to a single continuous band of charcoal (inertinite). Vitrinite between large inertinite clasts is principally collodetrinite. The detrovitrinite layers between those containing charcoal horizons contain scattered liptinite, mineral matter, macroscopic and/or microscopic inertinite

(Fig. 4.16 C). Some telovitrinite layers also contain scattered inertodetrinite and mineral matter. There are 3 charcoal horizons in total in one lithotype unit (Fig. 4.14). Fusinite and semifusinite clast sizes range from >425µm to 5.1mm. Some macroscopic inertinite clasts show gradational reflectance from qualitatively low reflecting semifusinite to qualitatively high reflecting fusinite (not illustrated). LU2 contains comparable proportions of fusinite (27.3%; Fig. 4.3) and semifusinite (23.9%; Fig. 4.3). The majority of large inertinite clasts have not fragmented at the perimeter [as seen in 78(a) LU4 (Fig. 4.6H)]. One occurrence of qualitatively low reflecting (semifusinite) cuticle (macrinite *sensu* ICCP, 2001) is also observed (labelled 'M' in the centre of Fig. 4.16 C).

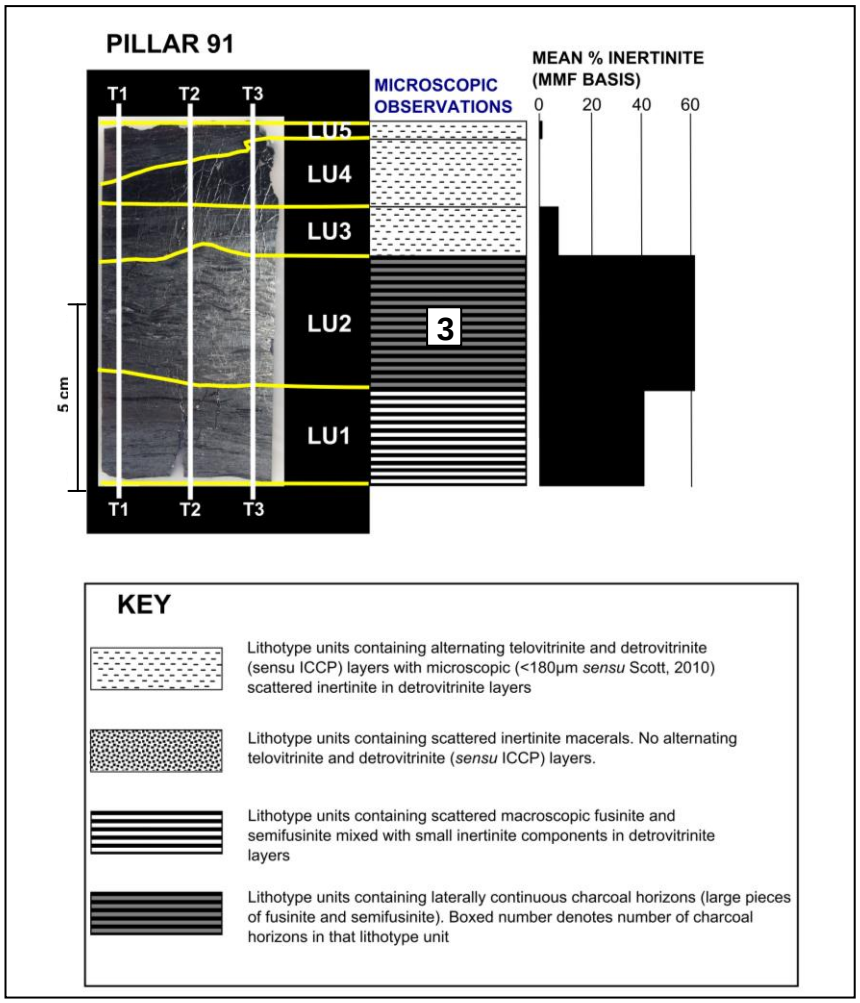

FIG. 4.14 Photograph of pillar 91 polished block highlighting the location and lateral variability of lithotype units (horizontal yellow lines) as well as transect positions (vertical white lines) for petrographic analysis. The central column is a visual representation of the variation in inertinite distributions between lithotype units in 91 and the bar chart on the right is the total inertinite content (mmf basis) for each lithotype unit.

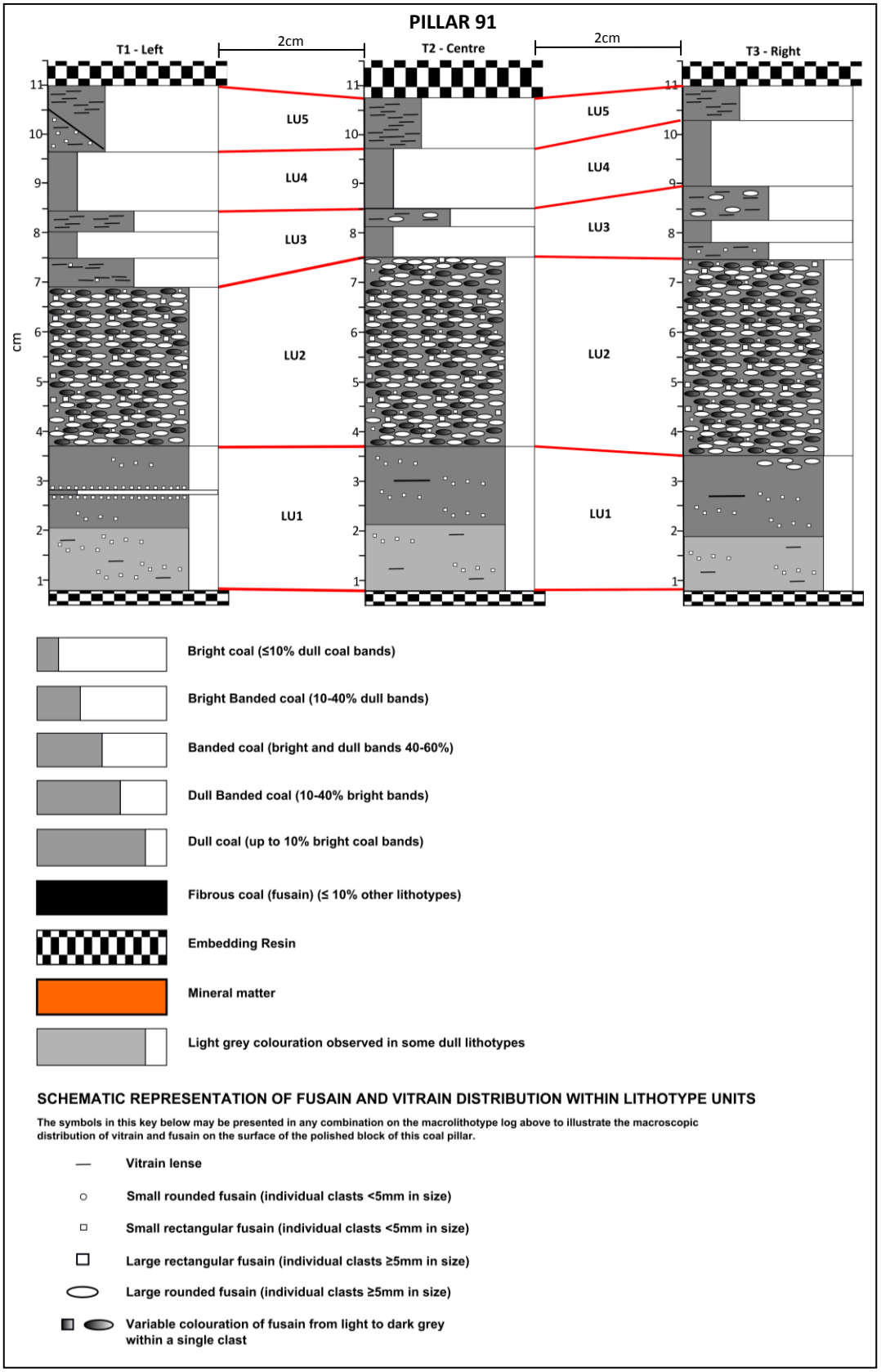

FIG. 4.15 Macrolithotype logs of pillar 91 showing location of lithotype unit divisions through the three transects studied (red lines), lateral variation in both lithotype unit thickness and position and fusain distribution in hand specimen. Lithotype units are described using Diessel's (1965) brightness scheme and patterns of vitrain and fusain distribution are own terms, this study. The vertical scale is in cm. Transect positions are shown on a photograph of the polished block in Fig. 4.14.

See overleaf for Fig. 4.16

FIG. 4.16

Representative images showing the range of inertinite distribution both within and between lithotype units from pillar 91 LU1-LU5. Scale bar in **A** corresponds to 100µm and is the same for all images. FOV = field of view in given T = transect.

Labels in white boxes represent inertinite, vitrinite and liptinite maceral groups, *sensu* ICCP (1998, 2001) (defined in Table 2.3): F = fusinite, SF = semifusinite, In = inertodetrinite, M = macrinite, TV = telovitrinite, DV = detrovitrinite, L = liptinite and mineral matter = MM.

A, B = 91 LU1. **A - (**T1 FOV 18) Detrovitrinite layer near the top of LU1 containing well spaced microscopic inertinite (inertodetrinite and macrinite), liptinite and mineral matter. **B -** (T1 FOV1) Detrovitrinite layer containing closely packed inertinite macerals and mineral matter.
C, D = 91 LU2. **C -** (T1 FOV 47) Alternating telovitrinite and detrovitrinite layers with well spaced inertinite, liptinite and mineral matter in detrovitrinite layers. Note the central clast of macrinite (labelled M) has a semifusinite qualitative reflectance and a jagged perimeter and is therefore likely to be a cuticle. **D -** (T3 FOV 75) Macroscopic clasts of fusinite and semifusinite. These clasts are part of a layer that can be traced across the width of the block and are therefore part of a charcoal horizon.
E, F = 91 LU3. **E - (**T3 FOV 82) Alternating telovitrinite and detrovitrinite layer with microscopic inertinite, liptinite and mineral matter in the detrovitrinite (collodetrinite; Table 2.3). **F -** (T2 FOV 84) Telovitrinite and detrovitrinite layer with scattered inertodetrinite and a rare piece of fusinite in the detrovitrinite layer.
G, H = 91 LU4. **G –** (T1 FOV 96) Telovitrinite layer with rare inertodetrinite. **H -** (T3 FOV110) Alternating telovitrinite and detrovitrinite layers with microscopic qualitatively high reflecting inertodetrinite scattered in detrovitrinite layers.
I, J = 91 LU5. **I -** (T1 FOV 104**)** Alternating telovitrinite and detrovitrinite layers with scattered qualitatively high reflecting inertodetrinite, macrinite as well as mineral matter in the detrovitrinite (collodetrinite; Table 2.3). **J -** (T3 FOV 119**)** Rare piece of fusinite in a thin detrovitrinite layer between telovitrinite layers.

FIG. 4.16

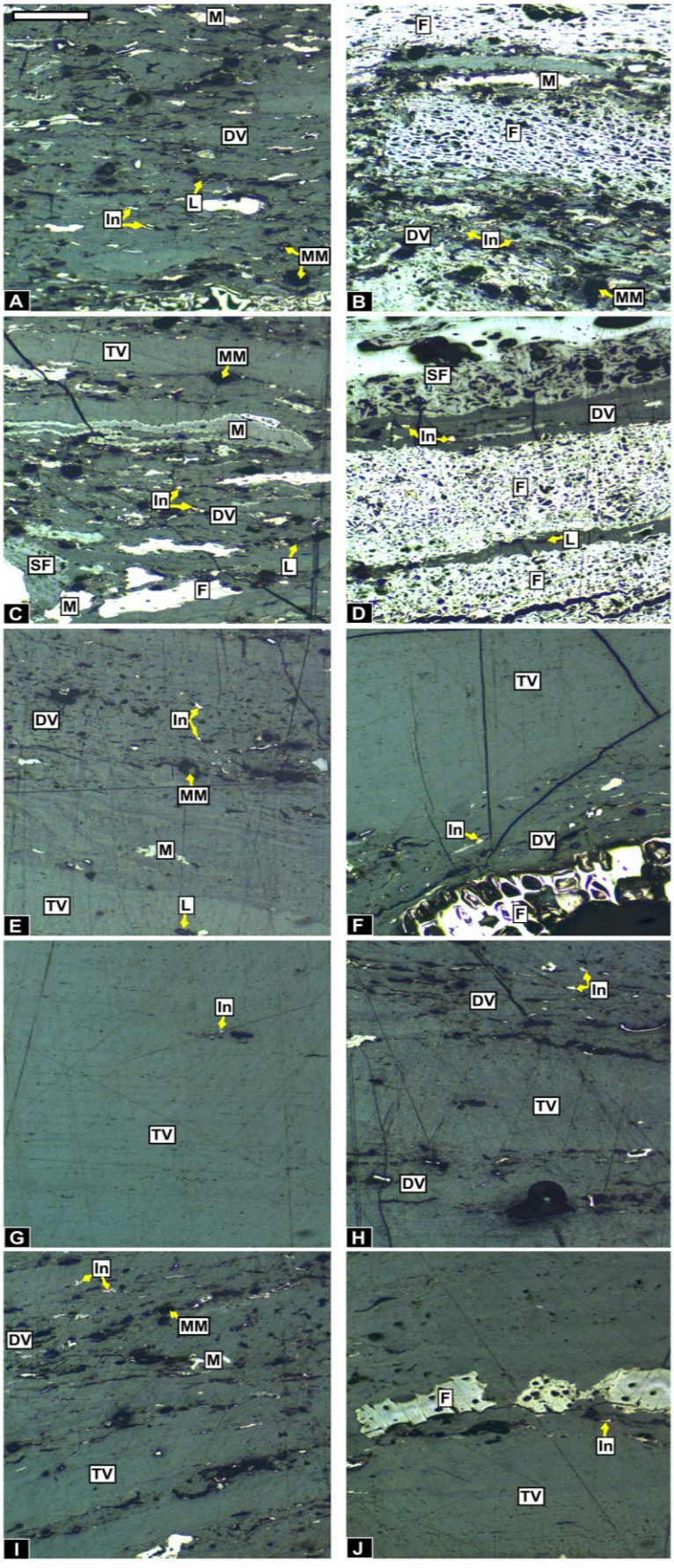
A
M
DV
L
In
MM
B
F
M
F
DV
In
MM
C
TV
MM
M
In
DV
SF
L
F
M
D
SF
DV
In
F
L
F
E
DV
In
MM
M
TV
L
F
TV
In
DV
F
G
In
TV
H
DV
In
TV
DV
I
In
MM
DV
M
TV
J
F
In
TV

4.3.6 Other entities in pillars 78(a), 88(a) and 91 of variable reflectance

All coal pillars contain entities, these were observed in varying amounts, scattered in detrovitrinite layers [1 in 78(a), 34 in 88(a) and 2 in pillar 91]. They show varying qualitative reflectance and as a result would be classified as different maceral groups according to ICCP terminology, from liptinite (Fig. 4.17 A) to vitrinite (Fig. 4.17 C). Those of qualitatively high reflectance (Fig. 4.17 E, G) would be classified as macrinite (*sensu* ICCP, 2001).

These entities are more abundant in dull lithotype units in pillar 88(a) and all contain fragments of plant material which may (Fig. 4.17 A, B, G) or may not be identifiable (Fig. 4.17 C - F). The entities range from 150µm (Fig. 4.17 C, D) to 1.1mm (Fig. 4.17 G) along their longest axis, some have irregular edges (4.17 A, B, G), and contain a range of plant material from cuticle (not illustrated) to spores (plate 4.17 A, B, G).

Pillar 91 contains two of these entities, one of high qualitative reflectance (Fig. 4.17 G) and one of liptinite colouration (not illustrated). Pillar 88(a) LU2 and LU4 contains 27 of these entities of liptinite colouration (Fig. 4.17 A), 2 of qualitative vitrinite reflectance (Fig. 4.17 C) and 5 of qualitative fusinite reflectance (Fig. 4.17 E).

See overleaf for Fig. 4.17

FIG. 4.17

Comparative reflectance (**A, C, E, G**) and fluorescence (**B, D, F**) images illustrating the range in size, morphology and qualitative reflectance of entities (labelled E in white box) observed in pillars 88(a) and 91. Scale bars correspond to 100µm. FOV = field of view in given T = transect.

Labels in white boxes represent the inertinite maceral group, *sensu* ICCP (2001): F = fusinite, M = macrinite.

A, B - 88(a) LU4 (T1 FOV 36) Montage of 4 images. **A –** Reflectance microscopy image of an entity with liptinite colouration, **B -** Orange fluorescence of entity, well preserved spores are only observed in the fluorescence image.

C, D – 88(a) LU2 (T2 FOV 41). **C –** Reflectance microscopy image of an entity with vitrinite qualitative reflectance, smaller size and more rounded morphology than seen in **A, E, G**. Discernible but unidentifiable plant material with liptinite colouration can also be observed inside the entity. **D** – Note the lack of fluorescence compared to **B**.

E, F - 88(a) LU2 (T2 FOV 25-26). **E -** Entity of qualitative fusinite reflectance (macrinite *sensu* ICCP, 2001) and a rounded morphology. Discernible plant material is observed in this entity. **F –** Note the lack of fluorescence compared to **B**.

G – 91 LU1 (T1) Montage of 4 images illustrating a large qualitatively fusinite reflecting entity containing spores. This entity did not fluoresce (not illustrated).

FIG. 4.17

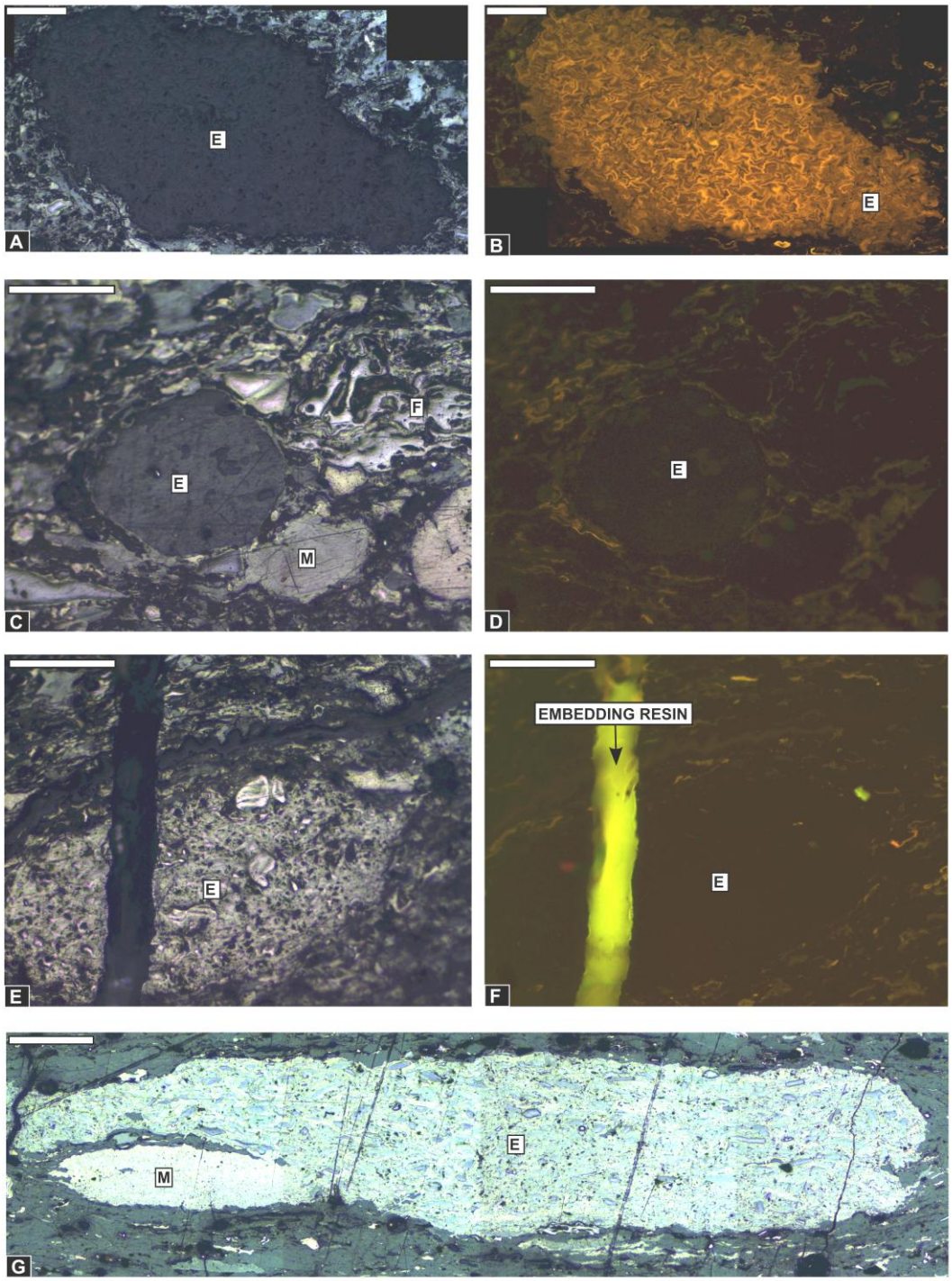

4.4 DISCUSSION

4.4.1 Comparison to previous published petrographic work

The randomly sampled coal pillars used in this study demonstrate an approach to interpreting wildfire history over a short time interval in the Late Permian Period. Pillar 78(a) contains a mean inertinite content of 27.6% mineral matter free basis (2 sd = 2.5; Table 4.2) which is comparable to previously published work (33%) (Pakh and Artser, 2003; Fig. 7.2). Pillar 88(a) contains far more inertinite [48% mineral matter free basis (2 sd = 4.7); Table 4.2] than documented by Pakh and Artser (2003) (22%; Fig. 7.2) as does pillar 91 with 34.9% inertinite mineral matter free basis (2 sd = 1.8) compared to 21% for seam 91 (Pakh and Artser, 2003; Fig. 7.2). These discrepancies suggest that there are both within, and between, seam variations in inertinite content which may relate to variability in wildfire occurrence in the peat-forming environment during the formation of each seam. The difference in inertinite contents may also indicate a record of either more fire events or a greater volume of charcoal produced during fire events for the time interval represented by the pillar compared to the totality of seams 88 and 91.

The Pakh and Artser (2003) data (Fig. 7.2) represent a summary of exploration data collected over many years and therefore are likely to be representative of the seams as a whole, however, their analysis is on crushed coals which, unlike *in situ* coal pillars, do not retain their inertinite distribution and therefore cannot be used in this type of study to interpret wildfire history.

4.4.2 Peat-forming environments

The peats were formed in extensive mire systems (Gore, 1983) that existed for considerable periods of time, producing coals often in excess of 10 metres thick (see chapter 3; Fig. 4.1 C).

Pillars 78(a) and 91 have low %ash (<9.4 % dry basis) and %total sulphur (<1.3 % dry ash free basis) (Appendix 5), thus suggesting formation in an ombrotrophic, rain-fed, peat-forming environment (Moore, 1987; Scott, 1989b). These form thick, zoned peats with domed topography (Moore, 1987; Scott, 1989b) although this morphology was not observed in the field.

Pillar 88(a) contains some lithotype units (LU2 and LU4) that have liptinite (sporinite) contents >10% (Fig. 4.3) and are therefore classed as sapropelic (Cook and Sherwood, 1991). Those rich in sporinite are termed cannel coals which form in freshwater lakes (Taylor et al., 1998). The sapropelic lithotype units (LU2, LU4) are interspaced with bright and banded lithotype units (LU3, LU5, LU7) which have lower %ash (7.16-17.6%) and liptinite contents (1.5-3.3%). The sapropelic lithotype units may represent small mire lakes on the peat surface of an ombrotrophic mire, similar to that illustrated in McCabe (1984, Fig. 9).

4.4.3 Other entities observed in coal pillars 78(a), 88(a) and 91

4.4.3.1 Identification

Pillars 78(a), 88(a) and 91 contain isolated entities which are scattered in detrovitrinite layers and range in size from 150μm (4.17 C, D) to 1.1mm (4.17 G). They contain fragments of identifiable plant material (commonly spores; Fig. 4.17 A, B, G), and are more abundant in dull lithotype units [88(a) LU2 and LU4].

The morphology of some of these entities (Fig. 4.17 A, B, E-G) is comparable to millipede coprolites observed by Scott and Taylor (1983) in Carboniferous coal balls. These are cylindrical and contain fragmented, identifiable plant material (Scott, 1977). The specimens in these coal pillars are widely scattered in detrovitrinite layers and none are associated with, or contained within, plant material. Millipedes are saprophagous detritus feeders (Kevan, 1968) consuming soft wood and decaying plant material, in particular, leaves (Cloudsley-Thompson, 1958; Raw, 1967; Wallwork, 1970). However, the coprolite illustrated in Fig. 4.17 (C, D) has a more rounded morphology and was therefore likely to have been formed by a different type of arthropod.

In coal seams coprolites have only previously been extensively documented in Carboniferous coal balls (Baxendale, 1979; Scott, 1977; Scott and Taylor, 1983) and reflected light images of coprolites in coal itself are rare (e.g. Hower et al., 2011). This work is the first documentation of coprolites in Permian coal.

Recognition of coprolites in these coal pillar samples is not straightforward. For example, some of these ‘coprolites’ appear to consist entirely of well preserved

spores (or possibly pollen) (Fig. 4.17 A, B). Experimental work on modern millipedes has shown that spore exines are resistant enough to be preserved whole in faecal pellets (Chaloner, 1976). Spore feeding appears to have been prevalent in the Carboniferous (Scott et al., 1985) and coprolites have been shown to contain significant numbers of spore exines which have remained entire through digestion (Scott, 1977; Chaloner et al., 1991) and may even consist of a single taxon (e.g. Rothwell and Scott, 1988). This quantity of spores in a coprolite may suggest a diet of sporivory (Scott, 1977), or an organism feeding on a spore eater, or an organism with a diet of spore-rich litter (Chaloner et al., 1991).

Although the entities in the coal pillars (Fig. 4.17) may represent coprolites, the preservation of entire spores suggests that they may represent detached sporangia (or possibly pollen organs). It may be possible to differentiate coprolites from sporangia. Previous work by Wellman et al. (2003) on Ordovician samples, recognised coprolites by their lack of covering (no sporangial wall) around the entity and an interior composition of mixed fragmented plant material (different spore types and cuticle). However, the sporangial walls may only be a few cells thick and as a result may not be well preserved (Collinson, personal communication) and may therefore be difficult to identify. Entities containing spores and no other plant material may be interpreted as either detached sporangia (or possibly pollen organs) or coprolites (e.g. Fig. 4.17 A, B) whereas entities consisting of mixed fragments of plant material may be interpreted as coprolites (e.g. Fig. 4.17 C-G).

4.4.3.2 Coal petrographic classification of coprolites / sporangia

The presence of animal remains such as coprolites and arthropod cuticle in coal are often overlooked in coal petrography (Bartram et al., 1987; Scott, 2002; Hower et al., 2011). There is currently no inertinite maceral category for charred coprolites (Scott and Glasspool, 2007). The qualitatively low reflecting entities described in section 4.3.6 would be classified petrographically as liptinite (Fig. 4.17 A) or vitrinite (Fig. 4.17 C) according to ICCP terminology (ICCP, 1998). The qualitatively high reflecting coprolites (Fig. 4.17 E, G) would be classified as macrinite under the ICCP (2001) inertinite scheme (Hower et al., 2011). However, the macrinite maceral definition does not encompass all of the morphological variation seen in the coprolites nor the wide qualitative reflectance variation from liptinite to fusinite.

Coprolite distribution is also not comparable to the macrinite definition as the entities do not appear as bands or lenses [an aspect of the definition of groundmass macrinite, as referred to in the comments section of the ICCP (2001) scheme], nor are they an amorphous matrix. The origins of macrinite macerals are poorly understood and some believe their formation may be related to fungal activity (e.g. Hower et al., 2009). As an approach to addressing this issue Hower et al. (2011) have proposed introducing a subdivision of macrinite termed 'copromacrinite'. This still does not address the range in qualitative reflectance seen in these entities or the difficulty in distinction of some coprolites from sporangia.

4.4.3.3 Charred entities

The coprolites or sporangia show variable qualitative reflectance from liptinite (Fig. 4.17 A) to fusinite (Fig. 4.17 E, G) and corresponding decreasing fluorescence with increasing qualitative reflectance (Fig. 4.17 B>D>F) which provides evidence for variable degrees of charring. These coprolites or sporangia may be uncharred (Fig. 4.17 A, B) to partially charred (Fig. 4.17 C, D) to fully charred (Fig. 4.17 E-G).

If these entities are coprolites, and were produced by millipedes (detritus feeders) then it is possible they (Fig. 4.17 C - F) may have been charred during a surface fire. However, the coprolites (both charred and uncharred) are relatively rare and distributed sporadically throughout the coal pillars. This is in contrast to faecal pellets observed in modern peat-forming environments by Cohen et al. (1987) which occur in clusters, not as isolated entities as seen here. This suggests that the entities in the coal pillars have been transported, as charcoal separates into different size fractions during water transport (Vaughan and Nichols, 1995; Nichols et al., 2000) and therefore, it may not be possible to link the occurrence of individual charred coprolites to wildfire types.

4.4.4 Interpretation of wildfire type and occurrence in pillar 78(a)

4.4.4.1 Evidence for wildfires: charcoal occurrence

Charcoal is present in all ten lithotype units in pillar 78(a), ranging from 3 - 59% (Fig. 4.4) thus providing evidence for wildfire occurrence throughout the formation of the coal pillar. Pillar 78(a) has a total mean inertinite content of 27.6% mineral matter free (mmf) basis (2 sd = 2.5; Table 4.2) which suggests that individual fires

were producing large quantities of charcoal, or a that fires were very frequent in this mire environment during the Late Permian. This inertinite content is much higher than observed for modern peat-forming environments [~4.3% mineral matter free basis, see Glasspool and Scott (2010)]. Lithotype units show spatial variation in macroscopic fusain (Fig. 4.5) and temporal variation in microscopic inertinite distribution (Fig. 4.4). This variation in inertinite distribution is interpreted to represent wildfires of varying size, proximity and type throughout the formation of this 23cm *in situ* coal pillar.

4.4.4.2 Evidence for multiple surface fires

There are 11 charcoal horizons in pillar 78(a) in LU2, LU3, LU8 and LU10 (Fig. 4.4). These are interpreted to represent charred vegetation from surface fire events, which produce the most charcoal (Scott, 2010), and burn both living and dead plant material (originally derived from both surface and canopy) at low temperatures (Scott, 1989a; see data compilation in Scott and Jones, 1994; Scott, 2000; McParland et al., 2009b). Low temperature charcoal may be represented in coal as semifusinite (Jones et al., 1991, 1993; Scott and Jones, 1994; Scott, 2000; Scott and Glasspool, 2007). Semifusinite is the most abundant inertinite maceral in LU2 and LU3 (13 - 29%; Fig. 4.3) which suggests that these charcoal horizons formed in cool temperature fires. Furthermore, macroscopic fusinite and semifusinite clasts in charcoal horizons in LU2 and LU3 show gradational reflectance (e.g. Fig 4.6 D). This represents partially charred material, formed if either the fire burns quickly due to short fire duration, or if there are high levels of vegetation moisture (Patterson et al., 1987). However, in the upper inertinite-rich lithotype units (LU6, LU8, LU9 and LU10) qualitatively high reflecting fusinite is the dominant inertinite maceral (18 – 39%), followed by semifusinite (13 - 18%) suggesting higher temperature fires during this period of peat formation.

The macroscopic charcoal in these horizons may have been transported locally either by wind under some specific conditions (e.g. Tinner et al., 2006) or, more commonly, by water transport through overland flow (Komarek, 1973; Scott et al., 2000a; Scott, 2009, 2010). The occurrence of several charcoal horizons in a sequence (as seen here) may represent seasonal fire events whereas large catastrophic fire events would be represented by single, thick charcoal deposits

(Scott and Jones, 1994) which are not observed in any of the coal pillars.

4.4.4.3 Evidence for crown fires

Crown fires combust living vegetation from both canopy and understory trees (Davis, 1959; Scott and Jones, 1994), at high temperatures around 800°C - 900°C (Pyne et al., 1996). Microscopic charcoal (<180µm but more commonly <20µm) is generally interpreted as the windblown or water transported size fraction from regional crown fire events within 20 - 100km of the fire source (Clark and Patterson, 1997; Clark et al., 1998; Pitkänen et al., 1999; Ohlson and Tryterud, 2000; Scott et al., 2000a; Scott, 2002; Lynch et al., 2004; Collinson et al., 2007; Peters and Higuera, 2007; Conedara et al., 2009; Power et al., 2010). Charring temperatures >600°C can cause fragmentation of charcoal (Scott and Jones, 1991) and therefore crown fires may be identified in the sequence by the presence of microscopic, high reflecting charcoal (Patterson et al., 1987; Clark, 1988; Clark et al., 1998; Ohlson and Tryerud, 2000; Scott and Glasspool, 2007). High reflecting inertodetrinite (<10µm) is present in all lithotype units in small amounts (0.2 - 5%; Fig. 4.3) in detrovitrinite layers, which suggests charcoal production and dispersal from frequent background, crown fires.

The telovitrinite layers occurring between detrovitrinite layers (all lithotype units) either contain no inertinite macerals or occasional, widely spaced, scattered inertodetrinite. The presence of inertodetrinite in some of the telovitrinite layers confirms that these layers cannot be single compressed plant organs. The microscopic inertinite in detrovitrinite layers is therefore interpreted to represent background, regional fires followed by periods without fires (telovitrinite layers) enabling a build-up of fuel, as seen in modern fire events (e.g. Pierce et al., 2004).

4.4.4.4 Evidence for other small fires

A range of charcoal sizes including macroscopic charcoal (not in horizons) is observed in LU4-6 and LU9 (Fig. 4.6 H, J; Fig. 4.7 B, H). This charcoal may represent windblown or water transported larger pieces (as documented in modern fires by Scott et al., 2000a and Tinner et al., 2006) from more local fire events (Scott, 2010).

4.4.5 Interpretation of wildfire type and occurrence in pillar 88(a)

4.4.5.1 Evidence for wildfires: charcoal occurrence

Charcoal is present in all seven lithotype units in varying amounts (3% - 56%) with a pillar average of 48% mineral matter free (mmf) basis (2 sd = 4.7; Table 4.2). This provides evidence for wildfire occurrence during the formation of this coal pillar. A summary of the variation in inertinite distribution between lithotype units in pillar 88(a) is given in Fig. 4.9. Lithotype units show spatial variation in macroscopic fusain (Fig. 4.10) and temporal variation in microscopic inertinite distribution (Fig. 4.9). This variation of inertinite distribution between lithotype units is interpreted to represent wildfires of varying size, proximity and type throughout the formation of this 36cm *in situ* coal pillar.

4.4.5.2 Evidence for multiple surface fires

There are 26 charcoal horizons present in three lithotype units, two of which are sapropelic [LU2 16 horizons (Fig. 4.13), LU4 8 horizons; Fig. 4.9] and two in a banded lithotype unit (LU7; Fig. 4.9). Charcoal horizons are interpreted to represent transported charcoal from individual low temperature (semifusinite 7.5 - 16%; Fig.4.3) surface fire events (see section 4.4.4.2).

The base of LU7 is marked by a charcoal horizon, interpreted as being the result of a surface fire which suggests that an ombrotrophic peat-forming environment (terminating LU6; Fig. 4.9) must have established in order to produce litter that was then charred, or it represents material washed in from a separate fire event from outside of the peat-forming area. The majority of charcoal in this horizon is partially charred (Jones et al., 1993) material and, as with similar material in pillar 78(a), it may have formed as a result of the fire burning quickly or the plants having high levels of moisture (Patterson et al., 1987) which can also effect burning efficiency (Enache and Cumming, 2006).

Charcoal horizons in sapropelic lithotype units LU2 (16 horizons) (an example is illustrated in Fig. 4.13) and LU4 (8 horizons) are interpreted as being formed from influxes of charred material from surface fire events which settle out in the mire lake environment. Preservation of charcoal horizons in this depositional setting suggests limited reworking within the mire lake.

4.4.5.3 Evidence for crown fires

Lithotype units LU3 and LU5 contain the least amount of charcoal (2% and 10% respectively; Fig. 4.9) in thin detrovitrinite layers (<425µm wide) with, scattered inertodetrinite (2 - 3%), liptinite, mineral matter, and microscopic inertinite macerals (Fig. 4.11 F; Fig. 4.12 A, B). Lack of large charcoal particles (>200µm) suggests that this material is derived from a regional fire source (Clark et al., 1998). There is no low reflecting inertodetrinite in pillar 88(a) suggesting an origin from high temperature crown fires. However, the majority of LU3 and LU5 is telovitrinite (70 - 83%; Fig. 4.3; Fig. 4.11 E). This suggests intervals without local fire events and only infrequent background regional crown fires.

Microscopic charcoal (<180µm) is also abundant in sapropelic lithotype units (LU2, LU4) and includes both inertodetrinite (9 - 15%) and macrinite (7%). These macerals are scattered in every field of view throughout these lithotype units and may represent an elevated background regional, fire signal as observed in modern charcoal distributions by Power et al. (2010), or fragmented, water transported charcoal from surface fires.

4.4.5.4 Evidence for other small fires

The presence of semifusinite in six of seven lithotype units (3 - 16%; Fig. 4.3) is interpreted as charcoal produced during low temperature surface fires. Macroscopic charcoal is completely scattered throughout lithotype units LU2, LU4 and LU6. The maceral associations in these lithotype units include scattered inertinite (41 - 45%; Fig. 4.3), uncharred liptinite (4 - 16%; Fig. 4.3) and mineral matter (19 - 26%; Fig. 4.3). The combination of charred and uncharred material is likely to be a result of a portion of biomass being charred and producing charcoal during a fire and an amount remaining uncharred (Nichols et al., 2000; Scott, 2010). These components may later be transported together and mixed in the same lithotype unit producing the scattered distribution in the coal pillar.

4.4.6 Interpretation of wildfire type and occurrence in pillar 91

4.4.6.1 Evidence for wildfires: charcoal occurrence

Charcoal is present in all seven lithotype units in varying amounts (0.3% - 61%) with a pillar average of 34.9% mineral matter free basis (2 sd. = 1.8; Table 4.2). This

provides evidence for wildfire occurrence during the formation of this coal pillar. Lithotype units contain variation in macroscopic fusain (Fig. 4.15) and microscopic inertinite distribution (Fig. 4.14) which is interpreted as representing wildfires of varying size, proximity and type throughout the formation of this 10cm *in situ* coal pillar.

4.4.6.2 Evidence for multiple surface fires

There are 3 charcoal horizons present in LU2 (Fig. 4.14). These are interpreted to represent transported charcoal from surface fire events due to the large clast size (>425µm up to 5.1 mm). Lithotype units above LU2 (LU3-5 discussed in section 4.4.6.3) are inertinite poor (0.3 - 7.2%; Fig. 4.3) and the vitrinite component is primarily collodetrinite which is thought to be formed from cellulosic substances, not lignin-rich wood (ICCP, 1998). This suggests that the fire events in LU2 may have been stand replacing as no other local fire events are observed (see section 4.4.6.3) during the remaining time interval of coal pillar formation.

4.4.6.3 Evidence for crown fires

Lithotype units LU3-LU5 contain the least amount of charcoal (0.3 - 7.2%; Fig. 4.3) in detrovitrinite layers containing widely scattered high reflecting inertinite, liptinite, mineral matter and rare fusinite and semifusinite pieces (>425µm) (Fig. 4.16 E-J). This suggests infrequent background regional crown fires and no local fire events in the immediate peat-forming area. Rare occurrences of macroscopic fusinite and semifusinite clasts (>425µm) may represent windblown larger pieces of charcoal (as seen in modern fires e.g. Tinner et al., 2006).

4.4.7 Recognising ground fires in coal pillars

A charred peat surface would be represented by a continuous band (Cohen et al., 1987) of charred material (fusinite or semifusinite) whereas the charcoal horizons in the coal pillars studied are composed of large clasts of charcoal that are surrounded by thin layers of detrovitrinite (Fig. 4.8; Fig. 4.13) and therefore are interpreted to represent transported clasts of charcoal and not charred peat. There is no evidence for a charred peat surface in any of the coal pillars.

4.4.8 Comparisons between charcoal amount in pillars 78(a), 88(a) and 91

The three coal pillars contain differing amounts of charcoal but show comparable wildfire histories. This variation in quantity of charcoal between pillar 78(a) [mean of 27.6% (2 sd = 2.5); Table 4.2], pillar 91 [mean of 35% (2 sd = 1.8); Table 4.2] and pillar 88(a) [48% (2 sd = 4.7); Table 4.2] could be related to variations in the fuel load, the spread and temperature of the fire, and resulting charcoal production, and differences in the transport-depositional system.

4.4.9 An approach to calculating fire return intervals in deep time using *in situ* coal pillars

High inertinite contents have previously been observed in Permian coals (mean 44%; Glasspool and Scott, 2010), and during this study in Late Permian Russian coals [mean 28.3% own data seams 68-94; Fig. 7.2], compared to charcoal contents in modern peat-forming environments (mean of 4.3%; Glasspool and Scott, 2010). The inertinite provides evidence for wildfire occurrence in Permian peat-forming environments. The high inertinite content may suggest that fires may have been more frequent in the Permian than the present day (see Uhl and Kerp, 2003; Uhl et al., 2008) or that a larger volume of charcoal was produced during fire events compared to present day fires.

In order to provide a comparison to fire return intervals (FRI) in modern peat-forming environments an attempt has been made to devise a method to calculate FRI from charcoal horizons in coal pillars. The ranges of peat-forming variables and caveats affecting the calculation are discussed further in the sections below. There have been no previous attempts to address calculating FRI in deep time using *in situ* coal pillars and this approach presents a starting point towards developing a possible solution.

4.4.9.1 The FRI calculation

Prior to calculating FRI the coal first needs to be de-compacted to the original peat thickness, which requires an understanding of the potential range in peat:coal compaction ratios. In order to then convert this calculated peat thickness to a time interval of peat formation, an understanding of peat accumulation rates is also required.

Using charcoal horizons: FRI were calculated from the Late Permian *in situ* coal pillars using occurrences of charcoal horizons (Fig. 4.4; Fig. 4.8; Fig. 4.9; Fig. 4.13; Fig. 4.14), which are interpreted to represent transported charcoal from local surface fire events within the peat-forming environment (section 4.4.4.2; 4.4.5.2; 4.4.6.2). However, charcoal may be transported for long periods of time prior to deposition (Nichols et al., 2000) and can continue to accrue during non fire years as a result of surface run-off (Whitlock and Larsen, 2001). It is therefore possible that multiple charcoal horizons in a single lithotype unit may represent re-worked charcoal from a single fire event. It may be difficult to identify individual fire events in coal pillars and the calculated fire return intervals may, therefore, be longer than suggested in Table 4.3. If charcoal horizons do represent individual fire events then they correspond to a very short time interval. This will affect both accumulation rate and compaction ratio of the peat during coalification as charcoal compaction differs from that of peat. One possible approach to take account of these issues is to remove the thickness of charcoal horizons from the total lithotype unit thickness and use the remaining lithotype unit thickness to calculate a more representative original peat thickness (Table 4.3).

Peat: coal compaction ratios: De-compacting coal to its original peat thickness is not straightforward and there has been limited quantitative work on peat to coal compaction ratios. A good understanding of compaction in peat is needed to give meaningful compaction ratios (Shearer and Moore, 1996), as prior to coalification the peat is compacted both in the catotelm and from surface loading of the above ground biomass (including fallen trees and litter) (Elliott, 1985). Furthermore, Winston (1986) has demonstrated that different plant tissues may compact at different rates, thus making generalisations of compaction ratios difficult without palaeobotanical data. In addition, literature compiled by Ryer and Langer (1980) gives a range of estimated peat: coal compaction ratios from 1:1 to 30:1 but the median compaction ratio of 7:1 is considered to be more representative (Ryer and Langer, 1980). The median value, as well as the range in compaction ratios, is therefore considered in the FRI calculations (Table 4.3).

It may be possible to estimate peat to coal compaction ratios from these Permian coal pillars using secretinite which does not become compacted during coalification. The

difference in thickness between the secretinite and the same coal layer away from the secretinite can indicate the degree of compaction (Taylor et al., 1998), as illustrated in Fig. 4.18. Although this is just one example it suggests that Permian peat:coal compaction ratios may be towards the lower end of values given in Table 4.3.

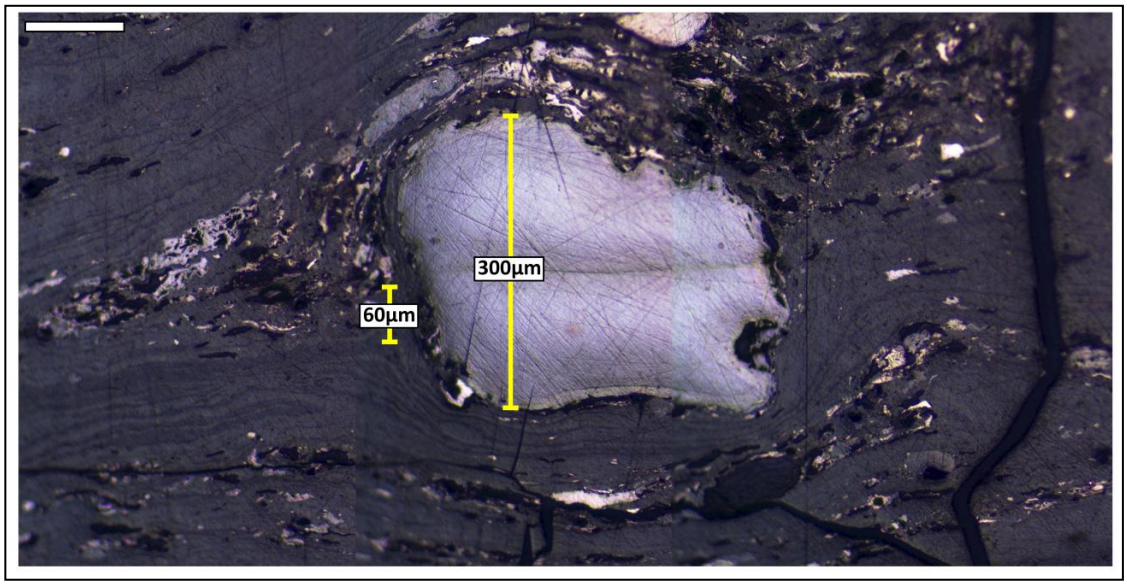

FIG 4.18 Montaged reflectance microscopy images (6 in total) from pillar 78(a) illustrating the potential peat to coal compaction ratio (5:1) for these Late Permian pillars calculated using the difference in thickness between an uncompacted secretinite clast (centre) and surrounding vitrinite layer.

Secretinite an inertinite maceral (Table 2.3) and inertinite (charcoal) has been shown, both in experimentally produced coal and in Carboniferous coal ball peels, to compact less than uncharred material (peat) with charcoal compaction ratios ranging from 1.3:1 to 2.5:1 (Winston, 1986; Shearer and Moore, 1996). The Permian coal pillars studied in this chapter have high inertinite contents and therefore detrovitrinite layers containing inertinite are likely to have undergone less compaction during coalification than telovitrinite layers containing no inertinite.

Calculating FRI for sapropelic lithotype units [88(a) LU2, LU4]: The median compaction ratio of 7:1 may be representative for humic coals but finer grained sapropelic coals [as seen in 88(a) LU2, LU4] may have formed under much higher compaction ratios, up to 20:1 (Taylor et al., 1998). Clearly this adds some uncertainty to any fire return interval calculation. However, sapropelic lithotype units in pillar 88(a) (LU2, LU4) also contain high inertinite contents [LU2 – 55%

(mineral matter free basis) and LU4 - 53% (mineral matter free basis); Fig. 4.9] with inertinite macerals scattered in every field of view (Fig. 4.11 C, D, G, H; Fig. 4.13) as charcoal has been shown to be less compactable than peat these lithotype units are unlikely to have undergone high compaction ratios during coalification. Moreover, these lithotype units also contain large quantities of quartz and kaolinite (LU2 – 18.7% and LU4 – 21.6%; Fig. 4.2; Fig. 4.3). Quartz is relatively incompressible compared to peat because of its low porosity (Weller, 1959; van Asselen et al., 2009). However, the effect of mineral matter on compaction may be negligible because of its scattered distribution (LU2 and LU4; Fig. 4.11 C, D, G, H) as opposed to occurring in bands.

It may not be possible to calculate FRI from sapropelic lithotype units using this method even though they contain charcoal horizons (Fig. 4.9; Fig. 4.13). The calculation requires the less compactable charcoal horizon thickness to be removed from the total lithotype unit thickness. Inertinite is distributed in every field of view in LU2 (Fig. 4.13) and LU4 throughout the entire lithotype unit, with little identifiable vitrinite (Fig. 4.11 C, G). Removal of charcoal in these lithotype units therefore removes the entirety of the lithotype unit thickness, considerably shortens the time interval for total pillar formation and implies that these lithotype units represent instantaneous depositional events. This is unlikely as 8 to 16 charcoal horizons are preserved which suggests time between depositional events allowing macroscopic pieces of charcoal to settle out in layers.

Peat accumulation rates: The upper uncompacted peat layer is the acrotelm (5-50cm), up to 90% of which is removed by aerobic decay (Clymo, 1987). The lower waterlogged layer is the catotelm which decomposes slowly and represents the majority of long-term peat accumulation (Clymo, 1987; Frolking et al., 2001; Yu et al., 2001; Moore et al., 2007). In modern temperate peat-forming environments there is a large amount of below ground productivity (Moore et al., 2007). Roots are likely to penetrate the catotelm while alive and may represent a major constituent of peat (Moore, 1987). However, the morphology of the rooting structure in this Permian peat-forming environment represents an unknown (Collinson and Scott, 1987), as roots may make a large but unquantifiable constituent of the Permian peat, accurately determining the accumulation rate is difficult.

In order for peat to accumulate at a continual rate in modern peat-forming environments the following conditions are required, high plant productivity, continuously rising water table, slow rates of litter decomposition, minimum influx of sediment and plant growth keeping pace with subsidence (Fielding, 1987; Cameron et al., 1989; Lamberson et al., 1996; Frolking et al., 2001; Moore et al., 2007; Jerrett et al., 2011b) all of which represent unknowns in ancient peat-forming environments. There are no modern temperate bog forests with high enough accumulation rates that could replicate the thickness of Permian coal seams (Moore, 1987). However, spectral analysis of geophysical data from a Late Permian Cathaysian coal seam by Wang et al. (2011) suggests that Late Permian peat accumulation rates were comparable to present day values. A range of modern peat accumulation rates from 0.2mm/a^{-1} (Aaby and Tauber, 1975) to 2mm/a^{-1} (Taylor et al., 1998) were therefore considered when calculating FRI in Table 4.3. 1mm/a^{-1} is highlighted as climate during the Permian in Siberia was temperate (Ziegler, 1990) and this value represents the most likely accumulation rate in a temperate peat-forming environment. The range of peat accumulation rates used here incorporates various vegetation types (herbaceous moss to woody conifers) so there is no reason to suggest that they cannot be applied to cordaite-dominated peat-forming environments.

Peat accumulation rates are unlikely to remain constant during seam, or even coal pillar formation. Periodic influxes of charcoal (either in charcoal horizons or scattered in detrovitrinite layers) do not represent periods of peat accumulation and may even represent instantaneous depositional events and therefore need to be considered separately from peat accumulation rates (see below for further discussion).

These modern peat accumulation rates may not be comparable to those in the Permian, as the vegetation is thought to have grown under elevated atmospheric oxygen conditions. Growth of modern plants under elevated atmospheric oxygen conditions (Quebedeaux and Hardy, 1975; Beerling et al., 1998) has shown that 35-40% O_2 may actually inhibit plant growth (Beerling et al., 1998). However, atmospheric oxygen models by Berner (2006, 2009) and Berner et al. (2003) have shown that oxygen levels may have only reached 30% during the Permian Period,

therefore it is unlikely that plant growth (hence peat accumulation) would have been inhibited during the time interval of seam formation. The wide range of modern peat accumulation rates used in this calculation should therefore take into account the elevated atmospheric oxygen compared to present levels.

The FRI calculation assumes a constant peat accumulation rate which is unlikely for the entire duration of seam formation and possibly even for the duration of coal pillar formation. Peat erosion has been observed in modern blanket bogs (Stevenson et al., 1990; Evans and Warburton, 2005). Basal erosion surfaces, interpreted as indicating a hiatus in peat formation, have been identified by Holdgate (1995) in Tertiary lignite and may represent time intervals of up to 300 ka. However, 'erosional hiatuses' in coal have been erroneously identified by some workers based on the presence of inertinite-rich dulling up sequences as they consider inertinite to be produced by oxidation and not wildfire (e.g. Lindsay and Herbert, 2002; Jerrett et al. 2011a,b). Thus, inertinite-rich lithotype units are therefore unlikely to represent hiatuses in peat accumulation.

Hiatuses in peat accumulation can also be caused by ground fires (Shearer et al., 1994) which can cause the soil to sterilise (Rein et al., 2008) and thus temporarily prevent or slow peat accumulation. However, this has not been taken into account in this study as there is no evidence for ground fires in any of these coal pillars (see section 4.4.7).

Significance of other charcoal not in horizons: Calculated FRI in Table 4.3 may be considered to represent conservative estimates of fire return interval (even allowing for the wide range in compaction ratios and accumulation rates) as the calculation is based on occurrence of charcoal horizons and not on all occurrences of macroscopic and microscopic charcoal. The calculation therefore does not represent all fire events during the interval of coal pillar formation. Other occurrences of charcoal were not incorporated into the calculation as these do not occur in a layer(s) that can be traced across the width of the block and therefore their thickness cannot be removed from the total lithotype unit thickness. For example pillar 91 (LU2) contains 3 charcoal horizons (Fig. 4.14) but the majority of the rest of LU2 is also macroscopic charcoal (Fig. 4.15) and if these individual pieces of charcoal were also removed, then the

interval of pillar formation would be even shorter than the calculation suggests (Table 4.3) thus fire return intervals would also be more frequent.

Alternating telovitrinite and detrovitrinite layers of varying thickness are observed in 78(a) LU1-LU10; 88(a) LU1, LU3, LU5, LU7; 91 LU1-5. Scattered charcoal in detrovitrinite layers provides evidence for wildfire occurrence. An approach to calculating all fire occurrences throughout the formation of these coal pillars may be to remove the thickness of all detrovitrinite layers containing inertinite from each coal pillar. This would give a very short, and potentially more representative FRI, but does not take into account the varying amounts of inertinite in each detrovitrinite layer (hence different fire types), or the possibility of reworking of charcoal over several detrovitrinite layers (therefore not a single event). In addition, some telovitrinite layers do not contain any macerals which suggests they are single compressed plant organs and do not represent long intervals of peat accumulation.

4.4.9.2 Application of the FRI calculation

This approach has been applied to three lithotype units [78(a) LU2, 88(a) LU7, 91 LU2] representing ombrotrophic mire depositional settings but with variation in both number of charcoal horizons [78(a) LU2, 4 horizons; 91 LU2, 3 horizons; 88(a) LU7, 2 horizons] and cumulative horizon thickness in the coal pillar (3mm to 6.2mm; Table 4.3) to demonstrate the range in potential fire return intervals in ombrotrophic mire depositional settings within these coal pillars. Mid value FRI range from: 7 years (extremes 0.5 to 143 years) for 78(a) LU2, to 70 years (extremes 5-1550 years) for 88(a) LU7, or 69 years (extremes 5-1485 years) for 91 LU2.

LU	LU thickness	Charcoal thickness	Corresponding peat thickness median compaction ratio 7:1 (range 1:1-30:1)	Peat accumulation rate	Duration of peat formation	Number of charcoal horizons	Fire return interval (FRI)
78(a) LU2	10mm	6.2mm	**26.6mm** (3.8 – 114mm)	0.2 mm/a^{-1}	**133 years** (19 – 570 years)	4	**33 years** (5 – 143 years)
			26.6mm (3.8 – 114mm)	1 mm/a^{-1}	**26.6 years** (3.8 – 114 years)		**7 years** (1 – 29 years)
			26.6mm (3.8 – 114mm)	2 mm/a^{-1}	**13.3 years** (1.9 – 57 years)		**3 years** (0.5 – 14 years)
88(a) LU7	23mm	3mm	**140mm** (20-600mm)	0.2 mm/a^{-1}	**700 years** (100 – 3000 years)	2	**350 years** (50 – 1550 years)
			140mm (20-600mm)	1 mm/a^{-1}	**140 years** (20-600 years)		**70 years** (10-300 years)
			140mm (20-600mm)	2 mm/a^{-1}	**70 years** (10-300 years)		**35 years** (5 – 150 years)
91 LU2	34mm	4.3mm	**207.9mm** (29.7-891mm)	0.2 mm/a^{-1}	**1039.5 years** (148.5-4455 years)	3	**346.5 years** (50-1485 years)
			207.9mm (29.7-891mm)	1 mm/a^{-1}	**207.9 years** (29.7-891 years)		**69.3 years** (10-297 years)
			207.9mm (29.7-891mm)	2 mm/a^{-1}	**104 years** (14.9-445.5 years)		**35 years** (5-149 years)

TABLE 4.3 An approach to calculating fire return intervals (FRI) using charcoal horizons demonstrated using three examples [78(a) LU2; 88(a) LU7; 91 LU2]. These lithotype units represent comparable environments of deposition in ombrotrophic mire settings but with variation in both number of charcoal horizons and cumulative charcoal horizon thicknesses. The thickness of the less compactable charcoal horizons is removed from the total lithotype unit thickness and the resulting value is used to determine the original peat thickness (over a range of compaction ratios). A range of peat accumulation rates is considered to calculate the duration of peat formation represented by this de-compacted peat thickness. Fire return interval is calculated by dividing the duration of peat formation by the number of charcoal horizons [see Conedara et al. (2009)].

It is possible to demonstrate how variable FRI can be once the caveats discussed above have been taken into account in the calculation. Using 78(a) LU2 as an example, this lithotype unit has the majority of its charcoal contained in four

charcoal horizons. Removal of the thickness of these charcoal horizons means the remaining LU thickness will potentially just represent peat accumulation and the compaction should remain relatively constant as it will not be influenced by other occurrences of charcoal outside of the four charcoal horizons. If peat accumulation of this lithotype unit occurred at a constant rate of $1mm/a^{-1}$ and was then compacted at a ratio of 5:1 during coalification (as suggested by Fig. 4.18), then if the charcoal horizons do in fact represent individual fire events, FRI would be 25 years or 100 years if all four charcoal horizons represent re-deposition from a single fire event. These values are less frequent than the calculated FRI in Table 4.3.

4.4.9.3 Comparison to modern FRI

Fire return intervals in modern peat-forming environments range from 200 - 750 years in subtropical environments (Spackman et al., 1976) to 200 - 1100 years for *Sphagnum* bogs and heathlands (Innes et al., 2004; Stähli et al., 2006; Muller et al., 2008) to 80 - 475 years in treed boreal peatlands (Turetsky and St.Louis, 2006; Ohlson et al., 2006) and 230 - 600 years for subalpine peatlands (Stähli et al., 2006). In addition, bogs in temperate latitudes also show longer fire return intervals than boreal bogs (~900 - 1000 years) (Wein and Moore, 1977; Lavoie and Pellerin, 2007). However, these values may not fully reflect the natural wildfire frequency as the human impact on fire regimes is not fully understood (e.g. Flannigan et al., 2009) and it is difficult to distinguish between anthropogenic and natural fires (Scott et al., 2000b; Bowman et al., 2011) as shown by studies of Holocene temperate ombrotrophic bogs which show natural fire return intervals that are ten times longer prior to the start of agricultural activity in the area (Lavoie and Pellerin, 2007). Therefore, although caution is required when comparing modern and ancient FRI both the mid-range FRI values calculated from these Late Permian coal pillars and the re-calculated values for 78(a) LU2 suggest shorter fire return intervals than seen in modern peat-forming environments.

4.5 CONCLUSIONS

There is currently no universal standard method for petrographic analysis of *in situ* coal pillars. Traditional petrographic techniques for maceral analysis use crushed coals but these do not retain original spatial or temporal context and therefore cannot be used for wildfire interpretation. *In situ* coal pillars are therefore considered to be

essential for research into palaeowildfire type, occurrence and frequency.

The three *in situ* coal pillars studied [78(a), 88(a), 91] represent coals formed in different environments of deposition within the peat-forming system. The low %ash (<9.4% dry basis) and low %total sulphur (<1.3% dry ash free basis) content of pillars 78(a) and 91 suggests formation in an ombrotrophic mire. In contrast the small particle size, high liptinite and low vitrinite in the two thickest lithotype units (LU2, LU4) of pillar 88(a) indicate sapropelic coal formed in a mire lake environment within an ombrotrophic peat-forming system. This is supported by the high %ash (19-21%) and mineral matter (19-22%) contents and the mixture of maceral components.

Coprolites or sporangia (or possibly pollen organs) are preserved in these coal pillars. These show variable qualitative reflectance and the high reflecting specimens may have been charred with the litter layer during surface fire events.

Wildfire derived charcoal (inertinite) is present in varying amounts in all lithotype units in all pillars averaging 27.6% in pillar 78(a), 35% in pillar 91 and 48% in pillar 88(a) (mineral matter free basis). For pillar 78(a) this value is similar to previous results from crushed coals (Pakh and Artser, 2003) but, pillars 88(a) and 91 contain more inertinite [88(a), 48%; 91, 35%] than documented in literature [88(a), 22%; 91, 21%]. Similar patterns of inertinite distribution are observed petrographically in all pillars either as, (1) microscopic charcoal (<180µm) which is scattered in detrovitrinite layers and is interpreted to represent a background, regional crown fire signal or (2) Scattered macroscopic charcoal in lithotype units 78(a) LU4-6, LU9, 88(a) LU1, 91 LU1 (Fig. 4.4; Fig. 4.9; Fig. 4.14) which may represent waterborne or windblown pieces of charcoal transported from local fires or (3) multiple charcoal horizons with macroscopic charcoal [e.g. Fig. 4.8; Fig. 4.13; 78(a) LU2, LU3, LU8, LU10; 88(a) LU2, LU4, LU7, 91 LU2] interpreted to represent charred litter or biomass from individual, local surface fire events within the peat-forming environment.

There are 3 charcoal horizons in pillar 91, 11 in pillar 78(a) and 26 in pillar 88(a). Twenty four of the twenty six charcoal horizons in pillar 88(a) occur in sapropelic lithotype units, LU2 and LU4. These lithotype units are also characterised by high

mineral matter contents (19-22%), scattered inertodetrinite (7%) and uncharred cuticle. The mix of charred and uncharred fractions may represent portions of charred and uncharred vegetation from the same area transported together. It is not possible to calculate fire return intervals for these sapropelic units using the method devised in section 4.4.9.

Charcoal horizons in three lithotype units from each pillar which represent comparable ombrotrophic mire depositional settings but variation in both number of charcoal horizons [78(a) LU2, 4 horizons; 88(a) LU7, 2 horizons; 91 LU2, 3 horizons] and cumulative charcoal horizon thicknesses in the coal pillar [78(a) LU2, 6.2mm; 91 LU2, 4.3mm; 88(a) LU7, 3mm] were used to demonstrate an approach to calculating fire return intervals (FRI). Mid-range values (7:1 peat to coal compaction ratio and 1mm/a^{-1} peat accumulation rate) give FRI of 7 years (extremes 0.5 to 143 years) for 78(a) LU2. Calculated FRI from 88(a) LU7 and 91 LU2 give comparable values of 69 years (extremes 5-1485 years) for 91 LU2 and 70 years (extremes 5-1550 years) for 88(a) LU7. The mid range values for these lithotype units demonstrate shorter FRI than seen in examples from modern peat-forming environments which range from 80 – 1100 years.

A record of both regional crown fires and local, surface fires is represented in these coal pillars. Despite the different depositional settings, and variations in mean inertinite content of the three coal pillars studied, they record similar wildfire type and occurrence in this Late Permian peat-forming environment.

CHAPTER 5

WITHIN SEAM VARIATION IN INERTINITE DISTRIBUTION AND IMPLICATIONS FOR INTERPRETING PALAEOWILDFIRE OCCURRENCE

5.1 INTRODUCTION

5.1.1 Factors influencing the production and dispersal of charcoal in modern wildfires

Petrographic work on three *in situ* coal pillars (see chapter 4) has shown that, total inertinite content, clast size of inertinite macerals, and their distribution vary temporally at a small scale between lithotype units, as well as between seams. It is therefore, also likely that inertinite content and distribution will vary within a single seam. In order to test this hypothesis, two additional *in situ* coal pillars from seams 78 and 88 have been studied using comparable petrographic techniques. Pillar 88(b), 1m from 88(a) (Fig. 5.1 A) and pillar 78(b) (Fig. 5.1 B) is 5km distant from 78(a). This study will document whether there is a range of inertinite content and distribution within a single seam.

The temporal variation in inertinite distribution observed between lithotype units may be related to charcoal production and dispersal from different wildfire types (chapter 4). Charcoal distribution, as a result of modern wildfire events, has also been shown to vary both spatially and temporally due to natural factors in addition to the fire type. Fires are complex natural phenomena whose burning characteristics vary spatially and temporally depending on the rate of fire spread, vegetation moisture, topography, climate, wind speed and direction, humidity, fuel types, fuel loading and local weather conditions during the fire (Peters and Higuera, 2007; DeLuca and Aplet, 2008; Belcher et al., 2010; Clay and Worrall, 2011). Furthermore, charcoal may be produced in large quantities at irregular intervals (Patterson et al., 1987). Experimental forest fires reported by Ohlson and Tryterud (2000) and Clark et al. (1998) suggest patchy and highly variable distribution of particles >0.5mm in size (Ohlson et al., 2006).

Lateral variation in charcoal distribution in peat profiles has been documented in the literature (e.g. Pitkänen et al., 2001; Ohlson et al., 2006) with only a few fire events able to be traced laterally across an entire site (Lavoie and Pellerin, 2007) and as a result little is known about spatial variability in the macroscopic charcoal record (Ohlson et al., 2006). Furthermore, mires and lake environments are not closed systems and charcoal may be lost (Patterson et al., 1987) over time by, burning from subsequent fires, slow chemical deterioration (only of the lower temperature charcoal; Ascough et al., 2011), biological degradation and physical fragmentation (Preston and Schmidt, 2006; Clay and Worrall, 2011). Therefore, the variability of these physical fire processes represent unknowns when interpreting wildfires in deep time. This necessitates the need to study more than one pillar in order to more fully interpret palaeowildfire occurrence in this Late Permian peat-forming environment.

5.2 METHODOLOGY

Coal pillars 78(b) and 88(b) (Fig. 5.1) were sampled from seams 78 and 88 using methods outlined in chapter 2.1.1. Production of polished blocks, petrography of *in situ* coal pillars, photography, XRD, and coal characterisation methodologies are the same as those used in chapter 4.2 (see also chapter 2.3, 2.4.2, 2.4.3, 2.4.5). Whole pillar inertinite averages were calculated (chapter 4.2.2) and presented in Table 5.1. Charcoal horizons were identified microscopically using the method in chapter 4.2.2.1.

Pillar	Transect	Total inertinite (%)	Standard deviation of transect means of inertinite (2 sd)	Whole pillar mean inertinite value (%)
78(b)	1	41.99	7.24	42.6
	2	39.35		
	3	46.50		
88(b)	1	34.35	5.14	37.1
	2	39.4		
	3	37.68		

TABLE 5.1 Pillar averages of inertinite point count data for each transect (using all points for that transect). The whole pillar mean inertinite content for each pillar is an average of the three total inertinite contents for each petrographic transect. The standard deviation for all transect means is also presented. All inertinite values are reported to a mineral matter free basis.

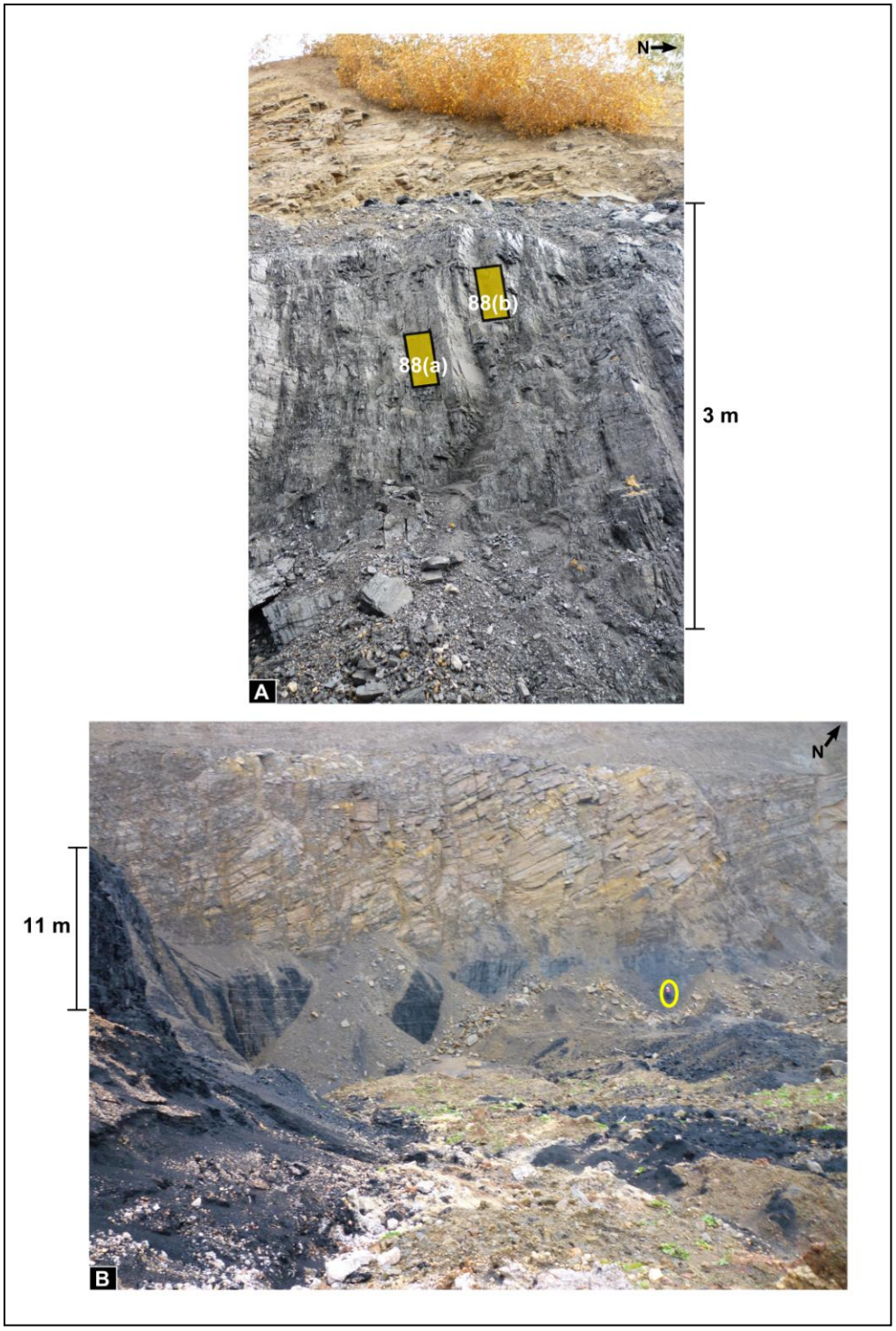

FIG. 5.1 Field photographs illustrating the position and size of sampled *in situ* coal pillars in relation to total seam thickness (compare to Fig. 4.1). **A** – Seam 88 (mine 1) and the position of pillars 88(a) (chapter 4) and 88(b) (this chapter) highlighted. **B –** Seam 78 (mine 1) 5km from pillar 78(a) (chapter 4). The yellow circle highlights the sampling locality of pillar 78(b) (this chapter).

5.3 RESULTS

5.3.1 Characterisation analysis and mineral content of pillars 78(b) and 88(b)

All lithotype units in both pillars have low %total Sulphur contents (<0.5% dry ash free basis) (Appendix 5). Pillar 78(b) ranges in %ash content from 4.4% (dry basis) (LU1-3; <1.9% mineral matter) to 12.96% (LU4-5; <10.7% mineral matter). Pillar 88(b) also shows a range from 3.2% ash (LU1-2; <3% mineral matter) to 6.3% (LU8; 6% mineral matter). Mineral matter in 78(b) and 88(b) pillars is predominantly quartz and kaolinite which is comparable to coal pillars from chapter 4 [78(a) and 88(a)] (compare Fig. 5.2 with Fig. 4.2). However, some lithotype units show variation in trace mineral content with 78(b) LU4-LU5 containing minor amounts of chlorite (Fig. 5.2) and 88(b) LU12 containing a trace of sulphur. However, 88(b) LU12 has one of the lowest %total Sulphur contents (0.23%; Appendix 5) suggesting these trace mineral occurrences are not present in large enough amounts to influence the overall properties of the coal.

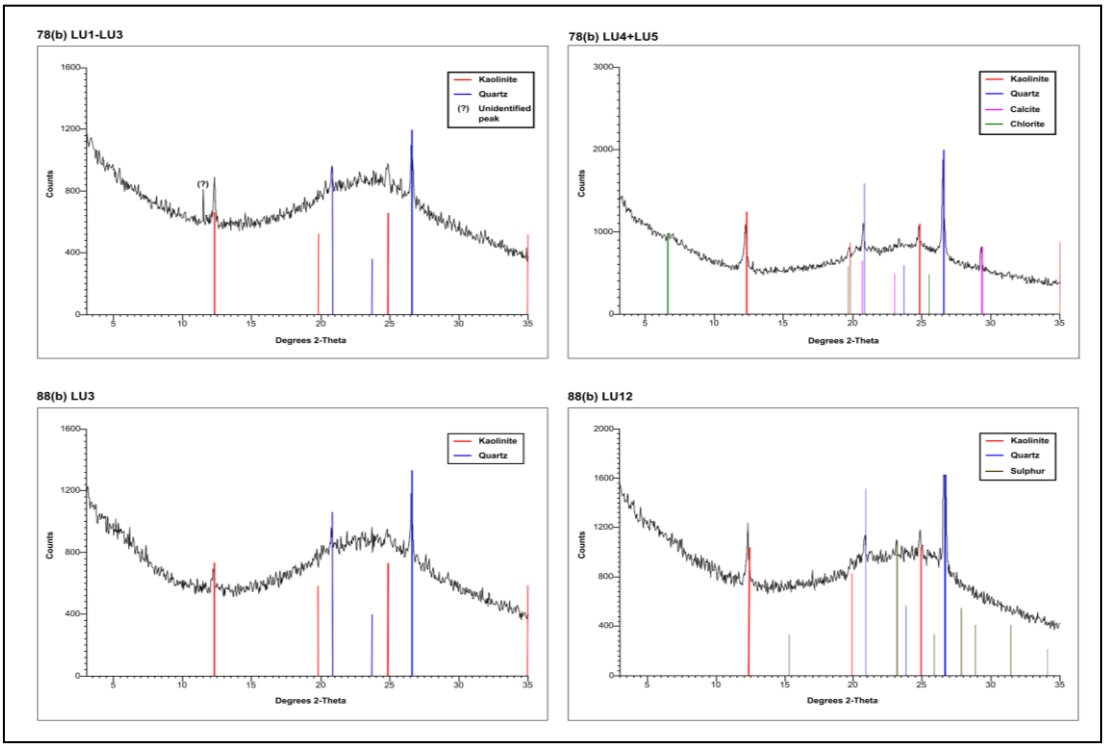

FIG. 5.2 XRD traces showing differences in mineral content both between coal pillars and between lithotype units in the same coal pillar. The area of elevated counts between 20-27 degrees 2-Theta on the background trace (black zig-zagged line) represents the organic matter content of the coal and the flatter the background trace, the higher the mineral content of the coal. The thickness of each coloured line represents the general abundance of that mineral scaled to the peak on the background trace. Red lines = kaolinite, blue = quartz, brown = Sulphur, pink = calcite, green = chlorite and a single unidentified peak [shown as (?)].

5.3.2 Petrographic results for coal pillars 78(b) and 88(b)

Comparable stacked bar charts of petrographic data for all lithotype units in pillars 78(b) and 88(b) are presented in Fig. 5.3 [compare to 78(a) and 88(a) in Fig. 4.3]. For raw petrographic point count data refer to Appendix 1.

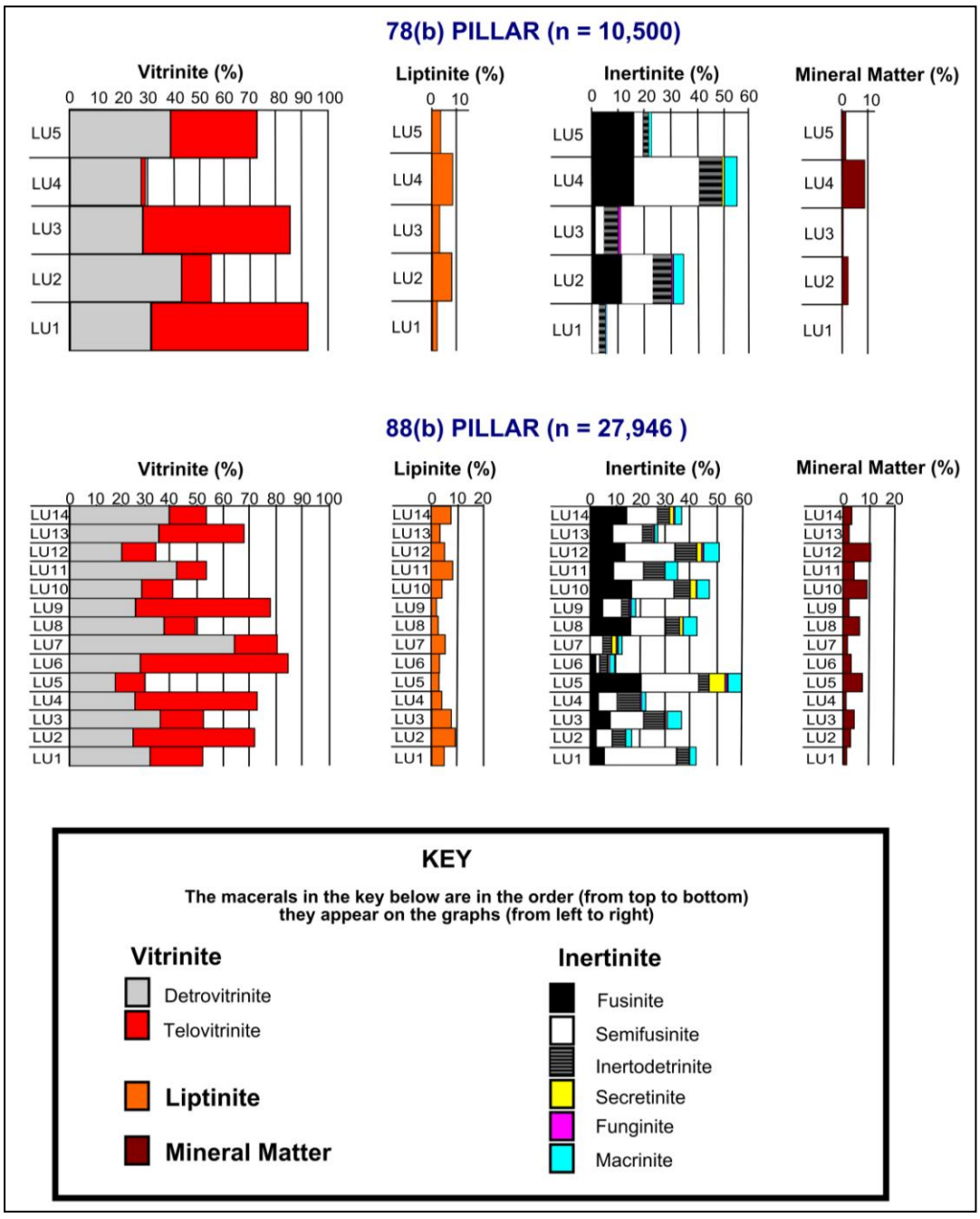

FIG. 5.3 Comparative stacked bar charts showing the petrographic point count results for the two coal pillars to a mineral included basis. Macerals were identified using ICCP schemes (1998; 2001) (defined in Table 2.3). The value next to the seam name corresponds to the total number of points counted for that pillar.

5.3.3 Inertinite distribution and abundance in pillar 78(b)

Petrographic results for individual lithotype units are illustrated in Fig. 5.3. The macroscopic appearance of the pillar is shown visually in a macrolithotype log (Fig. 5.5). The pillar is divided into five macroscopically distinct lithotype units (LU1-5) (Fig. 5.4; Fig. 5.5) which are bright (LU1, LU3), dull (LU2, LU4) and banded (LU5). Reflectance microscopy images representing each lithotype unit are presented in Fig. 5.6 and should be compared with Fig. 4.6 and Fig. 4.7.

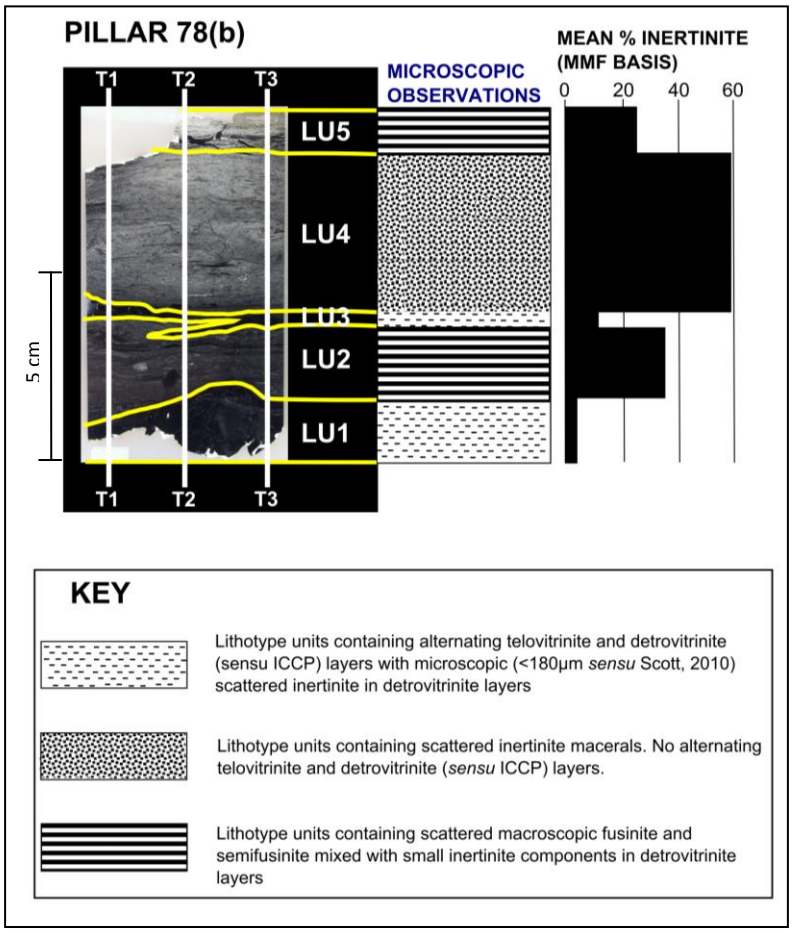

FIG. 5.4 Photograph of pillar 78(b) polished block highlighting the location and lateral variability of lithotype units (horizontal yellow lines across the block) as well as transect positions (white vertical lines) for petrographic analysis. The central column is a visual representation of the variation in inertinite distributions between lithotype units in 78(b) and the bar chart on the right is the total inertinite content (mineral matter free = mmf basis) for each lithotype unit.

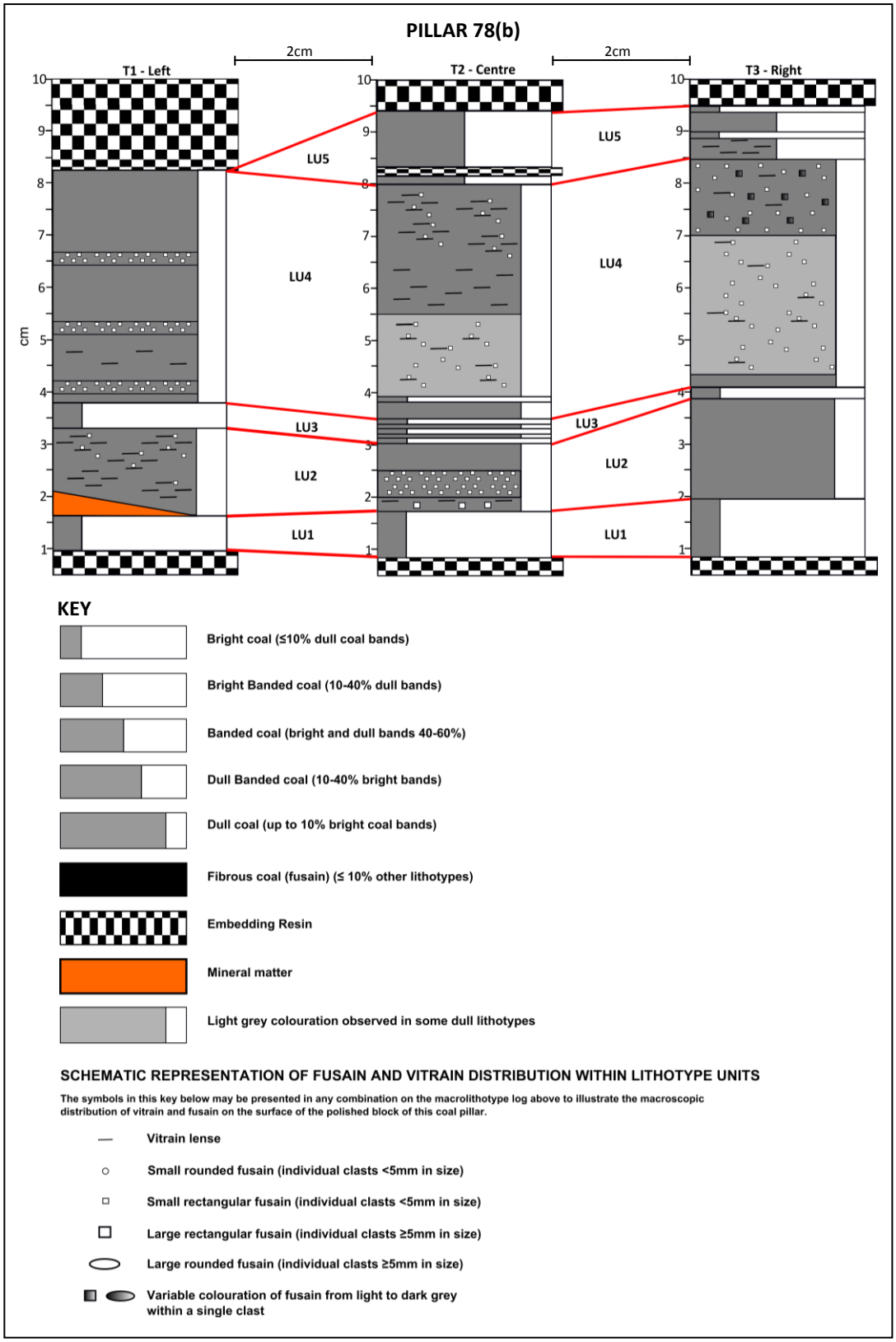

FIG. 5.5 Macrolithotype logs of pillar 78(b) showing location of lithotype unit divisions through the three transects studied (red lines), lateral variation in both lithotype unit thickness and position and fusain distribution in hand specimen. Lithotype units are described using Diessel's (1965) brightness scheme and patterns of vitrain and fusain distribution are own terms, this study. The vertical scale is in cm (shown in T1). Transect positions are shown on a photograph of the polished block in Fig. 5.4.

Inertinite is present in all five lithotype units (Fig. 5.4) from 5.8% (LU1) to 59% mineral matter free basis (LU4) with an overall pillar average of 42.6% mmf basis (2 sd = 7.2) (Table 5.1). Microscopically the majority of lithotype units contain alternating telovitrinite and detrovitrinite layers (Fig. 5.6 C, I). Patterns of inertinite distribution can be divided into three categories (as illustrated in Fig. 5.4).

(i) Detrovitrinite layers containing, scattered liptinite, mineral matter and microscopic inertinite (<180µm but commonly <20µm) (LU1, LU3; Fig. 5.6 B, F).

(ii) Detrovitrinite layers up to 3.4mm thick containing liptinite, inertodetrinite, macrinite, funginite (Fig 5.6 C, J) (LU2, LU5) and increasingly larger fusinite and semifusinite pieces (≤20mm) (LU2) (Fig. 5.6 D, I). Macroscopic inertinite clasts in LU2 and LU5 do not occur in layers that can be traced across the width of the block and therefore do not represent charcoal horizons (see definition, 4.2.2.1).

(iii) No alternating telovitrinite and detrovitrinite layers just a continuous single layer of detrovitrinite (LU4) with scattered inertinite, liptinite and mineral matter throughout (Fig. 5.6 G) which is visually comparable to 88(a) LU2, LU4, LU6 (chapter 4) but macerals in 78(b) LU4 are more discernible and hence identifiable due to the presence of more background vitrinite. This lithotype unit is also sapropelic (10% liptinite, mineral matter free basis; Appendix 1). Macroscopic clasts of fusinite and semifusinite (Fig. 5.6 H) can reach 1.3mm in size and occur in five concentrations throughout the LU. These inertinite clasts do not occur in a layer that can be traced across the block and are therefore not charcoal horizons (as in the definition in 4.2.2.1).

See overleaf for Fig. 5.6

FIG. 5.6

Representative images showing the range of inertinite distribution both within and between lithotype units from pillar 78(b) LU1-LU5. Scratches in the block are due to mineral grains that were plucked from the surface during polishing. Scale bar in **A** corresponds to 100µm and is the same for all images. FOV = field of view (given where known), T = transect.

Labels in white boxes represent inertinite, vitrinite and liptinite maceral groups, *sensu* ICCP (1998, 2001) (defined in Table 2.3): F = fusinite, SF = semifusinite, In = inertodetrinite, M = macrinite, Fu = funginite, TV = telovitrinite, DV = detrovitrinite, L = liptinite and mineral matter = MM.

A, B = 78(b) LU1. **A -** (T1) Telovitrinite layer containing no inertinite or liptinite macerals. **B** – (T3) Detrovitrinite layer, with scattered inertodetrinite, macrinite, liptinite and mineral matter.
C, D = 78(b) LU2. **C -** (T3) Alternating telovitrinite and telovitrinite layers with microscopic scattered inertodetrinite, macrinite, liptinite and mineral matter in detrovitrinite layers. **D -** (T2) Clasts of macroscopic fusinite and semifusinite in a detrovitrinite layer. These clasts do not occur in a layer that can be traced across the width of the block and are therefore not part of a charcoal horizon.
E, F = 78(b) LU3. **E** – (T2) Telovitrinite layer with rare microscopic inertinite. **F** – (T2) Scattered microscopic inertinite, liptinite and mineral matter in a detrovitrinite layer.
G, H = 78(b) LU4. **G –** (T1) No alternating telovitrinite and detrovitrinite layers, scattered inertinite, liptinite and mineral matter throughout. Note that there is more identifiable vitrinite than seen in 88(a) (compare to Fig. 4.11 C, G; Fig. 4.12 C, D). This pattern of maceral distribution represents the entirety of LU4. **H -** (T3) Macroscopic semifusinite and fusinite clasts. These do not occur in a layer that is traceable across the block and therefore not part of a charcoal horizon.
I, J = 78(b) LU5. **I –** (T2) Telovitrinite and detrovitrinite layers with scattered microscopic inertinite, liptinite, mineral matter and macroscopic fusinite. **J –** (T2) Scattered, microscopic inertinite macerals in a detrovitrinite layer.

FIG. 5.6

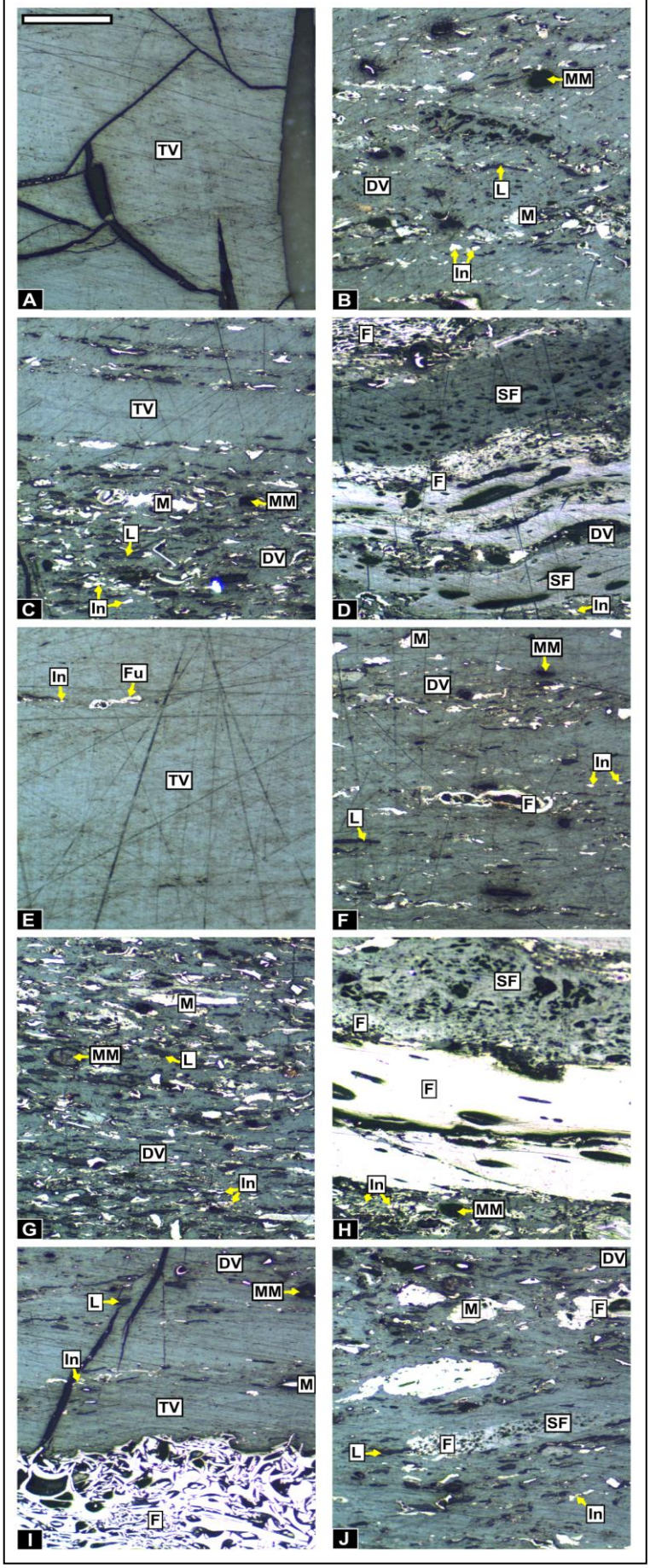
A
TV
B
MM
DV
L
M
In
C
TV
M
MM
L
DV
In
D
F
SF
F
DV
SF
In
E
In
Fu
TV
F
M
MM
DV
In
F
L
G
M
MM
L
DV
In
H
SF
F
F
In
MM
I
DV
L
MM
In
M
TV
F
J
DV
M
F
SF
L
F
In

5.3.4 Inertinite distribution and abundance in pillar 88(b)

Petrographic results are shown in Fig. 5.3. Macroscopically, the pillar can be sub-divided into 14 visually distinct lithotype units (Fig. 5.7; Fig. 5.8). Reflectance microscopy images representing each lithotype unit are shown in Figs. 5.9 - 5.11 and should be compared with Figs. 4.11 and 4.12.

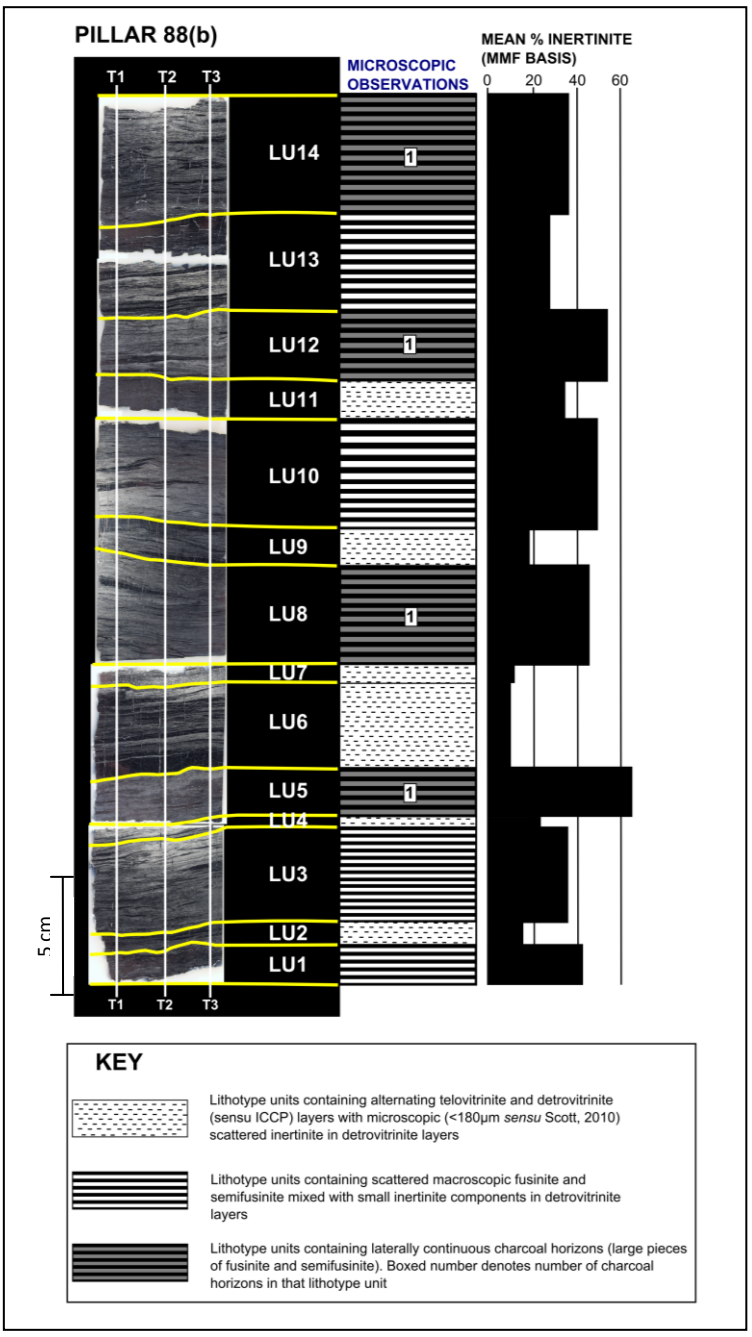

FIG. 5.7 Photographs of the polished blocks that make up pillar 88(b) highlighting the location and lateral variability of lithotype units (horizontal yellow lines across the block) as well as transect positions (white vertical lines) for petrographic analysis. The central column is a visual representation of the variation in inertinite distributions between lithotype units in 88(b) and the bar chart on the right is the total inertinite content (mmf basis) for each lithotype unit.

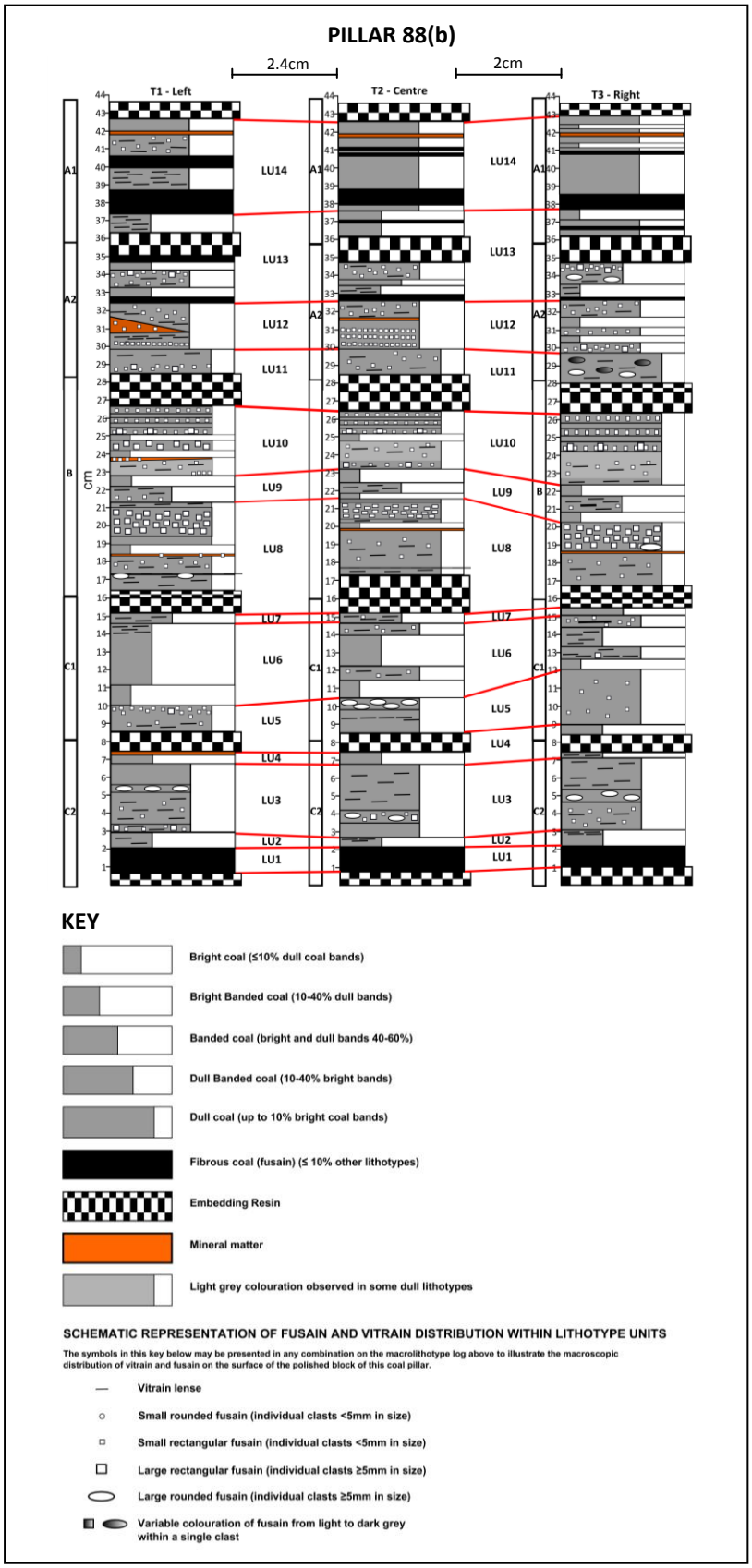

FIG. 5.8 Macrolithotype logs of pillar 88(b) showing location of lithotype unit divisions through the three transects studied (red lines), lateral variation in both lithotype unit thickness and position and fusain distribution in hand specimen. Lithotype units are described using Diessel's (1965) brightness scheme and patterns of vitrain and fusain distribution are own terms, this study. The vertical scale is in cm (shown in T1). Transect positions are shown on a photograph of the polished block in Fig. 5.7.

Pillar 88(b) contains inertinite in every lithotype unit from 9.8% (LU6) to 65.6% (LU5) mineral matter free basis (Fig. 5.7). The mean pillar average is 37.1% mmf basis (2 sd = 5.1) (Table 5.1).

Microscopically the lithotype units all contain alternating detrovitrinite and telovitrinite layers (illustrated in, Fig. 5.9 C, E, F, H; Fig. 5.10 H; Fig. 5.11 A). The majority of telovitrinite layers contain inertodetrinite, liptinite and mineral matter (Fig. 5.9 C, E, H; Fig. 5.10 H; Fig. 5.11 F). Inertinite distribution can be divided into the three categories also observed in pillars 78(a), 88(a) (chapter 4) and pillar 78(b) (this chapter).

(i) Detrovitrinite layers with scattered liptinite, mineral matter and microscopic inertinite (<180µm but commonly <20µm) (LU2, LU4, LU6, LU7, LU9, LU11; Fig. 5.7; Fig. 5.9 C, D, G, H; Fig. 5.10 A-D, F, G; Fig. 5.11 A, B) with 1-2 clasts of fusinite and semifusinite >425µm in size (e.g. Fig. 5.9 D). In addition, the inertodetrinite in LU6 is high reflecting and resembles fragments of cell walls (Fig. 5.10 B). Some of the vitrinite is collodetrinite (ICCP, 1998) and contains cutinite and clay minerals (Fig. 5.10 A, C; LU6, LU7).

(ii) Detrovitrinite layers containing scattered liptinite, mineral matter and microscopic and/or macroscopic inertinite occur in, LU1, LU3, LU10, LU13 (Fig. 5.7; Fig. 5.9 A, B, E, F; Fig. 5.10 H, I; Fig. 5.11 E, F). The macroscopic fusinite and semifusinite clasts (mostly ~3mm, up to 30mm in size) do not occur in layers that can be traced across the block and are therefore not classified as charcoal horizons (see definition 4.2.2.1). Clasts surrounded by vitrinite are typically larger than those associated with mineral matter and other inertinite macerals. Cutinite is also generally more abundant in detrovitrinite layers with macroscopic inertinite (LU13; Fig. 5.11 E). Fusinite and semifusinite clasts show variable qualitative reflectance from grey semifusinite with cuticle attached to white fusinite, to a continuum of reflectance from grey to white within a single clast (LU1; Fig. 5.9 A). Detrovitrinite layers above those containing macroscopic inertinite contain microscopic inertinite macerals (typically <20µm, a few fusinite and semifusinite clasts >425µm) and more liptinite (e.g. LU10; Fig. 5.10 H). The vitrinite is typically collodetrinite (ICCP, 1998) and contains high reflecting inertodetrinite (LU13).

(iii) Charcoal horizons are laterally continuous layers of macroscopic clasts of fusinite and semifusinite [e.g. LU5 (Fig. 5.9 J), LU8 (Fig. 5.10 E), LU12 (Fig. 5.12), LU14 (Fig. 5.11 H)] as opposed to a single continuous band of inertinite. Individual charcoal horizon thicknesses range from 1.3mm (LU12, LU14) to 3.4mm (LU5). Individual fusinite and semifusinite clasts (up to 4.7mm in length) in these horizons are of variable reflectance and each LU contains comparable portions of fusinite and semifusinite (Fig. 5.3). In LU8 the fusinite and semifusinite clasts in the charcoal horizon are surrounded by microscopic (<180µm) inertinite fragments which may be derived from the larger pieces (Fig. 5.10 E). Detrovitrinite layers between charcoal horizons contain either microscopic or macroscopic (>425µm) inertinite or a combination of sizes (Fig. 5.9 I; Fig. 5.10 D; Fig. 5.11 C, G). Some of the microscopic inertinite (<10µm) surrounding macroscopic inertinite clasts consists of high reflecting cell wall fragments [LU5, LU8, LU12, LU14 (labelled 'In' in, Fig. 5.9 I, Fig. 5.11 E)] particularly in detrovitrinite layers below and above those containing concentrations of macroscopic inertinite or charcoal horizons.

See overleaf for Fig. 5.9

FIG. 5.9

Representative images showing the range of inertinite distribution both within and between lithotype units from pillar 88(b) LU1-LU5. Scale bar in **A** corresponds to 100µm and is the same for all images. FOV = field of view in given T = transect.

Labels in white boxes represent inertinite, vitrinite and liptinite maceral groups, *sensu* ICCP (1998, 2001) (defined in Table 2.3): F = fusinite, SF = semifusinite, In = inertodetrinite, M = macrinite, TV = telovitrinite, DV = detrovitrinite, L = liptinite. Mineral matter = MM.

A, B = 88(b) LU1. **A –** (T2 FOV6) Central inertinite clast showing gradation in qualitative reflectance from grey (semifusinite) to white (fusinite) in a detrovitrinite layer containing scattered inertinite, liptinite and mineral matter. **B –** (T1) Macroscopic clasts of fusinite and semifusinite. One of the semifusinite clasts still has cuticle attached. These clasts do not occur in a layer that can be traced across the block and are therefore not part of a charcoal horizon.
C, D = 88(b) LU2. **C –** (T1) Telovitrinite and detrovitrinite layer with scattered inertinite macerals in detrovitrinite layer. **D –** (T3 FOV25) Detrovitrinite layer with scattered inertodetrinite, macrinite, liptinite and mineral matter and a rare macroscopic clast of semifusinite.
E, F = 88(b) LU3. **E -** (T3 FOV68) Alternating telovitrinite and detrovitrinite layers with microscopic (<180µm) scattered inertodetrinite and macrinite in detrovitrinite layers. **F -** (T3 FOV49) Macroscopic clasts of fusinite and semifusinite, these clasts do not occur in a layer that can be traced across the block and are therefore not part of a charcoal horizon.
G, H = 88(b) LU4. **G -** (T3 FOV2) Telovitrinite and detrovitrinite layers with scattered inertodetrinite, liptinite and mineral matter. **H -** (T1) Alternating telovitrinite and detrovitrinite layers with scattered microscopic inertinite macerals in detrovitrinite layers.
I, J = 88(b) LU5. **I -** (T3 FOV8) Scattered inertinite macerals of variable qualitative reflectance in a detrovitrinite layer. Note that some of the inertodetrinite pieces are angular and appear to be fragments of high reflecting cell walls. **J -** (T2 FOV116) Macroscopic fusinite clasts. These clasts occur in a layer that can be traced across the width of the block and therefore represent part of a charcoal horizon.

FIG. 5.9

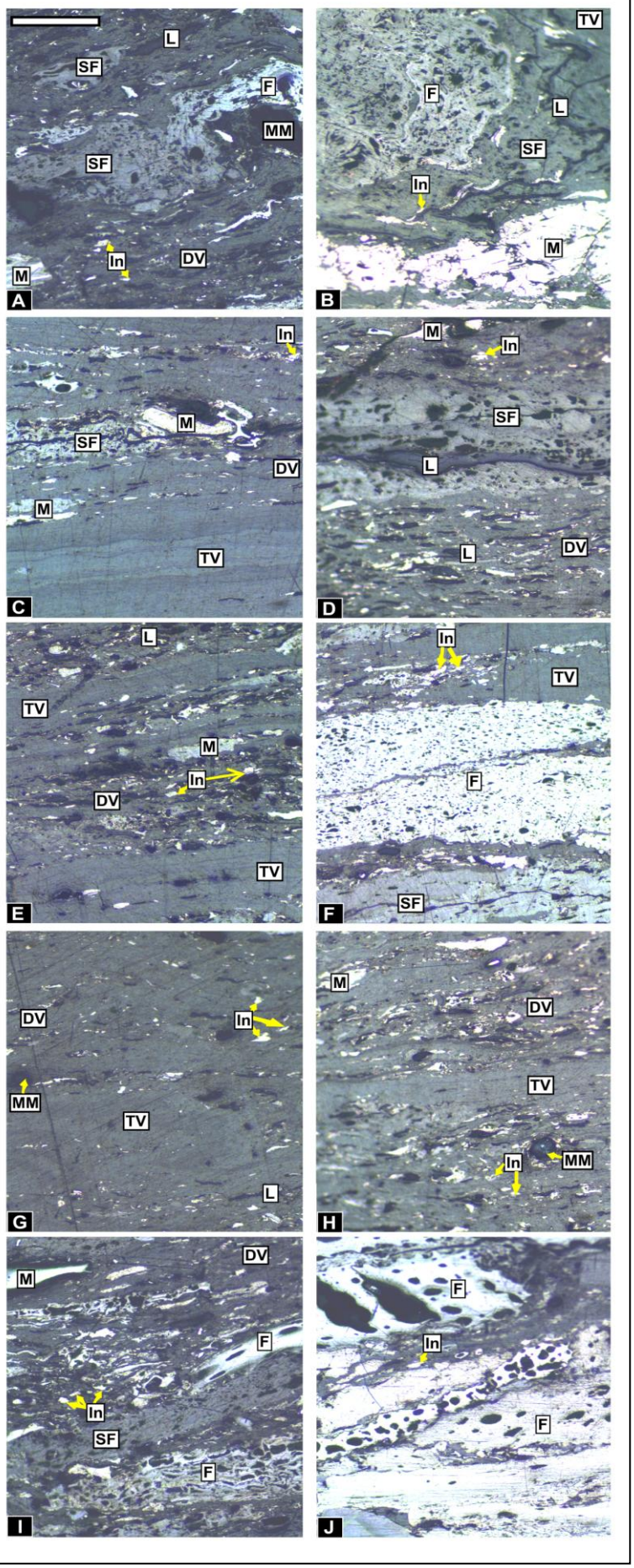
A
L
SF
F
MM
SF
In
DV
M
B
TV
F
L
SF
In
M
C
In
M
SF
DV
M
TV
D
M
In
SF
L
L
DV
E
L
TV
M
In
DV
TV
F
In
TV
F
SF
G
DV
In
MM
TV
L
H
M
DV
TV
In
MM
I
DV
M
F
In
SF
F
J
F
In
F

See overleaf for Fig. 5.10

FIG. 5.10

Representative images illustrating the range of inertinite distribution both within and between lithotype units from pillar 88(b) LU6-LU10. Scale bar in **A** corresponds to 100µm and is the same for all images. FOV = field of view in given T = transect.

Labels in white boxes represent inertinite, vitrinite and liptinite maceral groups, *sensu* ICCP (1998, 2001) (defined in Table 2.3): F = fusinite, SF = semifusinite, In = inertodetrinite, M = macrinite, TV = telovitrinite, DV = detrovitrinite, CG = corpogelinite, L = liptinite. Mineral matter = MM.

A, B = 88(b) LU6. **A -** (T2 FOV55) Telovitrinite and detrovitrinite (collodetrinite) layers with scattered qualitatively high reflecting inertodetrinite and liptinite in the collodetrinite layers. **B -** (T3 FOV42) Microscopic (<180µm) scattered inertinite macerals in a detrovitrinite layer. Note that some of the inertodetrinite particles appear to be fragments of cell walls.
C = 88(b) LU7 (T3 FOV84) Microscopic (<100µm) scattered high reflecting inertodetrinite, liptinite and mineral matter in detrovitrinite (collodetrinite).
D, E = 88(b) LU8. **D -** (T3 FOV20) Scattered inertinite, liptinite and mineral matter in a detrovitrinite layer. **E -** (T2 FOV39) macroscopic fusinite and semifusinite. These clasts occur in a layer that can be traced across the width of the block and therefore represent part of a charcoal horizon.
F, G = 88(b) LU9. **F -** (T1 FOV65) Scattered microscopic inertinite, corpogelinite, liptinite and mineral matter in a detrovitrinite layer. **G -** (T1 FOV72) Scattered inertinite, liptinite and mineral matter in detrovitrinite layers.
H, I = 88(b) LU10. **H -** (T3 FOV78) Alternating detrovitrinite and telovitrinite layers with scattered inertinite, liptinite and mineral matter in detrovitrinite layers. **I –** (T2 FOV104) Macroscopic high reflecting fusinite and macrinite. These clasts do not occur in a layer that can be traced across the block and are therefore not classed as a charcoal horizon.

FIG. 5.10

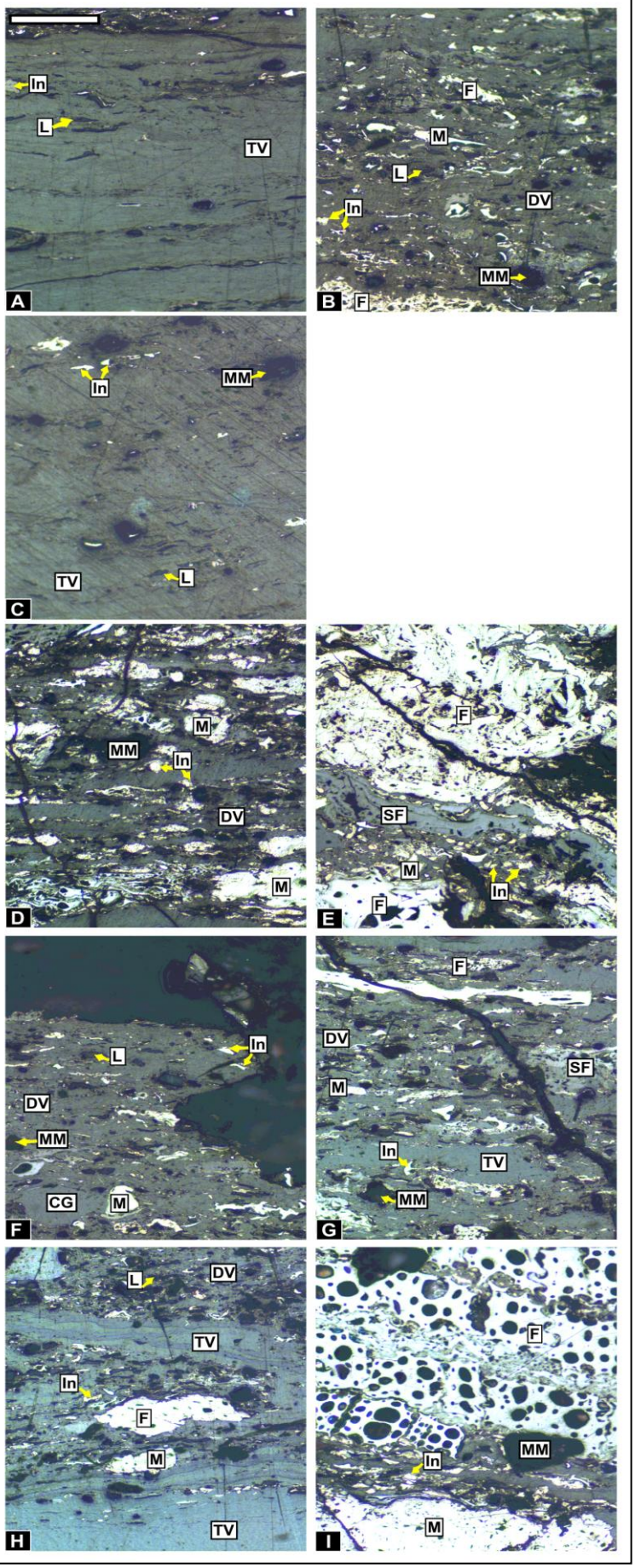
In
L
TV
A
F
M
L
DV
In
MM
B
F
In
MM
TV
L
C
M
MM
In
DV
M
D
F
SF
M
In
F
E
L
In
DV
MM
CG
M
F
F
DV
SF
M
In
TV
MM
G
L
DV
TV
In
F
M
TV
H
F
MM
In
M
I

See overleaf for Fig. 5.11

FIG. 5.11

Representative images illustrating the range of inertinite distribution both within and between lithotype units from pillar 88(b) LU11-LU14. Scale bar in the top left corner of image A corresponds to 100µm and is the same for all images. FOV = field of view in given T = transect.

Labels in white boxes represent inertinite, vitrinite and liptinite maceral groups, *sensu* ICCP (1998, 2001) (defined in Table 2.3): F = fusinite, SF = semifusinite, In = inertodetrinite, M = macrinite, Fu = funginite, TV = telovitrinite, DV = detrovitrinite, L = liptinite. Mineral matter = MM.

A, B = 88(b) LU11. **A –** (T1) Telovitrinite and detrovitrinite layers with scattered microscopic inertinite, liptinite and mineral matter in detrovitrinite layers. **B –** (T3 FOV2) Rare occurrence of macroscopic fusinite.
C, D = 88(b) LU12. **C -** (T3 FOV28) Detrovitrinite layer containing scattered inertinite macerals, liptinite and mineral matter. **D -** (T2 FOV56) Macroscopic fusinite and semifusinite clasts and scattered inertinite and liptinite macerals in a detrovitrinite layer. This lithotype unit also contains a charcoal horizon (part of which is illustrated in Fig 5.12).
E, F = 88(b) LU13. **E -** (T2 FOV68) Cuticle-rich (labelled 'L') detrovitrinite layer containing scattered inertinite macerals. Some inertodetrinite pieces are angular in shape and may represent fragments of cell walls. **F -** (T3 FOV85) Macroscopic clasts of fusinite. These do not occur in layer that can be traced across the block and are therefore not part of a charcoal horizon.
G, H = 88(b) LU14. **G -** (T1) Scattered inertinite, liptinite and mineral matter in a detrovitrinite layer. **H -** (T2 FOV29) Macroscopic clasts of fusinite and semifusinite. These clasts occur in a layer that can be traced across the width of the block and therefore represent part of a charcoal horizon.

FIG. 5.11

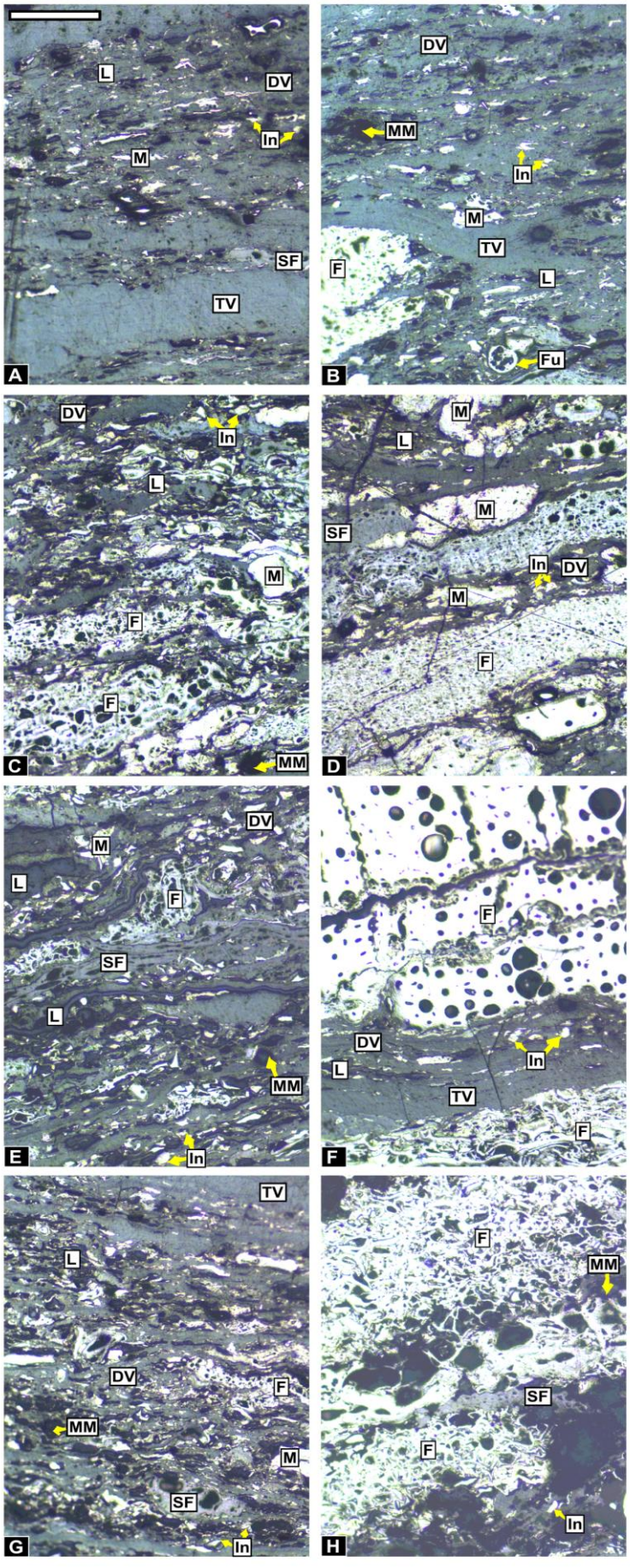
A
L
DV
In
M
SF
TV
B
DV
MM
In
M
TV
F
L
Fu
C
DV
In
L
M
F
F
MM
D
M
L
M
SF
In
DV
M
F
E
DV
M
L
F
SF
L
MM
In
F
F
DV
In
L
TV
F
G
TV
L
DV
F
MM
M
SF
In
H
F
MM
SF
F
In

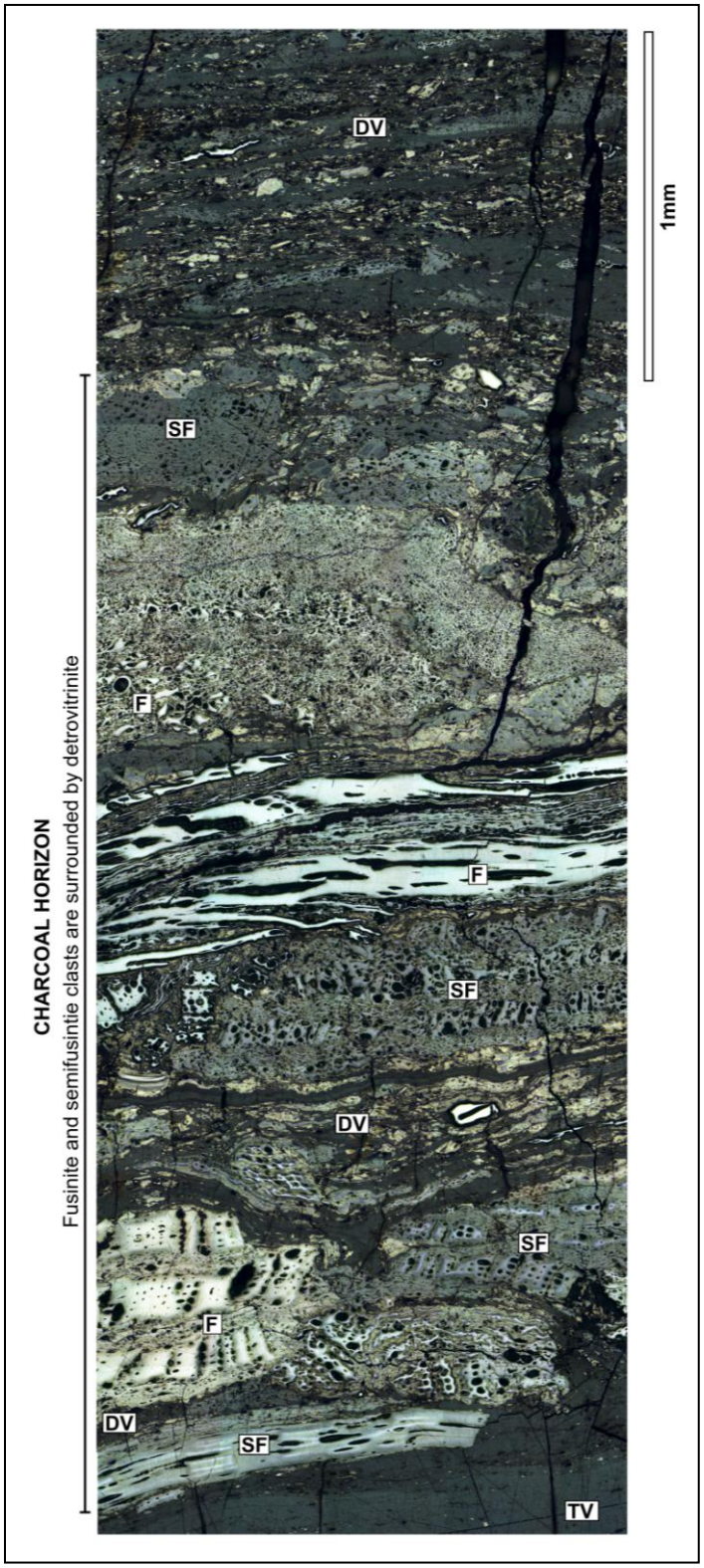

FIG. 5.12 Montaged images (n = 95) showing a representative 1.5mm by 4.5mm section of coal pillar 88(b) LU12 which contains one charcoal horizon (labelled). The charcoal horizon persists laterally across the block. There is a narrow detrovitrinite matrix between the macroscopic fusinite and semifusinite clasts which is typical for charcoal horizons. This is in contrast to the much wider detrovitrinite layer above the charcoal horizon and the telovitrinite layer below. Labels in white boxes correspond to: DV = detrovitrinite, TV = telovitrinite, F = fusinite, SF = semifusinite.

5.3.5 Other entities in pillars 78(b) and 88(b) of variable reflectance

Entities were observed in pillars 78(b) and 88(b) (Figs. 5.13 - 5.15) that would be classified petrographically as liptinite. They fluoresce from brown (Fig. 5.15 A) to orange (Fig. 5.14 B, D) to yellow (Fig. 5.14 F, H) and under high magnification (×50) (with ×10 eyepiece magnification) using fluorescence microscopy show variable internal structure from indiscernible (Fig. 5.14 F, H), to fragments of plant material (Fig. 5.14 B; Fig. 5.15 A), to clusters of entire spores (Fig. 5.14 D). In addition, some of the entities containing spores appear to have a partial thin cellular coating which has a bright yellow fluorescence (white arrows in Fig. 5.14 D, H).

Only one entity in all five coal pillars studied in this thesis (chapter 4 and this chapter) appears to be associated with plant material, in this case folded cuticle (illustrated in Fig. 5.13 B and Fig. 5.15). The cuticle and the entity show comparable fluorescence (Fig. 5.15 A) therefore the entity may contain cuticle.

In total pillar 88(b) has 101 entities of liptinite colouration (in: LU1, LU7, LU10, LU11, LU12 and LU14) and 94 of these occur in a single detrovitrinite layer in 88(b) LU10 between T2 and T3 (FOV 84), part of which is illustrated in Fig. 5.13 A and selected individual entities from this layer are shown in Fig. 5.14. They have a rounded to oblate spheroidal morphology (Fig. 5.13 A, B) and range from 100µm-425µm in size along the longest axis. In addition, several of these entities with liptinite colouration have telovitrinite perimeters [Fig 5.13 A (labelled ‘1’ and ‘2’); Fig. 5.14 E] which do not fluoresce (Fig. 5.14 F) but the liptinite interior consistently has a bright yellow fluorescence (Fig. 5.14 F). This telovitrinite perimeter is not observed in any other entities from any other lithotype units studied in this thesis (chapter 4, this chapter). Six entities also show a continuum of qualitative reflectance from low (comparable to vitrinite) to high (fusinite) (Fig. 5.13 C-E).

See overleaf for Fig. 5.13

FIG. 5.13

Representative images illustrating the range in occurrence of entities (labelled E in white box) (**A-E**), their associations with other macerals (**A-E**) or botanical entities (**B**) and variation in qualitative reflectance (**C-E)**. Scale bars correspond to 100µm. LU = lithotype unit, FOV = field of view in given T = transect.

A - 88(b) LU10 (T2 FOV84) Montage of 23 images illustrating a detrovitrinite layer which contains 94 entities of liptinite colouration, that show varying size and morphology (some entities are labelled). The entities labelled '1' and '2' both have telovitrinite perimeters and a higher magnification image of the entity labelled '1' is shown in Fig. 5.14 E, F.

B - 78(b) LU1 (T3) Montage of 6 images illustrating an entity of liptinite colouration which appears to be associated with folded cuticle. The entity (labelled '3') is shown in a high magnification image in Fig. 5.15 A, B.

C - 88(b) LU14 (T2 FOV74) Dark grey entity with qualitative reflectance comparable to vitrinite (entity itself highlighted by yellow circle).

D – 88(b) LU10 (T1 FOV128) Entity with comparable qualitative reflectance to semifusinite and containing higher reflecting components.

E – 88(b) LU14 (T2 FOV24) Entity of fusinite qualitative reflectance.

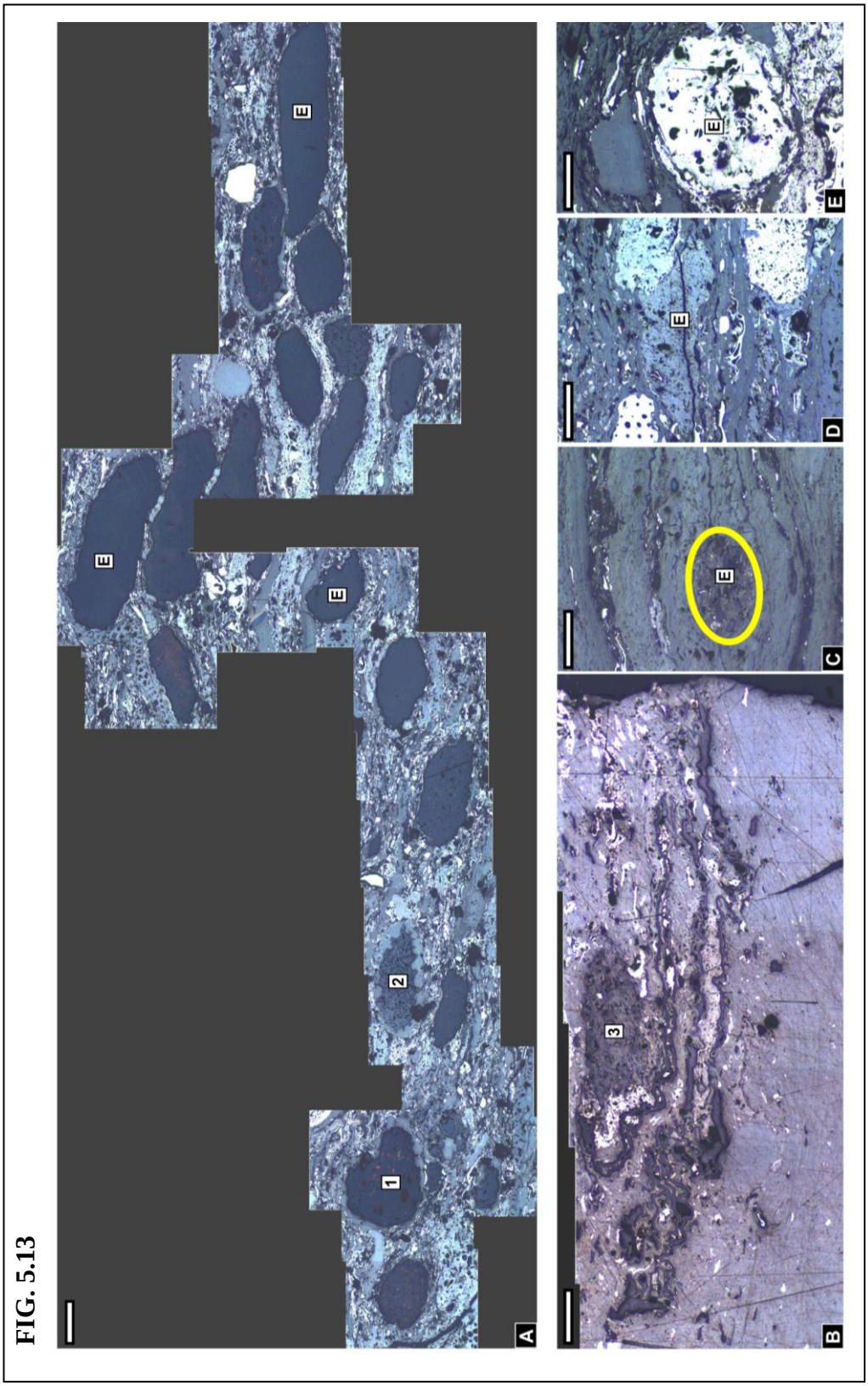

FIG. 5.13

See overleaf for Fig. 5.14

FIG. 5.14

Comparative reflectance (**A, C, E, G**) and fluorescence **(B, D, F, H)** high magnification (×50) images illustrating the variation in, composition, morphology and fluorescence of entities with liptinite colouration (labelled L). All images are from 88(b) LU10 (T2 FOV84) (Fig. 5.13 A). Scale bars in all images correspond to 100µm.

Labels in white boxes represent inertinite, vitrinite and liptinite maceral groups (*sensu* ICCP, 1998, 2001): F = fusinite, SF = semifusinite, In = inertodetrinite, M = macrinite, TV = telovitrinite, L = liptinite, MM = mineral matter.

A, B - Montage of 7 images showing an entity composed of indiscernible plant material which has a comparable fluorescence to spores (compare to **D**).

C, D - Montage of 2 images illustrating an entity which contains recognisable spores. The white arrows in **D** point to bright yellow fluorescing, possible cellular material that may be attached to the entity.

E, F - Montage of 8 images illustrating an entity with a telovitrinite perimeter **(E)** which does not fluoresce (see white arrows in **F**). All entities that have this telovitrinite perimeter all have a strong yellow fluorescing interior (**F**).

G, H – Montage of 2 images illustrating the range in morphology of these entities. This entity may contain spores (**H**). The white arrow in **H** points to bright yellow, fluorescing, possible cellular material that may be attached to the entity.

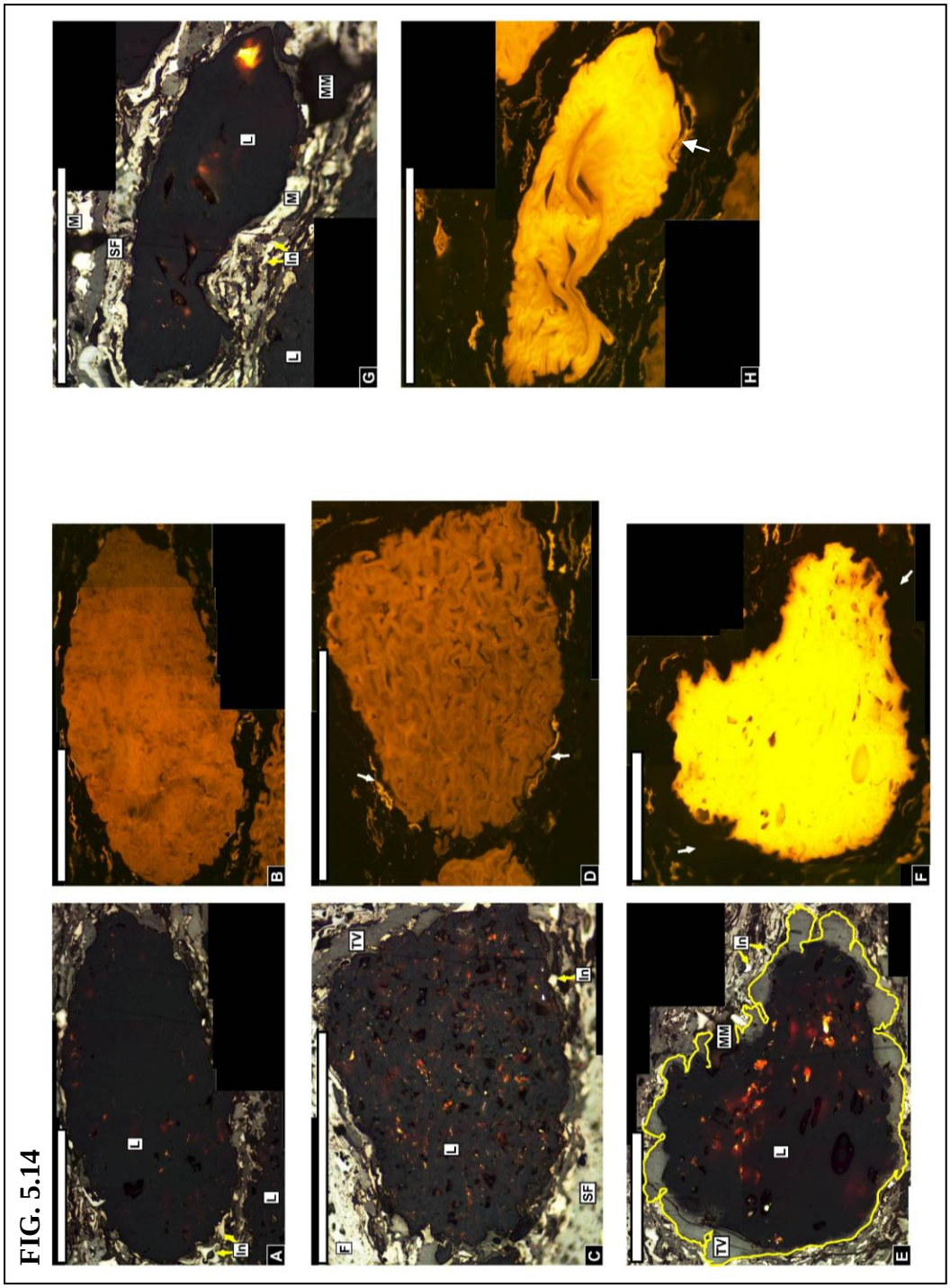

FIG. 5.14

FIG. 5.15

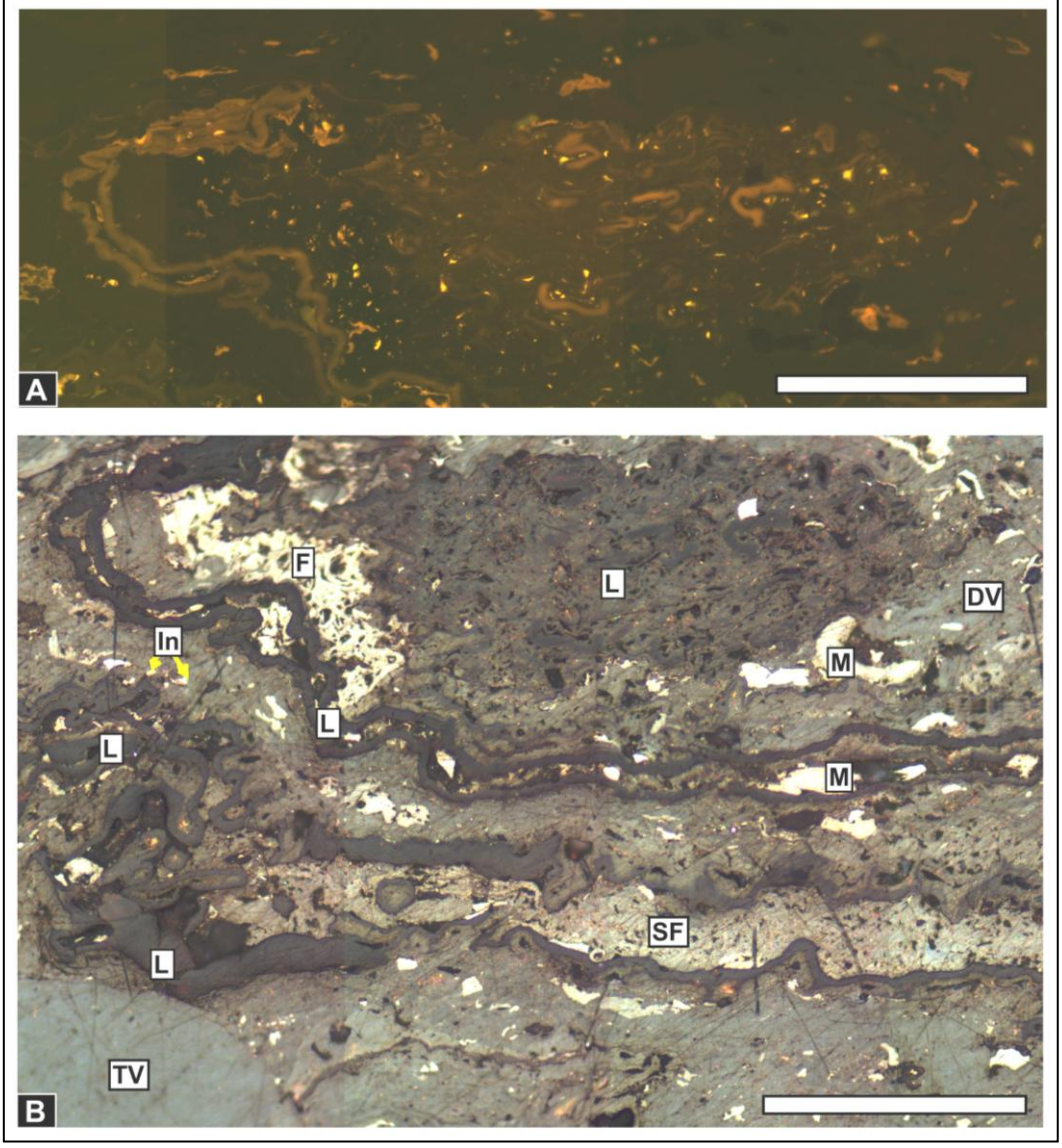

FIG. 5.15 Comparative high magnification montaged images showing both fluorescence **(A,** 5 images**)** and reflectance **(B,** 10 images**)** microscopy images of an entity of liptinite colouration from 78(b) LU1 associated with plant cuticle (compare to Fig. 5.13 B). Scale bars (bottom right) correspond to 100µm. Labels in white boxes represent inertinite, vitrinite and liptinite maceral groups (*sensu* ICCP, 1998, 2001): F = fusinite, SF = semifusinite, In = inertodetrinite, M = macrinite, TV = telovitrinite, DV = detrovitrinite, L = liptinite.

5.4 DISCUSSION

5.4.1 Environment of deposition

Environment of deposition of these Late Permian coal seams is discussed in chapter 3 and chapter 4.4.2. Pillar 78(b) (LU1-3, LU5) contains low %ash (4.4% dry basis) and low %total Sulphur contents (0.35% dry ash free basis) (Appendix 5). All lithotype units in pillar 88(b) also contain low %ash (<6.3% dry basis) and low

%total Sulphur (<0.47% dry ash free basis) (Appendix 5). These characteristics are typical of coals from an ombrotrophic mire setting (Cohen et al., 1987; Moore, 1987; Scott, 1989b). However, 78(b) LU4 has high %ash content (13% dry basis) and low %total Sulphur (0.4% dry ash free basis) and high liptinite content (10% mineral matter free basis) which is comparable to lithotype units from mire lake depositional settings [i.e. 88(a) LU2, LU4; chapter 4.4.2].

5.4.2 Coprolites and sporangia in pillars 78(b) and 88(b) of variable reflectance

The identification of entities is discussed in chapter 4.4.3.1 and their palaeoecological interpretation in section 4.4.3.3. The specimens observed in pillars 78(b) and 88(b) show, distribution in large numbers (Fig. 5.13 A), more variation in morphology (Fig. 5.13 A, C-E) and possible association with plant material (Fig. 5.13 B; Fig. 5.15) compared to pillars 78(a) and 88(a) (Fig. 4.17). The entities are primarily composed of spores (Fig. 5.14) with only one composed of cuticle (Fig. 5.13 B; Fig. 5.15).

In order to determine whether some of the specimens in Fig. 5.13 A were coprolites or sporangia, comparative high magnification (×50 objective, ×10 eyepiece magnification) reflectance and fluorescence images were taken (Fig. 5.14; Fig. 5.15). Identification is still not simple, for example, the interior of the entity shown in Fig. 5.14 B contains unrecognisable plant material but with the same fluorescence as the spores observed in Fig. 5.14 D. No attached sporangial wall was observed (Fig. 5.14 B) and the lack of recognisable plant material suggests that this may be a coprolite produced by a sporivore, or a detrivore, or it may represent a partially decomposed sporangia. Fig. 5.14 D shows fragments of a thin cellular layer around the exterior (white arrows). This is only observed under high magnification and suggests that this specimen may be a sporangium (or possible pollen organ). Fig. 5.14 G, H shows complex internal morphology and yellow fluorescence suggesting it has undergone a lower level of thermal alteration (Teichmüller, 1986) than specimens in Fig. 5.14 A-D. The interior appears to be spores and there appear to be small fragments possibly of sporangial wall attached (white arrow on Fig. 5.14 H) suggesting that this is also a sporangium (or possible pollen organ). In contrast, Fig. 5.13 B and Fig. 5.15 contain fragments of mixed plant material and the specimen can be identified as a coprolite.

Another feature not observed in specimens in pillars 78(a) or 88(a) are telovitrinite perimeters [Fig 5.13 A (labelled '1' and '2'); Fig. 5.14 E] which do not fluoresce, in contrast to the liptinite interior, which always has a bright yellow fluorescence (Fig. 5.14 F). This telovitrinite perimeter is only observed on a few specimens in a layer containing 94 (Fig. 5.13 A). The telovitrinite perimeter may represent liptinite transformed into liquid bituminous products (Teichmüller and Durand, 1983) which may be the result of charring. The fact that the specimen is not wholly vitrinite suggests that it has been partially charred, either at a low temperature or for a short duration. The bright yellow fluorescence suggests a lower level of thermal alteration (0-0.4% Ro) compared to the orange fluorescence seen in other specimens (0.4-1% Ro) (Teichmüller, 1986) which suggests that perhaps the charring sets the liptinite fluorescence at a lower level that is then not altered by the coalification process. An alternative interpretation is that the telovitrinite perimeter represents the thick wall of a sporangium or synangium.

5.4.3 Interpretation of wildfire type and occurrence in pillar 78(b)

5.4.3.1 Evidence for wildfires: charcoal occurrence

Inertinite is present in all lithotype units in varying amounts from 5.8% (LU1) to 59% (LU4) (Fig. 5.4) with an overall pillar average of 42.6% to a mineral matter free basis (2 sd= 7.2) (Table 5.1). The variation in inertinite content between lithotype units may be related to differences in wildfire occurrence and fire type in the peat-forming environment throughout the formation of this coal pillar.

5.4.3.2 Evidence for crown fires

Inertodetrinite is present in all lithotype units in varying amounts (1.3% - 8.5%; Fig. 5.3). The presence of microscopic (<180µm, but typically <20µm) qualitatively high reflecting charcoal (e.g. LU1, LU3, LU5; Fig. 5.6 B, F, J) is interpreted to represent wind or water transported charcoal dispersed from relatively frequent, high temperature regional crown fires (see discussion section chapter 4.4.4.3).

5.4.3.3 Evidence for other fire types

Charcoal horizons of macroscopic fusinite and semifusinite clasts have been interpreted to represent local surface fire events within the peat-forming environment (chapter 4.4.4.2). Charcoal horizons are absent from pillar 78(b) suggesting that

there are no local surface fire events during this time interval of peat formation. Occurrences of macroscopic charcoal clasts that do not occur in charcoal horizons (as seen in LU2, LU4, LU5; Fig. 5.6 D, H, I) may represent washed in water transported charcoal from other small surface fire events outside of the immediate peat-forming area.

Pillar 78(b) LU4 is a sapropelic lithotype unit representing deposition in a mire lake setting, comparable to pillar 88(a) LU2 and LU4 (chapter 4). Charcoal horizons have been observed in pillar 88(a) (chapter 4.4.5.2). There are five occurrences of macroscopic charcoal, dominated by low temperature semifusinite (27%; Fig. 5.3) in pillar 78(b) LU4 but no charcoal horizons. These occurrences may represent reworked transported charcoal from surface fires outside of the mire lake environment.

The microscopic appearance of modern charred peat is illustrated in Fig. 5.16 D. There is no evidence of charred peat or a charred peat surface in this coal pillar and therefore no evidence of ground fires.

5.4.4 Interpretation of wildfire type and occurrence in pillar 88(b)

5.4.4.1 Evidence for wildfires: charcoal occurrence

Inertinite is present in all lithotype units in varying amounts from 9.8% (LU6) to 65.6% (LU5) (Fig. 5.7) with an overall pillar average of 37.1% to a mineral matter free basis (2 sd= 5.1) (Table 5.1). The variation in inertinite content between lithotype units may be related to differences in wildfire occurrence and fire type throughout the formation of this coal pillar.

5.4.4.2 Evidence for surface fires

Charcoal horizons are present in four lithotype units (LU5, LU8, LU12 and LU14) with one per LU (Fig. 5.7; Fig. 5.12). These are interpreted to represent individual surface fire events (chapter 4.4.4.2). Lithotype units containing charcoal horizons contain comparable fusinite and semifusinite contents (Fig. 5.3) suggesting variable charring temperatures possibly due to variation in vegetation moisture (Patterson et al., 1987; Simoneit, 2002) or mosaic burning. Furthermore, fusinite and semifusinite clasts from charcoal horizons in LU8 (Fig. 5.10 E) and LU12 (Fig. 5.12) are

surrounded by microscopic (<180µm, but typically <20µm) charcoal that may have been fragmented from the macroscopic charcoal clasts. Different size fractions of charcoal are likely to become separated during water transport due to their waterlogging behaviour (Vaughan and Nichols, 1995; Nichols et al., 2000) whereas mixed size charcoal assemblages as seen in pillar 88(b) and in modern fires may represent limited transport history (Scott, 2010).

5.4.4.3 Evidence for crown fires

All lithotype units contain microscopic charcoal (<180µm, but typically <20µm) in varying amounts. Inertodetrinite (<10µm) ranges from 2.8% - 9.4% (Fig. 5.3) providing evidence for charcoal production and dispersal from frequent regional crown fires. In addition, rare pieces of fusinite and semifusinite >425µm are also observed in all lithotype units containing microscopic charcoal (e.g. Fig. 5.9 D) which may represent wind or water transported larger particles as seen in modern fires (e.g. Tinner et al., 2006).

5.4.4.4 Possible evidence for charred peat

There may be evidence for charred peat clasts (or peatified plant tissue from the litter layer) observed in LU3, LU8, LU10 and LU14 (Fig. 5.16). Previous work on charred peat is limited and examples which claim to represent charred peat in the literature (Petersen, 1998) show morphology more like vitrified charcoal (McParland et al., 2010) which is an amorphous material containing degassing pores not visually similar to experimentally charred peat. Experimental charring of modern *Taxodium* peat from the Okefenokee Swamp, Georgia by V. Hudspith (illustrated in Fig. 5.16 D), suggests that peat may not be fully charred until 600ºC. The putative 'charred peat' clasts in pillar 88(b) have a uniform qualitative high reflectance (Fig. 5.16 A-C) thus suggesting the clasts are fully charred and must have reached temperatures of ≥600ºC. These clasts are rare in pillar 88(b) and scattered sporadically in detrovitrinite layers, there is no evidence for an *in situ* charred peat surface in pillar 88(b). Therefore, the clasts may represent transported charred peat from a ground fire outside the immediate peat-forming environment or charred litter from deep in the litter layer and not charred peat.

FIG. 5.16

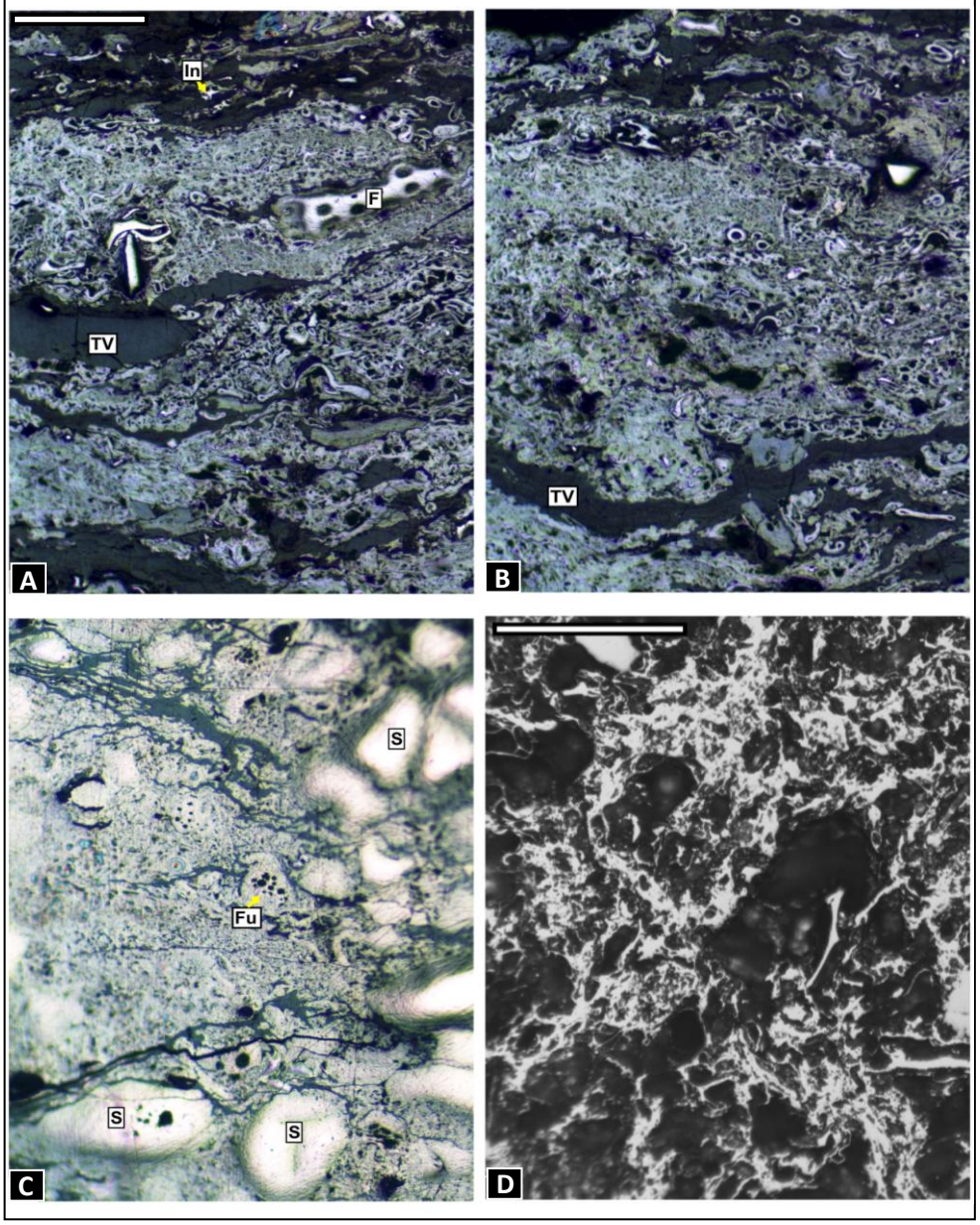

FIG. 5.16 Reflectance microscopy images showing the range in appearance of clasts interpreted as possible charred peat (**A-C**) compared to modern experimentally charred peat (**D**). Scale bars correspond to 100µm. Labels in white boxes represent inertinite, vitrinite and liptinite maceral groups (*sensu* ICCP, 1998, 2001) (defined in Table 2.3): F = fusinite, In = inertodetrinite, S = secretinite, Fu = funginite, TV = telovitrinite.

A, B – 88(b) LU14 (T2 FOV24) A mix of different cellular to almost porous components within a charcoal clast. Some of the cells are rounded and isolated suggesting a fungal origin.

C – 88(b) LU1 (T1) An isolated qualitatively high reflecting clast. The clast has poorly preserved cellular structure and contains some funginite (labelled 'Fu').

D - Black and white image showing an example of modern experimentally charred *Taxodium* peat from the Okefenokee Swamp, Georgia (courtesy of A. Cohen) charred for 1 hour at 600ºC.

5.4.4.5 Evidence for other small fires

Clasts of macroscopic charcoal that do not occur in charcoal horizons therefore do not represent individual surface fire events, are observed in pillar 88(b) LU1, LU3, LU5, LU8, LU10, LU12, LU13, LU14. This charred material is likely to represent transported material from surface fires outside of the immediate peat-forming environment.

5.4.5 Calculating fire return intervals

It is not possible to calculate fire return intervals for pillars 78(b) and 88(b) as 78(b) contains no charcoal horizons (Fig. 5.4) therefore no evidence for local surface fire events and 88(b) only contains one horizon per lithotype unit (in LU5, LU8, LU12, LU14) (Fig. 5.7).

5.4.6 Charcoal distribution and wildfire occurrence within seam 78

The randomly sampled coal pillars from seam 78 (a, b) represent samples 5 km apart. They are not lateral or temporal equivalents but represent an example of the potential range in inertinite type, content and distribution, hence fire occurrence, in the peat-forming environment during the time intervals represented by these pillars.

Previous published work by Pakh and Artser (2003) has shown that the mean inertinite content for seam 78 is 33% (Fig. 7.2), based on multiple crushed samples. Pillar 78(a) contains more macroscopic fusain than observed in pillar 78(b) (compare Fig. 4.5 to Fig. 5.5) so the total inertinite content of pillar 78(a) would be expected to be higher than 78(b). This is not the case, the mean inertinite content of pillar 78(a) is 27.6% mineral matter free basis (2 sd = 2.5; Table 4.2) and 78(b) is much higher at 42.6% mineral matter free basis (2sd =7.2) (Table 5.1). The higher average inertinite content for pillar 78(b) is a result of the thickest lithotype unit (LU4) which contains 59% inertinite (Fig. 5.3). When both pillar 78(a) and 78(b) are combined the average is lowered to 35.1% (mmf basis) which is comparable to Pakh and Artser (2003) data.

There is a significant difference in pillar length between pillars 78(a) (23cm) and 78(b) (10cm). Pillar 78(b) therefore probably represents a much shorter time interval of peat formation. The higher mean inertinite content observed for 78(b) does not

necessarily provide evidence for more wildfires than seen in 78(a) as this pillar does not represent an equivalent period of time. It is possible that if pillar 78(b) were extended vertically, in either direction, more inertinite-poor lithotype units may be encountered.

Charcoal is present in all lithotype units in both pillars, interpreted to represent production and dispersal of charcoal from wildfire events during the time interval represented by each coal pillar. There is a variation in environment of deposition as well as wildfire type and occurrence between these coal pillars. Pillar 78(a) represents an ombrotrophic mire depositional setting whereas pillar 78(b) represents a mire and mire lake setting [comparable to 88(a) LU2, LU4]. The charcoal distribution and therefore interpreted wildfire occurrence is different as there are no charcoal horizons in pillar 78(b) compared to 11 in pillar 78(a) hence no evidence for individual surface fire events in pillar 78(b)(chapter 4.4.4.2). Macroscopic charcoal is observed in pillar 78(b) in detrovitrinite layers which may represent transported charcoal from other small surface fires outside of the immediate peat-forming environment.

Variation in inertinite content, environment of deposition and wildfire types is unsurprising given the spacing between coal pillars (5 km) and the fact that they are not exact lateral equivalents, hence may represent different periods of time in the peat-forming environment. The degree of variation emphasises the need to study more than one coal pillar in order to reflect the range in inertinite content and distribution, in order to interpret wildfire history in this peat-forming environment.

5.4.7 Charcoal distribution and wildfire occurrence within seam 88

The seam 88 pillar samples are only 1m apart and pillar 88(b) was sampled above 88(a) (Fig. 5.1 A) and therefore represents a younger time interval in the period of overall seam formation, extending the record of fire history. These pillars represent differing environments of deposition with 88(b) representing an ombrotrophic mire environment compared to 88(a) which represents both ombrotrophic mire and mire lake [88(a) LU2, LU4] depositional settings. The change in depositional environment, within the time interval represented by coal pillar formation, will affect the inertinite distribution in the resulting coal pillar. Therefore, it is essential to study

more than one coal pillar in order to represent the potential range in depositional setting during seam formation.

Both the 88(a) and 88(b) coal pillars contain higher inertinite contents [88(a) 48%; 88(b) 37.1%; Table 4.2; Table 5.1] than observed in previous published work on bulk crushed coal samples from seam 88 by Pakh and Artser (2003) (22%). The combined average of 88(a) and 88(b) pillars gives 42.6% (mineral matter free basis). This may reflect either more wildfire events, or more charcoal being produced during a single fire event, during these intervals of pillar formation compared to the rest of seam 88. This variation also suggests that this small scale separation of coal pillars (1m) does not fully represent the range of inertinite content and distribution that may be seen within seam 88 [as the Pakh and Artser (2003) average is much lower].

Pillars 88(a) and 88(b) are the same length and therefore probably represent comparable time intervals in the peat-forming environment. Macroscopically 88(a) and 88(b) are completely different (compare Fig. 4.10 with Fig. 5.8). The majority of 88(a) is dominated by the dull mire lake sequence containing scattered vitrain and fusain throughout whereas 88(b) contains more variable fusain clast size and distribution, both between petrographic transects and compared to 88(a).

The presence of 26 charcoal horizons in lithotype units LU2, LU4, LU7 in pillar 88(a) provides evidence for frequent local surface fire events. There are only 4 charcoal horizons in 88(b) but frequent occurrences of macroscopic charcoal in detrovitrinite layers thus providing evidence for transported charcoal from other small surface fires. Fragmentation of macroscopic charcoal clasts may also be producing an elevated volume of background charcoal as observed in mire lake sequences in 88(a) LU2 and LU4.

5.4.8 Wildfire occurrence in comparable environments of deposition

5.4.8.1 Ombrotrophic mire

Coal pillars 78(a) and 88(b) were originally formed in an ombrotrophic mire setting (chapter 4.4.2; section 5.4.1). Charcoal is present in all lithotype units in both coal pillars and both coal pillars show comparable wildfire histories with local surface

fire events (charcoal horizons) interspersed with crown fires (microscopic scattered charcoal) and other small fires (scattered macroscopic charcoal clasts not in horizons). However, surface fire events are much more frequent for pillar 78(a) (11 charcoal horizons; chapter 4.4.9.2) compared to pillar 88(b) (4 charcoal horizons).

5.4.8.2 Mire with mire lake depositional setting

Sapropelic lithotype units in pillars 88(a) (LU2, LU4) and 78(b) (LU4) were originally formed in mire lakes (chapter 4.4.2; section 5.4.1). These lithotype units all contain high inertinite contents [41-45% in 88(a) LU2, LU4; 59% in 78(b) LU4]. Inertinite, liptinite and mineral matter are scattered throughout these lithotype units in every field of view with little identifiable vitrinite. Although this inertinite distribution means it is not possible to calculate FRI using the method in chapter 4.4.9, mire lake lithotype units in pillar 88(a) contain 24 charcoal horizons which provide evidence for frequent low temperature surface fire events and limited reworking in the mire lake (see chapter 4.4.5.2; Fig. 4.13). This is in contrast to 78(b) LU4 which contains no charcoal horizons but five concentrations of macroscopic charcoal thus, suggesting frequent local surface fire events but considerable reworking in the mire lake setting. Therefore, despite post-depositional taphonomic charcoal processes, lithotype units from mire lake depositional settings may represent comparable wildfire histories.

5.5 CONCLUSIONS

Two *in situ* coal pillars [78(b) and 88(b)] were analysed using petrographic techniques to assess within seam variation in inertinite content and distribution in seams 78 and 88 [to be compared with chapter 4; pillars 78(a) and 88(a)]. Pillars 78(b) and 88(b) represent different environments of deposition within the peat-forming environment. Pillar 78(b) (LU1-3, LU5) and pillar 88(b) have low %ash (<6.3% dry basis) and %total Sulphur (<0.5% dry ash free basis) contents and represent formation in an ombrotrophic mire. In contrast pillar 78(b) LU4 has high %ash (13% dry basis) and high liptinite content (10%) suggesting sapropelic coal formed in a mire lake environment within the ombrotrophic peat-forming system.

Inertinite is present in all lithotype units in both pillars in varying amounts averaging 42.6% in pillar 78(b) (mineral matter free basis) and 37.1% in pillar 88(b) (mmf

basis). Inertinite distribution shows the same patterns as seen in chapter 4 and occurs as, (1) microscopic charcoal (<180µm, but typically <20µm) which is scattered in detrovitrinite layers and is interpreted to represent a background, regional crown fire signal. (2) clasts of scattered macroscopic charcoal (Fig. 5.4; Fig. 5.7) which may represent waterborne or windblown pieces of charcoal transported from local surface fires, (3) scattered inertinite in every field of view representing charcoal re-working in a mire lake setting producing the scattered distribution [78(b) LU4] (4) charcoal horizons [e.g. Fig. 5.12; 88(b) LU5, LU8, LU12, LU14] interpreted to represent charred litter or biomass from individual, local surface fire events within the peat-forming environment. Fire return intervals could not be calculated using the approach outlined in chapter 4.4.9 from these pillars, as 78(b) contained no horizons and 88(b) only contained one horizon per lithotype unit. However, the presence of charcoal in all lithotype units provides evidence for frequent fire occurrence during these intervals of coal pillar formation.

There may be evidence for charred peat clasts in pillar 88(b) (Fig. 5.16 A-C). These are visually comparable to modern examples of charred peat (e.g. Fig. 5.16 D). However, these occur as isolated clasts scattered in detrovitrinite layers and therefore are likely to represent transported clasts from a ground fire outside of the immediate peat-forming environment. There is no evidence for a charred peat surface; hence an *in situ* ground fire in any of the coal pillars studied.

Coprolites or sporangia have been observed in all coal pillars [78(a), 88(a), 91, 78(b), 88(b)]. In addition, the telovitrinite perimeter seen on some entities may suggest that these are partially charred. Furthermore, the difference in liptinite fluorescence between entities, with and without the telovitrinite perimeter, may be related to the initial charring temperature.

Pillar 78(b) contains more inertinite (42.6%) than observed in pillar 78(a) (27.6% mineral matter free basis) but represents a shorter duration of peat formation. Pillars 88(a) and (b) represent comparable durations of peat formation but 88(b) contains less inertinite (37.1% mineral matter free basis) than pillar 88(a) (48% mmf basis) but far more than previous results from crushed coals (22% mmf basis; Pakh and Artser, 2003; Fig. 7.2) suggesting that wildfires may have been more frequent or

there was more charcoal produced during fire events than compared to the totality of seam 88. The variation in inertinite content and distribution, both between lithotype units from the same coal pillar and between coal pillars from the same seam, emphasises the need to study more than one pillar in order to understand the potential temporal variation in fire occurrence in this Late Permian peat-forming environment.

CHAPTER 6

QUANTIFYING REFLECTANCE OF INERTINITE MACERALS: PALAEOECOLOGICAL IMPLICATIONS

6.1 INTRODUCTION

6.1.1 Wildfire origin of inertinite macerals

Fusinite, semifusinite and inertodetrinite inertinite macerals are now generally accepted to represent charcoal derived from palaeowildfires (Scott, 1989a; Teichmüller, 1989; Sander and Gee, 1990; Diessel, 1992; Bustin and Guo, 1999; Scott et al., 2000b; Scott and Jones, 1994; Falcon-Lang, 2000; Glasspool, 2003a,b; Uhl and Kerp, 2003; Scott and Glasspool, 2007; Uhl et al., 2007; Glasspool and Scott, 2010; Scott, 2010). Macroscopic clasts of fusinite and semifusinite macerals in charcoal horizons from the Permian coals studied here have been interpreted to represent individual surface fire events (chapters 4.4.4.2; 4.4.5.2; 4.4.6.2; 5.4.4.2) whereas scattered inertodetrinite (<10µm *sensu* ICCP, 2001) has been interpreted to represent high temperature charcoal produced during crown fires (chapters 4.4.4.3; 4.4.5.3; 4.4.6.3; 5.4.3.2; 5.4.4.3).

6.1.2 Experimental charcoalification and charring temperatures

Laboratory based experimental charcoalification on a variety of modern plants from woody to non-woody to fungi (e.g. Correia et al., 1974; Jones et al., 1991; Scott and Jones, 1991; Guo and Bustin, 1999; Bustin and Guo, 1999; Scott and Glasspool, 2005, 2007; McParland et al., 2007, 2009b; Braadbaart and Poole, 2008; McParland, 2010) have all shown a positive relationship between increasing charring temperature and increasing mean random reflectance under oil (%Ro) (Fig. 6.1). When the initial charring temperature is unknown, charcoal can therefore be used as a temperature proxy. If the charring duration is also unknown then the inferred temperatures represent minimum charring temperatures (Scott and Glasspool, 2005; Scott et al., 2008; Ascough et al., 2010; Hudspith et al., 2010) because longer charring times slightly increase reflectance (Scott and Glasspool, 2005). For discussion of the implications of different charring durations and different calibration curves for inferring charring temperature see chapter 8.

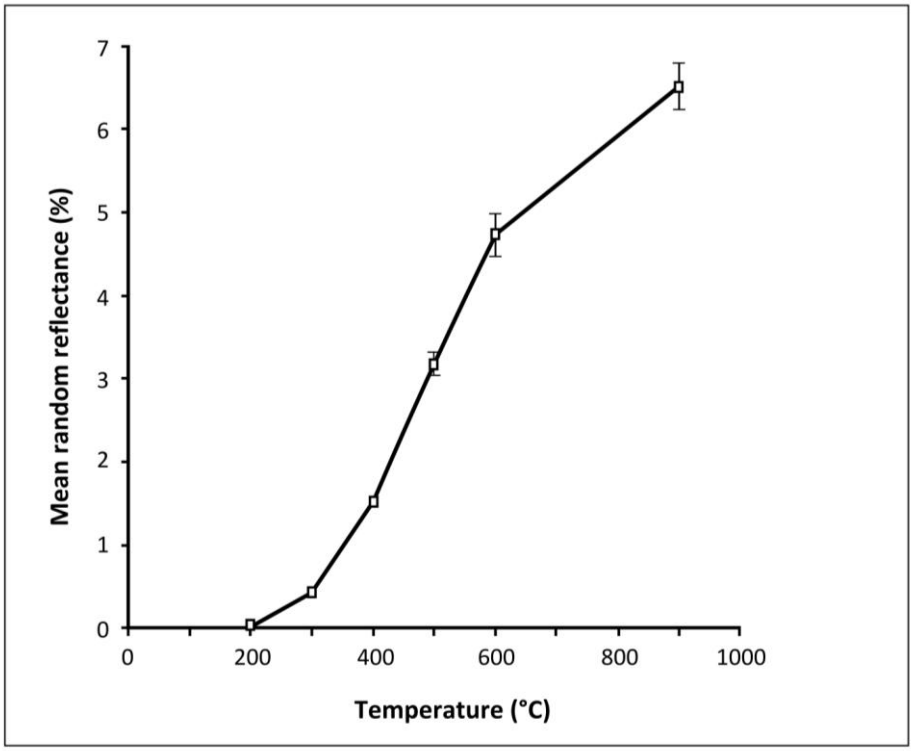

FIG. 6.1 Long duration temperature calibration curve constructed by experimental charcoalification of conifer wood (*Sequoia sempervirens*) charred for 24 hours under varying temperatures. Error bars correspond to 1 standard deviation (after Scott and Glasspool, 2005).

Reflectance measurements (%Ro random) in this chapter are therefore used to determine if there is temporal variation in reflectance of macroscopic charcoal from charcoal horizons both within and between coal pillars and the implications of this for interpreting palaeowildfire types. The reflectance of inertodetrinite particles, from lithotype units both with and without charcoal horizons, is also measured to determine whether inertodetrinite originates from high temperature crown fires (>600°C) and the implications of this for palaeowildfire interpretation.

6.2 METHODOLOGY

Reflectance values of vitrinite, inertodetrinite and macroscopic charcoal clasts from charcoal horizons from coal pillars: 78(a) (LU2, LU8), 88(a) LU7, 88(b) LU12, 91 LU2 (chapters 4 and 5) were measured. The samples have been selected because they are from comparable environments of deposition (ombrotrophic mires), contain macroscopic charcoal clasts in charcoal horizons and 78(a) LU2, 88(a) LU7 and 91 LU2 have been used to calculate fire return intervals in chapter 4.4.9.2.

Preparation of polished blocks is detailed in chapter 2.3. Polished blocks were studied under oil of RI 1.514 at 23°C using a Leica DM 2500 P reflectance microscope with a TIDAS MSP operating system and a ×50 objective (with ×10 eyepiece magnification). Reflectance (%Ro) points were measured manually using MSP200 v 3.20 software.

6.2.1 Vitrinite (telovitrinite) reflectance

Vitrinite reflectance was undertaken on lithotype units that contained large quantities of telovitrinite [pillar 78(a) LU7, pillar 88(a) LU7, pillar 88(b) LU6, pillar 91 LU3-5, Fig. 4.3, Fig. 5.3]. The system was calibrated using three reflectance standards (highest to lowest), GGG (gadolinium gallium garnet) (Ro 1.7486%), YAG (yttrium aluminium garnet) (Ro 0.929%) and spinel (Ro 0.393%). The standards were re-calibrated after every sample. A total of one hundred random points were measured within the lithotype unit, with one point measured per telovitrinite layer (for images of vitrinite see chapters 4 and 5).

Vitrinite shows anisotropy with increasing vitrinite reflectance, hence increasing rank (Hower and Davis, 1981). This causes the reflectance of vitrinite in high rank coals (vitrinite >1.3%Ro) to vary depending on the orientation of the surface that is sectioned (Taylor et al., 1998) therefore, the maximum reflectance value is typically used instead of the mean (Bustin, 1984). However, anisotropy is negligible in low and medium rank coals (subbituminous rank, this study; chapter 7) therefore the mean reflectance value is more appropriate to use than the maximum.

6.2.2 Inertodetrinite reflectance

Trial reflectance measurements were made of inertodetrinite particles (<10µm in size) (ICCP, 2001) in each studied lithotype unit. These showed a range of reflectance values, therefore the system was calibrated with four reflectance standards (highest to lowest), CZ (cubic zirconium) (Ro 3.188%), GGG (gadolinium gallium garnet) (Ro 1.7486%), YAG (yttrium aluminium garnet) (Ro 0.929%) and spinel (Ro 0.393%) and re-calibrated after every sample. One hundred measurements were taken of inertodetrinite particles along petrographic transects through each lithotype unit (transect positions illustrated in Fig. 6.3). Reflectance measurements were converted to temperature values using the 24 hour experimental charring

calibration curve from Scott and Glasspool (2005) (Fig. 6.1). For further discussion of temperature conversion see chapter 8.

6.2.3 Reflectance of macroscopic charcoal clasts in charcoal horizons

Charcoal horizons (defined in 4.2.2.1), formed from macroscopic fusinite and semifusinite (>425µm) clasts were measured as these are easy to locate microscopically and are laterally traceable across the polished block.

The system was calibrated using the four reflectance standards used to measure inertodetrinite. The standards were re-calibrated every hour. The clasts were measured by following the three vertical transects used for petrographic analysis (illustrated in: Fig. 4.4, Fig. 4.9, Fig. 4.14, Fig. 5.7, Fig. 6.3) in order to provide a comparable dataset. The horizons were numbered from the bottom (e.g. CH1) to the top (e.g. CH4) of the lithotype unit (Fig. 6.3).

The clasts were measured from the bottom to the top of each horizon. Fifty randomly distributed reflectance measurements were taken of each clast. This method was then repeated for all clasts in that horizon along the transect line and then for all three transects. The horizontal spacing between transects prevented the same clast being measured twice. Histograms of reflectance values were produced for individual charcoal horizons (combining all measurements for all macroscopic charcoal clasts from all three transects) (Fig. 6.3) and for all charcoal horizons combined for each lithotype unit (Fig. 6.4, Fig. 6.6, Fig. 6.7). Reflectance measurements were converted to temperature values using the 24 hour experimental charring calibration curve from Scott and Glasspool (2005) (Fig. 6.1). For further discussion of temperature conversion see chapter 8.

6.3 RESULTS

6.3.1 Vitrinite (telovitrinite) reflectance

Vitrinite reflectance values (Fig. 6.2) for individual lithotype units range between 0.41 - 0.64%Ro. The overall mean for all coal pillars is 0.56%Ro (2 sd = 0.08). Detrovitrinite was observed to have a lower qualitative reflectance than the measured telovitrinite. Vitrinite reflectance values should be normally distributed (Bustin and Guo, 1999) as seen in pillar 91 LU3-5. However, telovitrinite reflectance in 88(a)

LU7 shows a broad range and the highest standard deviation (0.41 - 0.62%; 2 sd = 0.1). Sapropelic lithotype units occur immediately below LU7 (Fig. 4.3; Fig. 4.9) therefore the vitrinite reflectance may have become suppressed with the large quantity of liptinite macerals (Taylor et al., 1998).

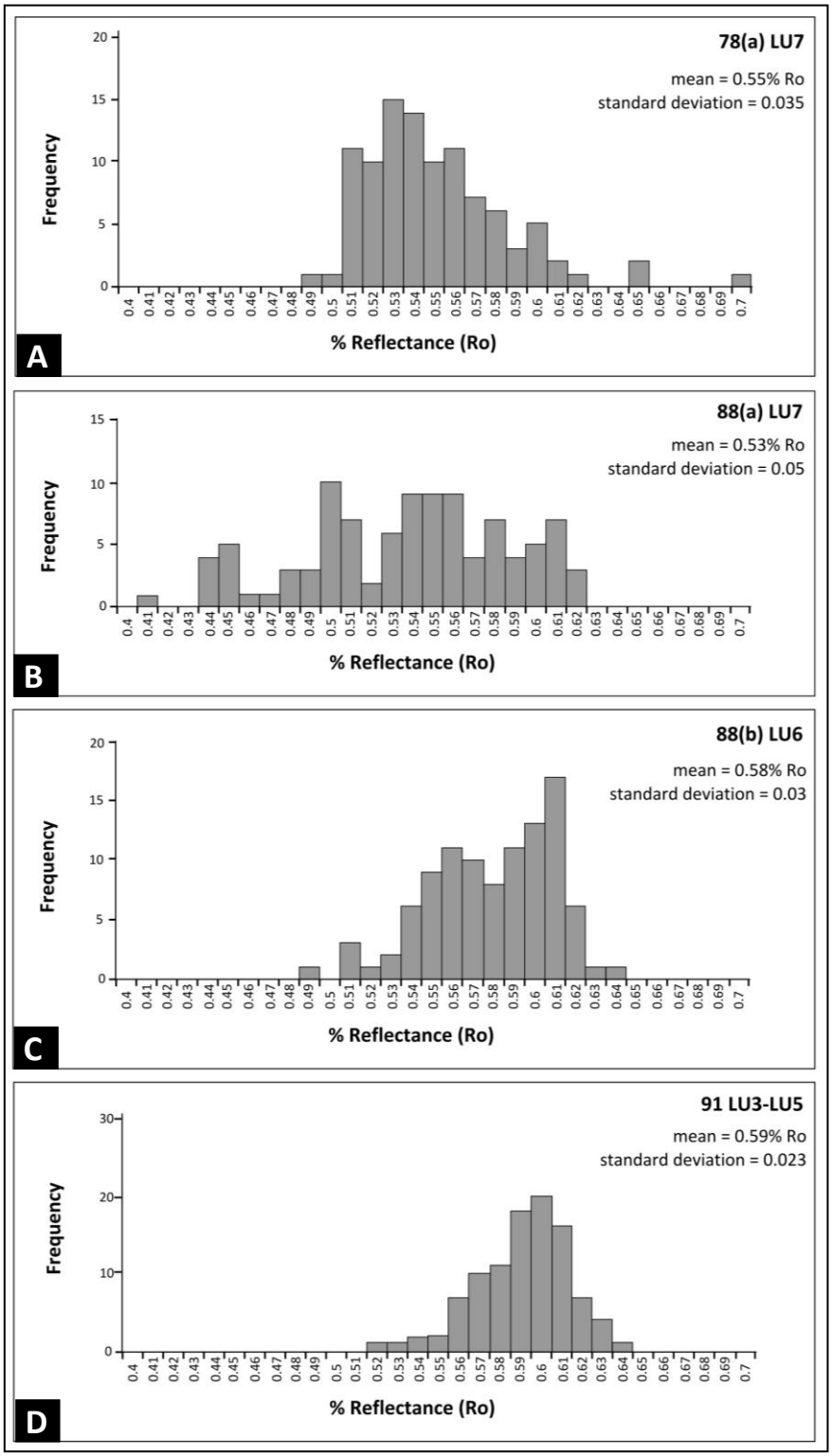

FIG. 6.2 Histograms showing the telovitrinite reflectance (%Ro random) for each coal pillar based on 100 mean random reflectance values from telovitrinite layers within that lithotype unit.

6.3.2 Reflectance values of macroscopic charcoal clasts from charcoal horizons compared to values from inertodetrinite

Comparative combined fusinite and semifusinite reflectance profiles of charcoal clasts from individual charcoal horizons are illustrated alongside the position and thickness of each lithotype unit relative to the entire coal pillar in Fig. 6.3. Raw reflectance data is presented in Appendix 2.

Coal pillar and LU	*Charcoal horizon*	*Ro mean (%)*	*Ro median (%)*	*Standard deviation (2 sd)*
78(a) LU2	CH1	0.90	0.80	0.86
	CH2	0.93	0.93	0.42
	CH3	0.99	1.06	0.62
	CH4	0.94	0.88	0.76
78(a) LU8	CH1	1.84	1.71	2.18
	CH2	1.62	1.60	1.02
	CH3	2.09	2.08	2.34
88(a) LU7	CH1	1.39	1.30	0.76
	CH2	1.19	0.97	1.26
88(b) LU12	CH1	1.50	1.50	0.66
91 LU2	CH1	2.08	1.74	2.3
	CH2	1.92	1.69	2.06
	CH3	1.77	1.63	1

TABLE 6.1 Summary of statistical data of combined macroscopic charcoal clasts from individual charcoal horizons (illustrated in Fig. 6.3).

FIG. 6.3 (overleaf) The images on the left of each set of histograms show photographs of the coal pillar polished blocks highlighting the position of lithotype units and vertical transect locations for petrographic analysis (see chapters 4 and 5). On the right of each pillar are comparative histograms showing reflectance data (%Ro random) of charcoal clasts from individual charcoal horizons from each pillar. The grey vertical lines represent 0.5%Ro intervals to assist comparison between and within coal pillars. For mean, median and standard deviation values see Table 6.1.

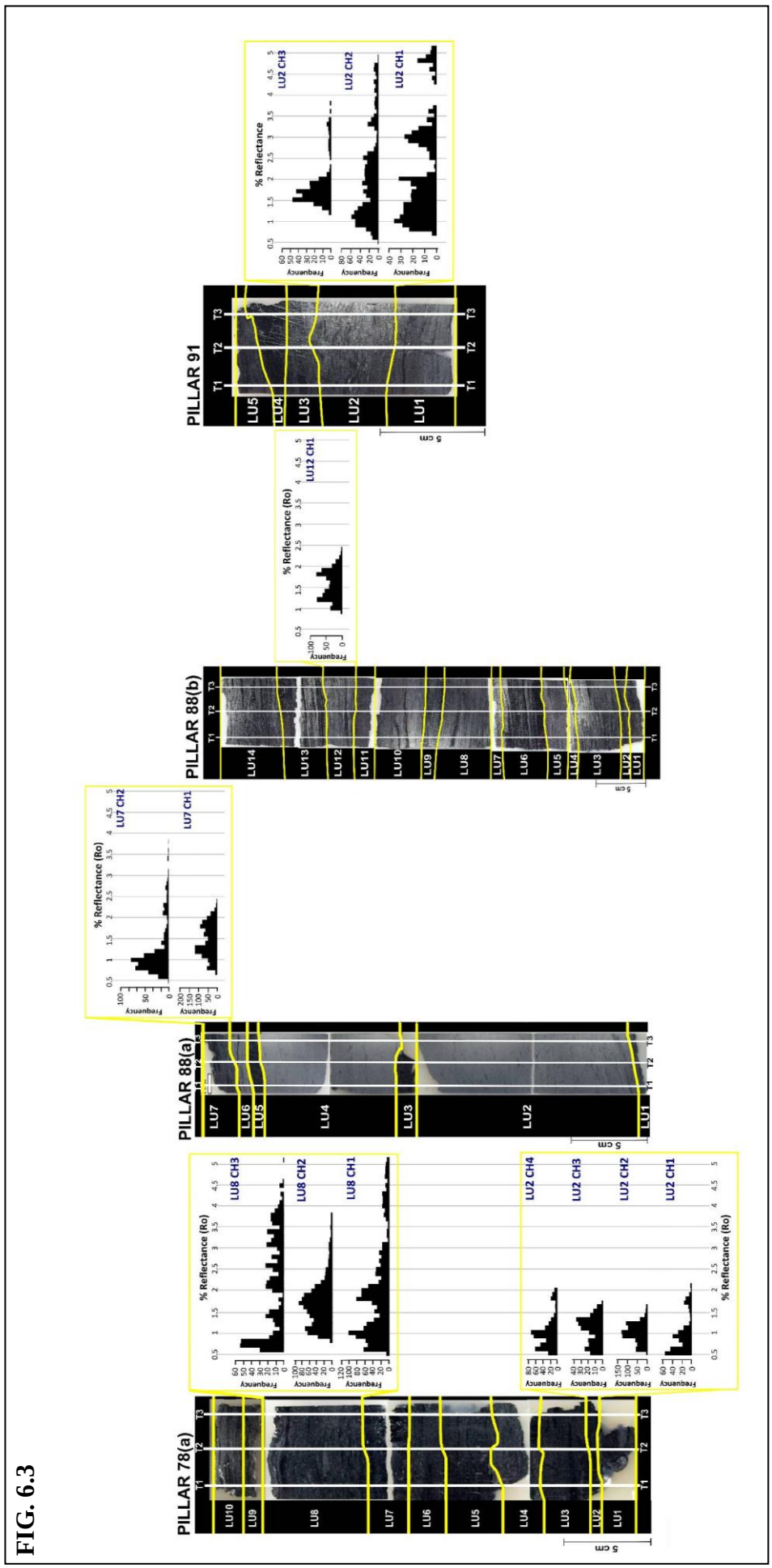
PILLAR 78(a)
PILLAR 88(a)
PILLAR 88(b)
PILLAR 91
% Reflectance (Ro)
% Reflectance
Frequency
5 cm

FIG. 6.3

Pillar 78(a) LU2: The distribution of the reflectance histogram for all macroscopic charcoal clasts from all charcoal horizons (Fig. 6.4 A) is right skewed and the spread of data is narrow (0.5 - 2.1%Ro). The most frequent category ranges from 0.9 - 1.3%Ro. In addition, 24.5% (n = 417) of all the data is within the range of measurements for telovitrinite (Fig. 6.2 A). The distribution of the inertodetrinite reflectance histogram is also slightly right skewed and measurements range from 0.8 - 3.3%Ro, and the most frequent category ranges from 1.3 - 1.7%Ro (Fig. 6.4 B). No inertodetrinite data are within the vitrinite reflectance range. Five inertodetrinite values are outliers (between 2.2 - 3.3%Ro) and are also not within the range of measured values for the macroscopic charcoal clasts in charcoal horizons.

78(a) LU2 contains four charcoal horizons (Fig. 6.3) and the spread of data varies between horizons. The reflectance histogram distribution in CH1, CH3 and CH4 is bimodal and right skewed. In CH1 the most frequent category ranges from 0.5 - 0.6%Ro (and a second smaller peak at 0.9%Ro). In CH2 (and CH4) the most frequent category ranges from 0.9 - 1%Ro. In CH3 the most frequent category ranges from 1.1 - 1.3%Ro. High reflecting charcoal is not common and only CH1 and CH4 have charcoal reflectance values >1.7%Ro.

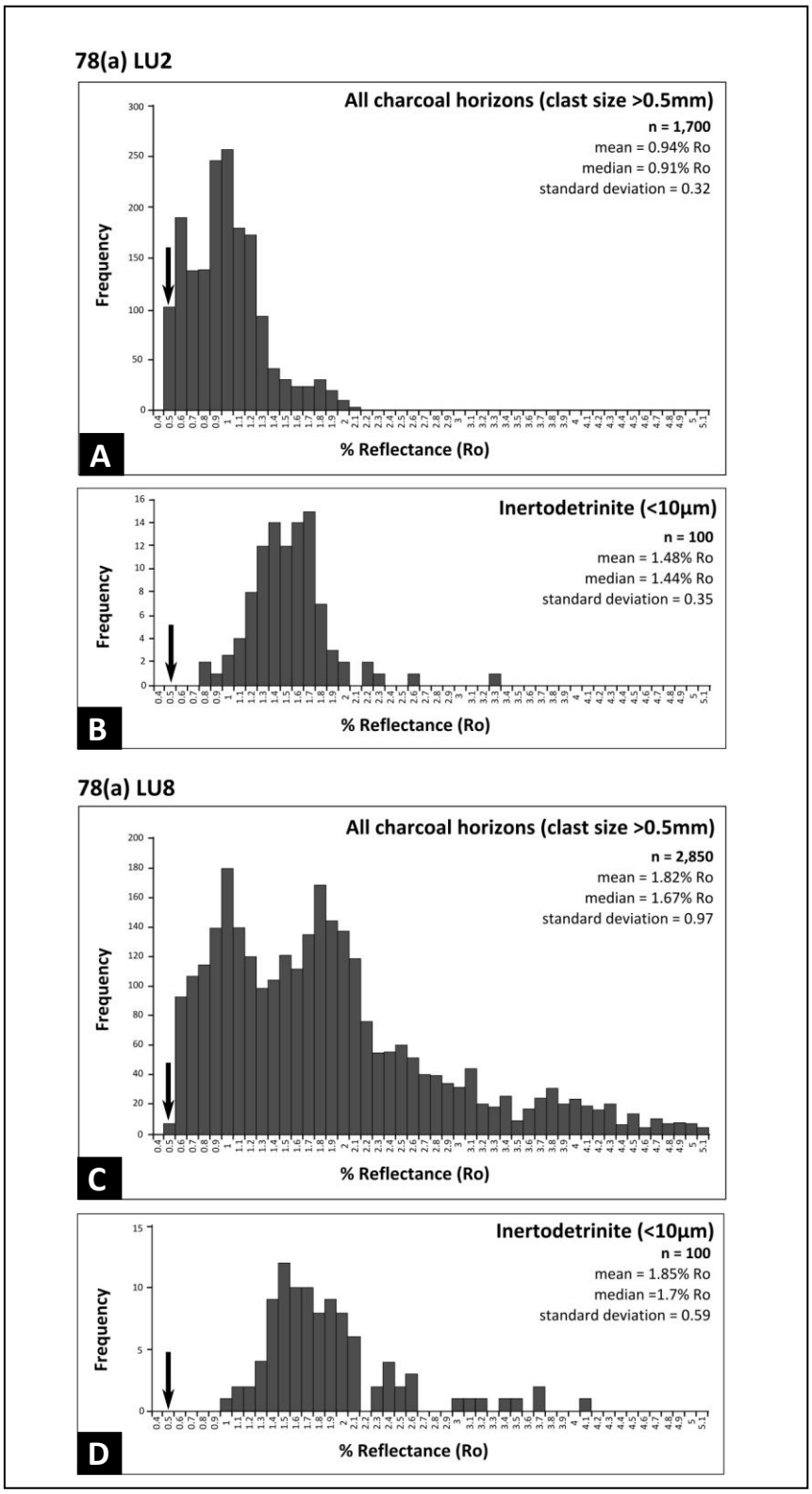

FIG. 6.4 Comparative histograms of reflectance values of charcoal clasts from charcoal horizons (macroscopic fusinite and semifusinite) and inertodetrinite from pillar 78(a) LU2 and 78(a) LU8. The black arrow represents the mean telovitrinite reflectance for that coal pillar. The vertical scale for the inertodetrinite graphs has been exaggerated in order to enable the distribution to be compared with the fusinite and semifusinite data.

Pillar 78(a) LU8: The distribution of the reflectance histogram for all macroscopic charcoal clasts from all charcoal horizons (Fig. 6.4 C) is bimodal and right skewed. There is a wide spread of data (0.5 - 5.1%Ro) compared to LU2, with only 6.8% (n = 195) of the data within the range of telovitrinite reflectance values (Fig. 6.2 A). The two most frequent categories range from 0.6 - 1.3%Ro and 1.4 - 2.1%Ro. The distribution of the inertodetrinite reflectance histogram (Fig. 6.4 D) is also right skewed but the spread of data is narrower than measured values for macroscopic charcoal clasts in charcoal horizons (1 – 4.1%Ro). No inertodetrinite values are within the vitrinite reflectance range. The most frequent category ranges from 1.4 - 2.1%Ro. The missing values in the inertodetrinite profile are all represented by values for macroscopic clasts in charcoal horizons, missing values in certain %Ro categories may be related to the small sample size (n = 100).

Reflectance measurements of inertodetrinite are represented by one measurement per particle, compared to 50 measurements per macroscopic charcoal clast for charcoal horizons. In order to therefore compare charcoal horizon reflectance data and inertodetrinite reflectance data the mean reflectance value of each macroscopic charcoal clast in each charcoal horizon is plotted (Fig. 6.5 A). The distribution of clast mean values (Fig. 6.5 A) has only a single value >4.1%Ro in contrast to the individual measured values (Fig. 6.4 C) with a number of values >4.1%Ro and ranging up to 5.1%Ro. There are very few macroscopic charcoal clasts (n = 12) with high Ro_{mean} values >2.5% (Fig. 6.5 A). Therefore, the higher reflectance values for macroscopic charcoal from charcoal horizons (Fig. 6.4 C) do not represent individual high reflecting clasts but within clast variation in reflectance.

LU8 contains three charcoal horizons (Fig. 6.3). The distribution of reflectance histograms of macroscopic charcoal clasts from individual charcoal horizons show CH1 and CH2 are bimodal with right skewed distributions whereas CH3 is right skewed but multimodal in distribution (Fig. 6.3). The most frequent category for CH1 ranges from 0.6 - 1.2%Ro (and 1.8 - 2.1%Ro). In CH2 the spread of data is narrower (0.8 - 3.7%Ro) but the most frequent categories are comparable to CH1 and range from 0.9 - 1.3%Ro and 1.4 - 2.1%Ro. CH3 has a wide spread of data (0.6 - 5.1%Ro) but the most frequent category ranges from 0.7 - 0.8%Ro.

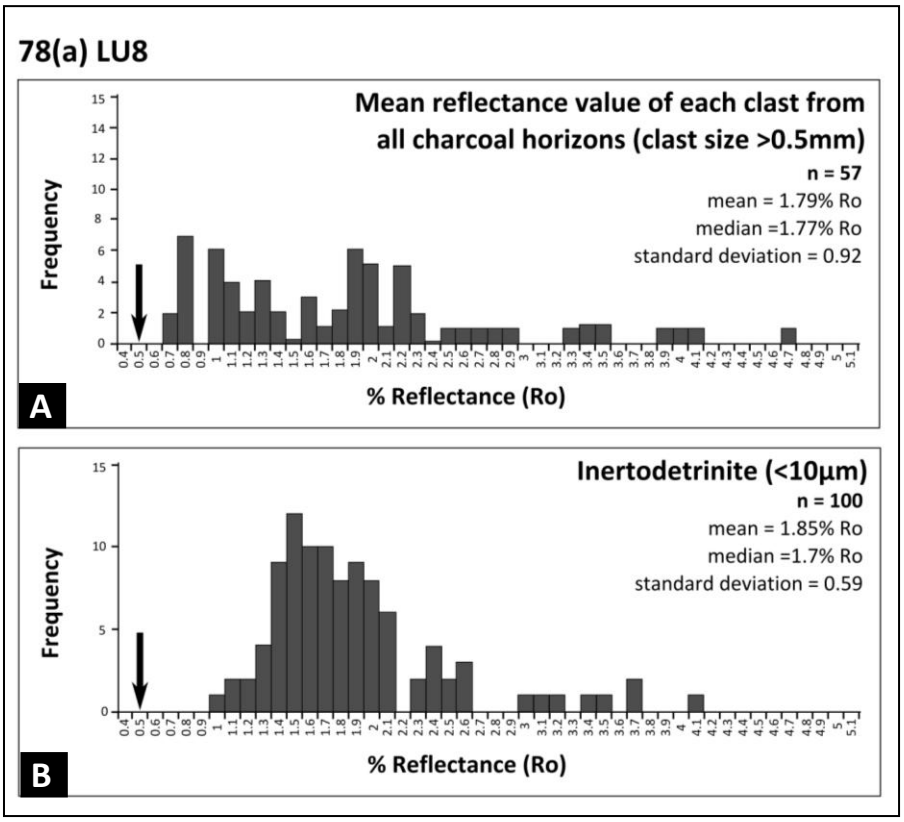

FIG. 6.5 Comparative histograms of reflectance values from pillar 78(a) LU8 **A -** the mean value of individual macroscopic charcoal clasts (n = 57) in all charcoal horizons and **B -** inertodetrinite. The black arrow represents the mean telovitrinite reflectance for that coal pillar.

Pillar 88(a) LU7: The distribution of the reflectance histogram for all macroscopic charcoal clasts from all charcoal horizons (Fig. 6.6 A) is right skewed. There is a wide spread of data (0.5 - 3.8%Ro) but the most frequent category ranges from 0.8 - 1.3% Ro, with 1.6% (n = 25) of the measured macroscopic charcoal clast values within the telovitrinite reflectance range (Fig. 6.2 B). The distribution of the inertodetrinite reflectance histogram (Fig. 6.6 B) shows a similar spread of values as the macroscopic charcoal clasts from charcoal horizons but with no values <0.9%Ro. No inertodetrinite data are within the vitrinite reflectance range. The most frequent category ranges from 1.8 - 1.9%Ro.

There are two charcoal horizons in LU7 (Fig. 6.3) and each has a different reflectance histogram distribution. CH1 is bimodal and the data has a narrow spread (0.7 – 2.4%Ro). The most frequent category ranges from 1.1 - 1.3%Ro (and 1.8 - 1.9% Ro). The histogram for CH2 is right skewed and the data has a wide spread (0.5 - 3.8%Ro) although the most frequent category ranges from 0.8 - 1%Ro.

Pillar 88(b) LU12: The distribution of the reflectance histogram for all macroscopic charcoal clasts from all charcoal horizons is bimodal and the data has a narrow spread (0.9 - 2.4%Ro). The most frequent categories range from 1.2 - 1.4%Ro and 1.7 - 1.9%Ro (Fig. 6.6 C). This is the only lithotype unit with no macroscopic charcoal values in the vitrinite reflectance range (Fig. 6.2 C). The distribution of the inertodetrinite histogram is right skewed and the data has a wide spread (0.9 - 3.7%Ro). The most frequent category ranges from 1.4 - 1.8%Ro (Fig. 6.6 D) which is comparable macroscopic charcoal clasts from charcoal horizons (Fig. 6.6 C). No inertodetrinite data are within the vitrinite reflectance range. Eight values are outliers compared to macroscopic charcoal reflectance values. These range from 2.6 - 3.7%Ro.

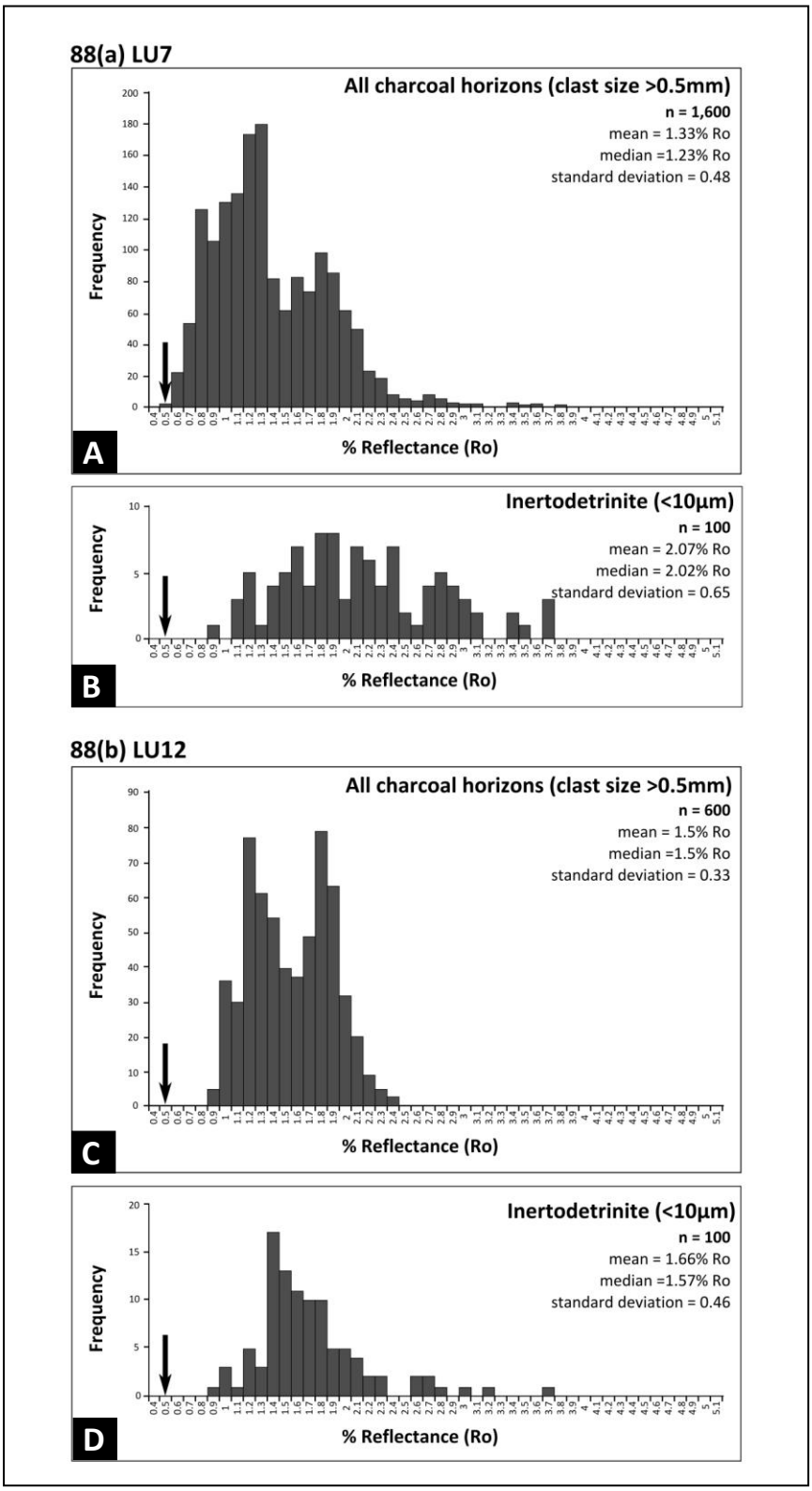

FIG. 6.6 Comparative histograms of reflectance values of charcoal clasts from charcoal horizons (macroscopic fusinite and semifusinite) and inertodetrinite from pillar 88(a) LU7 and 88(b) LU12. The black arrow represents the mean telovitrinite reflectance for that coal pillar. The vertical scale for the inertodetrinite graphs has been exaggerated in order to enable comparison with the fusinite and semifusinite data.

Pillar 91 LU2: The distribution of the reflectance histogram for all macroscopic charcoal clasts from all charcoal horizons is right skewed. The data has a wide spread (0.5 - 5.1%Ro). The most frequent category ranges from 0.9 - 2%Ro (Fig. 6.7 A), with 1% (n = 19) of the macroscopic charcoal reflectance values within the range for telovitrinite (Fig. 6.2 D). The distribution of the inertodetrinite reflectance histogram is also right skewed (Fig. 6.7 B) and has a narrower spread than the reflectance histogram for macroscopic charcoal in charcoal horizons (0.8 - 3.8%Ro). The most frequent category is 1.3%Ro. The six atypical values (3.2 - 3.8%Ro) are all within the spread of macroscopic charcoal data and are therefore unlikely to represent outliers. No inertodetrinite data are within the vitrinite reflectance range.

LU2 contains three charcoal horizons (Fig. 6.3). The reflectance histograms of each horizon have very different distributions. CH1 is trimodal with a wide spread (0.7 - 5.1%Ro) and no values between 3.8 - 4.2%Ro. The most frequent categories range from 0.8 - 2%Ro, 2.8 - 3.2%Ro and 4.8%Ro with the majority of values <2%Ro. CH2 has a right skewed distribution and a wide spread (0.5 - 4.9%Ro) and the most frequent category ranges from 0.9 - 1.4%Ro. The CH3 histogram is right skewed and the data spread is over a narrower range than CH1 or CH2 (1.2 – 3.8%Ro) the most frequent category ranges from 1.5 - 1.7%Ro. The inertodetrinite histogram distribution and spread is most comparable to the charcoal horizon histogram for CH3.

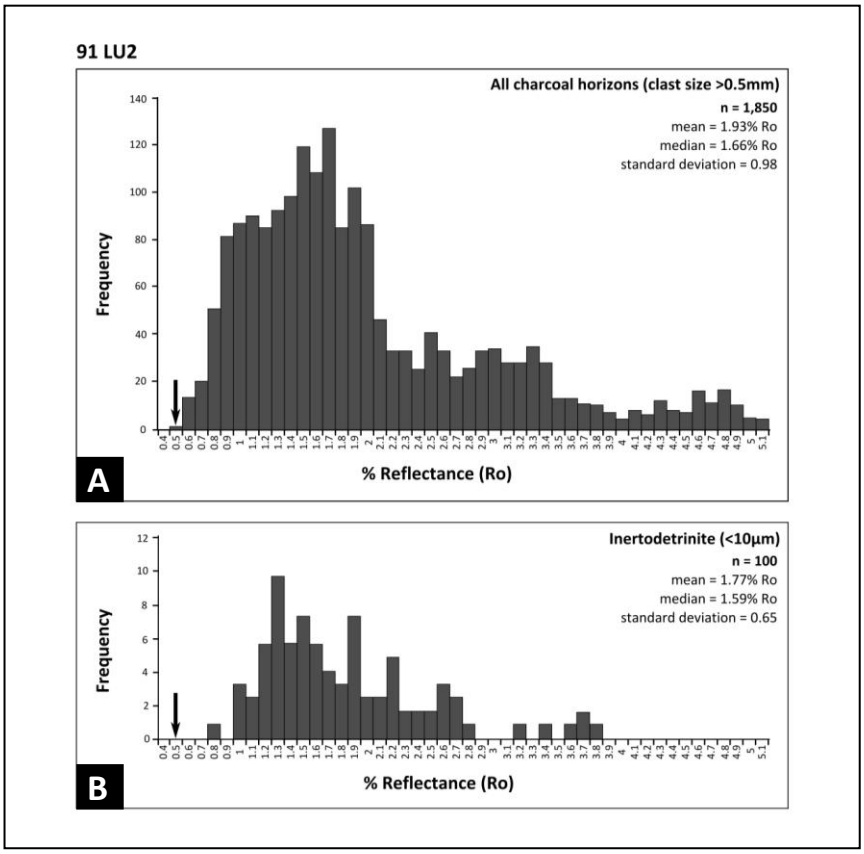

FIG. 6.7 Comparative histograms of reflectance values of charcoal clasts from charcoal horizons (macroscopic fusinite and semifusinite) and inertodetrinite from pillar 91 LU2. The black arrow represents the mean telovitrinite reflectance for that coal pillar. The vertical scale for the inertodetrinite graphs has been exaggerated in order to enable comparison with the fusinite and semifusinite data.

Total reflectance data for macroscopic charcoal clasts in charcoal horizons and inertodetrinite: Reflectance histograms, combining values for all macroscopic charcoal clasts in all charcoal horizons and all inertodetrinite data from lithotype units containing charcoal horizons are given in Fig. 6.8. Both histograms are right skewed. The macroscopic charcoal clast values have a wider spread (0.4 - 5.1%Ro) than inertodetrinite (0.7 - 4%Ro). The most frequent category for macroscopic charcoal clasts ranges from 0.5 - 2%Ro whereas inertodetrinite ranges from 1.4 - 1.9%Ro. All inertodetrinite values are within the range of values for macroscopic charcoal clasts from charcoal horizons.

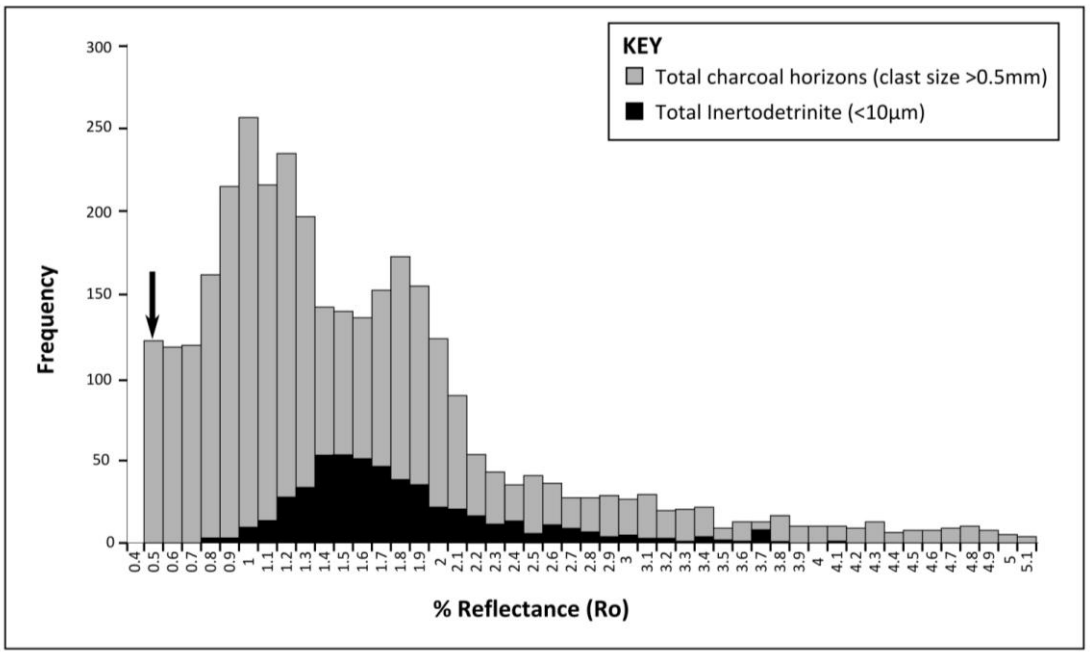

FIG. 6.8 Combined histograms of all random reflectance measurements (%Ro random) for macroscopic charcoal clasts in charcoal horizons (n = 8,600) and inertodetrinite (n = 500) from lithotype units containing charcoal horizons (Figs. 6.4, 6.6, 6.7). The black arrow represents the mean telovitrinite reflectance for all coal pillars (0.56%Ro).

6.3.3 Reflectance values of inertodetrinite from LU's that do not contain charcoal horizons

Histograms of inertodetrinite reflectance measurements for lithotype units containing charcoal horizons namely, 78(a) LU2, LU8; 88(a) LU7; 88(b) LU12 and 91 LU2, are given in (Fig. 6.4 B, D; 6.6 B, D; 6.7 B). Pillars 78(a) LU7, 91 (LU3-5) and 88(b) LU6 do not contain macroscopic clasts of charcoal in charcoal horizons but were observed during petrographic analysis to contain high reflecting inertodetrinite (chapters 4 and 5). The reflectance histogram distributions for these lithotype units are shown in Fig. 6.9.

The inertodetrinite reflectance values range from 0.8 – 4.7%Ro which is very similar to inertodetrinite from lithotype units containing charcoal horizons (0.8 – 4.1%Ro). The distribution of reflectance values varies both within and between coal pillars (Fig. 6.9) but the mean values are all within 0.34%Ro of each other. The lowest inertodetrinite values are all higher than mean vitrinite reflectance values for that lithotype unit (Fig. 6.2).

Pillar 78(a) LU7: The distribution, spread of data and most frequent category for this inertodetrinite reflectance histogram is comparable to inertodetrinite reflectance histograms from lithotype units containing charcoal horizons (compare Fig. 6.9 A to 6.4 B, D). The inertodetrinite histogram is right skewed. The spread of data is wide (0.8 - 3.8%Ro) and the most frequent category ranges from 1.3 - 1.9%Ro. The shape of the histogram is comparable to 78(a) LU8 (Fig. 6.4 D), but with a larger amount of higher reflecting values.

Pillar 88(b) LU6: The inertodetrinite reflectance histogram is right skewed and the data has a wider spread (1 – 4.7%Ro) than inertodetrinite measured in LU12 (compare Fig. 6.9 B to Fig. 6.6 D). The most frequent category is 1.6%Ro (majority of values <3%Ro). The outlying values in LU12 (2.6 - 3.7%Ro; Fig. 6.6 D) were also observed in LU6 (Fig. 6.9 B). However, there are three further outlying values (4.1 - 4.7%Ro) which are missing from the inertodetrinite reflectance histogram for LU12 in Fig. 6.6 B.

Pillar 91 LU3-5: Both inertodetrinite reflectance histograms are right skewed and have a narrower spread of data than seen in the macroscopic charcoal in horizons in LU2 (compare Fig. 6.9 C to Fig. 6.7). The most frequent category is 1.9%Ro which is higher than inertodetrinite in LU2 but in both inertodetrinite reflectance histograms the majority of measurements are <2.7%Ro. Three measured values are higher reflecting (4.1%Ro) than any observed in Fig. 6.7 B but are within the range of measurements for macroscopic clasts of charcoal in charcoal horizons (Fig. 6.7 A).

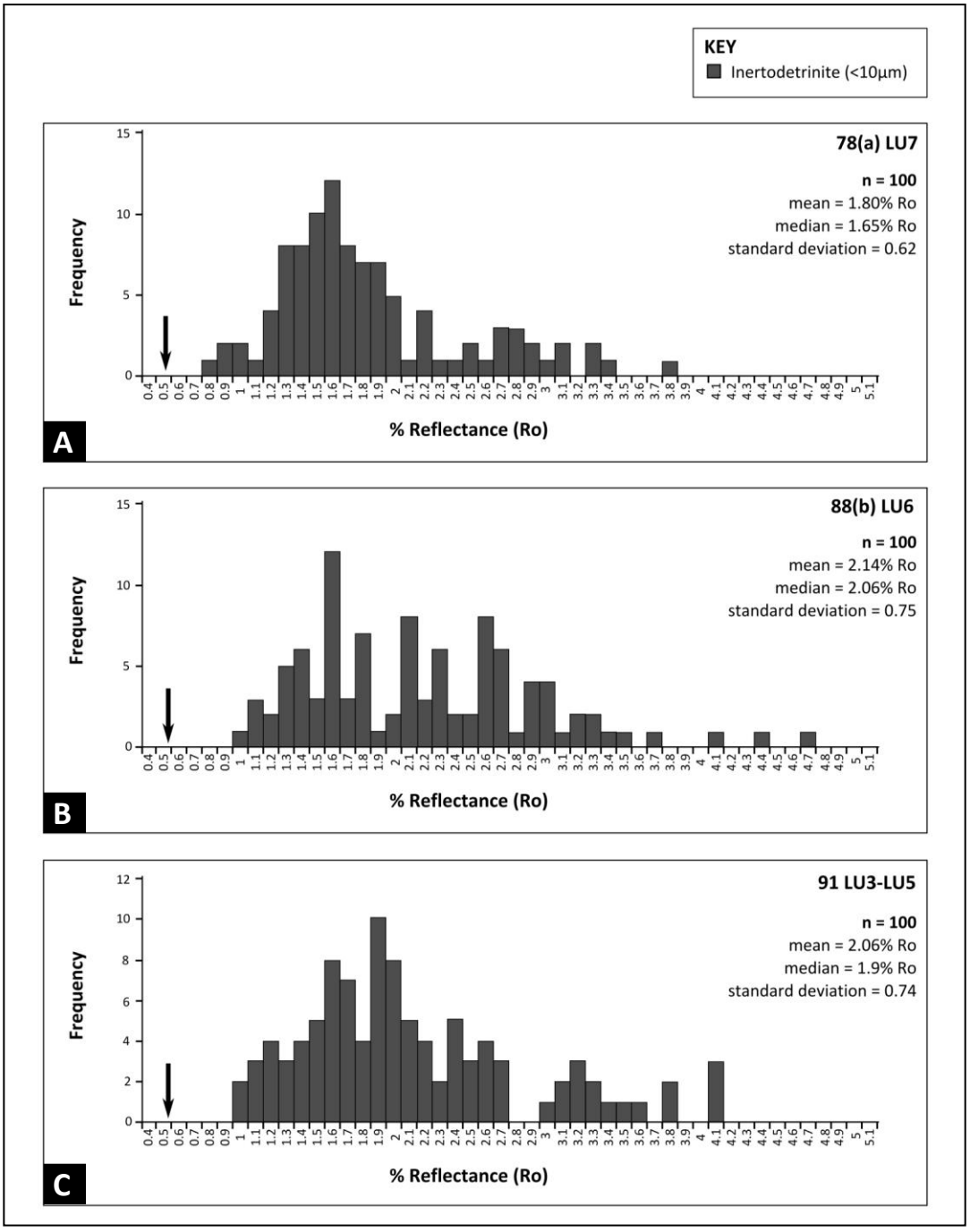

FIG. 6.9 Histograms showing the distribution of inertodetrinite reflectance values (%Ro random) from lithotype units that do not contain charcoal horizons. Data are presented with mean, median and standard deviations. The black arrow represents the telovitrinite mean reflectance value for that coal pillar.

6.3.4 Minimum charring temperatures derived from inertinite reflectance data

Inferred charring temperatures from (1) the mean, (2) the modified mean (3) the most frequent category ranges and (4) $3Ro_{max}$ are presented in Table 6.2 for macroscopic clasts of charcoal in charcoal horizons and Table 6.3 for inertodetrinite.

The reasoning behind the use of these various values is explained in the following text.

Extrapolating ancient charring temperatures using inertinite reflectance is not as straightforward as for modern charcoals. Increasing aromatisation during coalification may increase inertinite reflectance (Taylor et al., 1998; Smith and Smith, 2007). Fusinite already has high aromatisation which gives its high reflectance. In addition, fusinite is relatively inert during coalification due to the devolatisation which occurred during initial charring (Pyne et al., 1996; Taylor et al., 1998). Lower reflecting semifusinite is not chemically inert (Choudhury et al., 2008; Ascough et al., 2011) and its reflectance increases with vitrinite reflectance as maturation progresses (Bustin and Guo, 1999). These coals have low vitrinite reflectance values (0.56%Ro_{mean}; Fig. 6.2) therefore coalification may be considered to have had a negligible effect on fusinite and semifusinite reflectance. However, some of the reflectance measurements of macroscopic charcoal clasts in charcoal horizons are within the measured vitrinite range (Fig. 6.4 A, C; Fig. 6.6 A, C; Fig. 6.7 A). The reflectance values need to be higher than that of thermal maturation in order to confirm that these are charcoal (Glasspool et al., 2004) therefore these reflectance values probably represent the uncharred or partially charred areas of the macroscopic charcoal clasts (Jones et al., 1993). In order to take this into account, all values within the vitrinite reflectance range for each pillar (Fig. 6.2) were removed and the mean value was recalculated to give the 'modified mean' value, which therefore represents all charred material (Table 6.2).

The reflectance histograms for both macroscopic charcoal in charcoal horizons and inertodetrinite are not normally distributed (Fig. 6.4; Fig. 6.5; Fig. 6.6; Fig. 6.7; Fig. 6.9) which has also been noted in other inertinite reflectance assemblages (e.g. Spackman and Thompson, 1966; Bustin and Guo, 1999) and modern charcoal reflectance assemblages (e.g. McParland et al., 2009b). In a skewed distribution the median can give a better impression of the true central value instead of the mean so the median (Ro_{median}) is given in Table 6.1 and Table 6.2 as it is more robust in the presence of outliers. However, in pillars 78(a) and 88(a, b) the mean and median values are almost the same (Fig. 6.4; Fig. 6.6) and in multimodal reflectance histograms (e.g. 78(a) LU2 - CH1, CH4; 78(a) LU8 - CH1, CH3; 88(a) LU7 - CH2;

88(b) LU12; 91 LU2 - CH1, CH2; Fig. 6.3), especially those dominated by low reflecting charcoal, the median, mean and 'modified mean' values are not necessarily representative of the majority of the reflectance values.

By definition the mode represents the single most frequent value. However, the distribution of reflectance values for the majority of clasts in charcoal horizons is multimodal. Therefore, the mode only represents four of the thirteen charcoal horizons (Fig. 6.3). The range of most frequent values may therefore be considered to better represent each horizon where multiple peaks are observed and may therefore represent different fire temperature assemblages (Table 6.2). However, the most frequent category does not include the maximum reflectance values as these are often only represented by a couple of values. The maximum value (Ro_{max}) needs to be considered as these samples have been charred for unknown durations and therefore the maximum reflectance can be used to represent the minimum charring temperature (Scott and Glasspool, 2006). A single value may not be considered to be representative and therefore the mean of the three maximum reflectance values ($3Ro_{max}$) has been given as this may be a more appropriate approximation of minimum charring temperature (e.g. Hudspith et al., 2010).

TABLE 6.2 (overleaf) Summary table of measured reflectance values and inferred charring temperatures of macroscopic charcoal in charcoal horizons for all coal pillars. Inferred charring temperatures are extrapolated from the graph in Fig. 6.1 (Scott and Glasspool, 2005). Next to the charcoal horizon number the italicised value in brackets corresponds to the total number of measurements per horizon which is based on three vertical transects through each horizon (Fig. 6.3) and 50 random reflectance measurements per clast. The *n* value varies depending on the thickness of the charcoal horizon. Modified mean values remove all measured values within the telovitrinite reflectance range. Some charcoal horizons do not have charcoal clasts with reflectance values in the vitrinite reflectance range and therefore just the Ro_{mean} value is presented. $3Ro_{max}$ represents the mean of the three highest values. The most frequent category range represents the reflectance range for the majority of data for that histogram which can be uni- bi- or trimodal (Fig. 6.3).

Coal pillar and LU	*Charcoal horizon (n = no. of measurements)*	*Ro mean (%)*	*Charring temperature (°C)*	*Modified Ro mean (%)*	*Charring temperature (°C)*	*Ro max (%)*	*Charring temperature (°C)*	*3 Ro max (%)*	*Charring temperature (°C)*	*Most frequent range (%Ro)*	*Charring temperature (°C)*
78(a) LU2	**CH 1** *(n = 300)*	0.90	335	1.14	350	2.02	425	2.02	425	0.5 - 0.6 0.9	300 - 310 335
	CH 2 *(n = 700)*	0.93	335	0.99	340	1.61	400	1.60	400	0.9 - 1	335 - 340
	CH 3 *(n = 250)*	0.99	340	1.13	350	1.66	402	1.60	400	1.1-1.3	350 - 360
	CH 4 *(n = 450)*	0.94	335	1.1	350	2.0	422	1.97	420	0.6 0.9 - 1	310 335 - 340
78(a) LU8	**CH 1** *(n = 1,300)*	1.84	415	1.97	420	5.10	655	5.06	650	0.6 – 1.2 1.8 – 2.1	310 - 350 410 - 425
	CH 2 *(n = 950)*	1.62	400			3.74	530	3.66	520	0.9 – 1.3 1.4 – 2.1	335 – 360 365 - 425
	CH 3 *(n = 600)*	2.09	425	2.32	435	5.07	655	4.89	610	0.7 - 0.8	320 - 325
88(a) LU7	**CH 1** *(n = 1,100)*	1.39	365			2.38	435	2.35	435	1.1 – 1.3 1.8 – 1.9	350 - 360 410 - 420
	CH 2 *(n = 500)*	1.19	350	1.22	350	3.80	535	3.64	520	0.8 - 1	325 - 340
88(b) LU12	**CH 1** *(n = 600)*	1.50	395			2.37	435	2.33	435	1.2 – 1.4 1.7 – 1.9	350 - 365 405 - 420
91 LU2	**CH 1** *(n = 550)*	2.08	425			5.08	655	5.05	650	0.8 – 2 2.8 – 3.2 4.8	325 - 420 460 - 500 605
	CH 2 *(n = 850)*	1.92	420	1.95	420	4.89	610	4.77	605	0.9 – 1.4	335 - 365
	CH 3 *(n = 450)*	1.77	410			3.80	535	3.71	530	1.5 – 1.7	395 - 405

Coal pillar and LU	*Ro mean (%)*	*Charring temperature (°C)*	*Ro max (%)*	*Charring temperature (°C)*	*3 Ro max (%)*	*Charring temperature (°C)*	*Most frequent range (%)*	*Charring temperature (°C)*
78 (a) LU2	1.48	375	3.27	500	2.69	450	1.3 – 1.7	360 – 405
78(a) LU7	1.80	410	3.78	530	3.49	510	1.3 – 1.9	360 – 420
78(a) LU8	1.85	415	4	545	3.78	530	1.4 – 2.1	365 – 425
88(a) LU7	2.07	425	3.70	530	3.65	520	1.8 – 1.9	410 – 420
88(b) LU6	2.14	428	4.64	590	4.34	560	1.6	400
88(b) LU12	1.66	402	3.63	520	3.21	500	1 – 1.5 1.7 – 1.9	340 – 375 405 – 420
91 LU2	1.77	410	3.79	530	3.71	530	1.3	360
91 LU3-5	2.06	425	4.07	555	4.06	555	1.9	420

TABLE 6.3 Summary table of reflectance values and inferred charring temperatures of inertodetrinite for all coal pillars. Charring temperatures are extrapolated from the graph in Fig. 6.1 (Scott and Glasspool, 2005). The values correspond to 100 random reflectance measurements throughout a given lithotype unit. $3Ro_{max}$ represents the mean of the three highest values. The most frequent category range represents the reflectance range for the majority of data for that histogram which can be uni- or bimodal (Fig. 6.3). Rows highlighted in grey are inertodetrinite data from lithotype units containing macroscopic charcoal in charcoal horizons.

6.4 DISCUSSION

6.4.1 Charcoal characteristics of different wildfire types and temperatures

In chapters 4 and 5 patterns of inertinite distribution were interpreted to represent surface and crown wildfires. In terms of fire temperature it may be more appropriate to consider using the terms smouldering and flaming fires. Therefore, the wildfire types inferred in chapters 4 and 5 may need reconsidering.

Smouldering fires (ground fires) are a flameless type of combustion, advance slowly at low temperatures, and burn trunks, litter, duff, humus, peat and soils (Belcher et al., 2010). Combustion temperatures during smouldering fires are typically 300°C - 600°C (Lobert and Warnatz, 1993; Pyne et al., 1996; Muraleedharan et al., 2000; Otto et al., 2006) with a slow spread rate of 1 - 50mm/hr^{-1} (Rein et al., 2008). However, there is no evidence for ground fires, hence smouldering combustion, in any coal pillar.

Flaming surface and crown fires are short-lived (minutes) with a fast spread rate of 1m/hr^{-1} (Rein et al., 2008). Flaming surface fires can be initiated at low temperatures (300°C - 350°C) (Drysdale, 2011) and typically burn the surface litter and biomass at relatively low temperatures (300°C - 500°C) (Hartford and Frandsen, 1992). This is in contrast to flaming crown fires which are more intense, and combustion temperatures can be as high as 1500°C (Drysdale, 1998; Muraleedharan et al., 2000).

Flaming crown fires are high temperature fires (700°C - 1500°C) (Pyne et al., 1996; Drysdale, 1998). Fire temperatures >1000°C are likely to produce more ash than charcoal (e.g. Debano and Conrad, 1978; Boerner, 1982) therefore, crown fires are likely be represented by small amounts of very high reflecting charcoal (inertodetrinite). Most of the fuel consumed in a crown fire is small in size (<1cm)

(de Groot et al., 2004) and therefore produces large quantities of microscopic charcoal (Komarek et al., 1973; Pyne et al., 1996; Scott, 2010) which may be represented by inertodetrinite in coal. By contrast, flaming surface fires will be represented by low reflecting charcoal. Low temperature charcoal is robust during water transport and is therefore likely to be preserved as macroscopic pieces (Vaughan and Nichols, 1995; Nichols et al., 2000).

6.4.2 Interpreted minimum charring temperatures and fire types from macroscopic charcoal in charcoal horizons

Ro_{mean} and $Ro_{modified\ mean}$ of macroscopic charcoal clasts in all thirteen horizons indicate minimum charring temperatures of ≤435°C (Table 6.2). In six of the horizons inferred charring temperatures are ≤435°C even when using the single maximum Ro value (Table 6.2). These horizons are interpreted to represent low temperature surface fire events (chapters 4.4.4.2; 4.4.5.2; 4.4.6.2; 5.4.4.2) and much of the other low temperature charcoal in the other seven horizons is probably also derived from low temperature surface fire events.

In three charcoal horizons the inferred charring temperature derived from Ro_{max} is 530°C - 535°C and in four horizons it reaches >600°C (610°C - 655°C) (Table 6.2). These charcoal horizons may represent higher temperature fires but are still mostly within the range of modern surface fires (see section 6.4.1).

6.4.3 Temporal variation in minimum charring temperatures between charcoal horizons

There is temporal variation in the reflectance histograms of individual charcoal horizons both between lithotype units and between pillars (Fig. 6.3) which may suggest variation in wildfire temperature during these short intervals of coal pillar formation. Furthermore, in pillars with multiple charcoal horizons e.g. 78(a) LU2, 78(a) LU8, 88(a) LU7 (Fig. 6.3), individual horizons alternate between containing higher and lower reflecting charcoal. When using $3Ro_{max}$ the inferred charring temperature differences between individual horizons can range from 20°C - 120°C (Table 6.2) which provides evidence for variation in charring temperatures between individual fire events.

The thinnest lithotype unit [78(a) LU2; 10mm; Fig. 6.3] was noted to contain the most charcoal horizons and therefore represents the shortest fire return interval of all coal pillars (calculated as 0.5 – 143 years; 4.4.9.2). Inferred charring temperatures from all four horizons are <425°C (2.02% $3Ro_{max}$; Table 6.2) but the most frequent categories show that the majority of reflectance values represent inferred minimum charring temperatures of 300°C - 360°C (Table 6.2). This is in contrast to thicker lithotype units [78(a) LU8; 91 LU2; Fig. 6.3] which contain fewer horizons and therefore represent longer fire return intervals (calculated as 10 – 1485 years for 91 LU2; 4.4.9.2). Inferred charring temperatures are much higher 520°C - 650°C ($3Ro_{max}$ = 3.66 - 5.06%; Table 6.2) therefore less frequent fires have produced higher temperature charcoals.

6.4.4 Within clast variation in reflectance: implications for charring duration

Most pillars [with the exception of 88(b)] contain low reflecting charcoal in the vitrinite reflectance range (1% - 24.5%; Fig. 6.4 A, C; Fig. 6.6 A, C; Fig. 6.7 A). Many of the clasts in horizons are partially charred (4.4.4.2; 4.4.5.2). Jones et al. (1993) have documented a significant change in reflectance through a partially charred clast from 0.5%Ro in the inside to 2.5%Ro for the outer fusinite. The inner part needs only to have reached 180°C - 220°C to attain a measureable reflectance and thus to be partially charred. This reflectance will then increase further during coalification (Jones et al., 1993). Hammes et al. (2006) consider charring to be complete after 5h, therefore the partially charred macroscopic charcoal clasts in charcoal horizons were produced in short duration surface fires. In more intense charring temperatures, a layer of high reflecting charcoal (>5%Ro) can form around uncharred internal areas (Jones et al., 1993). A longer charring duration may fully char the clast, which would result in a more uniform reflectance throughout the clast. There are no wholly high reflecting clasts in charcoal horizons (as shown in Fig. 6.5 A, only 12 of 57 clasts have mean Ro random reflectance values >2.5%). The wide range in reflectance values within individual clasts suggests that a large proportion may have been partially charred during short duration surface fires. For further discussion of the implications of various charring durations on inferred charring temperatures, see chapter 8.

6.4.5 Wildfire origin of microscopic inertodetrinite (<10µm)

Inertodetrinite particles have inferred charring temperatures <425°C (using Ro_{mean} = 2.1%; Table 6.2) and <530°C (using $3Ro_{max}$ = <3.8%) for lithotype units with macroscopic clasts in charcoal horizons and <560°C (using $3Ro_{max}$ = 4.3%) for lithotype units without charcoal horizons. However, no inertodetrinite values are <0.8%Ro or 325°C. Experimental charcoalification has shown that cell walls become homogenised at temperatures >300°C - 325°C (McGinnes et al., 1971; Scott, 2000) and cell walls are homogenised in the inertodetrinite. This demonstrates that all inertodetrinite particles represent fully charred material.

These maximum reflectance values, hence minimum charring temperatures, of inertodetrinite are not indicative of the temperatures reached during flaming crown fires (see section 6.4.1). All fire types produce large quantities of airborne particulates (Patterson et al., 1987) and the microscopic inertodetrinite observed in lithotype units between those containing macroscopic charcoal in charcoal horizons may represent windblown charcoal from surface fires outside the immediate peat-forming environment.

Reflectance measurements of inertodetrinite particles from lithotype units containing charcoal horizons are all within the reflectance range of the macroscopic charcoal clasts from the charcoal horizons (Figs. 6.4 – 6.8). This suggests that both size fractions have been charred to the same temperatures and may derive from the same surface fire.

Crown fires are typically of short duration (see section 6.4.1) and consume varying sized fuel from foliage to twigs (Agee et al., 2002; Scott and Reinhardt, 2001). Foliar moisture varies considerably throughout the year, with live fuels containing up to 250% moisture (McAllister et al., 2012). Despite the high temperatures typical of crown fires (section 6.4.1), a short duration crown fire consuming fuel with high moisture contents may result in incomplete charring hence produce low temperature charcoal. Reflectance work on charcoal derived from modern flaming crown fires is needed to ascertain whether low temperature charcoal can be derived from crown fires. There may also be a continuum from surface to crown fires. The most common type of modern crown fire (active crown fire) includes both surface and crown fuels,

independent crown fires that burn without influence of surface fuels are very rare (Scott and Reinhardt, 2001). Therefore, the charcoal in these coal pillars could in fact be derived from contemporaneous surface and crown fires.

6.4.5.1 Implications for calculating fire return intervals

If inertodetrinite is windblown material derived from surface fires then surface fires may have been considerably more frequent than previously calculated (see chapter 4.4.9.2).

6.4.6 Preservation of macroscopic fusinite and semifusinite clasts in charcoal horizons: implications for relative fire proximity

All inferred charring temperatures of macroscopic charcoal (>425µm) from charcoal horizons and inertodetrinite are within the temperature range of modern surface fires (section 6.4.1). The combination of both lower (semifusinite) and relatively higher (fusinite) reflecting macroscopic charcoal in charcoal horizons may suggest a limited transport history (Vaughan and Nichols, 1995; Scott, 2010) as charcoals preferentially sort into separate fractions during water transport due to their buoyancy and waterlogging characteristics (Nichols et al., 2000). Charcoal formed at >600°C is brittle and susceptible to fragmentation (Scott and Jones, 1991; McParland et al., 2009a; Lancellotti et al., 2010). However, charring temperatures >600°C were inferred for macroscopic charcoal clasts from four charcoal horizons (Table 6.2). These high temperature macroscopic charcoal clasts are not fragmented therefore, suggesting that this charcoal is unlikely to have undergone extensive water transport (Clark, 1988).

6.5 CONCLUSIONS

Reflectance measurements of macroscopic charcoal clasts in charcoal horizons and inertodetrinite from *in situ* coal pillars have revealed that previous interpretations of palaeowildfire types (chapters 4 and 5) need to be reconsidered. Ro_{mean} and $Ro_{modified\ mean}$ reflectance values of macroscopic charcoal clasts from thirteen charcoal horizons, in all coal pillars, give inferred charring temperatures of ≤435°C. Macroscopic charcoal in charcoal horizons is therefore interpreted to be derived from low temperature surface fire events. There are no wholly high reflecting macroscopic charcoal clasts in charcoal horizons and most coal pillars [with the

exception of 88(b)] contain charcoal within the vitrinite reflectance range (1 - 24.5%). This suggests that a large proportion of charcoal in horizons has been partially charred in a short duration fire. Using Ro_{max} values, higher temperature charcoal is inferred for seven charcoal horizons (ranging from 530°C - 655°C), which is still within the temperature range of modern surface fires. There is evidence for temporal variation in fire temperatures within lithotype units with individual charcoal horizons alternating between containing lower and higher reflecting charcoal (Fig. 6.3). Less frequent fires have yielded higher temperature charcoals [78(a) LU8 and 91 LU2] whilst more frequent fires have yielded lower temperature charcoals [78(a) LU2].

Microscopic inertodetrinite from lithotype units both within and without charcoal horizons is within the range of measured reflectance values for macroscopic charcoal clasts from charcoal horizons. Using Ro_{mean} the inferred charring temperatures are < 425°C (or <560°C using $3Ro_{max}$). There is no evidence for very high reflecting charcoal, such as might have been formed within the temperature range of modern crown fires. Inertodetrinite from lithotype units containing charcoal horizons is therefore likely to be derived from the same surface fire event as the macroscopic charcoal clasts. Inertodetrinite from lithotype units without charcoal horizons is interpreted to represent windblown microscopic charcoal from surface fires outside of the immediate peat-forming environment.

Charcoal of different sizes and produced at different temperatures, can separate preferentially into size fractions during post-fire transport due to the waterlogging characteristics of the charcoal. The combination of both microscopic inertodetrinite and macroscopic charcoal clasts in horizons and the variation in reflectance within and between individual macroscopic charcoal clasts may therefore reflect a short transport history.

Interpretations of palaeowildfire type in chapters 4 and 5 were based on inertinite distribution and qualitative reflectance of inertinite macerals. Macroscopic clasts of charcoal (fusinite and semifusinite) in charcoal horizons were interpreted as representing low temperature surface fire events whereas microscopic inertodetrinite was interpreted as a windblown fraction from crown fires. Quantitative reflectance

measurements, hence inferred minimum charring temperatures, have now revealed that both macroscopic charcoal from charcoal horizons and microscopic inertodetrinite are derived from relatively low temperature surface fires. Inertodetrinite does not represent high temperature charcoal from flaming crown fires. These data therefore show that it is essential to quantify the reflectance of both macroscopic charcoal in horizons and microscopic inertodetrinite in order to interpret palaeowildfire types.

CHAPTER 7

THE EFFECT OF INERTINITE CONTENT AND DISTRIBUTION ON CHARACTERISATION PROPERTIES OF COAL

Mean coal properties (including maceral content and characterisation properties) are considered for coal purchasing decisions. The British standard (BS) for coal sampling regards a channel sample as representative of the entire seam (BS ISO 14180: 1998). However, inertinite is highly susceptible to fragmentation and if concentrated in horizons then the finer fractions of inertinite may be lost during mining and transport to the stockpile. Consequently, coal purchased from this stockpile may not necessarily reflect the same inertinite content of the seam as a whole. This has implications for purchasing strategies based solely on the BS analysis.

The majority of the seams in this study were in excess of 10m thick, which made it impossible to obtain full channel samples (BS ISO 14180: 1998) from any coal seam. Therefore, in this thesis, three sampling methods were adopted – (i) randomly selected samples from named seams (termed general samples herein) which can be argued to be as close to the BS sampling as was possible given the circumstances (ii) two size fractions from the stockpile (termed stockpile pieces and stockpile fine) to represent potentially purchased coal; (iii) individual lithotype units (LU's) from coal pillars from named seams to include those with and without inertinite concentrated in horizons.

In order to determine if inertinite distribution affects coal characterisation the following hypotheses will be tested:

i) LU's with inertinite clasts concentrated in horizons will differ from general samples from both the named seams and stockpile samples.

ii) The stockpile fine fraction will differ from stockpile pieces fraction and from lithotype units with inertinite clasts in horizons.

Inertinite contains less %volatile matter than vitrinite and liptinite (Marchioni, 1983; Mathews et al., 1997; Borrego et al., 2000) and therefore requires a higher temperature for ignition during combustion, and may pass through the furnace unburnt, resulting in poor burnout (Vleeskens and Nandi, 1986). This may result in inefficient combustion (Beeley et al., 1995) in power stations and a high carbon content of the ash, which means that the ash cannot then be utilised (Lester, 1994; Beeley et al., 1995; Cloke et al., 1997a).

In order to determine if inertinite distribution affects combustion behaviour the following hypothesis will be tested:

(i) Lithotype units with inertinite concentrated in horizons will yield more particles of pure inertinite when crushed and this may lead to poor burnout.

Problems with combustion experiments

It was originally expected that c. 10 gram sample size would be sufficient for DTF (Drop Tube Furnace) experiments. However, the coals in this study have high volatile contents so a larger sample size was required (c. 20 grams), which meant that individual lithotype units could not be studied. Furthermore, the analyses proved to be very time consuming and it was judged impractical to study more than a few samples. Therefore, it was not possible to determine if the distribution of inertinite affected combustion and led to poor burnout. Some initial results (Appendix 8) were obtained regarding the effect of varying inertinite content in seams, which are the first results of this kind for Permian coals from the Kuznetsk Basin.

7.1 INTRODUCTION

7.1.1 Coal maceral content and characterisation properties

The chemical properties of a given coal are determined using characterisation analyses (Borrego et al., 2000). These are subdivided into proximate (volatile and non-volatile organic coal components; %inherent moisture, %ash, %fixed carbon, %volatile matter) and ultimate analyses (%Carbon, %Hydrogen, %Nitrogen, %Oxygen, %total Sulphur) (Ward, 1984). Ranges in resulting data are due to coal rank and ranges between samples of the same rank are due to differences in

petrographic composition (Ward et al., 2005; Gupta, 2007; Suárez-Ruiz and Ward, 2008) or environment of deposition (%ash, %total Sulphur) (Scott, 1989b).

The relationship between coal petrography and certain coal characters is well established. Macerals have distinct chemical properties depending on the original plant material, alteration during deposition and rank (Crelling et al., 1992). Chemical characterisation data should represent an average of values of the individual maceral components in the coal (Borrego et al., 2000). Previous work on characterisation of density separated maceral groups has shown that, compared to vitrinite and liptinite, inertinite contains the lowest %Hydrogen, %Oxygen and %volatile matter and the highest %Carbon (Tsai, 1982; Dyrkacz et al., 1984; White et al., 1989; Speight, 1990; Mastalerz and Bustin, 1993; Borrego et al., 1997; Milligan et al., 1997; Hampartsoumian et al., 1998; Borrego et al., 2000; Su et al., 2001; Tang et al., 2005; Suárez-Ruiz and Ward, 2008). Fusinite, of the inertinite maceral group (Table 2.3), exhibits these characteristics more than other inertinite macerals (Borrego et al., 2000; ICCP, 2001; Ward et al., 2005). Ranges in values for these characterisation properties also depend on the coal rank (ICCP, 2001). Of all the characterisation properties, petrographic variation in coals of the same rank is most clearly expressed by differences in %volatile matter (Marchioni, 1983; Mathews et al., 1997; Borrego et al., 2000) which is dependent on the most dominant maceral group in a given sample (Smith and Smith, 2007). Therefore, data for individual separated maceral groups does not represent the characterisation properties of the coal that is commercially combusted, as this is a bulk sample containing all maceral groups. These known relationships between inertinite and characterisation properties will therefore be applied to the bulk coal samples (containing all maceral groups), from this study, to determine the extent to which inertinite content affects the overall characterisation properties of the coal.

Standard coal petrographic analysis is typically carried out on crushed coal samples which do not retain their inertinite distribution. Petrographic work on *in situ* coal pillars of known inertinite distribution (chapters 4 and 5) has shown that inertinite content and distribution can vary both spatially and temporally at a centimetre scale. Therefore, analysis of crushed coals may not fully represent the variation in inertinite content or distribution within a seam (chapter 5). Lithotype units from four *in situ*

coal pillars [78(a), 88(a), 88(b) and 91] and general seam samples from the same seams (78 and 88) are compared to document within seam variation in coal characterisation properties. Four repeating patterns of inertinite distribution have been observed in all lithotype units from all coal pillars (chapters 4 and 5). Characterisation data from all lithotype units are compared in order to determine whether the inertinite distribution affects the gross properties of the coal and if patterns of inertinite distribution can be identified from certain coal characters.

Characterisation data from two stockpile size fractions (chapter 2.1.3) are compared to data from all general seam samples (seams 68 to 94) as well as a 'combined stockpile' (see 7.2.2), produced in the laboratory of all worked seams (73 - 91) and an 'averaged stockpile', which is a mean of all characterisation data for individual general samples (73 - 91), in order to determine what seams are represented by the stockpiles.

7.2 METHODS

7.2.1 Field sampling: general samples and stockpiles

General samples were taken from thirteen coal seams numbered 68-94 (see chapter 2.1.2 for sampling techniques; chapter 3) and two stockpile size fractions (see chapter 2.1.3). Multiple general samples from the same seam were labelled in the field according to their position in the seam/ relation to other samples/ or Mine (1 or 2) location. Refer to Appendix 6 for specific sampling information for general seam samples as well as macroscopic description of each sample in hand specimen.

Due to seam access and availability not all worked seams from both Mines could be sampled during the sampling period. In addition, other Mines were also operational in the area therefore other seams (not studied in this thesis) may have been included in the two stockpile fractions.

7.2.2 Combined samples

As a direct comparison to the stockpile size fractions analysed, a combined stockpile was also produced in the laboratory, consisting of subsamples of all worked seams (22 samples; not including seams 68, 92 and 94) during the sampling period. There

is no petrographic data for the combined stockpile as it was produced after the general samples were pulverised.

Combined samples of all lithotype units from pillars 78(a) and 88(a) were also produced in the laboratory as a comparison to general seam samples from seams 78 and 88. Lithotype units were subsampled in proportions relative to lithotype unit thicknesses to more accurately represent the characterisation properties of the coal pillar as a whole.

7.2.3 Petrographic methodology

Preparation of polished blocks of crushed coal is described in chapter 2.3.2 and 2.3.3. Petrographic analysis was carried out using the methodology outlined in chapter 2.4.4 and macerals were identified using ICCP classification schemes (1998, 2001).

7.2.4 Vitrinite reflectance methodology

Vitrinite (telovitrinite) reflectance was undertaken on general seam and stockpile samples. For the ICCP definition of telovitrinite refer to Table 2.3. Refer to chapter 6.2 for microscopy methodology. The reflectance microscope was calibrated using the same reflectance standards as in chapter 6.2.1, from highest to lowest, GGG (gadolinium gallium garnet) (Ro 1.7486%), YAG (yttrium aluminium garnet) (Ro 0.929%) and spinel (0.393%). Three vertical traverses were taken of each crushed coal block (as in section 2.4.4) with a vertical step distance of 425µm (1 field of view). One measurement was taken per clast to ensure the maximum area of the block was covered and a minimum number of measurements were taken on a single clast. A total of 100 random reflectance measurements were taken per sample. For raw data see Appendix 7.

7.2.5 Characterisation methodology

Production of pulverised fuel for characterisation analysis is detailed in chapter 2.2. Characterisation analyses (proximate and ultimate) were carried out at the RWE Npower Fuel Characterisation Laboratory Facility in Swindon, following strict British Standard procedures (detailed in Appendix 3). Both proximate and ultimate

analyses are required to fully assess the extent to which the inertinite content and distribution affects the chemical properties of the coal.

All proximate and ultimate analyses were run in triplicate; any results outside of the narrow ranges set by the BS ISO standards were replicated (see Appendix 7 for raw data). %Inherent moisture and %ash are reported to an air dried (ad) basis whereas %volatile matter, calorific value, %Carbon, %Hydrogen, %Nitrogen, %Oxygen, %total Sulphur are reported to a dry ash free (daf) basis. Due to the small sample size of lithotype units from *in situ* coal pillars, proximate analyses of pillars; 78(a) LU1-10, 88(a) LU1-7, 88(b) LU1-14, 91 LU1-5 and ultimate analyses of pillars; 88(b) LU3, LU8-14 and 91 LU1-2 were undertaken at the Center of Applied Energy Research (CAER), Kentucky by J. Hower, according to American ASTM coal characterisation standards (ASTM standard D5142-04, 2004; ASTM standard D3176, 2009). Ultimate analyses were undertaken in both laboratories using the same equipment (CHN 2000 analyser) and results should therefore be within the British standard reproducibility limits (BS ISO 29541: 2010). The surfaces of coal pillars 88(b) and 91 had been exposed for several months prior to analysis and may therefore have been oxidised.

7.2.6 X-Ray Diffraction

XRD was undertaken on general samples from seams 78, 91(1) and 92 in order to identify petrographically point counted mineral matter. X-Ray Diffraction methodology is detailed in chapter 2.8.

7.2.7 Coal rank parameters

Coal rank represents the degree of metamorphism (coalification) that the peat has undergone during its burial history (Ward and Surárez-Ruiz, 2008). The chemical and physical alteration of material occurs in progressive rank stages from lignite, subbituminous, bituminous, anthracite to meta-anthracite (Taylor et al., 1998). The degree of coalification is primarily controlled by the maximum temperature reached and heating duration. The maximum temperature ultimately depends on the depth of subsidence, the geothermal gradient and heat conductivity from the under- and overlying rocks (Teichmüller, 1987a).

Vitrinite reflectance is normally used as the main coal rank parameter (Teichmüller, 1989) as it is unaffected by petrography or ash content unlike the other rank parameters given in Table 7.1. Assignment of rank of these Permian coal samples will therefore be based on vitrinite reflectance. There are no large faults or intrusive bodies in the study area (Fig. 3.1 B) that could cause localised elevated coal rank within individual seams. It is therefore likely that the coal seams in this study will be of comparable rank throughout the sequence. Consequently, any variations in chemical properties within and between seams are likely to be due to differences in petrographic composition.

Rank	%Carbon (daf basis)	%Volatile Matter (daf basis)	Calorific Value (MJ/Kg)	Vitrinite reflectance (% Ro random)	% Inherent moisture
Peat	60	64	16	0.25	75
Lignite	71	52	23	0.4	35
Subbituminous	80	40	33.5	0.6	25
High-volatile bituminous	86	31	35.6	0.97	8-10
Medium-volatile bituminous	90	22	36	1.47	
Low-volatile bituminous	91	14	36.4	1.85	
Semi-anthracite	92	8	36	2.65	
Anthracite	95	2	35.2	6.55	

TABLE 7.1 Coal rank parameters using German and North American classification schemes. Daf represents dry ash free basis (adapted from: Teichmüller, 1987b; Taylor et al., 1998; Suárez-Ruiz and Ward, 2008).

7.2.8 Critical R^2 value and correlation matrix

The statistical significance of the correlations observed between maceral groups and characterisation properties (see section 7.3.7) was assessed by calculating a critical R^2 value and using a symmetrical correlation matrix. The statistical significance of an R^2 value can be determined using a two-tailed t test (see Equation 7.1 below). The t-test is two-tailed as R may be significantly greater or smaller than zero. Statistical tables give a critical value of t based on 5% significance and n-2 degrees of freedom (Davis, 2002; Appendix 7).

$t = R\sqrt{(N-2)}/\sqrt{(1-R^2)}$

EQUATION 7.1: two-tailed t test with n-2 degrees of freedom (Davis, 2002).

The sample size of a data set can be used to determine a critical R^2 value above which a correlation can be considered to be statistically significant and below which the correlation could occur by chance. The critical R^2 value corresponds to the maximum R^2 value that could be obtained from 95% of a random collection of points (Davis, 2002; Appendix 7). As the sample size gets larger the size of the correlation needed for significance gets smaller. The critical value is dependent on sample size so remains the same (Davis, 2002). The hypothesis can be tested as to whether the observed sample correlation is significantly different from zero. The null hypothesis states that any non zero value for R^2 may arise randomly (Davis, 2002).

7.2.9 Drop Tube Furnace (DTF) experiments

Pilot-scale DTF experiments were undertaken on two size fractions of pulverised fuel (53µm - 75µm and 106µm - 125µm) from general seam samples 78, 88, 91(2) and a stockpile fraction (stockpile fine) in order to determine whether inertinite content influenced burnout. The work was completed as part of a collaborative project with A. Nuamah and E. Lester (University of Nottingham) and presented at the ICCS&T conference, Oviedo, 2011. The petrography was completed by V. Hudspith at Royal Holloway University of London and burnout and char morphology interpretation was undertaken by A. Nuamah and E. Lester at the University of Nottingham, therefore the work is presented as an extended abstract in Appendix 8.

7.3 RESULTS

Characterisation and petrographic data are presented graphically in Figs. 7.2 – 7.18. Summary tables of petrographic and characterisation data are given in Table A.4.1 and Appendix 6, for general seam and stockpile samples, and Appendix 5 for lithotype units (and chapters 4 and 5). Raw characterisation, petrographic point count data and vitrinite reflectance measurements are presented in spreadsheets in Appendix 1 and Appendix 7 (on appendix CD).

7.3.1 Determining coal rank

%volatile matter varies considerably between samples from <43% [general samples 91(2) and 92] corresponding to subbituminous rank (Table 7.1) to 24.3% - 30.8% [pillar 88(a); Appendix 5; Appendix 6] or medium-volatile bituminous rank (Table 7.1) thus suggesting that petrography is having an overriding effect on %volatile matter as opposed to rank.

Using %Carbon, only 22 of the 48 samples studied are in the high-volatile bituminous rank range (80.04% - 83.15%; Appendix 5; Appendix 6), and 19 samples are within the subbituminous rank range. The remaining samples were analysed at CAER [lithotype units from coal pillars 88(b) and 91] and have anomalously low %Carbon values (68.4% - 71.3%; Appendix 5) which incorrectly assigns these samples to lignite rank (Table 7.1). The potential causes for this variation are discussed further in section 7.4.1. Calorific value (dry ash free basis) was only measured for general and stockpile samples due to the small sample size of lithotype units. Values range from 23.9 MJ/Kg to 30.4 MJ/Kg (with one extreme outlying value, 13.3 MJ/Kg). As expected, there is a strong negative correlation between ash content and calorific value (R^2 = 0.97; Fig. A.4.1) and samples with %ash contents >12% have calorific values <25 MJ/Kg (Appendix 6). The remaining samples have low %ash contents and calorific values within the subbituminous rank range.

Vitrinite reflectance is a more reliable rank parameter than %Carbon, %volatile matter or calorific value. Mean random vitrinite reflectance values range from 0.49%Ro (seam 92) – 0.58%Ro (seam 84) with an overall mean of 0.53% (2 sd = 0.08) for all 13 coal seams and stockpile samples. All measurements are within the subbituminous rank range.

7.3.2 Identification of mineral matter and relation to %ash content

%Ash and mineral matter show a positive correlation for all samples (R^2 = 0.66) meaning that 66% of the variance in ash data is attributed to mineral matter (Fig. A.4.2). The majority of petrographically identified ‘mineral matter’ from *in situ* coal pillars (see chapter 4.3.1; Fig. 4.2; chapter 5.3.1; Fig. 5.2) and general samples, 78, 91(1) and 92 (Fig. 7.1) is quartz and kaolinite. This may explain the comparable %ash and mineral matter contents as quartz is inert during high temperature ashing

(Gluskoter, 1975; Lin and Guet, 1990). The seam 78 general sample also contains a trace of pyrite (Fig. 7.1) and correspondingly one of the higher %total Sulphur contents (0.63%), (Fig. 7.4).

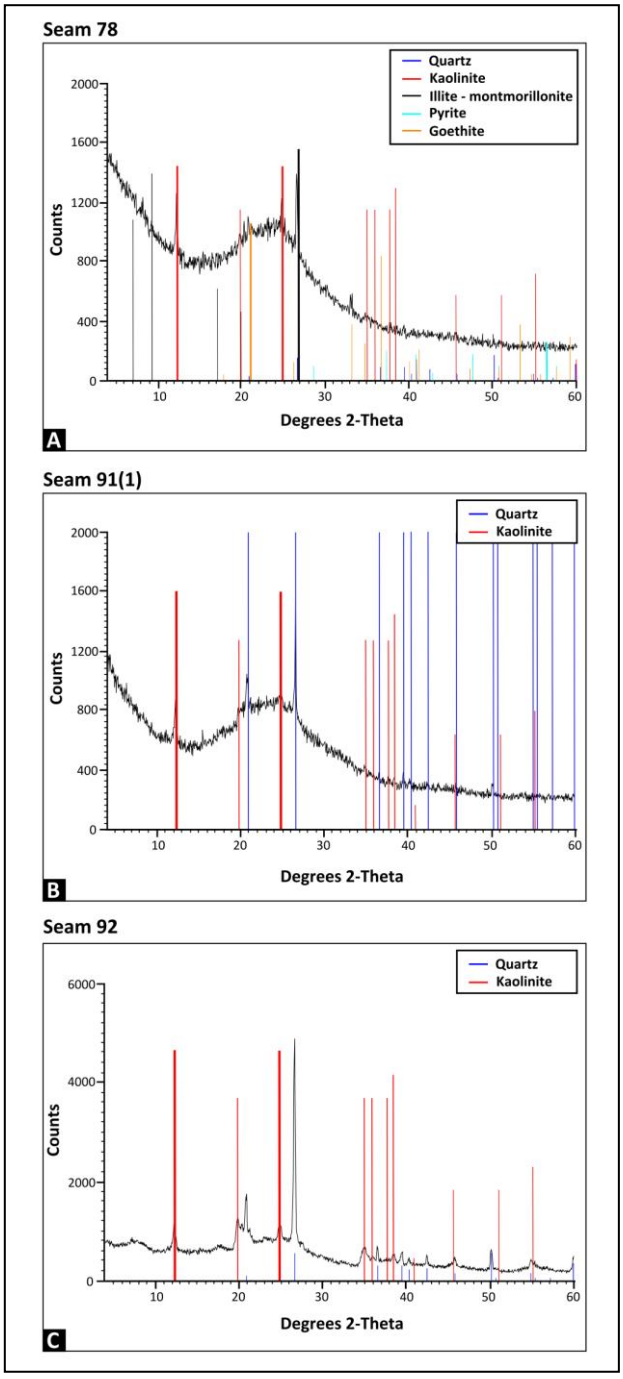

FIG. 7.1 XRD traces showing differences in mineral content between general crushed coal samples from seams 78, 91(1) and 92. The area of elevated counts between 20-27 degrees 2-Theta on the background trace (black zig-zagged line) represents the organic matter content of the coal and the flatter the background trace, the higher the mineral content of the coal (compare **A, B** to **C**). The thickness of each coloured line represents the general abundance of that mineral scaled to the peak on the background trace. Red lines = kaolinite, blue = quartz, black = illite - montmorillonite, light blue = pyrite, orange = goethite.

7.3.3 Inter- and intra-seam variation in inertinite content

Inertinite content (mineral matter free, mmf basis) of crushed general seam samples varies throughout the sequence (Fig. 7.2) and ranges from 7.1% (seam 92) to 50.2% (seam 81) but with a high overall mean of 28.3% (Fig. 7.3). There is also variation in inertinite maceral type between general samples from different seams. Fusinite is the most abundant inertinite maceral in four samples whereas semifusinite is more abundant in 15 samples (Fig. 7.3; Table A.4.1). Peaks in inertinite content broadly follow previous published work (Pakh and Artser, 2003; line graph in Fig. 7.2). Multiple general samples from the same seam show considerable within seam variation (see ranges in Fig. 7.2). For example, seam 78 (n = 6 samples) ranges from 12.6% (78 lower) to 33.2% (78 S2). However, the mean inertinite contents for both stockpile and general seam samples are very similar (Fig. 7.3) thus suggesting that the general seam samples may be well represented in both the stockpile fractions.

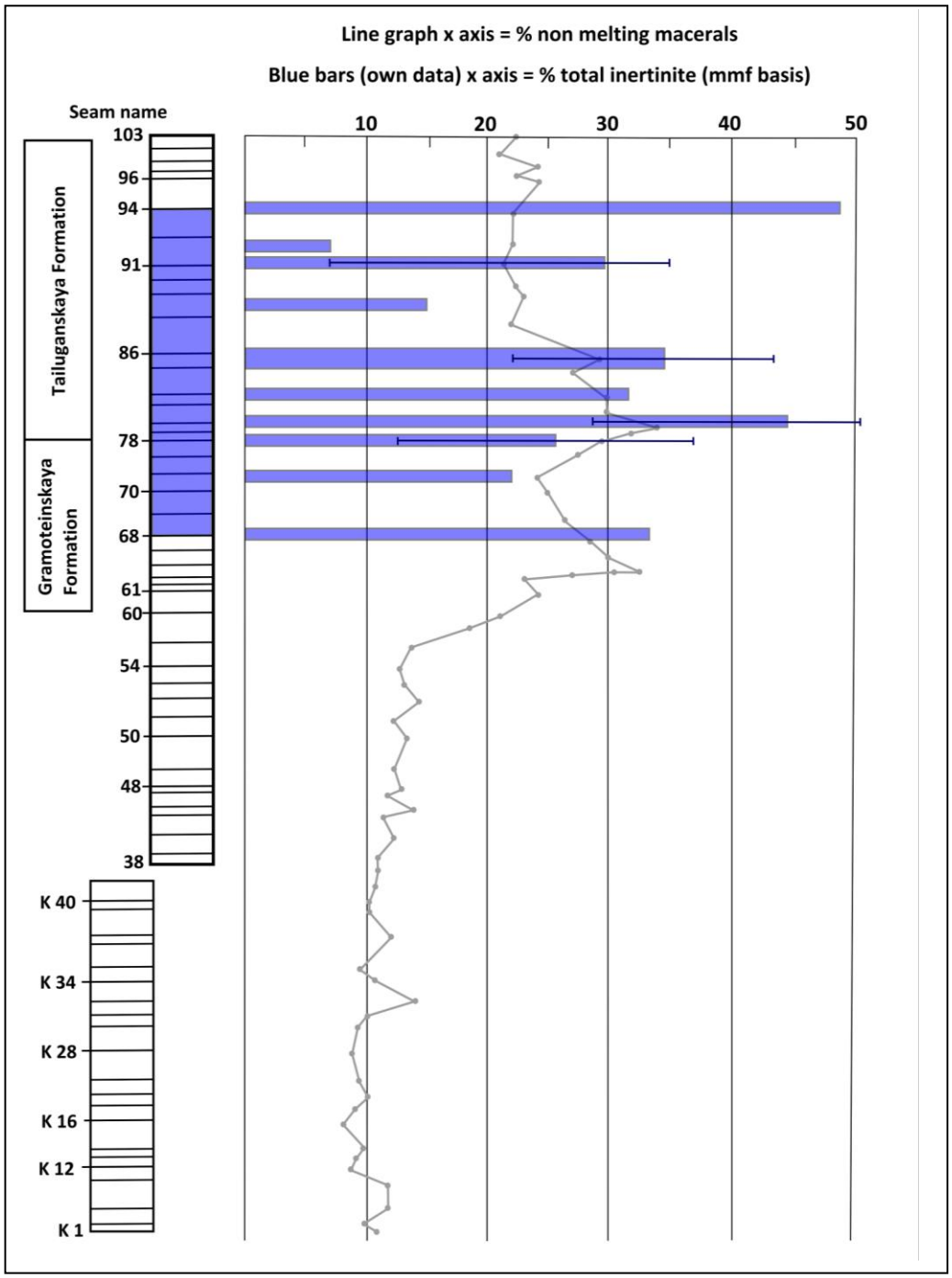

FIG. 7.2 Line graph (grey line) of non-melting macerals in Late Permian (Lopingian 260.4 ± 0.7Ma – 251 ± 0.4Ma) coal seams from the Kolchuginskaya Series, in the mining district, in the study area (adapted from Pakh and Artser, 2003). Non-melting macerals is a coking term representing total inertinite + 2/3 semivitrinite. Semivitrinite is a petrographic term for fusinite showing gradational reflectance from semifusinite to vitrinite and represents partially charred material (Snyman, 1989). Thirteen seams from this study numbered 68-94 are highlighted in blue on the left. Blue bars correspond to total mean inertinite contents (own data; mineral matter free basis) for individual seams from petrographic analysis of crushed general samples. Blue lines within bars represent ranges in inertinite content for multiple samples from the same seam. Seam 78 (n = 6 samples), seams 80-81 (n = 2 samples), seams 84-86 (n = 3 samples), seam 91 (n = 2 samples).

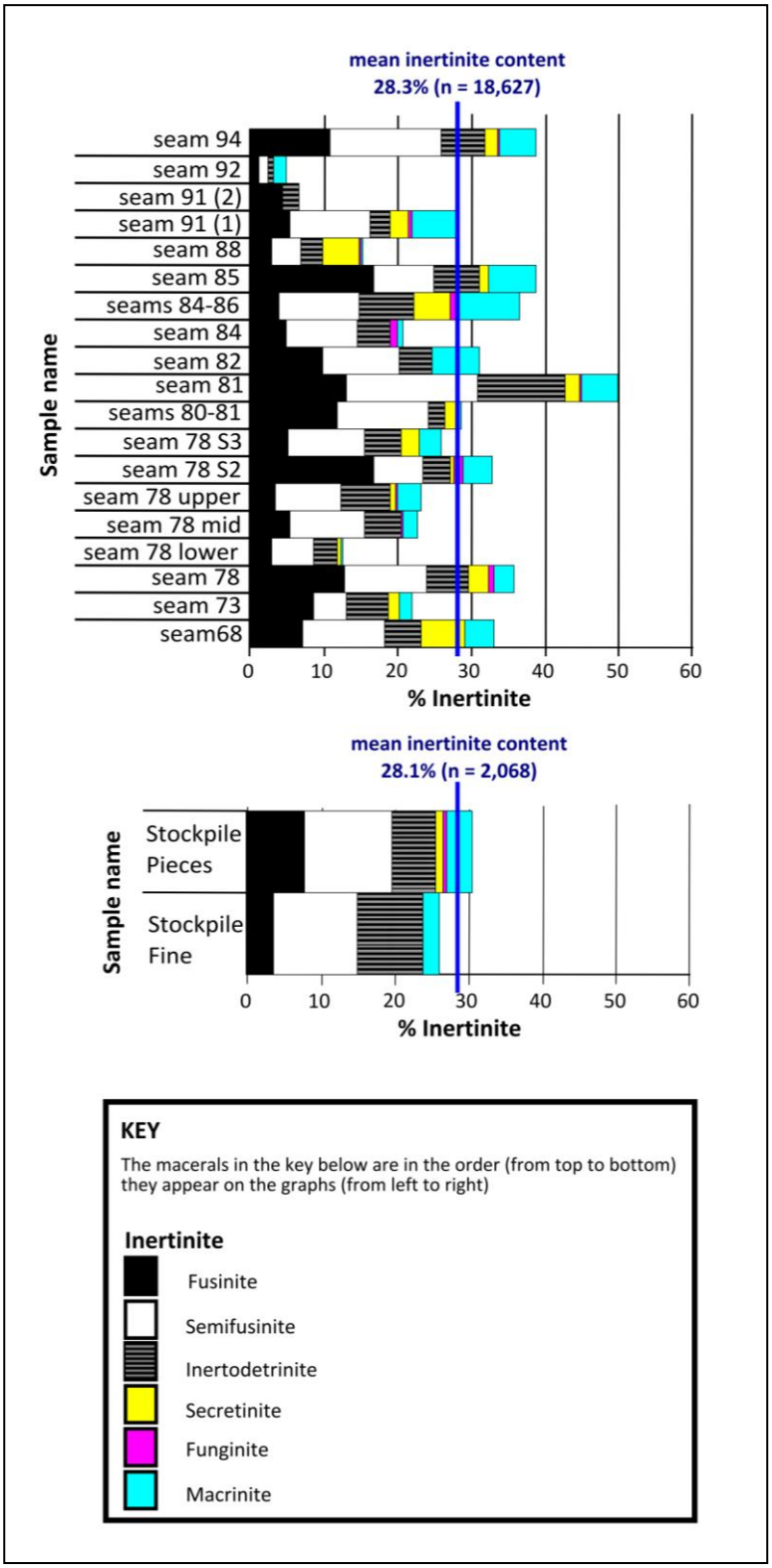

FIG. 7.3 Comparative stacked bar charts of inertinite maceral petrographic data from crushed general seam samples (top) and field stockpile size fractions (bottom) to a mineral matter free basis. The mean inertinite content for general seam samples and stockpiles is also presented and the value next to this corresponds to the total number of points counted for all general samples or stockpile fractions (both organic and inorganic).

7.3.4 Between seam variations in coal characterisation properties

%Total Sulphur is low for all general seam samples (<1.2% dry ash free basis; Fig. 7.4) but can vary considerably within a single seam e.g. seam 78 (0.26 - 1.18%) (Fig. 7.4). %Inherent moisture varies throughout the sequence (3.05 – 7.46%; Fig. 7.4) and higher values are associated with high vitrinite contents (up to 80%) for some samples (Fig. 7.4). %Volatile matter shows variation throughout the sequence, from 33.6% (84-86) to 43.3% [91(2)] (Fig. 7.4). The relationship between petrography and coal characters will be discussed further in section 7.3.7.

7.3.5 Comparison of petrographic and characterisation properties for general and stockpile samples

The petrography and characterisation results for general samples are comparable to stockpile samples (Fig. 7.4). The mean inertinite contents for stockpile fractions and general samples are also very similar (Fig. 7.3). The field stockpiles (fine and pieces), combined stockpile and averaged stockpile all contain low %ash (<10%), low mineral matter (<5%) and relatively high %total Sulphur (≤0.6%) therefore all worked seams (73 – 91) appear to be well represented in the field stockpile fractions (Fig. 7.4).

FIG. 7.4 (overleaf) Comparative bar charts illustrating between seam variation in coal characterisation properties and petrographic (organic and inorganic) point counts. The data for general samples (top) should be compared to field stockpile fractions, combined stockpile and averaged stockpile which all represent blends of seams 73 - 91 (bottom). The combined stockpile was produced from pulverised subsamples of general seams 73 - 91 (see section 7.2.2) and there is no petrographic data for this sample. The averaged stockpile is a mean of all characterisation and petrographic data for general samples from seams 73 - 91.

FIG. 7.4

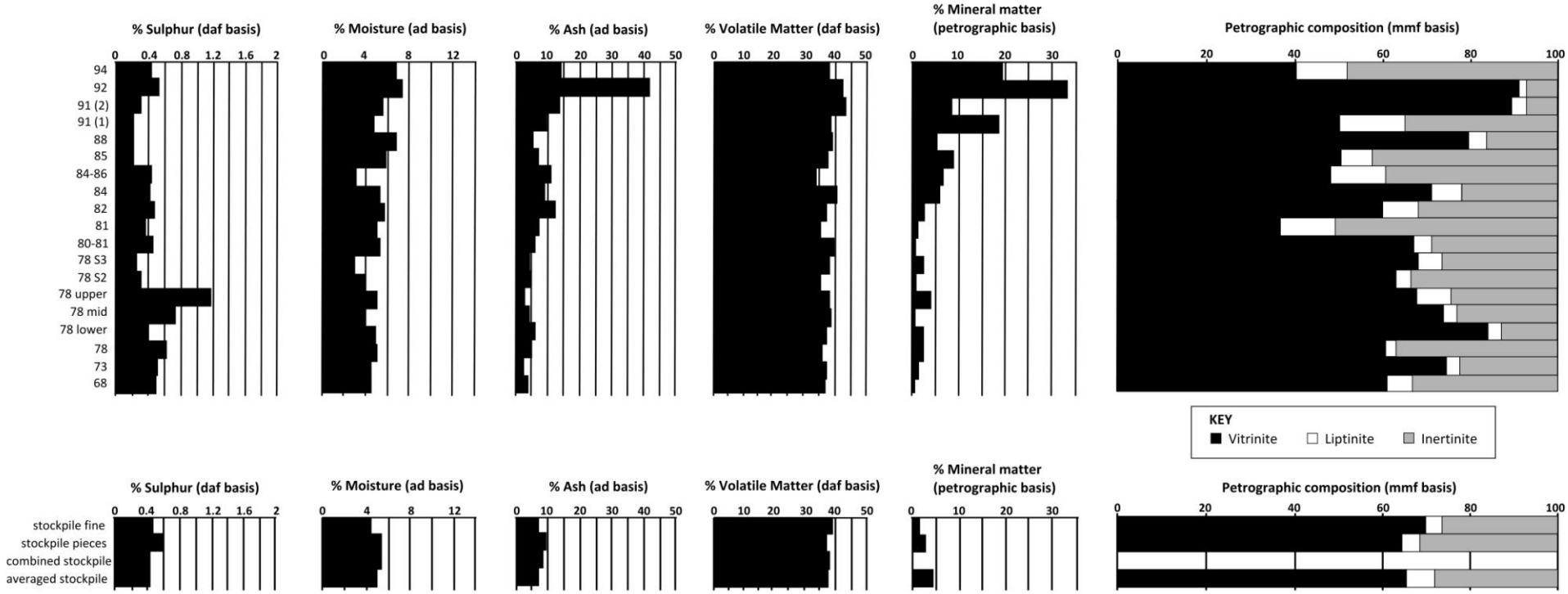
% Sulphur (daf basis)
% Moisture (ad basis)
% Ash (ad basis)
% Volatile Matter (daf basis)
% Mineral matter (petrographic basis)
Petrographic composition (mmf basis)
94
92
91 (2)
91 (1)
88
85
84-86
84
82
81
80-81
78 S3
78 S2
78 upper
78 mid
78 lower
78
73
68
KEY
Vitrinite
Liptinite
Inertinite
stockpile fine
stockpile pieces
combined stockpile
averaged stockpile

7.3.6 Within coal pillar variation in characterisation properties

7.3.6.1 Pillar 78(a)

The lithotype units from pillar 78(a) LU1-10 show no consistent relationships between any coal characters and petrography (Fig. 7.5). Both %ash and petrographically determined mineral matter are low in all lithotype units (%ash <7.5%, mineral matter <5.5%; Fig. 7.5). %Inherent moisture is also low (<5.5%) and decreases slightly from 78(a) LU1 to LU10. %Total Sulphur varies between lithotype units in pillar 78(a) from 0.7% – 1.27% (Fig. 7.5), which corresponds directly to higher mineral matter contents in 78(a) LU1 (9.3% mineral matter, 1.27% total Sulphur) and LU2 (6.7% mineral matter, 0.91% total Sulphur), suggesting that a proportion of mineral matter in LU1 and LU2 may be pyrite (see general sample 78 in Fig. 7.1). There is no correlation between %total Sulphur and mineral matter in any other lithotype units.

Variation in %volatile matter (32.3% - 39.7%) cannot be caused by rank variation at lithotype unit scale, and therefore is likely to be related to petrography. There is considerable variation in inertinite content between lithotype units (2.9% - 59.3%). Lithotype units with inertinite >45% [78(a) LU2, LU6, LU8, LU9] have slightly lower %volatile matter contents (<35.8%), (Fig. 7.5). However, 78(a) LU1 contains 14% inertinite and the second lowest %volatile matter (34.8%) which may be related to the relatively high mineral matter content (9.3%), (Fig. 7.5). The relationship between petrography and coal characters is discussed further in section 7.3.7.

7.3.6.2 Pillar 91

91 LU2 petrographically contains higher inertinite (61%), lower mineral matter (5%) and lower %ash content (7.3%) than LU1 (Fig. 7.5). Pillar 91 LU3-5 were analysed as a blend and therefore are not illustrated in Fig. 7.5. However, LU3-5 all have the same pattern of microscopic scattered inertinite distribution (Fig. 7.5) and all contain <10% inertinite. %Inherent moisture (5.5%) and %volatile matter (37.5%) are higher and %ash is lower (3.3%) than LU1-2 (Appendix 5). These properties are comparable to vitrinite-rich lithotype units from pillar 78(a).

FIG. 7.5

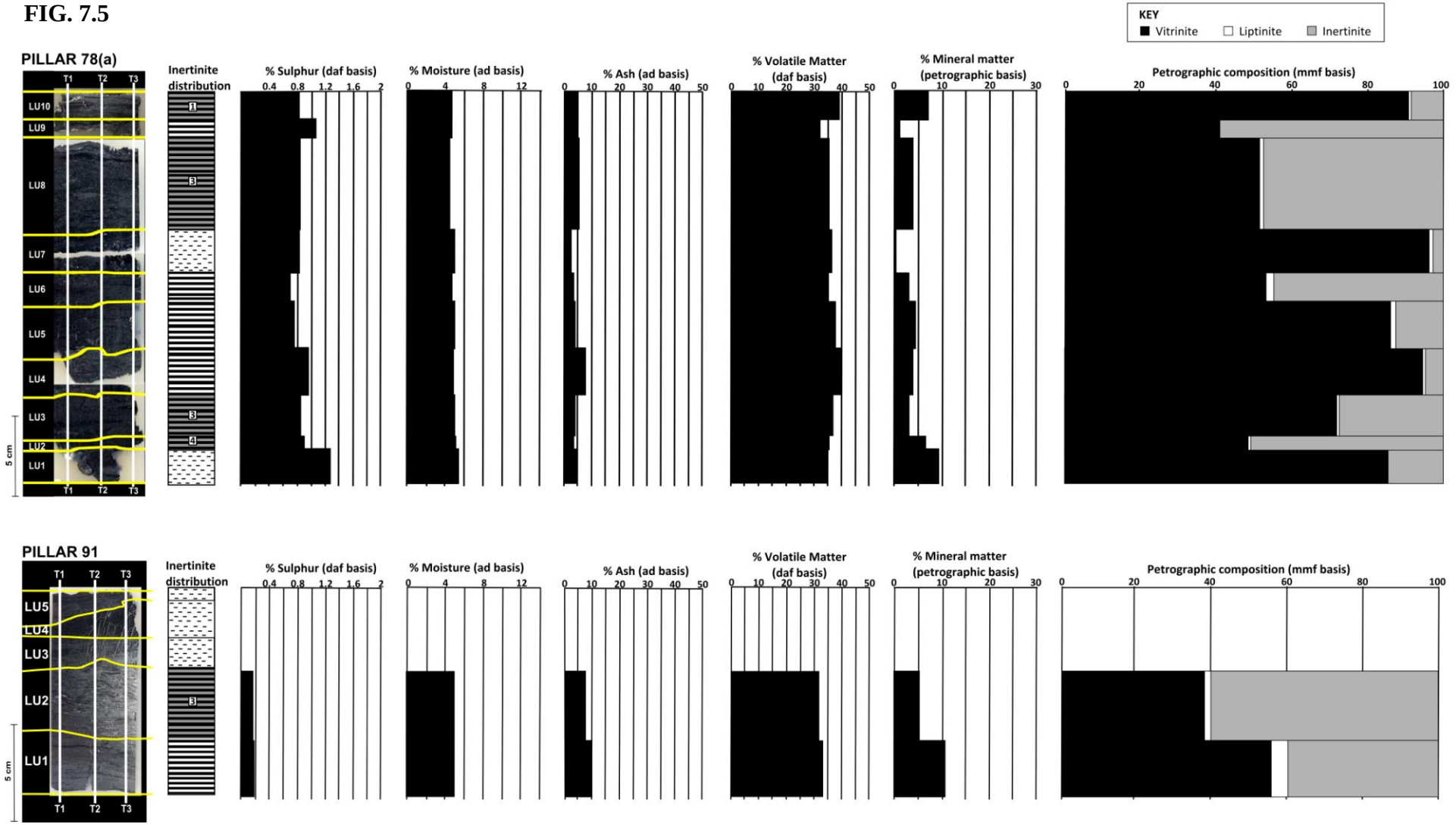
KEY
Vitrinite
Liptinite
Inertinite
PILLAR 78(a)
Inertinite distribution
% Sulphur (daf basis)
% Moisture (ad basis)
% Ash (ad basis)
% Volatile Matter (daf basis)
% Mineral matter (petrographic basis)
Petrographic composition (mmf basis)
T1
T2
T3
LU10
LU9
LU8
LU7
LU6
LU5
LU4
LU3
LU2
LU1
5 cm
PILLAR 91
Inertinite distribution
% Sulphur (daf basis)
% Moisture (ad basis)
% Ash (ad basis)
% Volatile Matter (daf basis)
% Mineral matter (petrographic basis)
Petrographic composition (mmf basis)
T1
T2
T3
LU5
LU4
LU3
LU2
LU1
5 cm

FIG. 7.5 Photographs (on left) of polished blocks from *in situ* coal pillars 78(a) and 91 illustrating lithotype unit position and relative thickness. On the right of each coal pillar are patterns of inertinite distribution between lithotype units (see key below), followed by comparative bar charts illustrating within pillar variation in both coal characterisation properties and petrography (organic and inorganic point counts). All bar charts are scaled relative to lithotype unit thickness. Lithotype units analysed as a blend (91 LU3-5) are not illustrated but data is presented in Appendix 5.

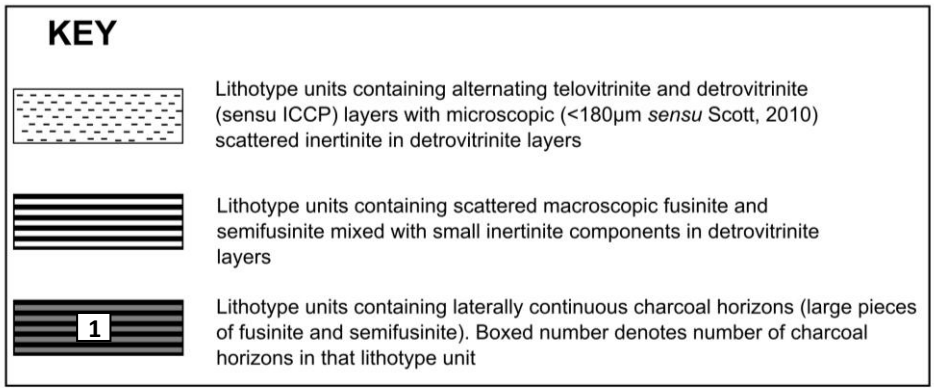

7.3.6.3 Comparison between pillars 88(a) and 88(b)

Pillars 88(a) and 88(b) represent different depositional settings (discussed in chapter 4.4.2; chapter 5.4.1; 5.4.8), which is reflected by variation in both coal characters and petrography between pillars (Fig. 7.6). All lithotype units in both pillars have low %total Sulphur (0.21% - 0.3%). The most vitrinite-rich lithotype units in pillar 88(a) LU3, LU5 (>89% mineral matter free basis), have the highest %inherent moisture (6.9%, 7.3%) and %volatile matter (31%, 31.5%) and lowest %ash (7.2%, 9.7%) and mineral matter (<2.5%), (Fig. 7.6). These characters are comparable to lithotype units from pillar 88(b) (Fig. 7.6) and vitrinite-rich lithotype units from pillar 78(a) and 91 (Fig. 7.5).

Sapropelic lithotype units were only observed in pillar 88(a) LU2, LU4. These are characterised by containing >10% liptinite (chapter 4.4.2). These lithotype units also contain >50% inertinite (Fig. 7.6), high %ash (18.8%, 20.9%), high mineral matter (18.3%, 21.6%) and low %volatile matter (25.4%, 24.3%), (Fig. 7.6).

7.3.6.4 Comparison between patterns of inertinite distribution

Four repeating patterns of inertinite distribution have been observed in all coal pillars (chapters 4 and 5; illustrated in Figs. 7.5 and 7.6). Refer to Figs. 7.5 and 7.6 throughout.

Microscopic inertinite: This type of inertinite distribution occurs in vitrinite-rich lithotype units (55.4% – 96.3%, mostly >80% mineral matter free basis) which all show slightly elevated %inherent moisture, low mineral matter (<4%) and low %ash (Fig. 7.5, Fig. 7.6) compared to other patterns of inertinite distribution. %Volatile matter is comparatively high for pillar 88(a) (LU3, LU5) (Fig. 7.6) but this trend is not observed for any other lithotype units containing microscopic inertinite (Fig. 7.5, Fig. 7.6).

Charcoal horizons: These lithotype units contain layer/s of macroscopic fusinite and semifusinite clasts (see definition, chapter 4.2.2.1). Charcoal horizons occur in varying numbers (1-16) in twelve lithotype units. Both lithotype units (Fig. 7.5, Fig. 7.6) and individual charcoal horizons (0.5-3mm) vary in thickness. This results in a wide range of inertinite contents from 8.4% [78(a) LU10] to 61.1% (91 LU1). Lithotype units containing charcoal horizons are therefore unlikely to show comparable coal characters. Lithotype units in pillars 88(a) and 88(b) that contain charcoal horizons show no relationship with %volatile matter. In pillars 78(a) and 91, %volatile matter depends on the inertinite content, not the distribution, and ranges from 31.8% (91 LU2, 61.1% inertinite) to 39.02% [78(a) LU10, 8.4% inertinite].

Macroscopic scattered inertinite: Lithotype units containing macroscopic scattered inertinite also contain a wide range of inertinite contents from 5% [78(a) LU4] to 59.3% [78(a) LU9] (Fig. 7.5; Fig. 7.6). %Volatile matter also varies between lithotype units depending on the amount of inertinite and ranges from 32.3% [78(a) LU9, 59.3% inertinite] to 39.6% [78(a) LU5, 5% inertinite].

Scattered inertinite in every field of view: This type of inertinite distribution is only observed in three lithotype units in pillar 88(a) LU2, LU4, LU6 (Fig. 7.6). LU2 and LU4 also contain charcoal horizons and are sapropelic (17.3% and 19.7% liptinite). The relationship between %volatile matter and liptinite content is discussed further in section 7.3.7.1. These lithotype units also contain high mineral matter (18.3 – 26.4%) and high %ash contents (18.8% – 20.9%). %Inherent moisture is slightly lower in relation to the rest of pillar 88(a) (Fig. 7.6). %Volatile matter contents are low (24.3% - 25.6%) which may be attributed to the high mineral matter or inertinite contents (53.1% - 56.02%).

FIG. 7.6

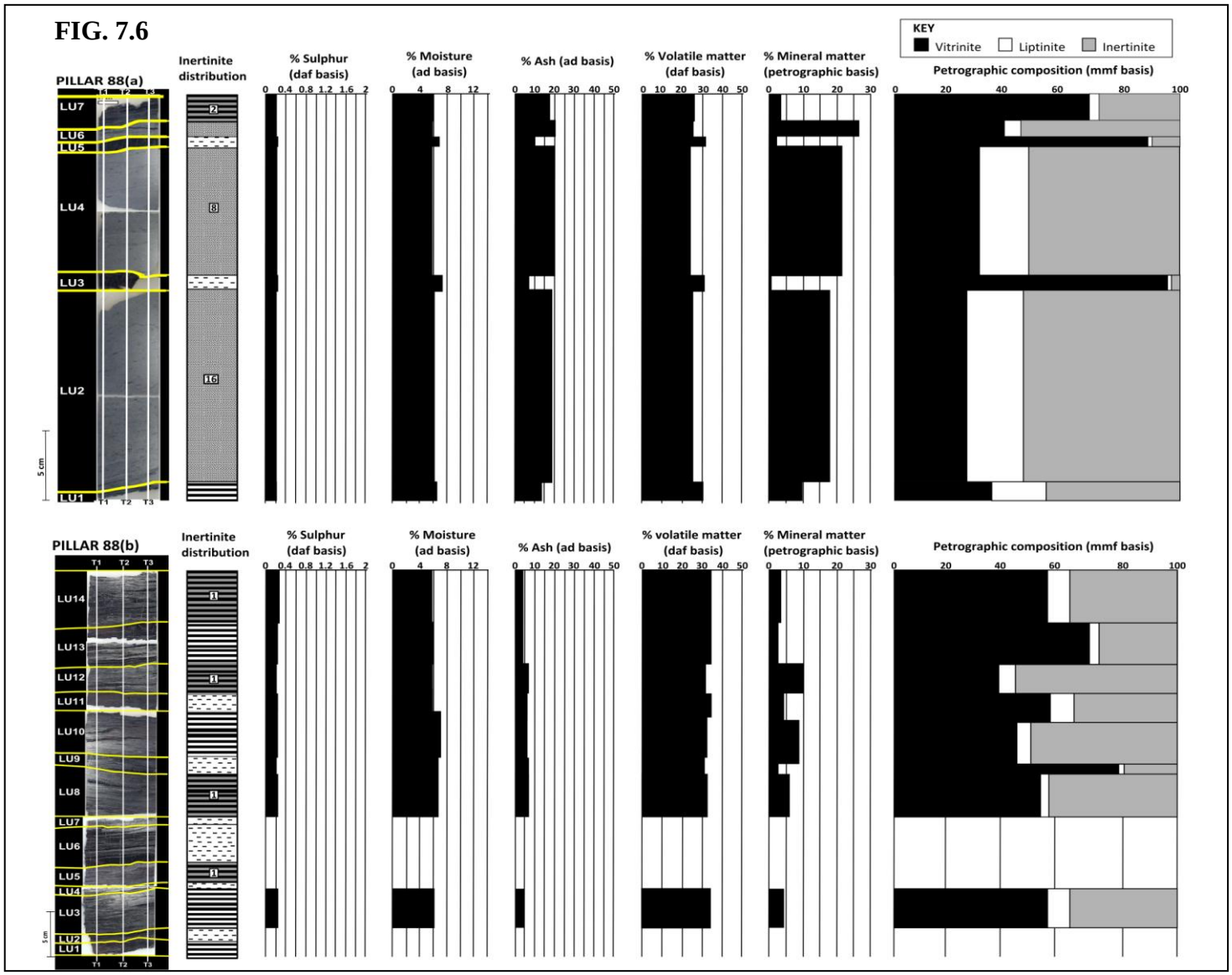
KEY
Vitrinite
Liptinite
Inertinite
PILLAR 88(a)
Inertinite distribution
% Sulphur (daf basis)
% Moisture (ad basis)
% Ash (ad basis)
% Volatile matter (daf basis)
% Mineral matter (petrographic basis)
Petrographic composition (mmf basis)
LU7
LU6
LU5
LU4
LU3
LU2
LU1
T1
T2
T3
5 cm
PILLAR 88(b)
% volatile matter (daf basis)
LU14
LU13
LU12
LU11
LU10
LU9
LU8

FIG. 7.6 Photographs (on left) of polished blocks from *in situ* coal pillars 88(a) and 88(b), 1m horizontal spacing (Fig. 5.1 A), illustrating lithotype unit position and relative thickness. On the right of each coal pillar are patterns of inertinite distribution between lithotype units (see key below), followed by comparative bar charts illustrating within pillar variation in both coal characterisation properties and petrography (organic and inorganic point counts). All bar charts are scaled relative to lithotype unit thickness. Lithotype units analysed as a blend [88(b) LU1-LU2, LU4- LU5, LU6 - LU7] are not illustrated but data is presented in Appendix 5.

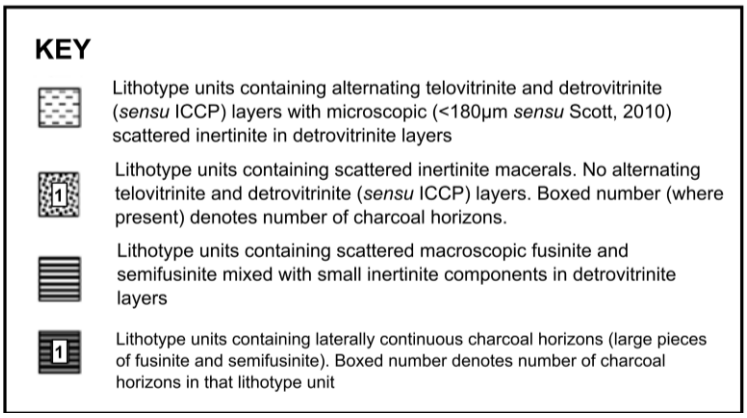

7.3.7 Petrography and characterisation properties

7.3.7.1 Vitrinite and liptinite

Vitrinite is the most abundant maceral group in 37 of the 48 samples studied (Figs. 7.4 - 7.6) and should therefore affect the characterisation properties of these samples more than liptinite or inertinite. However, vitrinite shows a weak correlation with %volatile matter in all samples (Fig. A.4.3; $R^2 = 0.29$) and a very weak correlation with %Carbon (Fig. A.4.4; Fig. A.4.5). Vitrinite has also been shown to have a positive correlation with %Oxygen (Tsai, 1982; Mastalerz et al., 1993). Although this trend is not clearly observed for these samples ($R^2 = 0.21$; Fig. A.4.6). However, caution should be taken when plotting %Oxygen as it is calculated by difference as opposed to determined analytically, and therefore contains accumulative errors of all individual components in the calculation (see Appendix 3 for calculation; Sen et al., 2009).

Liptinite is an aliphatic Hydrogen-rich maceral and should therefore show a positive correlation with %Hydrogen. Liptinite represents a small proportion of the total maceral content for most samples (<10% mineral matter free basis; n = 42; Figs. 7.4-7.6) and therefore shows no correlation with %volatile matter (Fig. A.4.7) or %Hydrogen (Fig. A.4.8) (see section 7.3.8). Sapropelic lithotype units from pillar

88(a) LU2, LU4, have the highest liptinite contents (17.3 - 19.7% mineral matter free basis; Appendix 5) but the lowest %Hydrogen (4.2 - 4.4% dry ash free basis; Appendix 5; Fig. A.4.8). This is due to the high inertinite content in these lithotype units (55.2%, 53.1%) which appears to have an overriding effect on the %Hydrogen content.

7.3.7.2 Inertinite content

Inertinite and %volatile matter: The general and stockpile samples show a negative correlation between inertinite content and %volatile matter (R^2 = 0.48; Fig. 7.7). A wide range of inertinite contents (4.8% - 49.6%) occupy a narrow range of %volatile matter (33.6% - 43.3%). The sample with the highest inertinite has one of the lowest %volatile matter contents (seam 81; Fig. 7.7).

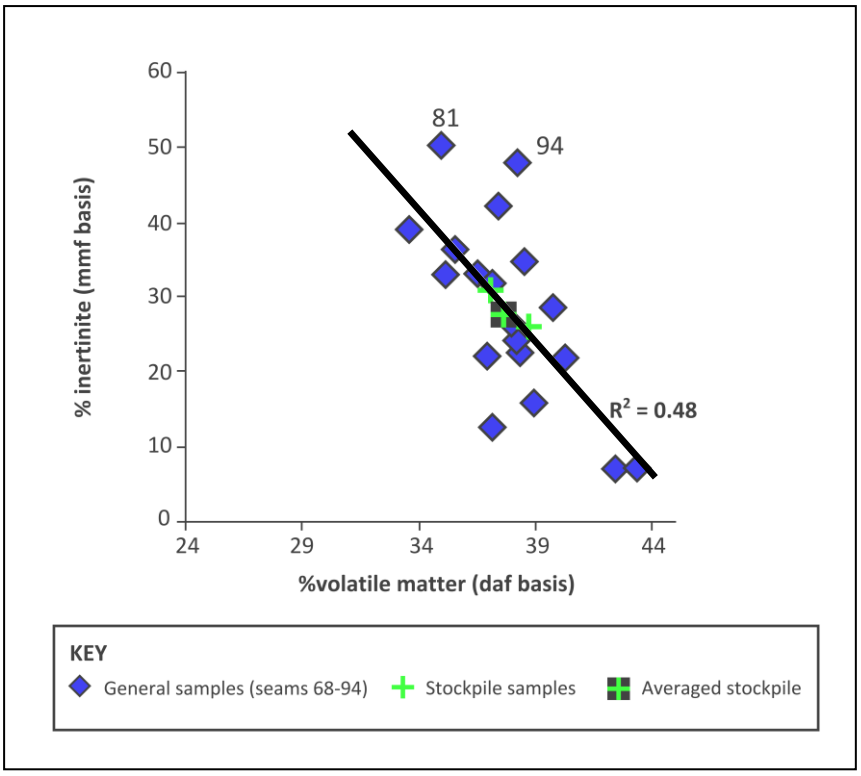

FIG. 7.7 Relationship between inertinite content and %volatile matter for general seam and stockpile samples analysed at RWE Npower. Samples with inertinite greater than vitrinite are labelled (81 and 94). Inertinite values are reported to a mmf (mineral matter free basis) and %volatile matter to a daf (dry ash free basis).

When all samples are plotted together there is a very weak correlation between inertinite and %volatile matter (Fig. 7.8; R^2 = 0.22). Samples with inertinite contents

greater than vitrinite do not have the lowest %volatile matter. Lithotype unit samples from individual coal pillars show a wide range of inertinite contents over a narrow %volatile matter range.

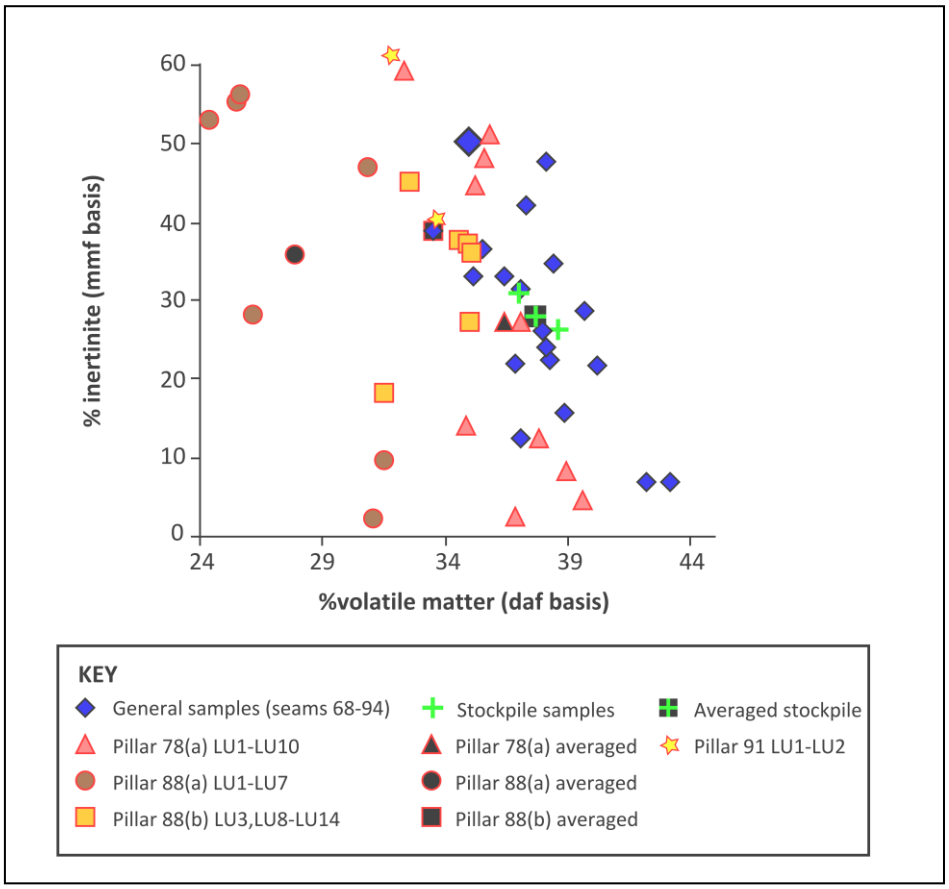

FIG. 7.8 Relationship between inertinite content and %volatile matter for all samples. Inertinite values are reported to a mmf (mineral matter free) basis and %volatile matter to a daf (dry ash free) basis. %Volatile matter of general and stockpile samples was analysed at RWE Npower. Lithotype units were analysed at CAER (symbols with red outlines).

Inertinite and %Carbon: There is a weak correlation between %Carbon and inertinite (R^2 = 0.28; Fig. 7.9), for the general and stockpile samples and no correlation when low %Carbon samples from seams 91(2) and 92 are removed (Fig. 7.10). There is only a very weak correlation when all samples analysed at RWE Npower are combined (Fig. 7.11; Fig. 7.12). The samples analysed at CAER [88(b), 91] have lower %Carbon values and show no correlation with inertinite content (Fig. 7.11). For further discussion on potential causes for the variation in %Carbon between laboratories refer to section 7.4.1.

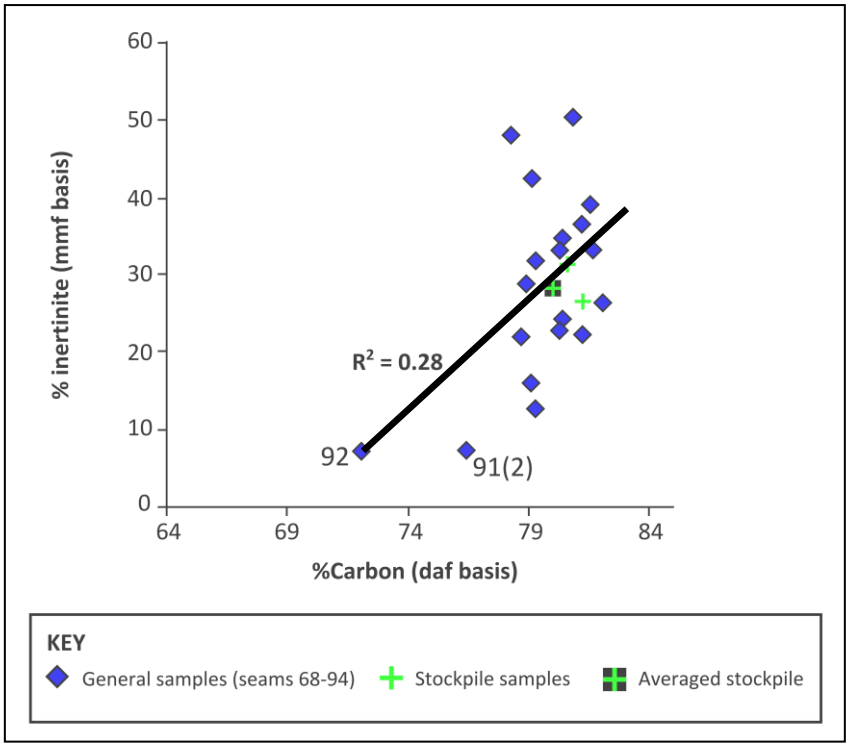

FIG. 7.9 Relationship between inertinite content and %Carbon for general and stockpile samples analysed at RWE Npower. Inertinite values are reported to a mmf (mineral matter free) basis and %Carbon to a daf (dry ash free) basis.

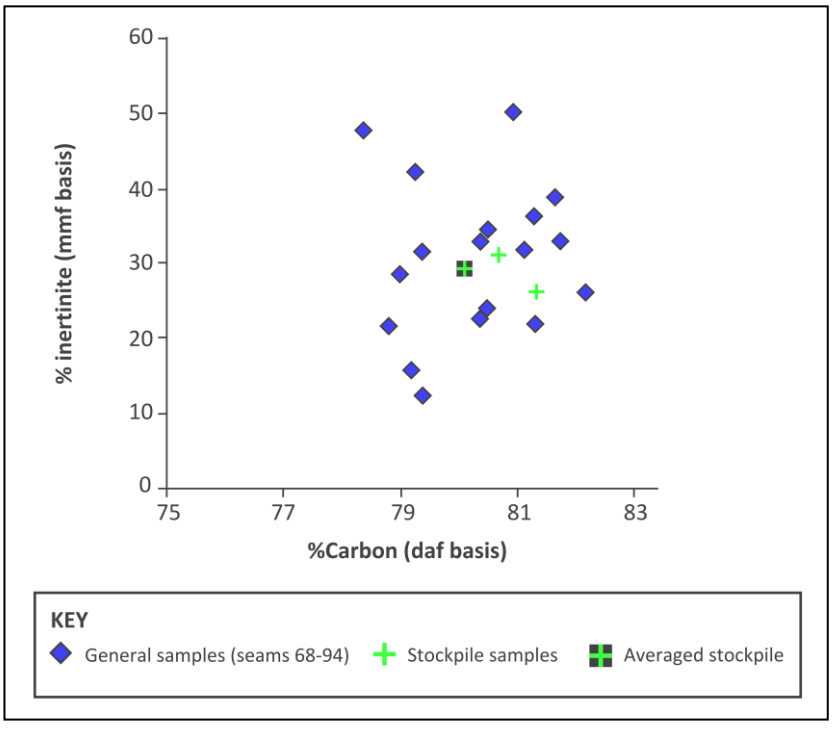

FIG. 7.10 Relationship between inertinite content and %Carbon for general and stockpile samples with low %Carbon outlying samples removed [seams 91(2), 92]. Inertinite values are reported to a mmf (mineral matter free) basis and %Carbon to a daf (dry ash free) basis.

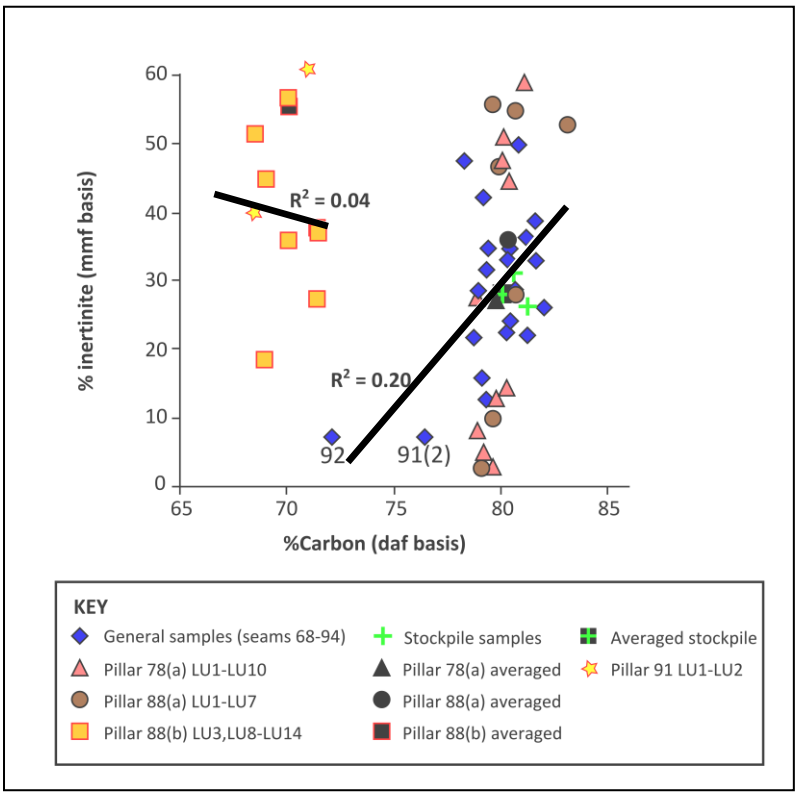

FIG. 7.11 Relationship between inertinite content and %Carbon for all samples. Inertinite values are reported to a mmf (mineral matter free) basis and %Carbon to a daf (dry ash free) basis. %Carbon of general and stockpile samples, and lithotype units from pillar 78(a) and 88(a) (symbols with black outlines) were analysed at RWE Npower. Lithotype units from pillars 88(b) and 91 were analysed at CAER (symbols with red outlines).

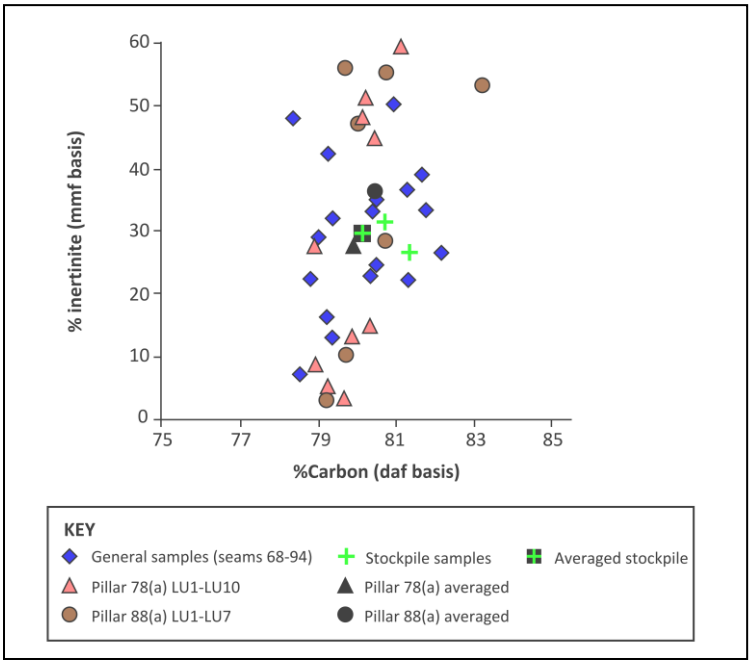

FIG. 7.12 Relationship between inertinite content and %Carbon for all samples analysed at RWE Npower. Outlying low %Carbon values from general seam samples 91(2) and 92 were also removed. There is no correlation between inertinite and %Carbon. Inertinite values are reported to a mmf (mineral matter free) basis and %Carbon to a daf (dry ash free) basis.

Inertinite and H/C ratio: Coals with high inertinite contents typically have low H/C ratios (White et al., 1989) because of the high %Carbon content of the charcoal structure (Speight, 1990). Samples that have the the highest H/C ratios have the lowest inertinite contents. Lithotype units analysed at CAER [pillars 88(b) and 91] have relatively low %Carbon contents, hence higher H/C ratios, than all samples analysed at RWE Npower (Fig. 7.13). Although the correlation for both trendlines is comparable (R^2 = 0.41 for RWE NPower samples, R^2 = 0.50 for CAER samples; Fig. 7.13). For further discussion of differences in %Carbon between laboratories see section 7.4.1.

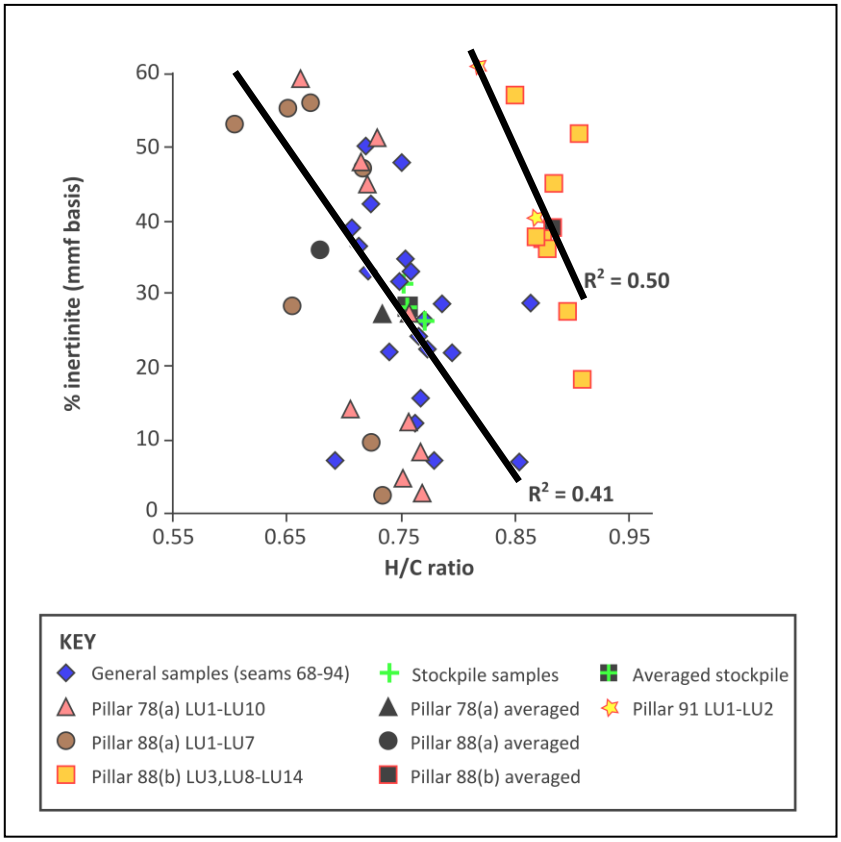

FIG. 7.13 Relationship between inertinite content and H/C (Hydrogen/ Carbon) ratio. Inertinite values are reported to a mmf (mineral matter free) basis. General and stockpile samples, and lithotype units from pillar 78(a) and 88(a) (symbols with black outlines) were analysed at RWE Npower. Lithotype units from pillars 88(b) and 91 were analysed at CAER (symbols with red outlines).

7.3.7.3 Inertinite distribution and characterisation

There is no relationship between inertinite distribution and %volatile matter. The proportion of inertinite has a stronger correlation with the %volatile matter than the distribution (see section 7.3.6.4). Only the inertinite distribution with scattered inertinite macerals in every field of view, typical of sapropelic lithotype units, consistently contains both high inertinite and correspondingly the lowest %volatile matter (Fig. 7.14).

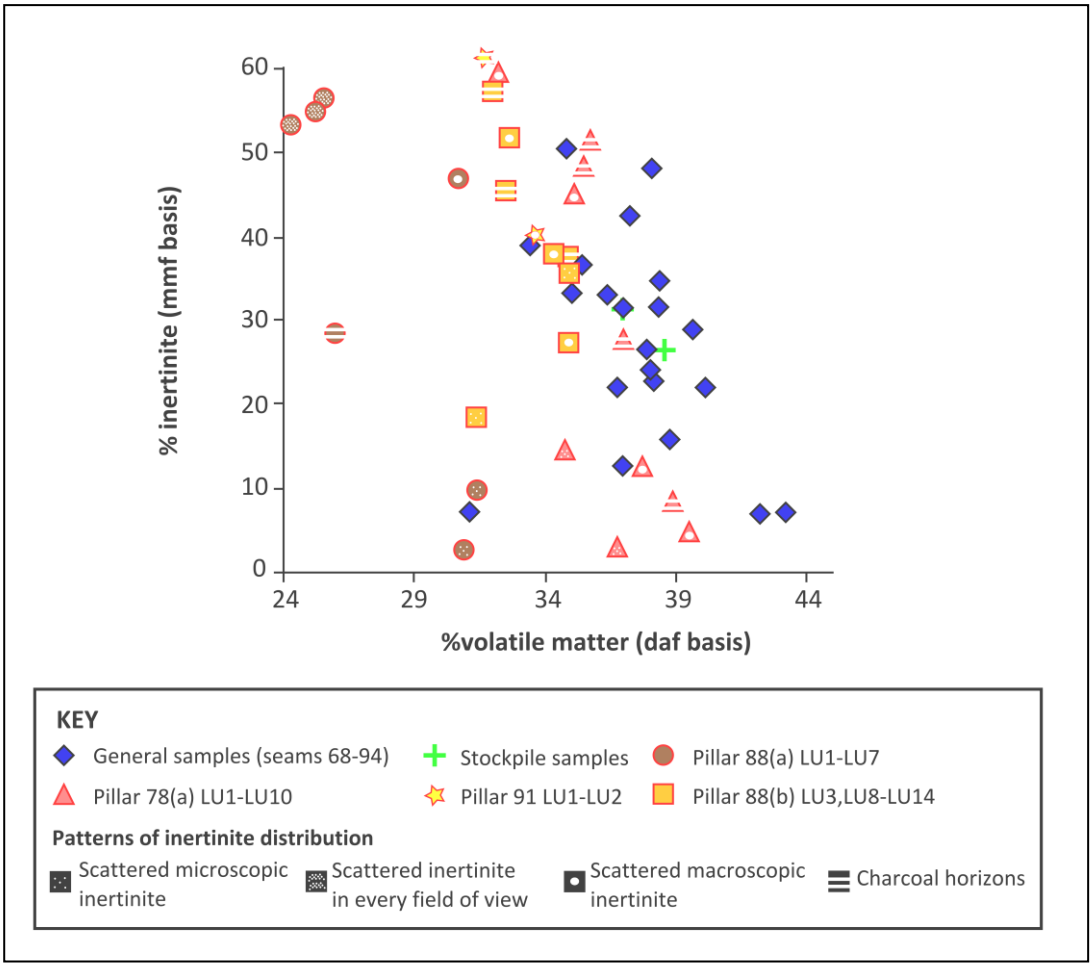

FIG. 7.14 Relationship between patterns of inertinite distribution and %volatile matter. Inertinite values are reported to a mmf (mineral matter free) basis and volatile matter is reported to a daf (dry ash free) basis. %Volatile matter of general and stockpile samples was analysed at RWE Npower. Lithotype units were analysed at CAER (symbols with red outlines).

7.3.8 Critical R^2 value and correlation matrix

A symmetrical correlation matrix was produced (Table 7.2) to ascertain whether any of the correlations between macerals and characterisation properties (observed in section 7.3.7) were statistically significant. The large sample size in this study (n = 48) means the critical R^2 value required for a correlation to be statistically significant is low, R^2 critical = 0.28 or 28% of the variance (see section 7.2.7 for methodology; Appendix 7). All correlations with R^2 values above the R^2 critical value are highlighted in Table 7.2.

The use of a critical R^2 value demonstrates that the petrographic composition of these Permian coals does influence certain coal characterisation properties. The lack of strong correlations between maceral groups and certain coal characters (section 7.3.7) may be due to the difference in values between laboratories. For further discussion refer to section 7.4.1. Vitrinite is the most abundant maceral group in 37 of the 48 Permian coal samples analysed (Figs. 7.4 – 7.6) and correlates with %volatile matter and %Hydrogen (Table 7.2) despite the apparent lack of correlation in Figs. A.4.7 and A.4.8. Inertinite is the second most abundant maceral group and correlates with %volatile matter, %Hydrogen and %Nitrogen as expected (see section 7.1.1) despite the lack of clear correlations observed in the biplots (section 7.3.7.2). Liptinite should correlate with %Hydrogen (section 7.1.1) but the correlation matrix shows the correlation is not statistically significant (Table 7.2; Fig. A.4.8), see section 7.4.2 for further discussion. None of the maceral groups correlate with %Carbon which appears to be more influenced by rank than petrographic composition in these coals.

The strongest correlations are between mineral matter, %ash and calorific value and have already been documented elsewhere (Figs. A.4.1, A.4.2; see sections 7.3.1, 7.3.2). The correlation between vitrinite and calorific value is also statistically significant (Table 7.2) which is unsurprising given that calorific value can be used as a rank parameter (section 7.3.1; Table 7.1).

	Vitrinite	Liptinite	Inertinite	Mineral Matter	%Moisture	%Ash	%Volatile Matter	%Carbon	%Hydrogen	%Nitrogen	%Total Sulphur	Calorific Value
Vitrinite	1											
Liptinite	-0.6239017	1										
Inertinite	-0.8825333	0.372441	1									
Mineral Matter	-0.5034217	0.321451	0.0867904	1								
%Moisture	-0.0766288	0.088128	-0.110181	0.387860739	1							
%Ash	-0.3032126	0.26141	-0.066256	0.810559258	0.4202901	1						
%Volatile Matter	0.4969913	-0.3053	-0.464216	-0.19927321	-0.2466011	-0.185553	1					
%Carbon	0.1175867	0.128825	-0.138607	-0.10746632	-0.4710436	-0.032806	0.048235	1				
%Hydrogen	0.48687292	-0.24131	-0.408468	-0.32719913	-0.0418929	-0.317429	0.747665	-0.408759	1			
%Nitrogen	0.4555646	-0.15577	-0.505421	-0.08932925	-0.2592593	0.0328116	0.507491	0.597769	0.1998827	1		
%Total Sulphur	0.32504419	-0.43164	-0.200843	-0.20682446	-0.3780897	-0.279811	0.365451	0.38609	-0.019881	0.3589	1	
Calorific value	0.35152086	-0.22138	0.1374797	-0.88623374	-0.7282168	-0.984194	0.030816	0.676017	0.1966586	0.0871	0.2766	1

TABLE 7.2 Correlation matrix of all characterisation properties against petrographic constituents. Grey highlight signifies any statistically significant positive correlations and yellow highlight represents any statistically significant negative corrections.

7.4 DISCUSSION

7.4.1 Inter-laboratory variation in characterisation results

7.4.1.1 Analytical technique

Pillar 78(a) LU5 was analysed as a 'standard' to compare results from both laboratories (Table 7.3). Ultimate analyses (%Carbon, %Hydrogen, %Nitrogen, %Oxygen) were undertaken at both laboratories using a Leco CHN2000 with different operators but the same operating conditions (see method in Appendix 3). However, the difference in %Carbon between laboratories (5.65%; Table 7.3) is significantly outside of the narrow reproducibility limit of 1.0% absolute set by British standards (BS ISO 29541: 2010) or 0.3% for ASTM standards (Schelkoph et al., 1983). However, the %Hydrogen, %Nitrogen and %total Sulphur are within the British standard reproducibility limits (BS 1016-106.4.2:1996; BS ISO 29541: 2010). Therefore, it is unlikely that the difference in %Carbon (Table 7.3) is due to analytical error. %Carbon values of lithotype units from pillars 88(b) and 91, analysed at CAER, are also significantly lower than those analysed at RWE Npower [general, stockpile and pillar 78(a) and 88(a) lithotype units illustrated in Figs. 7.11, 7.13, 7.15, 7.16 and 7.18]. Pillars 88(b) and 91 were exposed on the laboratory bench for several months prior to subsampling for characterisation analysis and may therefore be oxidised, which is likely to be causing the inconsistency in values between laboratories (discussed further in section 7.4.1.2).

%Volatile matter is the only characterisation analysis undertaken using a different methodology at both laboratories (see RWE Npower method in Appendix 3) but both values for pillar 78(a) LU5 are within the reproducibility limits for both British (4%; Appendix 3) and ASTM standards (2%; Schelkoph et al., 1983), (Table 7.3) therefore it is likely that the %volatile matter values for all samples analysed at CAER are also within the reproducibility limits (all lithotype units, all coal pillars).

Sample name	PROXIMATE ANALYSES (%)			ULTIMATE ANALYSES (%)				
	Moisture	Ash	Volatile matter	Carbon	Hydrogen	Nitrogen	Oxygen	Total Sulphur
78(a) LU5 (RWE Npower)	4.97	3.92	37.86	79.81	5.09	2.68	10.54	0.77
78(a) LU5 (CAER)	4.93	2.37	36.58	74.16	5.31	2.55	15.12	0.69

TABLE 7.3 Summary table of comparative characterisation results for a lithotype unit from pillar 78(a) LU5 analysed at both RWE Npower and CAER. Moisture and ash are reported to an air dried basis and volatile matter and ultimate analyses are reported to a dry ash free basis.

7.4.1.2 Oxidation

Oxidation can affect coal characterisation properties. Both laboratory-scale and field experiments have yielded comparable results, although quantification of deterioration in the coal is difficult (Banerjee et al., 2000). Values for %Carbon, %Hydrogen, %total Sulphur and calorific value have all been shown to decrease, whereas %inherent moisture and %Oxygen increase compared to un-oxidised coal (e.g. Huggins et al., 1980; Marchioni, 1983; Fredericks et al., 1983; Pisupati and Scaroni, 1993; Banerjee et al., 2000; Sen et al., 2009). The effect on %volatile matter is variable and difficult to quantify (Marchioni, 1983; Banerjee et al., 2000) and depends on both the rank of the coal and the form which oxygen is incorporated into the coal structure (Sen et al., 2009). The pillar 78(a) LU5 sample contains lower %Carbon (74.2%) and higher %Oxygen (15.1%), (Table 7.3; Fig. 7.15; Fig. 7.16) and slightly lower %total Sulphur (Table 7.3) than when the sample was originally analysed at RWE Npower which is consistent with an oxidised coal. Lithotype units from coal pillars, 88(b) and 91 also show low %Carbon and comparatively high %Oxygen (yellow highlight in Figs. 7.15, 7.16). %Oxygen is known to have an inverse relationship with %Carbon which is related to increasing rank (Neavel et al., 1986). Although caution should be taken when referring to %Oxygen (section 7.3.7.1) variation in %Oxygen is observed in the same sample, pillar 78(a) LU5 (10.5% - 15.1%; Table 7.3) which cannot be attributed to variation in rank. Furthermore, coal pillars 88(a) and 88(b) are from the same 3m thick seam (1m horizontal separation; Fig. 5.1 A) and are therefore also unlikely to be different ranks. It is therefore likely that these samples have been oxidised in the laboratory prior to analysis.

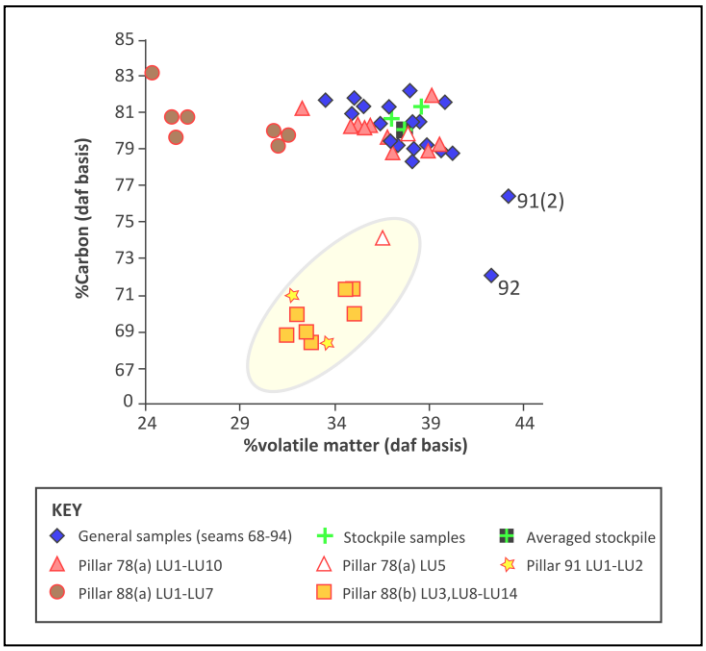

FIG. 7.15 Relationship between %Carbon and %volatile matter for oxidised samples (highlighted in the yellow circle). %Carbon and %volatile matter are reported to a dry ash free (daf) basis. %Volatile matter of general and stockpile samples was analysed at RWE Npower. Lithotype units were analysed at CAER (symbols with red outlines).

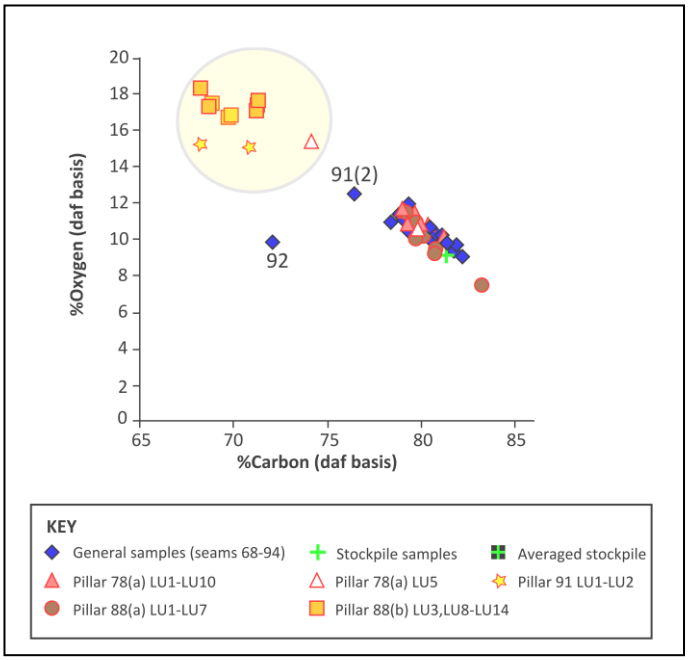

FIG. 7.16 Relationship between %Carbon and %Oxygen for oxidised samples (highlighted in the yellow circle). %Carbon and %Oxygen are reported to a dry ash free (daf) basis. General and stockpile samples were analysed at RWE Npower. Lithotype units were analysed at CAER (symbols with red outlines).

Seams 92 and 94 were observed in the field to be weathered (chapter 3.4; Fig. 3.12) and the general samples show characterisation results consistent with oxidised coal

(i.e. low %Carbon, calorific value, high %inherent moisture and %Oxygen; Fig. 7.4; Fig. 7.9; Fig. 7.11; Fig. 7.15; Fig. 7.16). Seam 91(2) also shows these characteristics (Fig. 7.9; Fig. 7.11; Fig. 7.15; Fig. 7.16). Oxidised coal can also be identified microscopically. Polished blocks were not reproduced for pillars 88(b) and 91 prior to characterisation analysis so qualitative determination of oxidation is not possible for these samples. Vitrinite is more readily oxidised than other maceral groups and can show the following features, micropores, microcracks, microfissures (Chandra, 1962; Crelling et al., 1979; Bruening and Cohen, 2005), variation in polishing relief (Bend and Kosloski, 1993) and dark reaction rims (Bustin, 1984; Lo and Cardott, 1995). A putative reaction rim (Fig. 7.17 A) and microfracturing of a clast (Fig. 7.17 D) is observed for general samples 91(2) and 94. These textures are rare in these samples and therefore do not provide unequivocal evidence for oxidation.

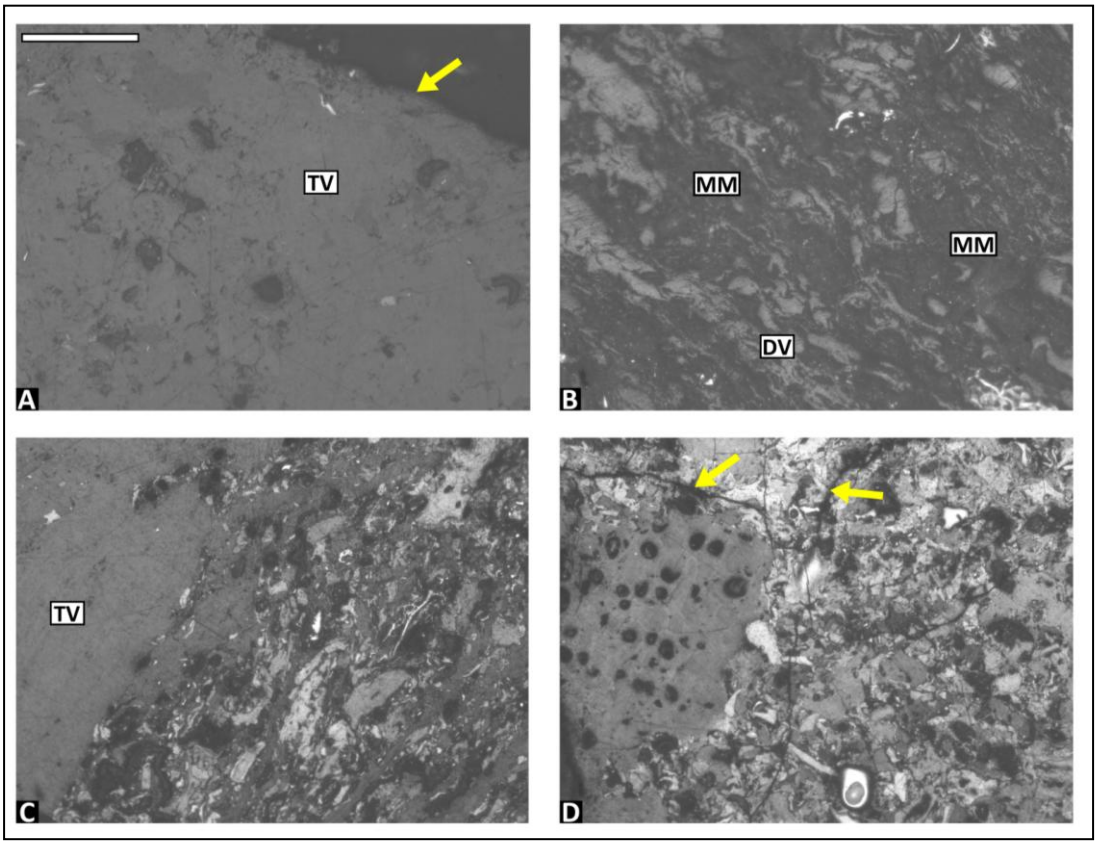

FIG. 7.17 Representative reflectance microscopy images of general crushed samples from seams 91(2), 92 and 94. Scale bar in **A** corresponds to 100µm and is the same for all images. Labels in white boxes represent: TV = telovitrinite, DV = detrovitrinite (*sensu* ICCP, 1998) and MM = mineral matter. **A –** Seam 91(2), possible dark reaction rim (yellow arrow) surrounding unaltered vitrinite particle. **B –** Seam 92, detrovitrinite dominated by mineral matter, no evidence for oxidation. **C, D –** Seam 94. **C -** Trimaceral clast with no oxidation textures observed in vitrinite. **D –** Microfracturing in a trimaceral clast (highlighted by yellow arrows).

General samples from seams 91(2), 92 and 94 all contain high mineral matter (8% - 33%; Fig. 7.4; Fig. 7.17 B) and corresponding %ash contents (14% - 41%; Fig. 7.4). Therefore the inorganic constituents in these samples may be contributing to these characterisation properties (Table 7.2) as opposed to oxidation. These samples also contain high %volatile matter contents (38% - 43%; Fig. 7.4; Fig. 7.7; Fig. 7.8; Fig. 7.15) and volatile decomposition products originating from the mineral phase of coal can contribute up to 45% of the total amount of %volatile matter in a coal (Slaghuis et al., 1991) which may account for the high %volatile matter contents in these samples.

7.4.2 The effect of inertinite on characterisation properties of bulk coal

Inertinite content does have a statistically significant correlation with %volatile matter (Table 7.2). The lack of strong correlations between inertinite and other characterisation properties may be a function of the limited number of samples containing >50% inertinite (n = 3 to a mineral included basis or n = 8 to a mineral matter free basis; Figs. 7.2 – 7.6). Whole coal samples have been shown to require 80% inertinite to have a significant effect on %volatile matter (e.g. Bostick et al., 1991). In addition, previous work by Van Niekerk (2008) on two Permian South African bituminous coals demonstrated that both inertinite-rich (87.7%) and vitrinite-rich (91.8%) samples had similar %Carbon values. Therefore %Carbon is more likely to be influenced by coal rank than petrography.

Significant quantities of liptinite in a sample may also contribute to %volatile matter. In order to counter this effect, Borrego et al. (2000) sampled coals with liptinite contents <5% for inertinite >40% and <2.5% liptinite for inertinite 30-40%. The general samples (studied here) with the highest inertinite contents also have high liptinite contents which is likely to be contributing to the %volatile matter (seam 81, 12.8% liptinite mmf basis; seam 94, 11.9% liptinite mmf basis). Only four samples have high inertinite and low liptinite contents [pillar 78(a) LU9, pillar 88(b) LU10, pillar 88(b) LU12 and pillar 91 LU2] but do show some of the lowest %volatile matter contents (31.8% - 32.8% dry ash free basis; Fig. 7.4; Fig. 7.8). Therefore, despite inertinite contents of up to 61% (pillar 91 LU2) the general seam samples, stockpiles and lithotype units from coal pillars, in this study, do not have inertinite in

sufficient enough quantities to influence the gross characterisation properties of the coal.

7.4.3 Inertinite content and combustion behaviour: Drop-Tube Furnace (DTF) experiments

Proximate analysis is the most basic data used by a power station to assess coal quality (Banerjee et al., 2000) and chemical analyses alone cannot be used to interpret combustion behaviour of the coal (Ballester and Jiménez, 2005). Experimental pilot-scale DTF experiments were therefore undertaken on three general samples [seam 78, 88, 91(2)] and a stockpile sample (stockpile fine) with varying inertinite contents (Table A.4.1). The samples with relatively low inertinite contents (seam 88 and stockpile fine; Appendix 8) showed the best burnout profiles, with less combustibles remaining at earlier residence times (Bostick et al., 1991), and produced the thinnest chars (Appendix 8). In contrast, samples with high inertinite contents [up to 30%; seams 91(2) and 78 S2] produced denser chars and showed poorer burnout (Appendix 8). However, the influence of inertinite content on burnout is not straightforward, as inertinite is typically associated with mineral matter in coal, and high mineral contents can also cause poor burnout (Beeley et al., 1995; Gibbins et al., 1999). Characterisation analysis of the unsieved seam 91(2) sample showed a high %ash content (13.7%; Appendix 8) therefore, mineral matter may also be contributing to the poorer burnout of this sample.

The association of mineral matter with inertinite can cause a slower ignition time, particularly for fusinite (200 ms), compared to vitrinite. This is significant for commercial pulverised fuel combustion as short furnace residence times (1 s) may mean inertinite-rich coals produce larger quantities of unburnt coal (Vleeskens and Nandi, 1986) which represents a loss in efficiency (Beeley et al., 1995). This can cause high %Carbon in ash which affects the sale and use of pulverised fuel ash (Lester, 1994; Beeley et al., 1995; Cloke et al., 1997a). Therefore, despite the weak correlations between inertinite content and distribution with characterisation properties, the inertinite content (and possibly also the mineral matter content) appears to be affecting the burnout of these coal samples.

7.4.4 Representation of seams in the field stockpiles

The two stockpile fractions, combined (subsamples from worked seams 73-91; see section 7.2.2) and averaged stockpile (averaged characterisation and petrographic data for general samples from seams 73 - 91) all yield very comparable characterisation results (Table 7.4). Therefore, the differences in petrography and coal characterisation properties between individual seams in the sequence (Fig. 7.4) do not affect the chemical properties of the overall stockpile. It is not possible to determine which seams are contributing to the field stockpiles as both size fractions are well represented by a mean of all the contributing seams (73 - 91).

Sample name	PETROGRAPHY (%)				PROXIMATE ANALYSES (%)			ULTIMATE ANALYSES (%)			
	Vitrinite	Liptinite	Inertinite	Mineral Matter	Moisture	Ash	Volatile matter	Carbon	Hydrogen	Nitrogen	Total Sulphur
Stockpile fine	68.8	3.5	25.9	1.8	4.41	7.07	38.72	81.32	5.25	2.75	0.47
Stockpile pieces	62.7	4.1	30.3	2.9	5.36	9.18	37.08	80.66	5.1	2.61	0.6
Combined stockpile (73 – 91)					5.36	8.26	37.93	80.04	5.07	2.52	0.44
Averaged stockpile (73-91)	63.3	5.8	26.6	4.3	4.93	6.91	37.69	80.1	5.09	2.48	0.45

TABLE 7.4 Comparative summary table of petrographic proximate and ultimate data for both field stockpile fractions, the laboratory produced combined stockpile and an averaged stockpile of general samples from worked seams during the sampling period (73 - 91). %Moisture and %ash are reported to an air dried basis and volatile matter and ultimate analyses are reported to a dry ash free basis.

7.4.5 Comparing coal pillars to general seam samples: Implications for within seam variation in coal characterisation properties

Petrography and characterisation properties vary between lithotype units in all *in situ* coal pillars (Figs. 7.5, 7.6, 7.8, 7.11, 7.13, 7.14). When all lithotype units for pillar 78(a) are blended, either as a combined or averaged sample (Table 7.5; Fig. 7.18), the resulting characterisation data are very comparable to the general seam 78

sample. However, there is also lateral and temporal variation in both petrography and characterisation properties within seam 78 between mines (Fig. 7.4). The lack of variation in characterisation properties between the seam 78 general sample and the combined and averaged pillar 78(a) sample suggests that the general sample may comprise similar lithotype units as pillar 78(a) or may have originated from a similar position in the seam.

This is in contrast to characterisation data for pillars 88(a) and 88(b) which do not represent the general seam 88 sample (Fig. 7.18; Table 7.5). The general sample did not contain any dull bands and therefore contains lower %inertinite, %ash and higher %volatile matter compared to pillar 88(a) (Table 7.5). The dull bands (sapropelic lithotype units) in pillar 88(a) comprise a small proportion of the overall seam (Fig. 5.1 A) but drastically affect the coal quality if sampled. There is considerable within seam variation in coal characterisation properties and coal quality in seam 88 depending on the position in the seam that is sampled.

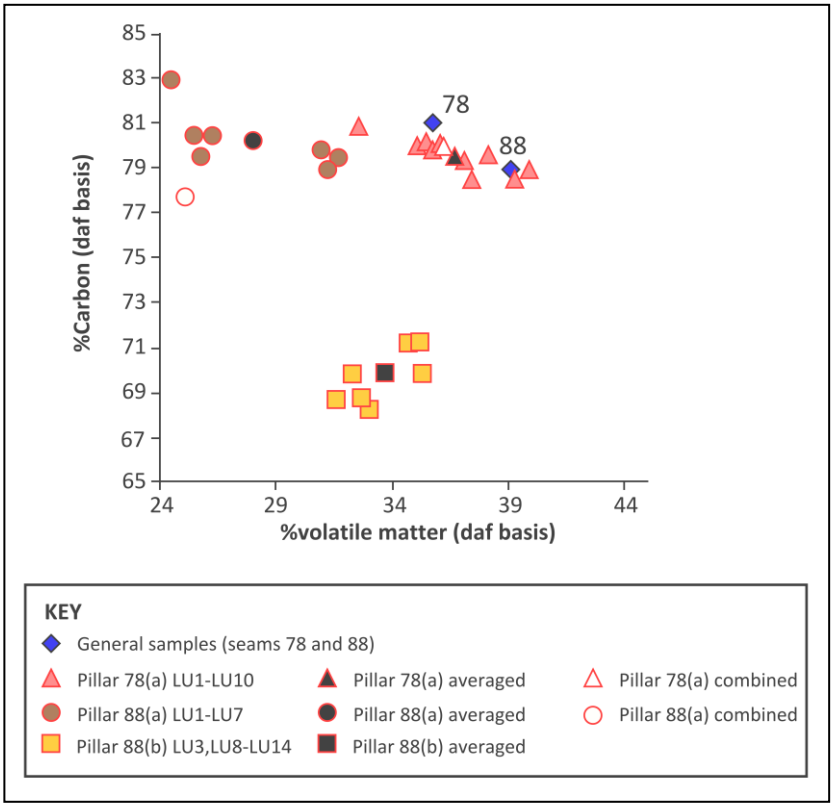

FIG. 7.18 Relationship between %Carbon and volatile matter for lithotype units from coal pillars 78(a), 88(a) and 88(b), combined samples from 78(a) and 88(a) and averages of 78(a) and 88(a) compared with general samples from seams 78 and 88. %Carbon and %volatile matter are reported to a dry ash free basis. General samples were analysed at RWE Npower. Lithotype units were analysed at CAER (symbols with red outlines).

Sample name	*PETROGRAPHY (%)*				*PROXIMATE ANALYSES (%)*			*ULTIMATE ANALYSES (%)*			
	Vitrinite	**Liptinite**	**Inertinite**	**Mineral matter**	**Moisture**	**Ash**	**Volatile matter**	**Carbon**	**Hydrogen**	**Nitrogen**	**Total Sulphur**
78(a) combined					4.97	3.81	35.97	80.15	4.99	2.61	0.8
78(a) averaged	67.1	0.9	28.1	4	4.91	4.32	36.45	79.86	4.91	2.49	0.9
General sample 78	59.7	2.3	35.6	2.4	5.02	5	35.54	81.27	4.86	2.47	0.63
88(a) combined					5.94	19.35	24.9	77.87	4.19	2.27	0.22
88(a) averaged	30.1	12.9	39.8	17.2	6.38	15.29	27.82	80.43	4.58	2.39	0.23
88(b) averaged (LU3, LU8-14)	50.7	5.2	38.7	5.4	6.32	5.34	33.57	70.01	5.2	2.23	0.25
General sample 88	75.5	4.1	15.1	5.3	6.81	5.34	38.92	79.16	5.1	2.41	0.23

TABLE 7.5 Comparative summary table of petrographic proximate and ultimate data for laboratory produced combined samples for pillar 78(a) and 88(a) combining subsamples of all lithotype units in those pillars. Averaged pillar compositions for 78(a), 88(a) and 88(b) averaging all lithotype unit data and comparing to general samples from seams 78 and 88. Moisture and ash are reported to an air dried basis and volatile matter, and ultimate analyses are reported to a dry ash free basis.

7.5 CONCLUSIONS

Bulk general samples (seams 68-94), stockpile fractions and lithotype units from four *in situ* coal pillars 78(a), 88(a), 88(b) and 91 were analysed using petrographic and characterisation techniques to document the effect of inertinite content and distribution on coal characterisation properties. Analysis of bulk coal (containing all maceral groups) is considered to be more representative of the coal that is commercially utilised unlike density separated maceral groups. The thirteen coal seams and stockpile size fractions studied have an overall mean random vitrinite reflectance of 0.53%Ro (2 sd = 0.08) therefore, all seams are within the subbituminous rank range.

Inertinite contents vary both between (7.1% – 50.2%) and within seams (e.g. seam 78, 12.6% - 33.2%), with a high overall mean of 28.3% which is very comparable to the mean of the two stockpile fractions (28.1%). There is only a weak correlation between inertinite content and coal characterisation properties; therefore, even with percentage values of up to 61.1% inertinite does not dominate the bulk properties of the coal. Within and between seam differences in both petrography and characterisation results do not appear to affect the overall stockpile composition which is well represented by a mean of all the contributing seams (73 – 91).

Patterns of inertinite distribution identified in coal pillars (chapters 4 and 5) do not correlate with any characterisation properties. Lithotype units containing microscopic inertinite show characteristics comparable to vitrinite-rich lithotype units. Sapropelic lithotype units (scattered inertinite in every field of view) typically contain low %volatile matter, high %ash and >50% inertinite. Lithotype units containing macroscopic inertinite (either scattered or contained in charcoal horizons) contain variable inertinite contents (5 - 61%) and the %volatile matter correlates with the amount of inertinite not the type of inertinite distribution.

Petrography and characterisation data also vary at lithotype unit scale (within and between pillars). When all lithotype units are combined or averaged, the pillar 78(a) blend is very comparable to the general 78 sample, suggesting the general sample may comprise comparable lithotype units or originate from a similar position in the seam to pillar 78(a). In contrast, neither pillar 88(a) nor pillar 88(b) represent the general 88 sample suggesting there is significant within seam variation in both petrography and characterisation properties depending on the position of the seam that is sampled.

The surfaces of pillars 88(b) and 91 were exposed in the laboratory for several months prior to ultimate analysis and discrepancies in values between laboratories may be due to oxidation of these samples. These samples all contain low %Carbon, high %Oxygen and low calorific value which are characteristics consistent with oxidised coal. General samples from seams 91(2), 92 and 94 also show characterisation trends comparable to oxidised coal but microscopically show no clear evidence for oxidation. These samples have high mineral matter and %ash

contents (14% – 41%). The inorganic constituents in these samples therefore appear to influence the characterisation properties of the coal as a whole more than the organic maceral content.

Pilot-scale Drop Tube Furnace (DTF) experiments have demonstrated that the more inertinite-rich Russian Permian samples (30% inertinite) produced denser chars and poorer burnout curves than inertinite-poor equivalents. Therefore, inertinite content may affect burnout more than characterisation properties in these coals.

CHAPTER 8

DISCUSSION

8.1 SAMPLING COAL SEAMS

Prior to fieldwork in Siberia no information was available regarding the Mines, seam thicknesses, or number of seams that could be sampled, therefore a sampling strategy could not be devised until reaching the Mine localities. In addition, seams were also commonly >10m thick (Fig. 3.2; Fig. 3.5 A; Fig. 3.7; Fig. 3.9 A; Fig. 4.1 C) therefore sampling a continuous pillar throughout the whole seam or ply sampling (e.g. Glasspool, 2000) was not possible or practical. The British Standard for coal sampling suggests a pillar width of 400mm (BS ISO 14180: 1998) and extraction using a chain saw. However, once the coal pillar is embedded in resin the resulting polished blocks are limited in size due to the dimensions of the reflectance microscopy stage. The pillar width suggested by the British Standard is too wide to enable appropriate polished blocks to be produced. Furthermore, chainsaws were not available in the field. Therefore, pillar sampling localities were based on features such as fractures and protrusions in the coal seam that enabled extraction using a geological hammer. The limitations of the sampling equipment meant that adjacent pillars could not be sampled, hence the spacing between pillars 88(a) and 88(b) (Fig. 5.1 A). As a consequence, the coal pillars studied are small in relation to total seam thickness (Fig. 4.1; Fig. 5.1). Although the coal pillars cannot be considered to represent the entire seam they do provide an insight into the potential variation in inertinite distribution, hence wildfire occurrence, for the duration of coal pillar formation (chapters 4 and 5).

Mining operations had to be stopped during sampling, so the time spent at each seam was limited, as was seam access. In the coal sampling standard, manual sampling is considered to be less desirable than mechanical sampling from a moving stream of material (BS ISO 18283: 2006). However, the latter was not possible for this study. In order to reduce bias replicate samples were taken in the form of multiple loose coal pieces from each seam. These were combined for characterisation analyses to

represent, as far as possible, the potential variation in coal characterisation properties in the seam (chapter 7).

8.2 PETROGRAPHIC METHODOLOGY

8.2.1 Evaluation of the point count/ transect methodology

There is currently no standardised methodology for petrographic analysis of *in situ* coal pillars. Previous methodologies all initially subdivide the pillars into visually distinct units (this study; Glasspool, 2000, 2003a; Collinson et al., 2007). Different graticules can be used for the point counting of macerals, either the Kötter (n =20; this study; Hacquebard, 1951, 1993), crosshair (n = 1; Beaton et al., 1993; Glasspool, 2000, 2003a; Jerret et al., 2011b,c), or a Whipple grid (n = 100; Belcher et al., 2003; Collinson et al., 2007) hence differences exist in surface area of the coal pillar covered in each analysis. Using a ×20 objective with a ×10 eyepiece magnification the Kötter graticule covers 50µm × 50µm, whereas the Whipple grid covers 125µm × 125µm (Fig. 8.1). The total number of points counted also varies depending on both the graticule used and the step distance, therefore points ranged from 20 points per mm (Glasspool, 2000), to 40 points per mm (or 120 points per mm combining the 3 transects; this study) to 100 points per lithotype (Belcher et al., 2003) to up to 1000 points per lithotype (Collinson et al., 2007). The British standard for coal petrographic analysis used in industry, suggests that a minimum of 500 points should be counted in total per crushed coal sample (BS 6127-3, 1995). This only applies to determinations made on small circular blocks of crushed coal (as used in chapter 7) but some workers also apply this method to coal pillars (e.g. Davies et al., 2005; Jerrett et al., 2011b,c). 500 points is a very small count size and unlikely to be representative of a whole coal pillar.

In order to justify the number of points counted during petrographic analysis (this thesis) a method has been used to demonstrate that the British standard of 500 points may not fully represent the proportion of macerals within a coal pillar. Individual point counts of petrographic data from pillar 78(a) LU8 (n = 13,363) (Appendix 1) were assigned a random number which were then randomly sorted to generate a hypothetical petrographic composition. From this hypothetical composition, the first 500, 1000, 2000, 5000 and 10,000 points were taken to represent a petrographic

transect. This process was repeated five times (termed runs) to test the reproducibility of the proportion of macerals counted (Appendix 1). For a given run of 500 points, maceral groups have a 2 sd of 4.6%, 5.9%, 1.3%, 0.8% for vitrinite, inertinite, mineral matter and liptinite respectively (Table 8.1). Whilst, for 5000 counts the expected precision for a given maceral group is 0.4%, 0.5%, 0.2%, 0.2% (2 sd) for the maceral groups listed above respectively (Table 8.1). This clearly demonstrates that 500 points are insufficient to confidently reflect the actual petrographic composition of this lithotype unit which represents a portion of a coal pillar. Therefore, 500 counts are extremely unlikely to adequately represent an entire coal pillar.

It is probably currently not meaningful to compare petrographic data for *in situ* coal pillars due to these differences in methodologies. A standardised petrographic methodology for coal pillars needs to be produced. In order to compare data obtained using the Kötter graticule with those that might result from using the Whipple grid, the coal pillars would need to be re-analysed which is too time consuming to be completed within the timeframe of this study. One prediction is that the Kötter graticule, which counts fewer points in a smaller surface area, might record only a single charcoal clast hence possibly over represents inertinite. However, this effect has been partly offset by counting three transects.

Number of points	Number of runs	Averaged maceral composition			
		Vitrinite (%)	*Inertinite (%)*	*Mineral matter (%)*	*Liptinite (%)*
500	1	52.6	41.8	4.4	1.2
	2	48.2	46.8	4	1
	3	47	48.8	3.8	0.4
	4	48.2	48.6	2.8	0.4
	5	47	48.2	4.4	0.4
	2 sd	**4.6**	**5.9**	**1.3**	**0.8**
2,000	1	50.7	44.1	4.3	1
	2	49.5	46.2	3.7	0.7
	3	49	46.9	3.6	0.5
	4	48.7	47.1	3.7	0.6
	5	48.4	46.5	4.6	0.6
	2 sd	**1.8**	**2.4**	**0.9**	**0.4**
5,000	1	49.1	46	4.1	0.8
	2	48.9	46.5	4	0.6
	3	49.2	46.2	3.9	0.6
	4	49.2	46.2	3.9	0.6
	5	48.7	46.6	4	0.7
	2 sd	**0.4**	**0.5**	**0.2**	**0.2**
10,000	1	49.1	46.2	4	0.7
	2	49.4	46	3.9	0.7
	3	49.2	46.3	3.9	0.7
	4	49.4	45.9	4	0.7
	5	49.2	46.3	3.8	0.7
	2 sd	**0.3**	**0.4**	**0.2**	**0**

TABLE 8.1 Hypothetical petrographic compositions of 78(a) LU8 based on actual point count data for a given number of counts. The reproducibility improves with the number of points counted. ≥5,000 points need to be counted in order to represent the petrographic composition of this lithotype unit (see Appendix 1 for complete data table).

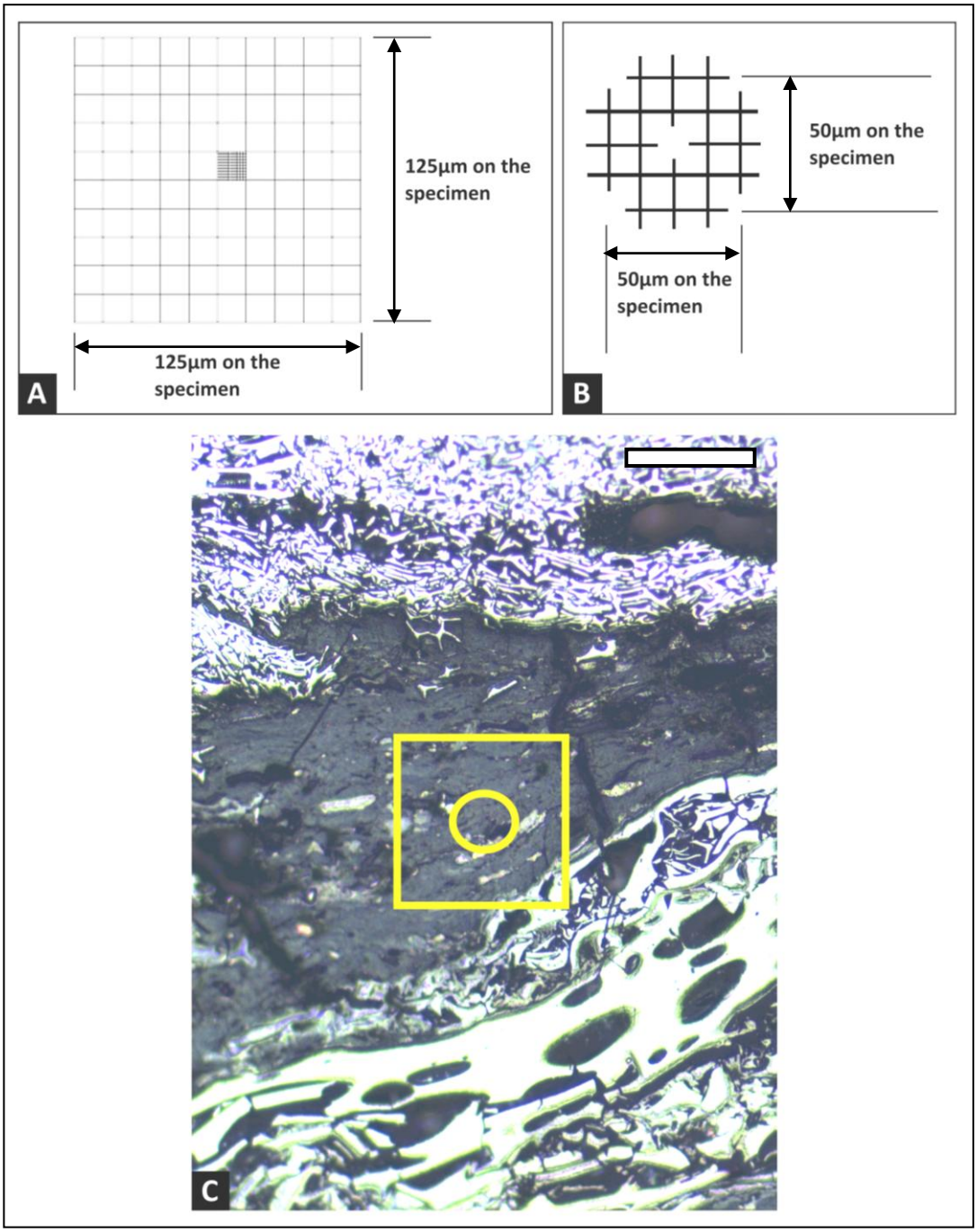

FIG. 8.1 Schematic representation of the different graticules used for *in situ* coal pillar petrographic analysis. During point counting, all crosshairs on the graticule are counted. **A –** 10 by 10 row Whipple grid (n = 100) used for petrographic analysis of coal pillars by Belcher et al. (2003) and Collinson et al. (2007). **B** – Industry standard Kötter graticule (n =20) used for coal petrographic point counting in this study (BS 6127-4: 1990). **C** - Representative reflectance microscopy image of one of the coal pillar samples (×20 objective, ×10 eyepiece magnification) illustrating the size of the Kötter graticule (yellow circle) and the Whipple grid (yellow square) in relation to one another. Scale bar in **C** 100µm.

The petrographic methodology devised in chapter 2.4 was based on the coal petrographic British Standard (BS 6127-4, 1990). The Kötter graticule only covers 15% of the total field of view (Fig. 8.1), or sixteen squares of the Whipple grid, and therefore counting 20 points in a 50µm × 50µm area represents a smaller surface area of the sample than the 100 points covered by the Whipple grid (illustrated in Fig. 8.1 C). In order to demonstrate that the use of the Kötter graticule is representative of the proportion of macerals in a given lithotype unit, a transect along pillar 78(a) block B2, LU4-LU7 (Fig. 4.5) was petrographically point counted, both with a vertical step distance of 425µm (or one field of view) compared to data from continuous adjoining graticules (i.e. 62.5µm vertical step distance). This is a very time-consuming task, counting >19,000 points takes >10 times as long as 1,500 points (Table 8.2) and despite discrepancies between the different vitrinite macerals the variation between the three maceral groups is negligible (Table 8.2), showing that the 425µm step distance for transect analysis retrieves data representative of the transect as a whole. The reduced size of the Kötter graticule (compared to the Whipple grid) may also be compensated for by the use of three transects (transect positions illustrated in, Fig. 4.4; Fig. 4.9; Fig. 4.14; Fig. 5.4; Fig. 5.7; Fig. 6.3) per pillar as opposed to one (e.g. Belcher et al., 2003; Glasspool, 2000, 2003a).

Vertical step distance	Detrovitrinite (%)	Telovitrinite (%)	Total vitrinite (%)	Liptinite (%)	Fusinite (%)	Semifusinite (%)	Inertodetrinite (%)	Secretinite (%)	Funginite (%)	Macrinite (%)	Total inertinite (%)	Mineral matter (%)	Total number of points counted using the Kötter graticule
T2 (425µm)	27.3	38	65.3	3.6	12.7	6	2	0	0.7	4.7	27	5	1,556
T2 (62.5µm)	49.8	19.6	69.4	2.3	11	6	3.1	1	0.6	2.4	24.3	4	19,408

TABLE 8.2 Comparative petrographic data for pillar 78(a) block B2 (LU4-LU7) illustrating the difference between point count data with a vertical step length of 425µm (or 1 field of view, used in this thesis) (top row) compared to point count data for adjoining graticules (bottom row) using the Kötter graticule for both methods. See appendix 1 for raw petrographic point count data.

Traverses need to be systematically spaced in order to give consistent estimates of area covered (Chayes, 1956; Beaton et al., 1993). Analysis of multiple transects was considered essential in this study to account for the macro- and microscopic spatial variation in charcoal distribution (chapters 4 and 5). The horizontal spacing between the three transects (~20mm) was designed to account for the maximum charcoal particle size of 30mm [pillar 88(b); chapter 5] thus ensuring that the minimum number of points are counted on the same clast. The variation in whole pillar mean inertinite content, between individual transects for all coal pillars, ranged from 1.84% (pillar 91) to 7.15% [pillar 78(b)] (Table 4.2; Table 5.1). Coal pillars containing sapropelic lithotype units showed the largest variation in total inertinite content between transects due to their high inertinite content (>50%) and scattered distribution of inertinite in every field of view [pillar 88(a) LU2, LU4; pillar 78(b) LU4; chapter 4; chapter 5]. Additional transects may be required to fully account for the lateral variation in inertinite content in sapropelic lithotype units. However, maceral identification in these lithotype units is incredibly time-consuming due to the small particle size of inertinite macerals. In addition, the identification of liptinite macerals must be cross checked using fluorescence microscopy in every field of view if there is high mineral matter content (as in chapter 4). The difference in inertinite contents between transects for sapropelic lithotype units does not affect palaeoecological interpretations of the petrographic data (chapters 4 and 5). The use of three transects adequately accounts for variation in the other types of inertinite distribution observed in this study. Therefore, the use of three transects appears to be appropriate for petrographic analysis of the coal pillars in this study.

8.2.2 Would automated petrographic analysis be useful for palaeoecological work?

Manual coal petrographic analysis is indeed a very time-consuming technique, particularly the analysis of coal pillars. In this study >7,000 points have been counted per coal pillar. Therefore, only five *in situ* coal pillars could be analysed petrographically in the timeframe of this study. The petrographic variation observed both within and between coal pillars (chapter 4, chapter 5) emphasises the need for multiple pillars to be analysed in order to more fully interpret Late Permian wildfire

occurrence using coal pillars. In order to analyse multiple pillars in a short time period the use of automated petrographic analysis could be considered.

Automated coal petrography uses image analysis software to produce reflectance profiles of the coal (including resin) (illustrated in Fig. 8.2) by assigning individual pixels in reflectance microscopy images a grey-scale value (0 – 255) that is then calibrated against a measured reflectance value (e.g. Chao et al., 1982; Pratt, 1993; O'Brien et al., 2003). Automated petrographic analysis has currently primarily been used for industrial applications (e.g. Chao et al., 1982; Pratt, 1993; Cloke et al., 1995a,b; Lester et al., 2002; O'Brien et al., 2003; Choudhury et al., 2007) as some workers consider manual petrographic analysis "prone to fatigue and boredom" and therefore counts in excess of 500 points on crushed coals are rarely reported in the literature (Borrego et al., 2000).

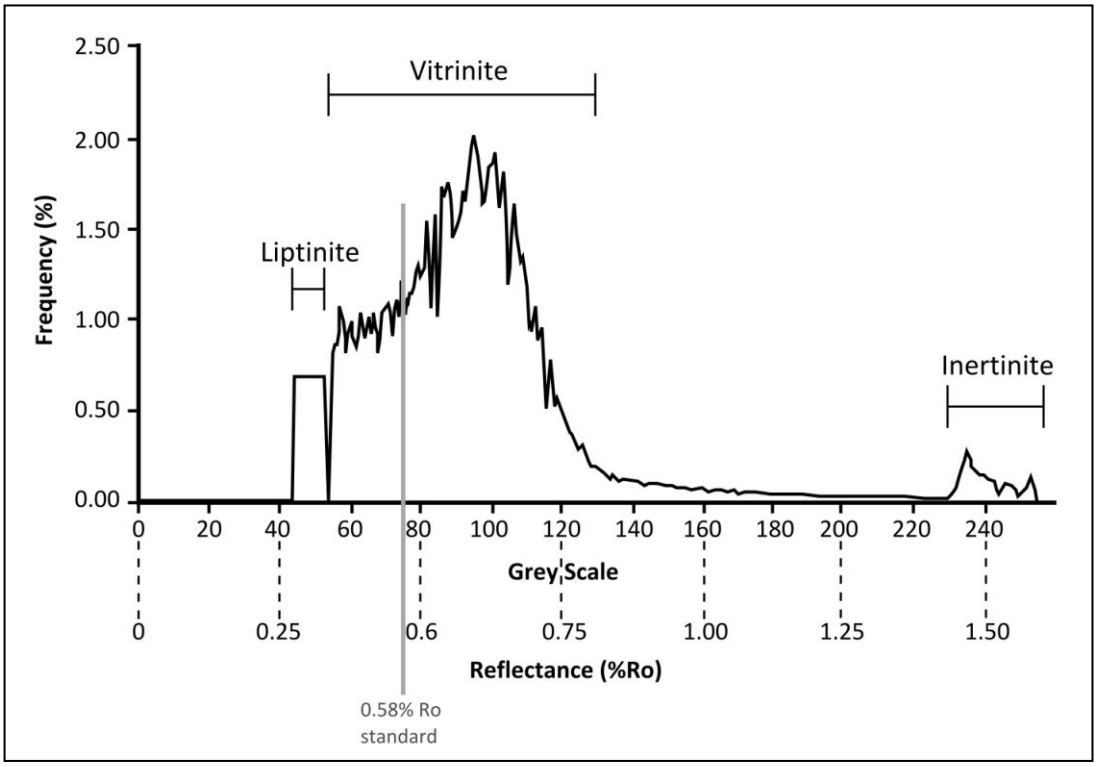

FIG. 8.2 Typical grey-scale histogram produced using automated image analysis (after Cloke et al., 1997b).

The advantage of an automated image analysis system would be to remove the time consuming and subjective nature of manual petrographic analysis (Cloke et al., 1997b; O'Brien et al., 2003). Automated petrographic analysis is not available using

the Royal Holloway University of London reflectance microscope. However, manual petrographic analysis is in any case currently more appropriate for the type of detailed petrographic work on *in situ* coal pillars used in this thesis for palaeoenvironmental reconstruction, as it is not yet possible to recognise the individual macerals within the maceral groups, or to determine their distribution in the coal, using automated petrographic analysis.

In automated petrographic analysis the system is calibrated using reflectance standards (also used for measuring charcoal reflectance; chapter 6). Currently, the automated system is only calibrated with a single low reflecting Leitz sapphire standard (0.58%Ro or 120 grey-scale units; Fig. 8.2) (Bostick et al., 1991; Cloke et al., 1995b) as this represents mid-range vitrinite reflectance for a bituminous coal. As a result, the high reflecting inertinite in a sample cannot be accurately measured because there is no high reflecting standard for calibration. Resulting published reflectance profiles therefore rarely show inertinite with >2%Ro values (Fig. 8.2; Cloke et al., 1997b; Lester et al., 2002; Choudhury et al, 2007; Choudhury et al., 2008). Furthermore O'Brien et al. (2003) only consider inertinite macerals to cover the reflectance range 2.4%Ro – 4%Ro with all values >4%Ro interpreted as "bright minerals". Measured reflectance values of fusinite clasts in Permian coal pillars can reach 5.1%Ro (chapter 6) and experimentally produced charcoal can reach up to 7%Ro at temperatures of 1,100°C (McParland et al., 2009b). Therefore, currently the automated method will miss all the high reflecting charcoal, hence high temperature fires. Automated petrographic analysis needs further development if it is to be applied for palaeoecological purposes.

8.2.3 Problems with the ICCP classification scheme for inertinite macerals

Inertinite macerals were identified in this thesis according to internationally recognised coal petrographic standards (ICCP, 1998, 2001; Table 2.3). Coal petrography is based on a visual classification scheme and therefore the identification of macerals can be highly subjective. In addition peat (the parent material of coal) is an extremely heterogeneous material and resulting coal macerals will potentially show considerable morphological variation according to the plane of section, botanical affinity, post depositional alteration and any transport induced

alteration. It may therefore be unrealistic to classify each maceral according to a single idealised image as in the 1994 ICCP (2001) inertinite maceral group classification scheme (Scott, 2002; Scott and Glasspool, 2007).

In particular, fusinite, semifusinite and inertodetrinite macerals are accepted to represent charcoal derived from palaeowildfires (Scott and Glasspool, 2007) and their distribution and reflectance has been used to aid interpretation of palaeowildfire occurrence and type from *in situ* coal pillars (chapters 4, 5, 6; see also Hudspith et al., 2012; Appendix 9). Therefore, critical evaluation of the classification scheme of these macerals is given below. Refer to chapters 4 and 5 for reflectance microscopy images of inertinite macerals and Table 2.3 for ICCP (2001) maceral definitions.

8.2.3.1 Problems with fusinite classification

"Fusinite is a maceral of the inertinite maceral group, showing highly reflecting, well preserved cellular structure of at least one complete cell of parenchyma, collenchyma, or sclerenchyma" (ICCP, 2001).

In the ICCP (2001) classification scheme fusinite (illustrated in Figure 2; pg 461; ICCP, 2001) has a grey colouration and is not visually the highest reflecting inertinite maceral in the image and should therefore technically be classified as semifusinite (*sensu* ICCP, 2001). Fusinite is also defined by having well preserved cellular structure. The majority of fusinite clasts in the coal pillars in this study have poorly preserved cellular structure (e.g. Fig. 4.6 D, E; Fig. 4.8; Fig. 4.11; Fig. 4.12; Fig. 4.13; Fig. 4.16 B, D, J; Fig. 5.6 D, H, I; Fig. 5.9 A, B, D, F, I; Fig. 5.10 E; Fig. 5.11 C, D, H; Fig. 5.12) and therefore some clasts, despite attaining high visual reflectance, cannot be classified as fusinite according to ICCP (2001). The implications for identifying inertinite macerals according to visual reflectance and morphology is discussed further in section 8.2.4.

High temperature charcoal can be brittle and fragment during transport (Scott and Jones, 1991; McParland et al., 2009b) therefore fragments of fusinite less than one cell in size are classified as inertodetrinite (Fig. 5.9 I; Fig. 5.10 B; Fig 5.11 E). Furthermore, partially charred clasts, commonly observed in charcoal horizons in

coal pillars, could be classified as different maceral groups depending on the area intersected by the graticule (i.e. fusinite, semifusinite, vitrinite) (Jones et al., 1993; Brown et al., 1994; Scott, 2002; Scott and Glasspool, 2007). See section 8.2.4 for implications of classifying inertinite according to cellular preservation and visual reflectance.

8.2.3.2 Problems with semifusinite classification

"Semifusinite is a maceral of the inertinite maceral group that shows intermediate reflectance and structure between humotelinite/vitrinite and fusinite in the same coal or sedimentary rock" (ICCP, 2001).

The physical properties section of the ICCP (2001) definition defines semifusinite as ranging from grey to white in colour which further complicates maceral identification. Visually high reflecting inertinite clasts with poor cellular preservation have to be classified as semifusinite according to ICCP (2001). See section 8.2.4 for implications of classifying inertinite according to cellular preservation and visual reflectance.

8.2.3.3 Inertodetrinite size definition

Inertodetrinite is defined as "Discrete small inertinite fragments of varying shape" (ICCP, 2001).

The "small" size of inertodetrinite is not formally defined in ICCP (2001). Scott and Glasspool (2007) suggested a size range of 2-50µm which encompasses the microscopic (or windblown) charcoal size fraction used by Quaternary researchers (Clark et al., 1998; Pitkänen et al., 1999; Ohlson and Tryterud, 2000; Lynch et al., 2004; Peters and Higuera, 2007; Conedara et al., 2009). However in this study it was appropriate that data should be comparable with others produced using the ICCP standard method. In the ICCP (2001) scheme inertodetrinite is suggested as being <10µm in the comments section of the definition. Therefore, this size was used in this study during petrographic analysis of *in situ* coal pillars (chapters 4 and 5). The use of the smaller size (10µm) for inertodetrinite (this study) does not affect wildfire interpretation because it is well within the size fraction for windblown charcoal.

8.2.4 Quantifying reflectance of inertinite macerals: implications for maceral definitions and palaeoecological interpretations

As indicated above (section 8.2.3) fusinite and semifusinite macerals were identified according to the ICCP (2001) classification scheme based on their visual, not measured, reflectance. All macerals in the Permian coals were initially identified using ICCP definitions (chapters 4, 5, 7). In addition, the reflectance of inertodetrinite and macroscopic clasts of fusinite and semifusinite were also measured to aid palaeowildfire interpretation (chapter 6). When the measured reflectance values are combined with macerals identified according to visual reflectance (*sensu* ICCP, 2001) there is an overlap between macerals visually identified as both fusinite and semifusinite over the reflectance range, 0.7%Ro – 2.4%Ro (Fig. 8.3). An overlap between inertinite identified according to both measured reflectance values and petrographic classification (ICCP, 2001) has previously been documented in the literature for other coals (e.g. Bostick et al., 1991; Crosdale et al., 2002). It would appear that, especially for low reflecting inertinites, visual reflectance is a poor indicator of measured reflectance, thus emphasising the need for reflectance measurements of inertinite to aid interpretation of palaeowildfire types in coal pillars.

Fusinite and semifusinite macerals are also distinguished according to their structure (ICCP, 2001) (see section 8.2.3.1, 8.2.3.2). Visually high reflecting inertinite clasts with poorly preserved cellular structure (e.g. the 2%Ro semifusinite image in Fig. 8.3) are classified petrographically as semifusinite (*sensu* ICCP, 2001; section 8.2.3.2). These clasts occur in pillars 78(a), 88(a) and 88(b) they have measured reflectance values from 1.2% - 2.4%Ro and account for the majority of the overlap in reflectance values. Therefore, the amount of higher temperature charcoals may be underestimated if palaeoecological interpretations are only based on visual petrographic data not using measured reflectance. In contrast, well structured low reflecting clasts may be erroneously classified as fusinite (Fig. 8.3) if the clast is surrounded by visually lower reflecting clasts or if the clast is partially charred and shows a continuum of visual reflectance from vitrinite to semifusinite within a single clast. The majority of macroscopic charcoal clasts in charcoal horizons are partially charred (chapter 4, chapter 6.4.4) and therefore ‘fusinite’ counts could be

overrepresented in these coal pillars. Therefore, for future petrographic analysis on coal pillars, the current ICCP (2001) inertinite classification scheme needs to be used in conjunction with reflectance histograms to more accurately interpret palaeowildfire types.

Jones et al. (1997) and Scott and Glasspool (2007) have already proposed classifying inertinite macerals according to measured reflectance to aid wildfire interpretation. They proposed a value of >2%Ro for fusinite which corresponds to a charring temperature of >400°C and <2%Ro or <400°C for semifusinite (Jones et al., 1997). This fusinite-semifusinite boundary at 2%Ro was based on modern charcoalification experiments not measurements of coal macerals. It was possible to distinguish between fusinite and semifusinite visually, irrespective of the visual reflectance of surrounding clasts, at a measured reflectance value of 2.5%Ro and above (Fig. 8.3). Therefore, the Permian coals suggest that a value of ≥2.5%Ro could be used to define fusinite.

Inferring charring temperatures from reflectance values is not always straightforward as calibration curves of experimentally charred material can vary depending on charring duration and plant type used (McParland et al., 2009b; McParland, 2010). Using these different calibration curves 2.5%Ro can be reached at different charring temperatures but all are <700°C which is still within the range of low temperature surface and ground fires (see chapter 6.4.1). For further discussion of the implications on interpreted Permian charcoal temperatures and wildfire interpretation see section 8.4.

FIG. 8.3 (overleaf) Stacked histograms with representative images of either fusinite and/or semifusinite clasts for a given reflectance value showing that visual appearance is a poor guide to measured reflectance value. Furthermore, poorly structured high reflecting material would be classified as semifusinite which could be taken to imply a low charring temperature. Alternatively low reflecting structured material, which should be classified as semifusinite, might be wrongly classified as fusinite if emphasis was placed on the structure not the reflectance value and if surrounded by low reflecting clasts. The range in reflectance values for each image shown is given in the table below the figure.

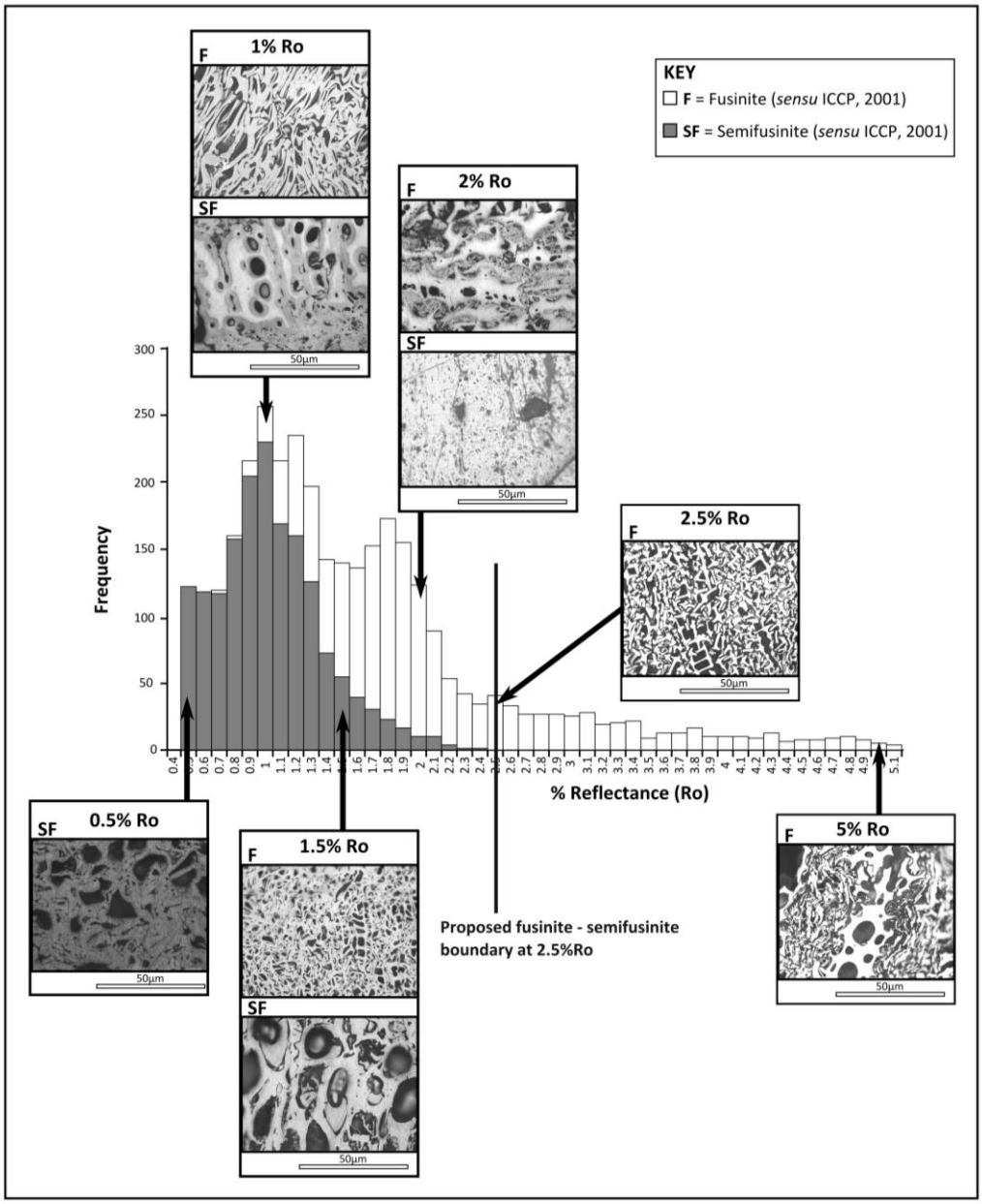

Reflectance value represented in diagram	*Sample name*	*Petrographic identification (F = fusinite, SF = semifusinite)*	*%Ro mean*	*%Ro min*	*%Ro max*
0.5% Ro	78(a) LU8 CH1 T2 clast 14	SF	0.79%	0.5%	1.1%
1.0% Ro	91 LU2 CH2 T3 clast 2	F	1.12%	0.94%	1.34%
	88(b) LU12 T1 clast 2	SF	1.3%	0.95%	1.6%
1.5% Ro	91 LU2 CH3 T2 clast 4	F	1.53%	1.2%	1.8%
	78(a) LU8 CH2 T2 clast 4	SF	1.56%	1.05%	1.94%
2.0% Ro	78(a) LU8 CH1 T2 clast 13	F	1.94%	1.44%	2.55%
	88(a) LU7 CH1 T2 clast 10	SF	2.03%	1.78%	2.3%
2.5% Ro	91 LU2 CH2 T2 clast 7	F	2.43%	2.15%	2.68%
5.0% Ro	91 CH1 T3 clast 3	F	4.73%	4.23%	5.08%

8.3 IMPLICATIONS OF THE PETROGRAPHIC TECHNIQUE USED FOR CHARACTERISATION PROPERTIES OF COAL

Whole coal bulk characterisation analysis of the Permian coals in this study (both general samples and lithotype units from coal pillars) showed weak correlations between inertinite content and distribution with various characterisation properties (chapter 7). However, previous work on bulk coals with maceral proportions determined from automated petrography reflectance histograms show good relationships with %volatile matter (Bostick et al., 1991), %Carbon and %Hydrogen (O'Brien et al., 2003) thus suggesting that automated petrographic analysis may be more appropriate for industrial than palaeoecological usage (see section 8.2.2 for further discussion). Manual petrographic analysis for industry is carried out on crushed coals that do not retain their original inertinite distribution and therefore cannot be used for the type of detailed petrographic analysis required for palaeowildfire interpretation (this study). Petrographic analysis of crushed coals is a small aspect of the overall characterisation of a coal for industry. The amount of low reflecting (<1.3%Ro) inertinite in a coal can correlate well with good burnout behaviour (Cloke et al., 1997a,b; Choudhury et al., 2007). Therefore, the use of a reflectance profile (see section 8.2.2; Fig. 8.2) as opposed to manual petrographic analysis where the macerals are determined based on visual reflectance (see section 8.2.3) may be more informative to predict the burnout behaviour of the coal than manual petrographic analysis.

8.4 IMPLICATIONS OF VARIATIONS IN CALIBRATION CURVES FOR INTERPRETATION OF PERMIAN CHARRING TEMPERATURES

Charring temperatures (chapter 6) were inferred using the 24 h experimental charring calibration curve for *Sequoia* (conifer) wood from Scott and Glasspool (2005) (illustrated in Fig. 6.2). The conifer *Sequoia* was thought to be an appropriate modern relative of the Permian Cordaite peat-forming vegetation because Cordaites are extinct but are the sister taxon to conifers. The 24 h calibration curve was chosen firstly because Permian peats have undergone long duration heating during coalification, which has raised the reflectance of the uncharred material (now vitrinite) by 0.56%Ro_{mean} and may therefore also have altered the reflectance of the low reflecting inertinite (charcoal) over time. Secondly, reflectance values are known

to stabilise after 24 h of heating (Scott and Glasspool, 2005). However, these coals are relatively low rank (subbituminous to high-volatile bituminous; chapter 7) therefore coalification may be considered to have had a negligible effect on the charcoals with reflectance values >0.6%Ro (see chapter 6.3.4). Furthermore, temperature/ reflectance value calibrations vary between different studies (see Table 8.3).

In order to consider the maximum potential variation in charring temperatures of these Permian charcoals the extreme ranges in temperatures extrapolated from a range of 1 h and 24 h charring calibration curves are presented in Table 8.3. Using the extremes, the highest Permian charcoal reflectance values fall within the temperature range for flaming crown fires (>700°C) which corresponds to reflectance values from >4%Ro to >5.2%Ro depending on the calibration used (Table 8.3). Of all the Permian reflectance values from this study, only 2.5% of all data are >4%Ro (n = 235 from 9,400) and no values are >5.2%Ro (Ro_{max} 5.1%). Therefore, even using the most extreme ranges in minimum charring temperatures only a very small proportion of the charcoal in the Permian coal pillars are within the temperature range for crown fires. This supports the interpretation that the majority of the Permian charcoal is derived from surface fires (chapter 6). However, crown fires may only be represented in the fossil record by small amounts of very high reflecting charcoal (see chapter 6.4.1; section 8.5.2).

Study	Charring duration	Range in reflectance data for all macroscopic clasts from all charcoal horizons (%Ro)	Range of inferred minimum charring temperatures	Range in reflectance data for all inertodetrinite particles (%Ro)	Range of inferred minimum charring temperatures
McParland et al. (2009b) *(Quercus)*	1 h	0.4% – 5.1% (1.1%)	340°C - 900°C (435°C)	0.7% – 4% (1.5%)	385°C - 720°C (485°C)
	24 h	0.4% – 5.1% (1.1%)	300°C – 800°C (350°C)	0.7% – 4% (1.5%)	320° C- 660°C (395°C)
Scott and Glasspool (2007) (*Sequoia*)	1 h	0.4% – 5.1% (1.1%)	325°C - 660°C (350°C)	0.7%– 4% (1.5%)	330°C - 610°C (450°C)
Scott and Glasspool (2005) (*Sequoia*)	24 h	0.4% - 5.1% (1.1%)	300°C – 655°C (350°C)	0.7% – 4% (1.5%)	320°C –545°C (395°C)
McParland (2010) *(Pinus)*	1 h	0.4% – 5.1% (1.1%)	350°C – 950°C (450°C)	0.7% – 4% (1.5%)	400°C –750°C (500°C)
	24 h	0.4% – 5.1% (1.1%)	300°C - 800°C (350°C)	0.7% – 4% (1.5%)	310°C - 650°C (400°C)
McParland (2010) all plant types	1 h	0.4% – 5.1% (1.1%)	300°C - 950°C (350°C)	0.7% – 4% (1.5%)	400°C - 700°C (500°C)
	24 h	0.4% – 5.1% (1.1%)	300°C - 800°C (350°C)	0.7% – 4% (1.5%)	310°C - 650°C (400°C)

TABLE 8.3 Summary table showing the potential ranges of inferred minimum charring temperatures for all Permian charcoal data (both macroscopic fusinite and semifusinite clasts from charcoal horizons and inertodetrinite; chapter 6), when reflectance values are extrapolated from calibration curves from different studies and different charring durations. Highlighted in grey is the 24 h calibration curve used in chapter 6 and the resulting minimum charring temperatures. Inferred charring temperatures from the most frequent value (mode) are given in brackets. The 1 h Sequoia calibration curve from Scott and Glasspool (2005) only has a maximum reflectance value of 4%Ro. The gradient of the line was extended above the graph to infer minimum charring temperatures at 5.1%Ro, so the inferred temperature (660°C) may underestimate the actual charring temperature, but this does not affect the palaeoecological interpretation of the data. See text for further discussion.

8.5 IDENTIFYING ANCIENT FIRE TYPES AND WILDFIRE DERIVED PRODUCTS USING EVIDENCE FROM MODERN FIRES

8.5.1 Post fire charcoal: alteration and transport

Charcoal is one of the most stable, slowly cycling compounds in terrestrial and marine systems (Abiven et al., 2011; Ascough et al., 2011) but the post depositional

decomposition of charcoal is still poorly understood (Schmidt et al., 2011). Charcoal is not a completely inert material (Preston and Schmidt, 2006; Ascough et al., 2010, 2011; Schmidt et al., 2011) and can be lost from the system due to chemical oxidation, degradation, fragmentation, transport, solubilisation, or subsequent fires (Preston and Schmidt, 2006; Ascough et al., 2010; Kane et al., 2010; Abiven et al., 2011). Therefore, the charcoal preserved in the sedimentary record might only represent a small proportion of the total charcoal produced in the original wildfire event. However, the rate of post-depositional diagenetic alteration of charcoal is slower in an anoxic peat than in soil (Preston and Schmidt, 2006). Low temperature charcoal (≤400°C) is highly susceptible to chemical oxidation and may be preferentially lost from the system (Ascough et al., 2010, 2011) yet the majority of charcoal clasts in charcoal horizons are low temperature charcoals formed at ≤435°C (chapter 6; Table 6.2; Fig. 6.3; Table 8.3) suggesting that the Permian peat-forming mire environment has resulted in good charcoal preservation.

8.5.2 Is there a bias against crown fire charcoal in the fossil record?

Crown fires occur at much higher temperatures than surface fires (see chapter 6.4.1). High temperature favours the evolution of volatiles whereas low temperature promotes the production charcoal (Pyne, 1996). In flaming crown fires more than 80% of the foliage is normally consumed and most of the emissions are entrained in a convection column associated with flaming fronts (Pyne, 1996; Bertschi et al., 2003). Up to 10% of the remaining material may be mineral ash (see section 8.5.4 for further discussion) which currently cannot be recognised in coal. Crown fires may be represented by small amounts of very high reflecting charcoal (see chapter 6.4.1; section 8.4) and therefore crown fires may not be well represented or recognised in the fossil record due to the small amount of charcoal preserved during each crown fire event.

8.5.3 Identifying ground fires in the fossil record

Prescribed and experimental burning has shown that peat can burn (e.g. Rein et al., 2008; Clay et al., 2010; Clay and Worrall, 2011) and therefore if a ground fire affects peat there should be evidence, in the form of charred peat, in the fossil record. Cohen et al. (1987) consider that a charred peat surface would be represented as a

continuous band of charcoal. However, charcoal horizons observed in Late Permian *in situ* coal pillars in this study are interpreted to represent transported charcoal from surface fires and there is no evidence of continuous charcoal bands (as all charcoal clasts in charcoal horizons are separated by uncharred material) (discussed in chapter 4). Charcoal horizons are observed in modern peat cores but these are not illustrated in the literature and therefore the charcoal could be derived from any type of fire.

Rare charcoal clasts that are visually comparable to experimentally charred peat have been observed in pillar 88(b) (see chapter 5.4.4.4; Fig. 5.16) but the scarcity of this material in pillar 88(b), and its absence from all four other coal pillars, suggests an absence of ground fires during the intervals of pillar formation in the Late Permian.

Ground fires are smouldering fires (discussed in chapter 6.4.1). Initial ignition depends on the moisture content of the peat, values <55% ± 2% can lead to >90% mass loss during smouldering combustion (Rein et al., 2008). A large proportion of organic material in a smouldering fire may be volatilised during combustion (50-86%) and only a very small amount (~4%) is typically preserved as charcoal (Bertschi et al., 2003; Clay and Worrall, 2011). It may therefore not be possible to identify ground fires in the fossil record from charcoal occurrence alone.

Smouldering ground fires produce large quantities of smoke (Pyne, 1996). The tar droplets produced during smouldering combustion can condense on cooler surfaces such as surface litter (Hartford and Frandsen, 1992). Franzén and Malmgren (2012) have reported 'tar' particles ('tar foam') with varying morphology in Holocene peat. Some of these SEM images of 'tar foam' particles are visually comparable to coprolites (e.g. Cohen et al., 1987) and parts of charred fungal sclerotia (illustrated in Scott et al., 2010) and have likely been misidentified as tar. Therefore, there currently appears to be no record of tar being preserved either from modern or ancient wildfires, which may be due to poor preservation potential of tar or a lack of recognition.

During a ground fire the overlying surface litter can be slightly charred at temperatures of up to 300ºC (Hartford and Frandsen, 1992). Jones et al. (1993)

suggest that charring temperatures of 180°C - 220ºC are sufficient to produce a measureable reflectance (see chapter 6.4.4). Therefore, it might be possible to recognise a ground fire indirectly in coal by the presence of very low reflecting charcoal that was present in the litter layer and was charred by an underlying ground fire. However, the coals in this study have vitrinite reflectance values of 0.56%Ro_{mean} therefore any low reflecting charcoal ≤0.6%Ro (≤300°C) will be overprinted by rank changes during coalification. Furthermore, re-charring experiments by McParland et al. (2009a) have demonstrated that charcoal reflectance represents the highest temperature event to which the material was subjected. Calculated fire return intervals were high in this Permian peat-forming environment (chapter 4.4.9) therefore, subsequent surface fires (at higher temperatures) would probably have overprinted any record of low temperature charcoal from ground fires.

Overall therefore, ground fires may be poorly represented in the fossil record. Future work should focus on alternative methods, other than charcoal occurrence, to identify ground fires to improve understanding of palaeowildfire occurrence in deep time.

8.5.4 Representation of other products produced during wildfires in the fossil record

Charcoal is not the only material produced during a wildfire. Black carbon represents a continuum of products from partially charred biomass to graphite and soot particles (Schmidt and Noak, 2000; Masiello, 2004; Preston and Schmidt, 2006; Hammes et al., 2007; DeLuca and Aplet, 2008; Clay and Worrall, 2011). There is currently no method for identifying other wildfire products such as mineral ash and tar (see section 8.5.3) in the fossil record. These other products may be the only evidence for crown and ground fires (see sections 8.5.2, 8.5.3). Further investigation is therefore required in order to aid interpretation of ancient wildfire types in coal pillars.

Ash: There is currently no accepted definition for ash produced during wildfires therefore the use of the term ‘ash’ can be misleading in the literature as it can incorporate both mineral ash and charcoal (e.g. Arcenegui et al., 2008; Bodí et al. 2011; Dlapa et al., 2012; Santín et al., 2012). Furthermore, some climate modellers

also classify both soot and ash as the same entity (Bond and Bergstrom, 2006). In the subsequent text in this section, 'ash' refers to the mineral ash remaining after complete combustion of organic material.

Only high severity fires can produce substantial quantities of mineral ash (Cerdá and Doerr, 2008). Typically mineral ash is readily removed from a burn site by wind or water erosion (Bodí et al., 2011) consequently, only smalls amounts are stored in the soil compared to charcoal (Santín et al., 2012). However, of the small amount of material remaining, up to 40% of the mineral ash may be stored in soil after exceptionally high severity fire events (Goforth et al., 2005). Mineral ash can range from 3.9µm - 250µm in size (Gabet and Bookter, 2011) and hence should be microscopically identifiable. Mineral ash composition is dependent on the original vegetation, the mineral content and combustion temperature, and typically contains high concentrations of Ca, K, Mg, Si, Mn, P, Fe and Al (Pereira and Úbeda, 2010; Gabet and Bookter, 2011; Dlapa et al., 2012). Potentially this wildfire mineral ash might be recognisable in the fossil record. However, the occurrence of mineral ash could not be used to interpret a single fire event as its distribution is patchy, it can be reworked by surface or wind erosion, or can be moved downward by precipitation percolating through the soil (leaching) (Boerner, 1982).

Coal contains inorganic material, in the Permian samples only 66% of the inorganic residue obtained after high temperature ashing can be accounted for by petrographically recognised mineral matter not derived from plants (chapter 7; Fig. A.4.2). Therefore, if wildfire derived mineral ash can be characterised, it may be possible to use techniques such as ICP-AES or XRF analysis to identify wildfire derived mineral ash in peat or coals. Another possibility would be to examine the morphologies of mineral particles to see if they are plant derived (phytoliths). Permian silica phytoliths have been reported in the literature (e.g. Carter, 1999) and in modern peats, plant phytoliths may be the dominant inorganic constituents (Cohen et al., 1987). Therefore, the occurrence of concentrations of phytoliths (in a peat or coal) may be related to wildfire events (Cohen et al., 1987) or the phytoliths themselves may show evidence of burning (ongoing work S.Y. Smith personal communication).

Pyrosynthetic Polycyclic Aromatic Hydrocarbons (pPAH): are carbonaceous organic toxins that can be produced in small amounts during partial combustion from wildfires (Belcher et al., 2009; Marynowski and Simoneit, 2009; Marynowski et al., 2011). pPAH are rapidly redistributed post fire and can be transported intercontinentally (García-Falcón et al., 2006; Zhang and Tao, 2009). At lower combustion temperatures pPAHs can condense into mineral ash particles (Preston and Schmidt, 2006), but distinguishing them from mineral ash depends on the burning conditions (García-Falcón et al., 2006) therefore, pPAHs could not be used to identify the presence of mineral ash in the fossil record. Wildfire derived pPAHs could be used to aid interpretation of palaeowildfire types as their size relates to the temperature of formation, with a larger number of hydrocarbon rings corresponding to higher temperature fires (Finkelstein et al., 2005). pPAH are persistent in the fossil record but there are still issues in the literature regarding the identification of those derived from biomass burning (discussed in Belcher et al., 2003, 2005, 2009).

Soot particles: Microscopic observations (SEM) of soot particles produced during a recent wildfire primarily consisted of plant fragments <30µm in size (Belcher et al., 2005). Other 'soot' morphologies reported from ancient sediments in the literature may actually represent hydrocarbon not biomass burning (Belcher et al., 2005). Soot particles, formed within flames, may range from 30nm to <100µm (Preston and Schmidt, 2006) so there is potentially a size continuum from soot to microscopic charcoal (inertodetrinite). It is therefore unlikely that soot produced from biomass burning can provide any more information about wildfire type than other microscopic charcoals in the same samples.

8.6 COMPARISON TO SOUTHERN HEMISPHERE PERMIAN COALS

There are few published records of charcoal from the Permian in the Northern Hemisphere (Scott, 2000). However, Permian coals from South Africa (Glasspool, 2000, 2003a), India (Stach et al., 1982; Choudhury et al., 2007, 2008), Australia (Diessel, 1992, 2010) and China (Shao et al., 2003; Zhuang et al., 2007; Glasspool and Scott, 2010) all contain high inertinite (charcoal) contents, with an overall mean of ~38.9% for coals from the Changhsingian Stage (Glasspool and Scott, 2010).

The most well studied major Permian Southern Hemisphere coal deposits are in Australia. Therefore, comparisons will be restricted to this geographic region. The predominant Permian peat-forming vegetation was not Cordaites but deciduous *Glossopteris* (Taylor et al., 1989; Retallack, 1999; Michaelsen and Henderson, 2000; Glasspool, 2000a; Fielding and Alexander, 2001; Greb et al., 2006). Lycopods and Sphenophytes were the main herbaceous flora (Hunt, 1989; Glasspool, 2003a, 2003b; McLoughlin, 2009). The Permian climate in Australia was cool temperate and long-lived mire environments produced thick, laterally extensive, coal measures during the Late Permian (McLoughlin, 2009) comparable to the Russian sequence (chapter 3).

The climate was much colder in Australia than Russia during the Permian with evidence for four glaciations (Jones and Fielding, 2004; Fielding et al., 2008; Frank et al., 2008; Birgenheier et al., 2009) which may have perturbed fire activity during these periods due to the lack of available fuel. However, there is no evidence for glacial events in Australia in the Late Permian (Fig. 8.4) and Late Permian (Changhsingian) Australian coals have a wide range of inertinite contents from 18.8% - 57.9%, with a high overall mean of 41.2% (Glasspool and Scott, 2010). Inertinite contents are comparable for both the Russian (Fig. 7.2) and Australian coals (Fig. 8.4). This suggests that there was widespread wildfire occurrence throughout the Permian in both Hemispheres. Inertinite macerals in Permian Australian coals mainly consist of semifusinite or inertodetrinite (Hunt, 1989; Diessel, 1992; Beamish and Crosdale, 1998), comparable to the Russian coals in this study, thus suggesting that palaeowildfire types may have been comparable for both Australia and Russia during the Permian.

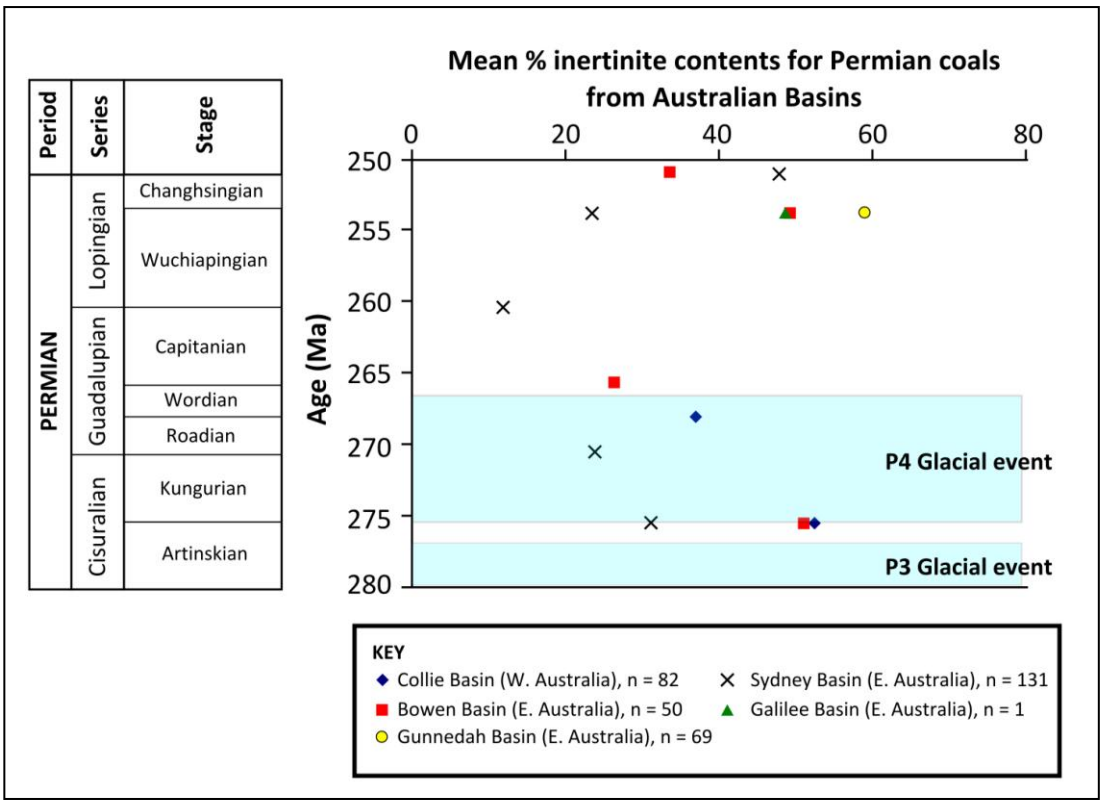

FIG. 8.4 Stratigraphic variation in inertinite content from coals Early (Artinskian) to Late Permian (Changhsingian) in age, from both E and W Australia (after: Diessel, 2010). The blue shaded regions denote glacial events from Fielding et al. (2008). Numbers in the key give total sample numbers (crushed coal) from that basin from Diessel (2010). Compare with Fig. 7.2 for Russian values. The stratigraphic chart on the left is after Gradstein et al. (2004).

8.7 FUTURE WORK

1. Sample lateral coal pillars at varying distances, both horizontally and vertically, within seams 78, 88 and 91 to document the extent of spatial variation in inertinite content and distribution to further aid palaeowildfire interpretation in the Late Permian peat-forming environment.

2. Analyse the coal pillars studied in this thesis using automated petrographic methods using a range of reflectance standards (instead of a single low reflectance standard) to attempt to develop a less time-consuming petrographic methodology for analysis of coal pillars.

3. Petrographic analysis of Early Permian coal pillars from the Kuznetsk Basin, Russia to document variations in palaeowildfire occurrence during the Permian Period.

4. Detailed petrographic and reflectance analysis of *in situ* coal pillars from a Southern Hemisphere Australian coal basin of comparable Late Permian age to determine if palaeowildfire occurrence, palaeowildfire type and fire return intervals were comparable to the Russian coals studied in this thesis.

5. Further study in the visual appearance of other wildfire derived products (such as tar and ash) from modern fires, as alternative means to recognising fires in deep time, in particular ground and crown fires that may not produce large quantities of charcoal.

6. Apply the petrographic methodology devised in this thesis to coal pillars previously studied using different methodologies, as the first step to producing a standard petrographic methodology for coal pillars.

CHAPTER 9

CONCLUSIONS

The thirteen Late Permian coal seams studied in this thesis were sampled from two open cast mines in the Kuznetsk Basin, Russia. The seams represent deposition in a temperate, long-lived mire environment (seam thickness >10m) on a floodplain (Davies et al., 2010) as part of a large single channel fluvial system. Charcoalified woods studied from fragmental bands (seam 78), abundant leaf and stem impressions, and permineralised plant axes were observed in interseam sediments. These all show gross morphologies consistent with Cordaitaleans, which were the dominant Angaran Permian peat-forming vegetation (Meyen 1982; Oshurkova, 1996; Krassilov, 2000; Rees et al., 2002). Growth rings were also observed in permineralised plant axes thus suggesting growth in a seasonal climate.

Detailed petrographic analysis was undertaken on five randomly sampled *in situ* coal pillars to interpret palaeowildfire occurrence, type and frequency in this Late Permian peat-forming environment. The low %ash (<10% air dried basis) and low %total Sulphur (<1.3% dry ash free basis) of three coal pillars suggests formation in an ombrotrophic mire environment [pillar 78(a), 88(b) and 91]. In contrast, in pillars 88(a) and 78(b), the small particle size, high liptinite content (>10%), high %ash (up to 21% air dried basis) and mineral matter contents (up to 22%) represent sapropelic coal formed in a mire with mire lake depositional setting.

Inertinite macerals are considered to represent charcoal derived from wildfires (Glasspool and Scott, 2010). Inertinite is present in all lithotype units in all coal pillars, therefore providing evidence for wildfire occurrence throughout the duration of coal pillar formation. There is variation in inertinite content both within and between seams, with whole pillar averages of 27.6% in pillar 78(a), 42.6% in pillar 78(b), 48% in pillar 88(a), 37.1% in pillar 88(b), 35% in pillar 91 (to a mineral free basis). All coal pillars show repeating patterns of inertinite distribution, (1) microscopic charcoal (<10µm) scattered in detrovitrinite layers, interpreted to represent a background, regional fire signal from surface fires and possibly some

crown fires. (2) Pieces of widely scattered macroscopic charcoal which may represent waterborne or windblown pieces of charcoal transported from local surface fires. (3) Charcoal horizons interpreted to represent charred litter or biomass from individual local surface fire events within the peat-forming environment. In addition the mire lake lithotype units contain (4) scattered inertinite in every field of view. Despite differences in inertinite content and distribution and environment of deposition between coal pillars, all show comparable wildfire histories.

An approach to calculating fire return intervals (FRI) in deep time was devised based on occurrence of charcoal horizons in three coal pillars. The charcoal horizons vary in both number and cumulative charcoal horizon thickness. Mid-range values (7:1 peat to coal compaction ratio and $1mm/a^{-1}$ peat accumulation rate) give FRI of 7 years (extremes 0.5 to 143 years) for 78(a) LU2, 69 years (5 – 1,485 years) for 91 LU2 and 70 years (5 – 1550 years) for 88(a) LU7. The mid range values for these Permian peat-forming environments demonstrate shorter FRI than seen in examples from modern peat-forming environments, which range from 80 to 1,100 years.

Pillar 78(b) contains more inertinite than observed in pillar 78(a) but represents a shorter duration of peat formation. Pillars 88(a) and (b) represent comparable durations of peat formation but 88(b) contains less inertinite than pillar 88(a) though far more than previous results from crushed coals from seam 88 (22% mmf basis; Pakh and Artser, 2003). This suggests that wildfires may have been more frequent, or there was more charcoal produced during fire events, in some intervals during formation of seam 88. The variation in inertinite content and distribution, both between lithotype units from the same coal pillar and between coal pillars from the same seam, emphasises the need to study more than one pillar in order to understand the potential temporal variation in fire occurrence in this Late Permian peat-forming environment.

In order to confirm interpretations of palaeowildfire types (surface or crown fire) it was necessary to measure the reflectance of both the macroscopic charcoal clasts from charcoal horizons and microscopic inertodetrinite. The $\%Ro_{mean}$ of all charcoal clasts from all thirteen charcoal horizons give inferred minimum charring temperatures of ≤435°C using the 24 h experimental charring calibration curve for

Sequoia wood from Scott and Glasspool (2007) confirming the interpretation that charcoal horizons contain charcoal derived from low temperature surface fires. In addition, there are no wholly high reflecting macroscopic charcoal clasts in charcoal horizons and most coal pillars [with the exception of 88(b)] contain some charcoal within the vitrinite reflectance range. This suggests that a large proportion of charcoal clasts in horizons may have been partially charred in a short duration fire. There is evidence for temporal variation in fire temperatures within lithotype units with individual charcoal horizons alternating between containing lower and higher reflecting charcoal (chapter 6). Less frequent fires have yielded higher temperature charcoals [78(a) LU8 and 91 LU2] whilst more frequent fires have yielded lower temperature charcoals [78(a) LU2].

Microscopic inertodetrinite from lithotype units with and without charcoal horizons has reflectance values within the range of macroscopic charcoal clasts from charcoal horizons. This shows that inertodetrinite may be derived from the same fire type as charcoal clasts. However, inferred charring temperatures can vary depending on the experimental charring calibration curves used. Using calibration extremes, a small number of Permian charcoal reflectance values (n = 235 from 9,400) yield inferred temperatures within the range of modern crown fires (>700°C) and may therefore represent charcoal derived from crown fires. Furthermore, a large proportion of the plant material is volatilised during modern crown fires, so that a small amount of very high reflecting charcoal may be the only representation of crown fires in the fossil record.

There is no evidence for a charred peat surface, hence no evidence for an *in situ* ground fire, in any of the coal pillars studied. The majority of organic material is consumed during a smouldering ground fire (Rein et al., 2008; Clay and Worrall, 2011). Therefore, it may not be possible to identify the occurrence of ground fires in the fossil record by charcoal occurrence alone. Future work should concentrate on developing methods for recognising other products derived from wildfire (such as mineral ash and tar) in order to aid interpretation of palaeowildfire types in deep time.

Inertinite contents in crushed coal in all thirteen coal seam general samples (68-94) show a range throughout the sequence from 7.1% - 50.2% with a high overall mean of 28.3%. These are comparable to the lithotype units in coal pillars which range from 0.34% to 61% with pillar means from 27% - 48%. Bulk characterisation analysis of both general and lithotype unit samples demonstrate that even 61.1% inertinite is not sufficient to affect the coal characterisation properties of the coal. Despite the lack of correlation between inertinite content and characterisation, pilot scale Drop Tube Furnace (DTF) experiments have demonstrated that more inertinite-rich samples (>30% inertinite) produce slightly denser chars and show poorer burnout than inertinite-poor equivalents. Therefore, inertinite content may affect the burnout more than characterisation properties in these coals.

Modelled atmospheric oxygen levels were high during the Permian Period (Berner et al., 2003; Berner, 2006). Southern Hemisphere Gondwanan Permian coal deposits formed in cool temperate peat-forming environments comparable to Russian coals. Despite differences in vegetation (*Glossopteris* compared to Angaran cordaites) this study on Russian material has shown that there are high inertinite contents in coals from both hemispheres. As suggested by Glasspool and Scott (2010) high inertinite contents may be linked to elevated atmospheric oxygen.

REFERENCE LIST

Aaby, B., Tauber, H., 1975, Rates of peat formation in relation to degree of humidification and local environment, as shown by studies of a raised bog in Denmark. Boreas 4, 1-17.

Abiven, S., Hengartner, P., Schneider, M.P.W., Singh, N., Schmidt, M.W.I., 2011, Pyrogenic carbon soluble fraction is larger and more aromatic in aged charcoal than fresh charcoal. Soil Biology & Biochemistry 43, 1615-1617.

Agee, J.K., Wright, C.S., Williamson, N., Huff, M.H., 2002, Foliar moisture content of Pacific Northwest vegetation and its relation to wildland fire behaviour. Forest ecology and Management 167, 57-66.

Allen, J.R.L., 1970, A quantitative analysis of climbing ripples and their cross-laminated deposits. Sedimentology 14, 5-26.

Allen, J.R.L., 1971, Instantaneous sediment deposition rates deduced from climbing-ripple cross-lamination. Journal of the Geological Society 127, 553-561.

Allen, J.R.L., 1973, A classification of climbing-ripple cross-lamination. Journal of the Geological Society 129, 537-541.

Anshits, N.N., Mikhailova, O.A., Salanov, A.N., Anshits, A.G., 2010, Chemical composition and structure of the shell of fly ash non-perforated cenospheres produced from the combustion of the Kuznetsk coal (Russia). Fuel 89, 1849 - 1862.

Arcenegui, V., Guerrero, C., Mataix-Solera, J., Mataix-Beneyto, J., Zornoza, R., Morales, J., Mayoral, A.M., 2008, The presence of ash as an interference factor in the estimation of the maximum temperature reached in burned soils using near-infrared spectroscopy (NIR). Catena 74, 177-184.

Ascough, P.L., Bird, M.I., Francis, S.M., Thornton, B., Midwood, A.J., Scott, A.C., Apperley, D., 2011, Variability in oxidative degradation of charcoal: Influence of production conditions and environmental exposure. Geochimica et Cosmochimica Acta 75, 2361-2378.

Ascough, P.L., Bird, M.I., Scott, A.C., Collinson, M.E., Cohen-Ofri, I., Snape, C.E., Le Manquais, K., 2010, Charcoal reflectance measurements: implications for structural characterization and assessment of diagenetic alteration. Journal of Archaeological Science 37, 1590-1599

Ashley, G.M., Southard, J.B., Boothroyd, J.C., 1982, Deposition of climbing-ripple beds: a flume simulation. Sedimentology 29, 67-79.

ASTM standard D3176-09, 2009, Standard practice for ultimate analysis of coal and coke. ASTM International, West Conshocken, PA, 2009.

ASTM Standard D5142-04, 2004, Standard test methods for proximate analysis of the analysis sample of coal and coke by instrumental procedures. ASTM International, West Conshocken, PA, 2004, 517-520.

Ballester, J., Jiménez, S., 2005, Kinetic parameters for the oxidation of pulverised coal as measured from drop tube tests. Combustion and Flame 142, 210-222.

Banerjee, D., Hirani, M., Sanyal, S.K., 2000, Coal-quality deterioration in a coal stack of a power station. Applied Energy 66, 267 – 275.

Bartram, K.M., Jeram, A.J., Selden, P.A., 1987, Arthropod cuticles in coal. Journal of the Geological Society 144, 513-517.

Baxendale, R.W., 1979, Plant-bearing coprolites from North American Pennsylvanian coal balls. Palaeontology 22, 537-548.

Beamish, B.B., Crosdale, P.J., 1998, Instantaneous outbursts in underground coal mines: An overview associated with coal type. International Journal of Coal Geology 35, 27-55.

Beaton, A.P., Kalkreuth, W., MacNeil, D., 1993, The geology, petrology and geochemistry of coal seams from the St. Rose and Chimney Corner coalfields, Cape Breton, Nova Scotia, Canada. International Journal of Coal Geology 24, 47-73.

Beeley, T.J., Crelling, J.C., Gibbins, J.R., Scott, A.C., Williamson, J., 1995, Observations of maceral and mineral heterogeneity in pulverised coals. International Conference on Coal Science, Oviedo, Elsevier, 203-206.

Beerling, D.J., Lake, R.A., Berner, R.A., Hickey, L.J., Taylor, D.W., Royer, D.L., 2002, Carbon isotope evidence implying high O_2/CO_2 ratios in the Permo-Carboniferous atmosphere. Geochimica et Cosmochimica Acta 66, 3757-3767.

Beerling, D.J., Woodward, F.I., Lomas, M.R., Wills, M.A., Quick, W.P., Valdes, P.J., 1998, The influence of Carboniferous palaeoatmospheres on plant function: an experimental and modelling assessment. Philosophical Transactions of the Royal Society London B 353, 131-140.

Belcher, C.M., Collinson, M.E., Sweet, A.R., Hildebrand, A.R., Scott, A.C., 2003,

Fireball passes and nothing burns – The role of thermal radiation in the Cretaceous-Tertiary event: Evidence from the charcoal record of North America. Geology 31, 1061-1064.

Belcher, C.M., Collinson, M.E., Scott, A.C., 2005, Constraints on the thermal energy released from the Chicxulub impactor: new evidence from multi-method charcoal analysis. Journal of the Geological Society of London 162, 591-602.

Belcher, C.M., Finch, P., Collinson, M.E., Scott, A.C., Grassineau, N.V., 2009, Geochemical evidence for combustion of hydrocarbons during the K-T impact event. PNAS 106, 4112 - 4117.

Belcher, C.M., Yearsley, J.M., Hadden, R.M., McElwain, J.C., Rein, G., 2010, Baseline intrinsic flammability of Earth's ecosystems estimated from paleoatmospheric oxygen over the past 350 million years. PNAS 107, 22448-22453.

Bend, S.L., Kosloski, D.M., 1993, A petrographic examination of coal oxidation. International Journal of Coal Geology 24, 233-243.

Berner, R.A., 2005, The carbon and sulphur cycles and atmospheric oxygen from middle Permian to middle Triassic. Geochimica et Cosmochimica Acta 69, 3211-3217.

Berner, R.A., 2006, GEOCARBSULF: A combined model for Phanerozoic atmospheric O_2 and CO_2. Geochimica et Cosmochimica Acta 70, 5653-5664.

Berner, R.A., 2009, Phanerozoic atmospheric oxygen: new results using the GEOCARBSULF model. American Journal of Science 309, 603-606.

Berner, R.A., Beerling, D.J., Dudley, R., Robinson, J.M., Wildman Jr, R.A., 2003, Phanerozoic atmospheric oxygen. Annual Review of Earth and Planetary Sciences 31, 105-134.

Berner, R.A., Petsch, S.T., Lake, J.A., Beerling, D.J., Popp, B.N., Lane, R.S., Laws, E.A., Westley, M.B., Cassar, N., Woodward, F.I., Quick, W.P., 2000, Isotope fractionation and atmospheric oxygen: implications for Phanerozoic O_2 evolution. Science 287, 1630-1633.

Bertschi, I., Yokelson, R.J., Ward, D.E., Babbitt, R.E., Susott, R.A., Goode, J.G., Hao, W.M., 2003, Trace gas and particle emissions from fires in large diameter and belowground biomass fuels. Journal of geophysical research 108, 1-12.

Bibler, C.J., Marshall, J.S., Pilcher, R.C., 1998, Status of worldwide coal mine

methane emissions and use. International Journal of Coal Geology 35, 283-310.

Birgenheier, L.P., Fielding, C.R., Rygel, M.C., Frank, T.D., Roberts, J., 2009, Evidence for dynamic climate change on sub-10^6-year scales from the Late Paleozoic glacial record, Tamworth Belt, New South Wales, Australia. Journal of Sedimentary Research 79, 56-82.

Blackford, J.J., 2000, Charcoal fragments in surface samples following a fire and the implications for interpretation of subfossil charcoal data. Palaeogeography, Palaeoclimatology, Palaeoecology 164, 33-42.

Bodí, M.B., Mataix-Solera, J., Doerr, S.H., Cerdà, A., 2011, The wettability of ash from burned vegetation and its relationship to Mediterranean plant species type, burn severity and total organic carbon content. Geoderma 160, 599-607.

Boerner, R.E.J., 1982, Fire and nutrient cycling in temperate ecosystems. BioScience 32, 187-192.

Bond, T.C., Bergstrom, R.W., 2006, Light absorption by carbonaceous particles: an investigative review. Aerosol Science and Technology 40, 27-67.

Borrego, A.G., Álvarez, D., Menéndez, R., 1997, Effects of inertinite content in coal on char structure and combustion. Energy & Fuels 11, 702-708.

Borrego, A.G., Marbán, G., Alonso, M.J.G., Álvarez, D., Menéndez, R., 2000, Maceral effects in the determination of proximate volatiles in coals. Energy & Fuels 14, 117-126.

Bostick, N.H., Betterton, W.J., Gluskoter, H.J., Nazrul Islam, M., 1991, Petrography of Permian "Gondwana" coals from boreholes in northwestern Bangladesh, based on semiautomated reflectance scanning. Organic Geochemistry 17, 399-413.

Bowman, D.M.J.S., Balch, J.K., Artaxo, P., Bond, W.J., Carlson,J.M., Cochrane, M.A., D'Antonio, C.M., DeFries, R.S., Doyle, J.C., Harrison,S..P., Johnston, F.H., Keeley, J.E., Krawchuk, M.A., Kull, C.A., Marston, J.B., Moritz, M.A., Prentice, I.C., Roos. C.I., Scott, A.C., Swetnam, T.W., van der Werf, G. R., and Pyne, S.J., 2009, Fire in the Earth System. Science 324, 481-484.

Braadbaart, F., Poole, I., 2008, Morphological, chemical and physical changes during charcoalification of wood and its relevance to archaeological contexts. Journal of Archaeological Science 35, 2425–2674.

Brierley, G.J., Ferguson, R.J., Woolfe, K.J., 1997, What is a fluvial levee?. Sedimentary Geology 114, 1-9.

Brown, S.A.E., Scott, A.C., Glasspool, I.J., Collinson, M.E., 2012, Cretaceous wildfires and their impact on the Earth system. Cretaceous Research 36, 162-190.

Brown, R.E., Scott, A.C., Jones, T.P., 1994, Taphonomy of plant fossils from the Viséan of East Kirkton, West Lothian, Scotland. Transactions of the Royal Society of Edinburgh: Earth Sciences 84, 267-274.

Bruening, F.A., Cohen, A.D., 2005, Measuring surface properties and oxidation of coal macerals using the atomic force microscope. International Journal of Coal Geology 63, 195-204.

BS 1016-104.1: 1999, ISO 11722: 1999, Methods for analysis and testing of coal and coke, part 104: Proximate analysis, section 104.1 Determination of moisture content of the general analysis test sample, first edition 1999-05-01, 1-5.

BS 1016-104.3:1998, ISO 562: 1998, Methods for analysis and testing of coal and coke, part 104: Proximate analysis, section 104.3: Determination of volatile matter content, second edition, 1998-02-01, 1-6.

BS 1016-104.4: 1998, ISO 1171, Solid mineral fuels – Determination of ash, third edition, 1997-12-15, 1-8.

BS 1016-105:1992, Methods for analysis and testing of coal and coke, part 105: Determination of gross calorific value, 1-11.

BS 1016-106.4.2: 1996, British Standard, methods for analysis and testing of coal and coke – part 106: Ultimate analysis of coal and coke – Section 106.4 Determination of total sulphur content – subsection 106.4.2 high temperature combustion method.

BS 1017-1:1989, Methods for sampling of coal.

BS ISO 29541: 2010, Solid mineral fuels. Determination of total carbon, hydrogen and nitrogen content. Instrumental method, 1-22.

BS ISO 14180:1998, British Standard, solid mineral fuels – guidance on the sampling of coal seams. ISBN 0580301141. London 1-14.

BS ISO 17246: 2005, Coal – Proximate analysis, International Standard, First edition 2005-05-01, 1-2.

BS ISO 17247: 2005, Coal – Ultimate analysis, International Standard, First Edition, 2005-05-01, 1-4.

BS ISO 18283: 2006, British Standard, hard coal and coke – manual sampling. ISBN 9780580627767. London 1-80.

BS 6127.3: 1995, ISO 7404-3:1994, British Standard, Petrographic analysis of bituminous coal and anthracite – Part 3: method of determining maceral group composition of bituminous coal and anthracite.

BS 6127.4: 1990, ISO 7404-4:1988, British Standard, Petrographic analysis of bituminous coal and anthracite – Part 4: method of determining microlithotype division, carbominerite and minerite composition

Bustin, R.M., 1984, Coalification levels and their significance in the Groundhog coalfield, north-central British Columbia. International Journal of Coal Geology 4, 21-44.

Bustin, R.M., Guo, Y., 1999, Abrupt changes (jumps) in reflectance values and chemical compositions of artificial charcoals and inertinite in coals. International Journal of Coal Geology 38, 237-260.

Cai, H.-Y., Megaritis, A., Messenböck, R., Dix, M., Dugwell, D.R., Kandiyoti, R., 1998, Pyrolysis of coal maceral concentrates under pf-combustion conditions (I): changes in volatile release and char combustibility as a function of rank. Fuel 71, 1273-1282.

Cameron, C.C., Esterle, J.S., Palmer, C.A., 1989, The geology, botany and chemistry of selected peat-forming environments from temperate and tropical latitudes. International Journal of Coal Geology 12, 105-156.

Carcaillet, C., Bouvier, M., Fréchette, B., Larouche, A.C., Richard P.J.H., 2001, Comparison of pollen-slide and sieving methods in lacustrine charcoal analyses for local and regional fire history. The Holocene 11, 467-476.

Carter, J.A., 1999, Late Devonian, Permian and Triassic Phytoliths from Antarctica. Micropalaeontology 45, 56-61.

Cerdá, A., Doerr, S.H., 2008, The effect of ash and needle cover on surface runoff and erosion in the immediate post-fire period. Catena 74, 256-263.

Chaloner, W.G., 1976, The evolution of adaptive features in fossil exines. In: Greuter, W., Zimmer, B. (eds.), Proceedings of the XIV International Botanical Congress, 301-316.

Chaloner, W.G., Creber, G.T., 1973, Growth rings in fossil woods as evidence of

past climates. In: Tarling, D.H., Runcorn, S.K. (eds.), Implications of Continental Drift to the Earth Sciences. Academic Press, London, 425 - 437.

Chaloner, W.G., Scott, A.C., Stephenson, J., 1991, Fossil evidence for plant-arthropod interactions in the Palaeozoic and Mesozoic. Philosophical Transactions of the Royal Society London B 333, 177-186.

Chandra, D., 1962, Reflectance and microstructure of weathered coals. Fuel 41, 185-193.

Chao, E.C.T., Minkin, J.A., Thompson, C.L., 1982, Recommended procedures and techniques for the petrographic description of bituminous coals. International Journal of Coal Geology 2, 151-179.

Chayes, F., 1956, Petrographic modal analysis. John Wiley & Sons, New York, 113.

Chi, T., Zhang, H., Yan, Y., Zhou, H., Zheng, H., 2010, Investigations into the ignition behaviours of pulverized coals and coal blends in a drop tube furnace using flame monitoring techniques. Fuel 89, 743-751.

Choudhury, N., Biswas, S., Sarkar, P., Kumar, M., Ghosal, S., Mitra, T., Mukherjee, A., Choudhury, A., 2008, Influence of rank and macerals on the burnout behaviour of pulverized Indian coal. International Journal of Coal Geology 74, 145-153.

Choudhury, N., Boral, P., Mitra, T., Adak, A.K., Choudhury, A., Sarkar, P., 2007, Assessment of nature and distribution of inertinite in Indian coals for burning characteristics. International Journal of Coal Geology 72, 141-152.

Clark, J.S., 1988, Particle motion and the theory of charcoal analysis: Source area, transport, deposition and sampling. Quaternary Research 30, 67-80.

Clark, J S., Patterson III, W.A., 1997, Background and local charcoal in sediments: scales of fire evidence in the palaeo record, in: Clark, J.S., et al. (eds.), Sediment records of biomass burning and global change. NATOASI Series I 51, Springer Verlag, Berlin, 23-48.

Clark, J. S., Royall, P.D., 1995, Particle-size evidence for source areas of charcoal accumulation in Late Holocene sediments of Eastern North American Lakes. Quaternary Research 43, 80-89.

Clark, J.S., Lynch, J., Stocks, B.J., Goldammer, J.G., 1998, Relationships between charcoal particles in air and sediments in west-central Siberia. Holocene 8, 19-29.

Clay, G., Worrall, F., Rose, R., 2010, Carbon budgets of an upland blanket bog managed by prescribed fire. Journal of Geophysical Research 115, 1-14.

Clay, G.D., Worrall, F., 2011, Charcoal production in a UK moorland wildfire - How important is it?. Journal of Environmental Management 92, 676-682.

Cloke, M., Lester, E., Gibb, W., 1997a, Characterization of coal with respect to carbon burnout in p.f.-fired boilers. Fuel 76, 1257-1267.

Cloke, M., Gilfillan, A., Lester, E., 1997b, The characterization of coals and density separated coal fractions using FTIR and manual and automated petrographic analysis. Fuel 76, 1289-1296.

Cloke, M., Lester, E., Allen, M., Miles, N.J., 1995a, Repeatability of maceral analysis using image analysis systems. Fuel 74, 654-658.

Cloke, M., Lester, E., Allen, M., Miles, N.J., 1995b, Automated maceral analysis using fluorescence microscopy and image analysis. Fuel 74, 659-669.

Cloudsley-Thompson, J.L., 1958, Spiders, scorpions, centipedes and mites. Pergamon Press Inc., New York.

Clymo, R.S., 1987, Rainwater-fed peat as a precursor of coal. In: Scott, A.C., (ed). Coal and Coal-bearing Strata: Recent Advances. Geological Society Special Publication 32, Blackwell Scientific Publications, 17-23.

Cocks, L.R.M., Torsvik, T.H., 2007, Siberia, the wandering northern terrane, and its changing geography through the Palaeozoic. Earth-Science Reviews 82, 29-74.

Cohen, A.D., Spackman, W., Raymond Jr, R., 1987, Interpreting the characteristics of coal seams from chemical, physical and petrographic studies of peat deposits, in: Scott A.C., (ed.), Coal and Coal-bearing strata: Recent advances. Geological Society Special Publication 32, 107-125.

Collinson, M.E., Scott, A.C., 1987, Implications of vegetational change through the geological record on models for coal-forming environments. In: Scott, A.C., (ed). Coal and Coal-bearing Strata: Recent Advances. Geological Society Special Publication 32, Blackwell Scientific Publications, 67-85.

Collinson, M.E., Steart, D.C., Scott, A.C., Glasspool, I.J., Hooker, J.J., 2007, Episodic fire, runoff and deposition at the Palaeocene-Eocene boundary. Journal of the Geological Society London 164, 87-97.

Conedara, M., Tinner, W., Neff, C., Meurer, M., Dickens, A.F., Krebs, P., 2009, Reconstructing past fire regimes: methods, applications, and relevance to fire

management and conservation. Quaternary Science Reviews 28, 555-576.

Cook, A.C., Sherwood, N.R., 1991, Classification of oil shales, coals and other organic-rich rocks. Organic Geochemistry 17, 211-222.

Correia, M., Maury, R., Arai, F., 1974, Mesure par leur pouvoir réflecteur, des temperatures de carbonisation des bois fossilisés dans les formations volcanique. Bulletin Centre Recherches de Pau (Société Nationale des Pétroles d'Aquitaine) 8, 527–536.

Crelling, J.C., Hippo, E.J., Woerner, B.A., West Jr., D.P., 1992, Combustion characteristics of selected whole coals and macerals. Fuel 71, 151-158.

Crelling, J.C., Schrader, R.H., Benedict, L.G., 1979, Effect of weathered coal on coking properties and coke quality. Fuel 58, 542-546.

Crosdale, P.J., Sorokin, A.P., Woolfe, K.J., Macdonald, D.I.M., 2002, Inertinite-rich Tertiary coals from the Zeya-Bureya Basin Far Eastern Russia. International Journal of Coal Geology 51, 215-235.

Davies, C., Allen, M.B., Buslov, M., 2004, Field observations from the Kuznetsk Basin, West Siberia. West Siberian Basin project. Report 4 – December 2004. CASP confidential report.

Davies, C., Allen, M.B., Buslov, M.M., Safonova, I., 2010, Deposition in the Kuznetsk Basin, Siberia: insights into the Permian-Triassic transition and the Mesozoic evolution of Central Asia. Palaeogeography, Palaeoclimatology, Palaeoecology 295, 1-2, 307-322.

Davies, C., Marshall, J., Harland, M., Whitham, A., Buslov, M., 2007, Vitrinite reflectance analysis from the southern margin of the West Siberian Basin. West Siberian Basin project. Phase II report 10 – March 2007. CASP confidential report.

Davies, R., Diessel, C., Howell, J., Flint, S., Boyd, R., 2005, Vertical and lateral variation in the petrography of the Upper Cretaceous Sunnyside coal of eastern Utah, USA – implications for the recognition of high-resolution accommodation changes in paralic coal seams. International Journal of Coal Geology 61, 13-33.

Davis, K.P., 1959, Forest fire-control and use. McGraw-Hill, New York, 584.

Davis, J.C., 2002, Statistics and data analysis in geology: Third Edition. John Wiley & Sons, Inc. New York.

Debano, L.F., Conrad, C.E., 1978, Effect of fire on nutrients in a chaparral

ecosystem. Ecology 59, 489-497.

De Grave, J., Buslov, M.M., Van Den Haute, P., Metcalf, J., Dehandschutter, B., McWilliams, M.O., 2009, Multi-method chronometry of the Teletskoye graben and its basement, Siberian Altai mountains: new insights on its thermo-tectonic evolution. Geological Society, London, Special Publications 324, 237-259.

De Groot, W.J., Bothwell, P.M., Taylor, S.W., Wotton, B.M., Stocks, B.J., Alexander, M.E., 2004, Jack pine regeneration and crown fires. Canadian Journal of Forest Research 34, 1634-1641.

DeLuca, T.H., Aplet, G.H., 2008, Charcoal and carbon storage in forest soils of the Rocky Mountain West. Frontiers in Ecology and the Environment 6, 18–24.

Demchuk, T.D., 1993, Petrology of fibrous coal (fusain) and associated inertinites from the Early Paleocene of the central Alberta Plains. International Journal of Coal Geology 24, 211-232.

Diessel, C.F.K., 1965, Correlation of macro- and micro-petrography of some New South Wales Coals. 8th Commonwealth Mining and Metallurgical Congress, 6, Melbourne, Australia and New Zealand Publ., 669-677.

Diessel C.F.K., 1992, Coal bearing depositional systems, Springer-Verlag .

Diessel, C.F.K., 2010, The stratigraphic distribution of inertinite. International Journal of Coal Geology 81, 251-268.

Dlapa, P., Bodí, M.B., Mataix-Solera, J., Cerdà, A., Doerr, S.H., 2012, FT-IR spectroscopy reveals that ash water repellency is highly dependent on ash chemical composition. Catena (2012), DOI 10.1016/j.catena.2012.02.011.

Domeier, M., Van der Voo, R., Torsvik, T.H., 2012, Palaeomagnetism and Pangea: The road to reconciliation. Tectonophysics 514-517, 14-43.

Drysdale, D., 1998, An introduction to Fire Dynamics, 2nd Ed. John Wiley & Sons Ltd, Chichester, UK.

Drysdale, D., 2011, An introduction to fire dynamics, 3rd Ed. Wiley Blackwell, 260.

Dyrkacz, G.R., Bloomquist, C.A.A., Ruscic, L., 1984, Chemical variations in coal macerals separated by density gradient centrifugation. Fuel 63, 1166-1173.

EIA Energy Investigation Agency, 2010, Country analysis briefs: Russia Energy Data, Statistics and Analysis – Oil, Gas, Electricity, Coal. http://www.eia.doe.gov

Elliott, R.E., 1985, Quantification of peat to coal compaction stages, based especially

on phenomena in the East Pennine Coalfield, England. Proceedings of the Yorkshire Geological Society 45, 163-172.

Enache, M.D., Cumming, B.F., 2006, Tracking recorded fires using charcoal morphology from the sedimentary sequence of Prosser Lake, British Columbia (Canada). Quaternary Research 65, 282-292.

Evans, M., Warburton, J., 2005, Sediment budget for an eroding peat-moorland catchment in northern England. Earth Surface Processes and Landforms 30, 557-577.

Evtushenko, V.E., Fefelov, G.G., Nadler, Yu. S., Sharapenko, A.P., Sorokin, P.V., Tsader, Z.S., Turkin, V.A., Vasilieva, N.A., Yuzvitsky, A.Z., 1975, Field Excursion Guidebook for the Kuznetsk Basin. Moscow, Publishing office "Nauka", 172.

Falcon-Lang, H.J., 2000, Fire ecology of the Carboniferous tropical zone. Palaeogeography, Palaeoclimatology, Palaeoecology 164, 339–355.

Falcon-Lang, H.J., Bashforth, A.R., 2005, Morphology, anatomy, and upland ecology of large cordaitalean trees from the Middle Pennsylvanian of Newfoundland. Review of Palaeobotany and Palynology 135, 223-243.

Falcon-Lang, H.J., Scott, A.C., 2000, Upland ecology of some Late Carboniferous cordaitalean trees from Nova Scotia and England. Palaeogeography, Palaeoclimatology, Palaeoecology 156, 225-242.

Falkner, A., 1987, Coal examination on a mesoscopic scale. Research Methods Papers, 617-619.

Fielding, C.R., 1987, Coal depositional models for deltaic and alluvial plain sequences. Geology 15, 661-664.

Fielding, C.R., Alexander, J., 2001, Fossil trees in ancient fluvial channel deposits: evidence of seasonal and longer-term climatic variability. Palaeogeography, Palaeoclimatology, Palaeoecology 170, 59-80.

Fielding, C.R., Frank, T.D., Birgenheier, L.P., Rygel, M.C., Jones, A.T., Roberts, J., 2008, Stratigraphic imprint of the Late Palaeozoic Ice Age in eastern Australia: a record of alternating glacial and nonglacial climate regime. Journal of the Geological Society, London 165, 129-140.

Finkelstein, D.B., Pratt, L.M., Curtin, T.M., Brassell, S.C., 2005, Wildfires and seasonal aridity recorded in Late Cretaceous strata from south-eastern Arizona, USA. Sedimentology 52, 587-599.

Flannigan, M., Stocks, B., Turetsky, M., Wotton, M., 2009, Impacts of climate change on fire activity and management in the circumboreal forest. Global Change Biology 15, 549-560.

Frank, T.D., Thomas, S.G., Fielding, C.R., 2008, On using Carbon and Oxygen isotope data from glendonites as paleoenvironmental proxies: a case study from the Permian system of eastern Australia. Journal of Sedimentary Research 78, 713-723.

Franzén, L.G., Malmgren, B.A., 2012, Microscopic charcoal and tar (CHAT) particles in peat: a 6500-year record of palaeo-fires in southern Sweden. Mires and Peat 10, 1-25.

Fredericks, P.M., Warbrooke, P., Wilson, M.A., 1983, Chemical changes during natural oxidation of a high volatile bituminous coal. Organic Geochemistry 5, 89-97.

Frolking, S., Roulet, N.T., Moore, T.R., Richard, P.J.H., Lavoie, M., Muller, S.D., 2001, Modeling northern peatland decomposition and peat accumulation. Ecosystems 4, 479-498.

Gabet, E.J., Bookter, A., 2011, Physical, chemical and hydrological properties of Ponderosa pine ash. International Journal of Wildland Fire 20, 443-452.

García-Falcón, M.S., Soto-González, B., Simal-Gándara, J., 2006, Evolution of the concentrations of Polycyclic Aromatic Hydrocarbons in burnt woodland soils. Environmental Science and Technology 40, 759-763.

Ghaly, R.A., Pyke, J.B., Ghaly, A.E., Ugursal, V.I., 1999, Physical and chemical properties of uncontaminated and diesel-contaminated peat. Energy Resources 21, 433-451.

Gibbins, J.R., Beeley, T.J., Crelling, J.C., Scott, A.C., Skorupska, N.M., Williamson, J., 1999, Observations of heterogeneity in large pulverised coal particles. Energy and Fuels 13, 592-601.

Gibling, M.R., 2006, Width and thickness of fluvial channel bodies and valley fills in the geological record: A literature compilation and classification. Journal of Sedimentary Research 76, 731-770.

Glasspool, I., 2000, The palaeoecology of a South African Early Permian, and a Late Permian Australian, Gondwana coal. Unpublished PhD thesis.

Glasspool, I., 2003a, Hypauthochthonous-allochthonous coal deposition in the Permian, South African, Witbank Basin No.2 seam; a combined approach

using sedimentology, coal petrology and palaeontology. International Journal of Coal Geology 53, 81-135.

Glasspool, I., 2003b, Palaeoecology of selected South African export coals from the Vryheid Formation, with emphasis on the role of heterosporous lycopods and wildfire derived inertinite. Fuel 82, 959-970.

Glasspool, I.J., Edwards, D., Axe, L., 2004, Charcoal in the Silurian as evidence for the earliest wildfire. Geology 32, 381-383.

Glasspool, I.J., Scott, A.C., 2010, Phanerozoic concentrations of atmospheric oxygen reconstructed from sedimentary charcoal. Nature Geoscience 3, 627-630.

Glorie, S., De Grave, J., Buslov, M.M., Zhimulev, F.I., Elburg, M.A., Van Den Haute, P., 2012, Structural control on Meso-Cenozoic tectonic reactivation and denudation in the Siberian Altai: Insights from multi-method thermochronometry. Tectonophysics 544-545, 75-92.

Gluskoter, H.J., 1975, Mineral matter and trace elements in coal, in: Babu, S.P., (ed), Trace elements in fuel. American Chemical Society, Washington, D.C. 141, 1-22.

Goforth, B.R., Graham, R.C., Hubbert, K.R., Zanner, W.C., Minnich, R.A., 2005, Spatial distribution and properties of ash and thermally altered soils after high-severity forest fire, southern California. International Journal of Wildland Fire 14, 343-354.

Gore, A.J.P., 1983, Introduction, in: Gore A.J.P., (ed.), Ecosystems of the world, 4A, mires: Swamp, Bog, Fen and Moor, General Studies. Elsevier, Amsterdam, 1-34.

Gradstein, F.M., Ogg, J.G., Smith, A.G., Agterberg, F.P., Bleeker, W., Cooper, R.A., Davydov, V., Gibbard, P., Hinnov, L.A., House, M.R., Lourens, L., Luterbacher, H P., McArthur, J., Melchin, M.J., Robb, L.J., Shergold, J., Villeneuve, M., Wardlaw, B.R., Ali, J., Brinkhuis, H., Hilgen, F.J., Hooker, J., Howarth, R.J., Knoll, A.H., Laskar, J., Monechi, S., Powell, J., Plumb, K.A., Raffi, I., Röhl, U., Sanfilippo, A., Schmitz, B., Shackleton, N.J., Shields, G.A., Strauss, H., Van Dam, J., Veizer, J., van Kolfschoten, Th., and Wilson, D., 2004, A Geologic Time Scale 2004. Cambridge University Press, 500.

Greb, S.F., DiMichele, W.A., Gastaldo, R.A., 2006, Evolution and importance of wetlands in earth history. In: Greb, S.F., DiMichele, W.A., (eds.) Wetlands

through time: Geological Society of America Special Paper 399, 1-40.

Guo, Y., Bustin, R.M., 1999, FTIR spectroscopy and reflectance of modern charcoals and fungal decayed woods: implications for studies of inertinite in coals. International Journal of Coal Geology 37, 29–53.

Gupta, R., 2007, Advanced coal characterization: A review. Energy Fuels 21, 451 - 460.

Hacquebard, P.A., 1951, The correlation by petrographic analyses of No. 5 seam in the St. Rose and Chimney Corner coalfields, Nova Scotia. Geological Survey of Canada Bulletin 19, 32.

Hacquebard, P.A., 1993, Petrology and facies studies of the Carboniferous coals at Mabou Mines and Inverness in comparison with those of the Port Hood, St. Rose and Sydney coalfields of Cape Breton Island, Nova Scotia, Canada. International Journal of Coal Geology 24, 7-46.

Hamad, A.M.BA., Jasper, A., Uhl, D., 2012, The record of Triassic charcoal and other evidence for palaeowildfires: Signal for atmospheric oxygen levels, taphonomic biases or lack of fuel?. International Journal of Coal Geology 96-97, 60-71.

Hammes, K., Schmidt, M.W.I., Smernik, R.J., Currie, L.A., Ball, W.P., Nguyen, T.H., Louchouarn, P., Houel, S., Gustafsson, Ö., Elmquist, M., Cornelissen, G., Skjemstad, J.O., Masiello, C.A., Song, J., Peng, P., Mitra, S., Dunn, J.C., Hatcher, P.G., Hockaday, W.C., Smith, D.M., Hartkopf-Fröder, C., Böhmer, A., Lüer, B., Huebert, B.J., Amelung, W., Brodowski, S., Huang, L., Zhang, W., Gschwend, P.M., Flores-Cervantes, D.X., Largeau, C., Rouzaud, J-N., Rumpel, C., Guggenberger, G., Kaiser, K., Rodionov, A., Gonzalez-Vila, F.J., Gonzalez-Perez, J.A., de la Rosa, J.M., Manning, D.A.C., López-Capél, E., Ding, L, 2007, Comparison of quantification methods to measure fire-derived (black/elemental) carbon in soils and sediments using reference materials from soil, water, sediment and the atmosphere. Global Biogeochemical Cycles 21, 1-18.

Hammes, K., Smernick, R.J., Skjemstad, J.O., Herzog, A., Vogt, U.F., Schmidt, M.W.I., 2006, Synthesis and characterisation of laboratory charred grass straw (*Oryza sativa*) and chestnut wood (*Castanea sativa*) as reference materials for black carbon quantification. Organic Geochemistry 37, 1629 - 1633.

Hampartsoumian, E., Nimmo, W., Rosenberg, P., Thomsen, E., Williams, A., 1998, Evaluation of the chemical properties of coals and their maceral group constituents in relation to combustion reactivity using multivariate analyses. Fuel 77, 735-748.

Harms, V.L., Leisman, G.A., 1961, The anatomy and morphology of certain cordaites leaves. Journal of Paleontology 35, 1041-1064.

Harris, T.M., 1957, A Liasso–Rhaetic flora in South Wales. Proceedings of the Royal Society of London B 147, 289–308.

Harrison, J.F., Kaiser, A., VandenBrooks, J.M., 2010, Atmospheric oxygen level and the evolution of insect body size. Proceedings of the Royal Society B 277, 1937-1946.

Hartford, R.A., Frandsen, W.H., 1992, When it's hot, it's hot…or maybe it's not! (Surface flaming may not portend extensive soil heating). International Journal of Wildland Fire 2, 139-144.

Hilliard, J.E., Cahn, J.W., 1961, An evaluation of procedures in quantitative metallography for volume fraction analysis. Transactions of the Metallurgical Society of AIME (American Institute of Mining, Metallurgical, and Petroleum Engineers) 221, 344-352.

Holdgate, G.R., Kershaw, A.P., Sluiter, I.R.K., 1995, Sequence stratigraphic analysis and the origins of Tertiary brown coal lithotypes, Latrobe Valley, Gippsland basin, Australia. International Journal of Coal Geology 28, 249-275.

Hower, J.C., Davis, A., 1981, Vitrinite reflectance anisotropy as a tectonic fabric element. Geology 9, 165-168.

Hower, J.C., O'Keefe, J.M.K., Eble, C.F., 2008, Tales from a distant swamp: Petrological and palaeobotanical clues for the origin of the sand coal lithotype (Mississippian, Valley Fields, Virginia). International Journal of Coal Geology 75, 119-126.

Hower, J.C., O'Keefe, J.M.K., Eble, C.F., Raymond, A., Valentim, B., Volk, T.J., Richardson, A.R., Satterwhite, A.B., Hatch, R.S., Stucker, J.D., Watt, M.A., 2011, Notes on the origin of inertinite macerals in coal: Evidence for fungal and arthropod transformations of degraded macerals. International Journal of Coal Geology 86, 231-240.

Hower, J.C., O'Keefe, J.M.K., Watt, M.A., Pratt, T.J., Eble, C.F., Stucker, J.D., Richardson, A.R., Kostova, I.J., 2009, Notes on the origin of inertinite

macerals in coals: observations on the importance of fungi in the origin of macrinite. International Journal of Coal Geology 80, 135-143.

Hudspith, V., Scott, A.C., Collinson, M.E., Pronina, N., Beeley, T., 2012, Evaluating the extent to which wildfire history can be interpreted from inertinite distribution in coal pillars: An example from the Late Permian Kuznetsk Basin, Russia. International Journal of Coal Geology 89, 13-25.

Hudspith, V.A., Scott, A.C., Wilson, C.J.N., Collinson, M.E., 2010, Charring of woods by volcanic processes: An example from the Taupo ignimbrite, New Zealand. Palaeogeography, Palaeoclimatology, Palaeoecology 291, 40-51.

Huggins, F.E., Huffman, G.P., Kosmack, D.A., Lowenhaupt, D.E., 1980, Mossbauer detection of goethite (α-FeOOH) in coal and its potential as an indicator of coal oxidation. International Journal of Coal Geology 1, 75-81.

Hunt, J.W., 1989, Permian coals of eastern Australia: geological control of petrographic variation. International Journal of Coal Geology 12, 589-634.

Ignatiev, I.A., Meyen, S.V., 1989, *Suchoviella* – Gen. Nov. from the Permian of Angaraland and a review of the systematics of cordaitanthales. Review of Palaeobotany and Palynology 57, 313-339.

Innes, J.B., Blackford, J.J., Simmons, I.G., 2004, Testing the integrity of fine spatial resolution palaeoecological records: microcharcoal data from near-duplicate peat profiles from the North York Moors, UK. Palaeogeography, Palaeoclimatology, Palaeoecology 214, 295-307.

International Committee for Coal and Organic Petrology (ICCP), 1963, International Handbook of Coal Petrography 2nd Edition. Centre National de la Recherché Scientifique, Paris, France.

International Committee for Coal and Organic Petrology (ICCP), 1998, The new vitrinite classification (ICCP System 1994). Fuel 77, 349-358.

International Committee for Coal and Organic Petrology (ICCP), 2001, The new inertinite classification (ICCP system 1994). Fuel 80, 459-471.

ISO 7404-2: 1985, Methods for the petrographic analysis of bituminous coal and anthracite – Part 2: Preparation of coal samples.

Jerrett, R.M., Davies, R.C., Hodgson, D.M., Flint, S.S., Chiverrell, R.C., 2011a, The significance of hiatal surfaces in coal seams. Journal of the Geological Society, London 168, 629-632.

Jerrett, R.M., Flint, S.S., Davies, R.C., Hodgson, D.M., 2011b, Sequence

stratigraphic interpretation of a Pennsylvanian (Upper Carboniferous) coal from the central Appalachian Basin, USA. Sedimentology 58, 1180-1207.

Jerrett, R.M., Hodgson, D.M., Flint, S.S., Davies, R.C., 2011c, Control of relative sea level and climate on coal character in the Westphalian C (Atokan) Four Corners Formation, Central Appalachian basin, U.S.A. Journal of Sedimentary Research 81, 420-445.

Jones, T.P., 1999, Polished blocks and reflected light microscopy. In: Jones, T.P., Rowe, N.P., (eds.), Fossil Plants and Spores: modern techniques. Geological Society, London, 82-86.

Jones, T.P., Chaloner, W.G., Kuhlbusch, T.A.J., 1997, Proposed bio-geological and chemical based terminology for fire-altered plant matter, in: Clark, J.S., Cachier, H., Goldammer, J.G., Stocks, B., (eds.), Sediment records of biomass burning and global change. NATO ASI Series 1, Springer, Berlin, 9-22.

Jones, A.T., Fielding, C.R., 2004, Sedimentological record of the late Paleozoic glaciation in Queensland, Australia. Geology 32, 153-156.

Jones, T.P., Scott, A.C., Cope, M., 1991, Reflectance measurements and the temperature of formation of modern charcoals and implications for studies of fusain. Bulletin de la Societé Geologique de France 162, 193-200.

Jones, T.P., Scott, A.C., Mattey, D.P., 1993, Investigations of "fusain transition fossils" from the Lower Carboniferous: comparisons with modern partially charred wood. International Journal of Coal Geology 22, 37-59.

Kane, E.S., Hockaday, W.C., Turetsky, M.R., Masiello, C.A., Valentine, D.W., Finney, B.P., Baldock, J.A., 2010, Topographic controls on black carbon accumulation in Alaskan black spruce forest soils: implications for organic matter dynamics. Biogeochemistry 100, 39-56.

Kevan, D.K. McE., 1968, Soil animals. London H.F. and G. Ltd., Witherby.

Komarek, E.V., 1973, Ancient fires. Proceedings of the Annual Tall Timbers Fire Ecology Conference, 12, 219-240.

Krassilov, V.A., 2000, Permian phytogeographic zonality and its implications for continental positions and climates. Paleontological Journal 34, 587-598.

Kurlenya, M.V., Cheskidov, V.I., 2001, Mineral mining technology: Prospects of coal mining in Siberia. Journal of Mining Science 37, 319-322.

Lamberson, M.N., Bustin, R.M., Kalkreuth, W.D., Pratt, K.C., 1996, The formation

of inertinite-rich peats in the mid-Cretaceous Gates Formation: implications for the interpretation of mid-Albian history of palaeowildfire. Palaeogeography, Palaeoclimatology, Palaeoecology 120, 235-260.

Lancelotti, C., Madella, M., Ajithprasad, P., Petrie, C.A., 2010, Temperature, compression and fragmentation: an experimental analysis to assess the impact of taphonomic processes on charcoal preservation. Archaeological and Anthropological Sciences 2, 307-320.

Lavoie, C., Pellerin, S., 2007, Fires in temperate peatlands (southern Quebec): past and recent trends. Canadian Journal of Botany 85, 263-272.

Leco Corporation, 1998, CHN 2000, instruction manual, Metals Energy mining Agriculture Geology, form no. 200-627, version 2.0.

Lenton, T.M., 2001, The role of land plants, phosphorus weathering and fire in the rise and regulation of atmospheric oxygen. Global Change Biology 7, 613-629.

Lester, E., 1994, The characterisation of coals for combustion. Unpublished PhD thesis.

Lester, E., Watts, D., Cloke, M., 2002, A novel automated image analysis method for maceral analysis. Fuel 81, 2209 - 2217.

Lin, Q., Guet, J.M., 1990, Characterization of coals and macerals by X-ray diffraction. Fuel 69, 821 - 825.

Lindsay, G., Herbert, C., 2002, Coal and conglomerate in the Newcastle Coal Measures-coeval facies or temporally unrelated?. International Journal of Coal Geology 51, 169 - 184.

Lo, H.B., Cardott, B.J., 1995, Detection of natural weathering of Upper McAlester coal and Woodford Shale, Oklahoma, U.S.A. Organic Geochemistry 22, 73-83.

Lobert, J.M., Warnatz, J., 1993, Chapter 2 - Emissions from the combustion process in vegetation. In: Crutzen, P.J., Goldammer, J.G. (eds.), Fire in the environment: The ecological, atmospheric, and climatic importance of vegetation fires. John Wiley & Sons, 15 - 35.

Lynch, J.A., Clark, J.S., Stocks, B.J., 2004, Charcoal production, dispersal, and deposition from the Fort Providence experimental fire: interpreting fire regimes from charcoal records in boreal forests. Canadian Journal of Forest Research 34, 1642 - 1656.

Malyshev, Y.N., 2000, Underground and open pit mining: Strategy for the development of the Russian coal industry. Journal of Mining Science 36, 57 - 65.

Marchioni, D.L., 1983, The detection of weathering in coal by petrographic, rheologic and chemical methods. International Journal of Coal Geology 2, 231 - 259.

Marynowski, L., Scott, A.C., Zatoń, M., Parent, H., Garrido, A.C., 2011, First multi-proxy record of Jurassic wildfires from Gondwana: Evidence from the Middle Jurassic of the Neuquén Basin, Argentina. Palaeogeography, Palaeoclimatology, Palaeoecology 299, 129 - 136.

Marynowski, L., Simoneit, B.R.T., 2009, Widespread Upper Triassic to Lower Jurassic wildfire records from Poland: Evidence from charcoal and pyrolytic polycyclic aromatic hydrocarbons. PALIOS 24, 785 - 798.

Masiello, C.A., 2004, New directions in black carbon organic geochemistry. Marine Chemistry 92, 201-213.

Mastalerz, M., Bustin, R.M., 1993, Electron microprobe and micro-FTIR analyses applied to maceral chemistry. International Journal of Coal Geology 24, 333 - 345.

Mastalerz, M., Bustin, R.M., Lamberson, M.N., 1993, Variation in chemistry of vitrinite and semifusinite as a function of associated inertinite content. International Journal of Coal Geology 22, 149 - 162.

Mathews, J.P., Hatcher, P.G., Scaroni, A.W., 1997, Particle size dependence of coal volatile matter: is there a non-maceral-related effect?. Fuel 76, 359 - 362.

McAllister, S., Grenfell, I., Hadlow, A., Jolly, W.M., Finney, M., Cohen, J., 2012, Piloted ignition of live forest fuels. Fire Safety Journal 51, 133-142.

McCabe, P.J., 1984, Depositional environments of coal and coal-bearing strata. In: Rahmani, R.A., Flores, R.M., (eds)., Sedimentology of coal and coal-bearing strata. Special Publication of the International Association of Sedimentologists 7, Blackwell Scientific Publications, Oxford, 2-30.

McElhinny, M.W., McFadden, P.L., 2000, Palaeomagnetism: continents and Oceans. Academic Press, San Diego, 386.

McGinnes, E.A., Kandeel, S.A., Szopa, P.S., 1971, Some structural changes observed in the transformation of wood into charcoal. Wood and Fiber 3, 77-83.

McKee, E.D., Crosby, E.J., Berryhill Jr, H.L., 1967, Flood deposits, Bijou Creek, Colorado, June 1965. Journal of sedimentary petrology 37, 829-851.

McLoughlin, S., 2009, Floristic patterns through the Late Carboniferous and Permian of Gondwana with particular emphasis on Australia. Lyell meeting 2009 - Late Palaeozoic terrestrial habitats and biotas. Oral presentation, The Geological Society, London, May 2009.

McParland, L.C., 2010, Utilisation of quantified reflectance values to determine temperature and processes of formation for human produced and archaeological charcoal. Unpublished PhD thesis.

McParland, L.C., Collinson, M.E., Scott, A.C., Campbell, G., 2009b, The use of reflectance for the interpretation of natural and anthropogenic charcoal assemblages. Archaeological and Anthrolopological Sciences 1, 249-261.

McParland, L.C., Collinson, M.E., Scott, A.C., Campbell, G., Veal, R., 2010, Is vitrification of charcoal a result of high temperature burning of wood?. Journal of Archaeological Science 37, 2679 - 2687.

McParland, L., Collinson, M.E., Scott, A.C., Steart, D., 2007, Ferns and fires: experimental charring of ferns compared to wood and implications for paleobiology, coal petrology and isotope geochemistry. PALAIOS 22, 528 – 538.

McParland, L.C., Hazell, Z., Campbell, G., Collinson, M.E., Scott, A.C., 2009a, How the Romans got themselves into hot water: temperatures and fuel types used in firing a hypocaust. Environmental Archaeology 14, 176-183.

Méndez, L.B., Borrego, A.G., Martinez-Tarazona, M.R., Menéndez, R., 2003, Influence of petrographic and mineral matter composition of coal particles on their combustion reactivity. Fuel 82, 1875-1882.

Meyen, S.V., 1982, The Carboniferous and Permian Floras of Angaraland (a synthesis). Biological Memoirs 7, 1-109.

Meyen, S.V., 1984, Basic features of Gymnosperm systematics and phylogeny as evidenced by the fossil record. Botanical Review 50, 1 - 111.

Michaelsen, P., Henderson, R.A., 2000, Facies relationships and cyclicity of high-latitude, Late Permian coal measures, Bowen Basin, Australia. International Journal of Coal Geology 44, 19-48.

Milligan, J.B., Thomas, K.M., Crelling, J.C., 1997, Temperature-programmed combustion studies of coal and maceral group concentrates. Fuel 76, 1249 - 1255.

Mogutcheva, N.K., Krugovykh, V.V., 2009, New data on the stratigraphic chart for Triassic deposits in the Tunguska syneclise and Kuznetsk Basin. Stratigraphy and Geological Correlation 17, 510-518.

Monastersky, R., 1988, Lessons from the flames. Science News 134, 314-317.

Moore, P.D., 1987, Ecological and hydrological aspects of peat formation. In: Scott, A.C., (ed). Coal and Coal-bearing Strata: Recent Advances. Geological Society Special Publication 32, Blackwell Scientific Publications, 7-15.

Moore, P., 2010, Taldinski – a Russian coal giant: Operation focus – Russia. International Mining, 25-28.

Moore, T.R., Bubier, J.L., Bledzki, L., 2007, Litter decomposition in temperate peatland ecosystems: the effect of substrate and site. Ecosystems 10, 949-963.

Morton, A., Davies, C., Allen, M., Buslov, M., Safonova, I., 2005, Provenance studies from the Permian – Mesozoic strata of the Kuznetsk Basin, W. Siberia. West Siberian Basin project. Report 5 – March 2005. CASP confidential report.

Morton, A., Davies, C., Whitham, A., Harland, M., Buslov, M., Safonova, I., 2007, Zircon and additional mineral chemical analysis from the Kuznetsk Basin and Krasnoyarsk Region, West Siberian Basin. West Siberian Basin project. Phase II report 9 – March 2007. CASP confidential report.

Muller, S.D., Richard, P.J.H., Talon, B., 2008, Impact of disturbance on the Holocene development of a temperate peatland (Southern Québec). Vegetation History and Archaeobotany 17, 713-721.

Muraleedharan, T.R., Radojevic, M., Waugh, A., Caruana, A., 2000, Emissions from the combustion of peat: an experimental study. Atmospheric Environment 34, 3033 - 3035.

Neavel, R.C., Smith, S.E., Hippo, E.J., Miller, R.N., 1986, Interrelationships between coal compositional parameters. Fuel 65, 312 - 320.

Nichols, G., 2009, Sedimentology and Stratigraphy: Second Edition. Wiley Blackwell, UK.

Nichols, G.J., Cripps, J.A., Collinson, M.E., Scott, A.C., 2000, Experiments in

waterlogging and sedimentology of charcoal: results and implications. Palaeogeography, Palaeoclimatology, Palaeoecology 164, 43-56.

O'Brien, G., Jenkins, B., Esterle, J., Beath, H., 2003, Coal characterisation by automated coal petrography. Fuel 82, 1067-1073.

Ohlson, M., Korbøl, A., Økland, R.H., 2006, The macroscopic charcoal record in forested boreal peatlands in southeast Norway. The Holocene 16, 731-741.

Ohlson, M., Tryterud, E., 2000, Interpretation of the charcoal record in forest soils: forest fires and their production and deposition of macroscopic charcoal. Holocene 10, 519-525.

Oshurkova, M.V., 1996, Palaeoecological parallelism between the Angaran and Euramerican provinces. Review of Palaeobotany and Palynology 90, 99-111.

Otto, A., Gondokusumo, R., Simpson, M.J., 2006, Characterization and quantification of biomarkers from biomass burning at a recent wildfire site in Northern Alberta, Canada. Applied Geochemistry 21, 166 - 183.

Pakh, E.M., Artser, A.S., 2003, Kuznetsky basin. Petrographic composition of coals. In: Coal Basins of Russia.v.2. Coal basins and coal fields of the Western Siberia (Kuznetsky, Gorlovsky, West-Siberian basins; coal fields of Altai Region and Republic Altai). – Moscow: Geoinformcentre, 2003, ISBN 5-900357-88-0, ISBN 5-900357-15-5, 604.

Patterson III, W.A., Edwards, K.J., Maguire, D.J., 1987, Microscopic charcoal as an indicator of fire. Quaternary Science Reviews 6, 3-23.

Patzek, T.W., Croft, G.D., 2010, A global coal production forecast with multi-Hubbert cycle analysis. Energy 35, 3109 - 3122.

Pearson, T., Scott, A.C., 1999, Large palynomorphs and debris. In: Jones, T.P., Rowe, N.P., (eds.), Fossil Plants and Spores: modern techniques. Geological Society of London, 20-25.

Pereira, P., Úbeda, X., 2010, Spatial distribution of heavy metals released from ashes after a wildfire. Journal of Environmental Engineering and Landscape Management 18, 13-22.

Peters, M.E., Higuera, P.E., 2007, Quantifying the source area of macroscopic charcoal with a particle dispersal model. Quaternary Research 67, 304-310.

Petersen, H.I., 1998, Morphology, formation and palaeo-environmental implications of naturally formed char particles in coals and carbonaceous mudstones. Fuel 77, 1177-1183.

Pierce, J.L., Meyer, G.A., Jull, A.J.T., 2004, Fire-induced erosion and millennial-scale climate change in northern ponderosa pine forests. Nature 432, 87-90.

Pisarevsky, S.A., Gladkochub, D.P., Donskaya, T.A., De Waele, B., Mazukabzov, A.M., 2006, Palaeomagnetism and geochronology of mafic dykes in south Siberia, Russia: the first precisely dated Early Permian palaeomagnetic pole from the Siberian craton. Geophysical Journal International 167, 649-658.

Pisaric, M.F.J., 2002, Long-distance transport of terrestrial plant material by convection resulting from forest fires. Journal of Paleolimnology 28, 349-354

Pisupati, S.V., Scaroni, A.W., 1993, Natural weathering and laboratory oxidation of bituminous coals: Organic and inorganic structural changes. Fuel 72, 531-542.

Pitkänen, A., Lehtonen, H., Huttunen, P., 1999, Comparison of sedimentary microscopic charcoal particle records in a small lake with dendrochronological data: evidence for the local origin of microscopic charcoal produced by forest fires of low intensity in eastern Finland. Holocene 10, 221-229.

Pitkänen, A., Tolonen, K., Jungner, H., 2001, A basin-based approach to the long-term history of forest fires as determined from peat strata. Holocene 11, 599-605.

Polyansky, O.P., Reverdatto, V.V., Fomin, A.N., 2004, Model reconstructions of subsidence in the Kuznetsk sedimentary basin. Russian Geology aand Geophysics 45, 678-687.

Power, M.J., Marlon, J.R., Bartlein, P.J., Harrison, S.P., 2010, Fire history and the Global Charcoal Database: A new tool for hypothesis testing and data exploration. Palaeogeography, Palaeoclimatology, Palaeoecology 291, 52-59.

Pratt, K.C., 1993, The use of composite and mosaic imaging of polished surfaces to enhance petrographic analysis of coal by image analysis. Organic Geochemistry 20, 759-768.

Preston, C.M., Schmidt, M.W.I., 2006, Black (pyrogenic) carbon: a synthesis of current knowledge and uncertainties with special consideration of boreal regions. Biogeosciences 3, 397-420.

Pyne, S.J., Andrews, P.L., Laven, R.D., 1996, Introduction to Wildland fire. J. Wiley & Sons, New York, 769.

Quebedeaux, B., Hardy, R.W.F., 1975, Reproductive growth and dry matter production of *Glycine max* (L.) Merr. in response to Oxygen concentration. Plant Physiology 55, 102-107.

Raw, F., 1967, Arthropods (except Acari and Collembola), in: Burges, A., Raw, F., (eds.), Soil Biology. Academic Press, London.

Rees, P.M., Ziegler, A.M., Gibbs, M.T., Kutzbach, J.E., Behling, P.J., Rowley, D.B., 2002, Permian phytogeographic patterns and climate data/ model comparisons. Journal of Geology 110, 1-31.

Reichow, M.K., Pringle, M.S., Al'Mukhamedov, A.I., Allen, M.B., Andreichev, V.L., Buslov, M.M., Davies, C.E., Fedoseev, G.S., Fitton, J.G., Inger, S., Medvedev, A.Ya., Mitchell, C., Puchkov, V.N., Safonova, I.Yu., Scott, R.A., Saunders, A.D., 2009, The timing and extent of the eruption of the Siberian Traps large igneous province: Implications for the end-Permian environmental crisis. Earth and Planetary Science Letters 277, 9-20.

Rein, G., Cleaver, N., Ashton, C., Pironi, P., Torero, J.L., 2008, The severity of smouldering peat fires and damage to the forest soil. Catena 74, 304-309.

Retallack, G.J., 1999, Postapocalyptic greenhouse paleoclimate revealed by earliest Triassic paleosols in the Sydney Basin, Australia. GSA Bulletin 111, 52-70.

Rothwell, G.W., Scott, A.C., 1988, *Heterotheca* Benson; lyginopterid pollen organs or coprolites?. Bulletin of the British Museum (Natural History) Geology 44, 41-43.

Rutledge, D., 2011, Estimating long-term world coal production with logit and probit transforms. International Journal of Coal Geology 85, 23-33.

RWE Npower Fuel Characterisation Laboratory (FCL) SOP manual, 2001, FCL/SOP/03, 12/09/2001, Method for determining Calorific Value by Parr 6400 bomb calorimeter, 1-6.

RWE Npower Fuel Characterisation Laboratory (FCL) SOP manual, 2009, FCL/SOP/06, 06/04/2009, Method for CHN analysis using Leco CHN2000, 1-11.

RWE Npower Fuel Characterisation Laboratory (FCL) SOP manual, 2009, FCL/SOP/07, 06/04/2009, Method for Sulphur determination using Leco SC144DR, 1-3.

RWE Npower Fuel Characterisation Laboratory (FCL) SOP manual, 2009, FCL/SOP/08, 06/04/2009, Method for volatile matter content, 1-2.

Ryer, T.A., Langer, A.W., 1980, Thickness change involved in the peat-to-coal transformation for a bituminous coal of Cretaceous age in Central Utah. Journal of Sedimentary Petrology 50, 0987-0992.

Sander, P.M., Gee, C.T., 1990, Fossil charcoal — techniques and applications. Review of Palaeobotany and Palynology 63, 269–279.

Santín, C., Doerr, S.H., Shakesby, R.A., Bryant, R., Sheridan, G.J., Lane, P.N.J., Smith, H.G., Bell, T.L., 2012, Carbon loads, forms and sequestration potential within ash deposits produced by wildfire: new insights from the 2009 'Black Saturday' fires, Australia. European Journal of Forest Research DOI: 10.1007/s10342-012-0595-8.

Schmidt, M.W.I., Noak, A.G., 2000, Black carbon in soils and sediments: Analysis, distribution, implications and current challenges. Global Biogeochemical Cycles 14, 777-793.

Schelkoph, G.M., Hassett, D.J., Weber, B.J., 1983, A comparative study of preparation and analytical methods for peat. In: Jarrett, P.M., (ed), Testing of peats & organic soils. The American Society for Testing and Materials (ASTM) STP 820, 99-110.

Schmidt, M.W.I., Torn, M.S., Abiven, S., Dittmar, T., Guggenberger, G., Janssens I.A., Kleber, M., Kögel-Knabner, I., Lehmann, J., Manning, D.A.C., Nannipieri, P., Rasse, D.P., Weiner, S., Trumbore, S.E., 2011, Persistence of soil organic matter as an ecosystem property. Nature 478, 49-56.

Scott, A.C., 1977, Coprolites containing plant material from the Carboniferous of Britain. Palaeontology 22, 59-68.

Scott, A.C., 1989a, Observations on the nature and origin of fusain. International Journal of Coal Geology 12, 443-475.

Scott, A.C., 1989b, Deltaic coals: an ecological and palaeobotanical perspective, in: Whateley, M.K.G., Pickering, K.T., (eds.), Deltas: Sites and Traps for Fossil Fuels. Geological Society Special Publication 41, 309-316.

Scott, A.C., 2000, The Pre-Quaternary history of fire. Palaeogeography, Palaeoclimatology, Palaeoecology 164, 281-329.

Scott, A.C., 2002, Coal petrology and the origin of coal macerals: A way ahead?. International Journal of Coal Geology 50, 119-134.

Scott, A.C., 2009, Forest Fire in the Fossil Record, in: Cerdà, A. and Robichaud, P. (eds). Fire Effects on Soils and Restoration Strategies. Science Publishers

Inc. New Hampshire, 1-37.

Scott, A.C., 2010, Charcoal recognition, taphonomy and uses in palaeoenvironmental analysis. Palaeogeography, Palaeoclimatology, Palaeoecology 291, 11-39.

Scott, A.C., Chaloner, W.G., Paterson, S., 1985, Evidence of pteridophyte-arthropod interactions in the fossil record. Proceedings of the Royal Society of Edinburgh 86B, 133-140.

Scott, A.C., Cripps, J.A., Collinson, M.E., Nichols, G.J., 2000a, The taphonomy of charcoal following a recent heathland fire and some implications for the interpretation of fossil charcoal deposits. Palaeogeography, Palaeoclimatology, Palaeoecology 164, 1-31.

Scott, A.C., Glasspool, I.J., 2005, Charcoal reflectance as a proxy for the emplacement temperature of pyroclastic flow deposits. Geology 33, 589–592.

Scott, A.C., Glasspool, I.J., 2006, The diversification of Paleozoic fire systems and fluctuations in atmospheric oxygen concentration. PNAS 103, 10861-10865.

Scott, A.C., Glasspool, I.J., 2007, Observations and experiments on the origin and formation of Inertinite group macerals. International Journal of Coal Geology 70, 55-66.

Scott, A.C., Jones, T.P., 1991, Microscopical observations of recent and fossil charcoal. Microscopy and Analysis 25, 13-15.

Scott, A.C., Jones, T.P., 1994, The nature and influence of fire in Carboniferous ecosystems. Palaeogeography, Palaeoclimatology, Palaeoecology 106, 91-112.

Scott, J.H., Reinhardt, E.D., 2001, Assessing crown fire potential by linking models of surface and crown fire behaviour. United States Department of Agriculture (USDA), forest service, Rocky Mountain research station, research paper RMRS-RP-29, 1-59.

Scott, A.C., Moore, J., Brayshay, B., 2000b, Introduction to fire and the palaeoenvironment. Palaeogeography, Palaeoclimatology, Palaeoecology 164, vii - xi.

Scott, A.C., Pinter, N., Collinson, M.E., Hardiman, M., Anderson, R.S., Brain, A.P.R., Smith, S.Y., Marone, F., Stampanoni, M., 2010, Fungus, not comet or catastrophe, accounts for carbonaceous spherules in the Younger Dryas 'impact layer'. Geophysical Research Letters, DOI: 10.1029/2010GL043345.

Scott, A.C., Sparks, R.S.J., Bull, I.D., Knicker, H., Evershed, R.P., 2008, Temperature proxy data and its significance for the understanding of pyroclastic density currents. Geology 36, 143–146.

Scott, A.C., Taylor, T.N., 1983, Plant/Animal interactions during the Upper Carboniferous. The Botanical Review 49, 259-307.

Sen, R., Srivastava, S.K., Singh, M.M., 2009, Aerial oxidation of coal – analytical methods, instrumental techniques and test methods: a survey. Indian Journal of Chemical Technology 16, 103-135.

Seward, A.C., 1919, Fossil plants: for students of botany and geology. Cambridge University Press, New York.

Shao, L., Jones, T., Gayer, R., Dai, S., Li, S., Jiang, Y., Zhang, P., 2003, Petrology and geochemistry of the high-sulphur coals from the Upper Permian carbonate coal measures in the Heshan Coalfield southern China. International Journal of Coal Geoology 1040, 1-26.

Shearer, J.C., Moore, T.A., 1996, Effects of experimental coalification on texture, composition and compaction in Indonesian peat and wood, Organic Geochemistry, 24, 127 - 140.

Shearer, J.C., Staub, J.R., Moore, T.A., 1994, The conundrum of coal bed thickness: A theory for stacked mire sequences. The Journal of Geology 102, 611-617.

Simoneit, B.R.T., 2002, Biomass burning – A review of organic tracers for smoke from incomplete combustion. Applied Geochemistry 17, 129 - 162.

Šimůnek, Z., Libertín, M., 2006, *Cordaites schatzlarensis* sp. nov. and *Samaropsis newberryi* (Andrews) from the Westphalian (Carboniferous) of the Žacléř area (Czech Republic). Review of Palaeobotany and Palynology 138, 43-62.

Slaghuis, J.H., Ferreira, L.C., Judd, M.R., 1991, Volatile material in coal: effect of inherent mineral matter. Fuel 70, 471-473.

Smith, J.R., Smith, J.W., 2007, A relationship between the carbon and hydrogen content of coals and their vitrinite reflectance. International Journal of Coal Geology 70, 79-86.

Snyman, C.P., 1989, The role of coal petrography in understanding the properties of South African coal. International Journal of Coal Geology 14, 83-101.

Spackman, W., Cohen, A.D., Given, P.H., Casagrande, D.J., 1976, The comparative study of the Okefenokee swamp and the Everglades-mangrove swamp-marsh

complex of southern Florida. Short course presentation of the Pennsylvanian State University, 403.

Spackman, W., Thompson, R., 1966, A coal constituent classification designed to evolve as knowledge of coal composition evolves. In: Int. Cong. Stratigraphie et Geologie du Carbonifere, 5th, Paris, 1963, Compte Rendu 1, 239-254.

Speight, J.G., 1990, Fuel science and technology handbook. Marcel Dekker Inc, New York and Basel.

Stach, E., 1982, The microlithotypes of coal and their strength, in: Stach, E., et al., Stach's Textbook of Coal Petrology. Gebrüder Borntraeger, Berlin-Stuttgart, 173-177.

Stähli, M., Finsinger, W., Tinner, W., Allgöwer, B., 2006, Wildfire history and fire ecology of the Swiss National Park (Central Alps): new evidence from charcoal, pollen and plant macrofossils. The Holocene 16, 805-817.

Stevenson, A.C., Jones, V.J., Battarbee, R.W., 1990, The cause of peat erosion: a palaeolimnological approach. New Phytologist 114, 727-735.

Stopes, M.C., 1919, On the four visible ingredients of banded bituminous coal. Proceedings of the Royal Society B., 90, London, 470-487.

Stopes, M.C., 1935, On the petrology of banded bituminous coals. Fuel 14, 4-13.

Su, S., Pohl, J.H., Holcombe, D., Hart, J.A., 2001, A proposed maceral index to predict combustion behaviour of coal. Fuel 80, 699-706.

Suárez-Ruiz, I., Ward, C.R., 2008, Chapter 2 – Basic factors controlling coal quality and technological behaviour of coal. In: Suárez-Ruiz, I., Crelling, J.C., (eds.), Applied coal petrology – The role of petrology in coal utilization. Academic Press publications, USA.

Suárez-Ruiz, I., Flores, D., Mendonço Filho, J.G., Hackley, P.C., 2012, Review of and update of the applications of organic petrology: Part 1, geological applications. International Journal of Coal Geology.
DOI: 10.1016/j.coal.2012.02.004.

Tang, L., Gupta, R., Sheng, C., Wall, T., 2005, The char structure characterization from the coal reflectogram. Fuel 84, 1268-1276.

Taylor, G.H., Liu, S.Y., Diessel, C.F.K., 1989, The cold-climate origin of inertinite-rich Gondwana coals. International Journal of Coal Geology 11, 1-22.

Taylor, G.H., Teichmüller, M., Davis, A., Diessel, C.F.K., Littke, R., Robert, P.,

1998, Organic Petrology. Gebrüder Bornstraeger, Berlin, Stuttgart.

Teichmüller, M., 1986, Organic petrology of source rocks, history and state of the art Advances in Organic Geochemistry 1985. Organic Geochemistry 10, 581-599.

Teichmüller, M., 1987(a), Recent advances in coalification studies and their application to geology. In: Scott, A.C., (ed.), coal and coal-bearing strata: recent advances. Geological Society Special Publication 32, 127 - 169.

Teichmüller, M., 1987(b), Organic material and very low-grade metamorphism. In: Frey, M., (ed.), Low temperature metamorphism, Blackie, Glasgow, 114-161.

Teichmüller, M., 1989, The genesis of coal from the viewpoint of coal petrology. International Journal of Coal Geology 12, 1-87.

Teichmüller, M., Durand, B., 1983, Fluorescence microscopical rank studies on liptinites and vitrinites in peat and coals, and comparison with results of the rock-eval pyrolysis. International Journal of Coal Geology 2, 197-230.

Thevenon, F., Williamson, D., Vincens, A., Taieb, M., Merdaci, O., Decobert, M., Buchet, G., 2003, A late-Holocene charcoal record from Lake Masoko, SW Tanzania: climatic and anthropogenic implications. The Holocene 13, 785 - 792.

Thomas, L., 1992, Handbook of Practical Coal Geology. John Wiley & Sons, Chicester, UK, 122

Tinner, W., Conedara, M., Ammann, B., Gaggelar, H.W., Gedye, S., Jones, R., Sagesser, B., 1998, Pollen and charcoal in lake sediments compared with historically documented forest fires in southern Switzerland since AD 1920. Holocene 8, 31-42.

Tinner, W., Hofstetter, S., Zeugin, F., Conedera, M., Wohlgemuth, T., Zimmermann, L., Zweifel, R., 2006, Long-distance transport of macroscopic charcoal by intensive crown fire in the Swiss Alps – implications for fire history reconstruction. Holocene 16, 287-292.

Tolonen, K., 1983, The post-glacial fire record, in: Wein R.W., MacLean D.A., (eds.), The Role of Fire in Northern Circumpolar Ecosystems. John Wiley & Sons, New York, 21-44.

Tsai, S.C., 1982, Coal science and technology 2 – Fundamentals of coal beneficiation and utilization. Elsevier Scientific Publishing Company, Amsterdam.

Turetsky, M.R., St. Louis, V.L., 2006, Disturbance in boreal peatlands, in: Weider, R.K., Vitt, D.H., (eds.), Ecological Studies, Vol. 188, Boreal Peatland Ecosystems. Springer-Verlag, Berlin, 359-379.

Uhl, D., Hamad, A., Kerp, H., Bandel, K., 2007, Evidence for palaeo-wildfire in the Late Permian palaeotropics—charcoalified wood from the Um Irna Formation of Jordan. Review of Palaeobotany and Palynology 144, 221–230.

Uhl, D., Jasper, A., Abu Hamad, A.M.B., Montenari, M., 2008, Permian and Triassic wildfires and atmospheric oxygen levels, in: DeSantis, A., Baker, R., Klug, B., Vanicek, P., Silva, L.J.H., Foyo, A., Ercanoglu, M., Dordevic, D., (eds.) Proceedings of the 1st WSEAS international conference on environmental and geological science and engineering (EG'08)-Environment and Geoscience, 179-187.

Uhl, D., Kerp, H., 2003, Wildfires in the Late Palaeozoic of Central Europe – The Zechstein (Upper Permian) of NW-Hesse (Germany), Palaeogeography, Palaeoclimatology, Palaeoecology 199, 1-15.

Van Asselen, S., Stouthamer, E., van Asch, Th.W.J., 2009, Effects of peat compaction on delta evolution: a review on processes, responses, measuring and modelling. Earth-Science Reviews 92, 35-51.

Van Niekerk, D., Pugmire, R.J., Solum, M.S., Painter, P.C., Matthews, J.P., 2008, Structural characterization of vitrinite-rich and inertinite-rich Permian-aged South African bituminous coals. International Journal of Coal Geology 76, 290-300.

Vaughan, A., Nichols, G.J., 1995, Controls on the deposition of charcoal: implications for sedimentary accumulations of fusain. Journal of Sedimentary Research A65 (1), 129-135.

Vleeskens, J.M., Nandi, B.N., 1986, Burnout of coals: Comparative bench-scale experiments on pulverized fuel and fluidized bed combustion. Fuel 65, 797 - 802.

Walker, S., 2000, Major coalfields of the world, CCC/32, June 2000. IEA Coal Research 2000, 131.

Wallwork, J.A., 1967, Acari, in: Burges A., Raw F., (eds.), Soil Biology. Academic Press, London.

Wang, H., Shao, L., Large, D.J., Wignall, P.B., 2011, Constraints on carbon accumulation rate and net primary production in the Lopingian (Late

Permian) tropical peatland in SW China. Palaeogeography, Palaeoclimatology, Palaeoecology 300, 152-157.

Ward, C.R., 1984, Coal geology and coal technology. Blackwell Scientific Publications. Melbourne, Australia.

Ward, C.R., Li, Z., Gurba, L.W., 2005, Variations in coal maceral chemistry with rank advance in the German Creek and Moranbah Coal Measures of the Bowen Basin, Australia, using electron microprobe techniques. International Journal of Coal Geology 63, 117-129.

Ward, C.R., Suárez-Ruiz, I., 2008, Chapter 1 – Introduction to applied coal petrology in: Suárez-Ruiz, I., Crelling, J.C., (eds), Applied coal petrology – The role of petrology in coal utilization. Academic Press Publications, USA.

Wein, R.W., Moore, J.M., 1977, Fire history and rotations in the New Brunswick Acadian Forest. Canadian Journal of Forest Research 7, 285-294.

Weller, J.M., 1959, Compaction of sediments. AAPG Bulletin 43, 273.

Wellman, C.H., Osterloff, P.L., Mohiuddin, U., 2003, Fragments of the earliest land plants. Nature 425, 282-284.

White, A., Davies, M.R., Jones, S.D., 1989, Reactivity and characterization of coal maceral concentrates. Fuel 68, 511-519.

Whitlock, C., Larsen, C., 2001, Chapter 5 – Charcoal as a fire proxy. In: Smol, J.P., Birks, H.J.B., Last, W.M., (eds.). Tracking environmental change using lake sediments. Volume 3: Terrestrial, Algal and Siliceous Indicators. Kluwer Academic Publishers, Dordrecht, The Netherlands, 1-23.

Wilson, L.R., Johnston, A.W., 1940, A new species of Cordaites from the Pennsylvanian strata of Iowa. Bulletin of the Torrey Botanical Club 67, 117-120.

Winston, R.B., 1986, Characteristic features and compaction of plant tissues traced from permineralized peat to coal in Pennsylvanian coals (Desmoinsian) from the Illinois basin. International Journal of Coal Geology 6, 21-41.

Yu, Z., Turetsky, M.R., Campbell, I.D., Vitt, D.H., 2001, Modelling long-term peatland dynamics. II. Processes and rates as inferred from litter and peat-core data. Ecological Modelling 145, 159-173.

Zhang, Y., Tao, S., 2009, Global atmospheric emission inventory of polycyclic aromatic hydrocarbons (PAHs) for 2004. Atmospheric Environment 43, 812 - 819.

Zhuang, X., Querol, X., Alastuey, A., Plana, F., Moreno, N., Andrés, J.M., Wang, J., 2007, Mineralogy and geochemistry of the coals from the Chongqing and Southeast Hubei coal mining districts, South China. International Journal of Coal Geology 71, 263-275.

Ziegler, A.M., 1990, Phytogeographic patterns and continental configurations during the Permian Period. Geological Society, London, Memoirs 12, 363-379.

APPENDIX 1

REFER TO APPENDIX CD

APPENDIX 2

REFER TO APPENDIX CD

APPENDIX 3

CHARACTERISATION METHODOLOGY

Proximate and ultimate analyses were carried out at the RWE Npower Fuel Characterisation Laboratory in Swindon. Prior to each analysis the sample container was rotated for >1 minute mechanically before weighing the desired amount of coal to thoroughly mix the sample and reduce sampling bias (BS 1016-104.1:1999). All samples were analysed in triplicate.

A.3.1 Proximate analysis

A.3.1.1 Moisture content (%)

The moisture on the surface of the coal (free moisture) needs to be removed prior to analysis. Coal is hygroscopic and atmospheric humidity within the laboratory varies which makes producing a limiting factor for reproducibility difficult. However, for <5% moisture the reproducibility is 0.10% and >5% = 0.15% (BS 1016-104.1:1999).

Free moisture determination: Coal is spread out evenly in a tray and left to air dry for 24 h at room temperature (Equation A.3.1). This ensures the sample moisture content is in equilibrium with laboratory humidity to minimise moisture variation during analyses (BS 1016-104.1:1999; Ghaly et al., 1999). Once air dried the coal is sub-sampled using a scoop (with a diameter twice that of the largest particle size), and increments are taken until 500g of subsample is obtained.

$$MC_{wet} = ((WW-DW)/WW) \times 100$$

Whereby:

MC_{wet} moisture content on a wet basis (as received basis) (%)

WW wet weight of the sample (in g)

DW dry weight of the sample (in g)

EQUATION A.3.1 Free moisture determination

Inherent moisture: Is the remaining moisture within the coal after the free moisture has been removed. It is measured using a Thermo Gravimetric Analyser (TGA 701).

0.9 - 1.5g of pulverised fuel in a ceramic crucible is combusted in a Nitrogen rich atmosphere (with a flow rate of 15× per hour). The temperature is raised step wise, from 25°C-110°C and is maintained until the sample reaches a constant mass (BS 1016-104.1:1999; Fig. A.3.1 E). The moisture content is calculated from the loss in mass (BS 1016-104.1:1999).

$$\omega M = \frac{m_2 - m_3}{m_2 - m_1} \times 100$$

whereby:
m_1 – is the mass in g of the empty dish
m_2 – is the mass of the coal sample
m_3 – is the mass in g of the dish and the sample after heating

EQUATION A.3.2 Inherent moisture determination

A.3.1.2 Inherent ash content (%)

Ash content is determined using a Thermo Gravimetric Analyser (TGA 701), after the moisture content has been calculated the furnace temperature is raised from 600-815°C in an O_2 atmosphere. The sample is continually weighed until the sample mass remains constant. The ash content is calculated from the mass of the residue in the crucible calculated on an air dried basis (BS 1016-104.4:1998; Fig. A.3.1 E).

Precision and repeatability:

Ash	Maximum acceptable difference between results (calculated to the same moisture content)	
	Repeatability limit	**Reproducibility limit**
< 10%	0.2% absolute	0.3% absolute
≥ 10%	2.0% of the mean result	3.0% of the mean result

TABLE A.3.1 - Ash content results required assuming the analysis is carried out by a single operator in the same laboratory on the same sample (repeatability limit column). For multiple operators in more than one laboratory studying the same sample, the mean of the results obtained need to be within the values shown in the reproducibility limit column of the table (BS 1016-104.4:1998)

A.3.1.3 Volatile Matter (%)

Volatile matter is calculated by measuring 1.0 ± 0.005g of air dried pulverised fuel in a fused silica crucible with a well fitting lid which is placed into a muffle furnace at 900°C in the absence of air for 7 minutes ± 5 seconds. The sample is then removed and placed into a desiccator (Fig. A.3.1 G) and re-weighed to determine the percentage of volatiles driven off during combustion (FCL/SOP/08, 2009). The volatile matter is calculated by the loss in mass after deducting the loss in mass due to moisture (BS 1016-104.3:1998). Mineral matter may cause additional mass loss during the analysis, the amount depends on the type and quantity of minerals present (BS 1016-104.3:1998). A correction is therefore made to convert to a dry ash free basis (daf) which removes the effect of volatiles released by mineral matter (Equation A.3.3).

$$VM\ (daf) = VM_{air\ dried} \times 100 / (100 - Moisture_{\ air\ dried} - Ash_{\ air\ dried})$$

EQUATION A.3.3 - Conversion of Volatile matter on an as received basis to dry ash free basis

Repeatability and Reproducibility:

Volatile Matter	Maximum acceptable difference between results (calculated to the same moisture content)	
	Repeatability limit	**Reproducibility critical difference**
Hard coal of volatile matter < 10%	0.3% absolute	0.5% absolute
Hard coal of volatile matter ≥ 10%	3.0% of the mean result	0.5% absolute or 4% of the mean result (whichever is greatest)

TABLE A.3.2 Precision of volatile matter content results required assuming the analysis is carried out by a single operator in the same laboratory on the same sample (repeatability limit). For multiple operators in more than one laboratory studying the same sample, the mean of the results obtained need to be within the values shown in the reproducibility critical difference column in the table (BS 1016-104.4:1998)

A.3.1.4 Fixed Carbon

Fixed Carbon represents the carbon in the coal after volatile matter has been driven off. It is used as an indicator of coke yield in the carbonization process and serves as a rank parameter (Ward, 1984). Fixed Carbon is calculated by difference, summing moisture, ash and volatile matter and taking from 100 (Equation A.3.4).

$$FC = 100 - (M_{ad} + A_{ad} + V_{ad})$$

Whereby:

M_{ad} is the moisture in the air dried sample

A_{ad} is the ash (air dried basis)

V_{ad} is the volatile matter (air dried basis)

EQUATION A.3.4 Calculation of Fixed Carbon content (BS 17246:2005)

A.3.2 Ultimate analysis

A.3.2.1 Carbon, Hydrogen, Nitrogen, Oxygen

The percentage of each of these elements is measured using a Leco CHN2000 (Fig. A.3.1 D). 0.14 - 0.2g of pulverised fuel sample is weighed, sealed in a tin foil cup which falls into a combustion chamber where furnace temperature and flow of oxygen cause combustion. The process converts any elemental C, H and N into CO_2, H_2O, N_2 and NO_x (NO_x reduced to N_2). These gases are then passed through IR (infrared) cells to determine C and H content and a TC (thermal conductivity) cell to determine N_2 content (Leco corporation, 1998). The system is calibrated using blanks and a synthetic standard, EDTA, of known C, H, N content (Table A.3.3) standard are periodically added to the run of samples to monitor drift during analysis (FCL/SOP/06, 2009).

Carbon (%)	Hydrogen (%)	Nitrogen (%)
41.07 ± 0.17	5.55 ± 0.02	9.57 ± 0.03

TABLE A.3.3 Known Carbon, Hydrogen and Nitrogen values of synthetic standard EDTA (produced by Leco corp. part no. 502-092).

A percentage of water from hydrous clay minerals is incorporated into the measured Hydrogen value (Ward, 1984) therefore a correction needs to be made for this additional moisture in order to calculate Hydrogen to an air dried basis (Equation A.3.5). Samples with high inherent moisture will be most affected by this correction.

Calculated H(ad) = H(ad) – (0.1119 × inherent moisture)

EQUATION A.3.5 Method for moisture correction of Hydrogen to give a true air dried basis.

Oxygen is not measured during the analysis but calculated by difference (Equation A.3.6).

$O_{ad} = 100 – (C_{ad} – H_{ad} - N_{ad} - \text{Total } S_{ad} - Ash_{ad} - Moisture_{ad})$

EQUATION A.3.6 Determining Oxygen content of coal (BS 17247:2005) on an air dried basis

A.3.2.2 Total Sulphur

A known mass of pulverised fuel (0.1g ± 0.020g) is weighed in a standard ceramic crucible boat and heated between 1250-1350°C in an oxygen rich atmosphere in a Leco SC-144DR Sulphur analyser (Fig. A.3.1 F). Total Sulphur is calculated from the amount of infrared absorption from exit gases (SO_2). The furnace is purged with O_2 between runs to clean the system (FCL/SOP/07, 2009). The data is collected using SC-144DR carbon/sulphur determinator software. A Leco low Sulphur coal standard (part no. 502-433, sulphur 0.24% (+/-) 0.03%, repeatability tested in three independent laboratories) is used for calibration and monitoring drift during analysis. Repeatability of Sulphur data should be 0.02%.

A.3.3 Other

A.3.3.1 Specific Energy (CV – calorific value in MJ/Kg)

Calorific value is measured using a Parr 6400 bomb calorimeter (Fig. A.3.1 A-C) in an oxygen rich atmosphere saturated with water vapour. Pulverised fuel (0.7-0.8g) is weighed in a crucible (Fig. A.3.1 B). A cotton thread fuse is attached to the bomb head (Fig. A.3.1 B). The bomb calorimeter is calibrated using benzoic acid (Parr instrument co. no. 3415) of known calorific value (26.454 ± 0.2 MJ/Kg).

The gross calorific value is calculated from the temperature rise of the water in the bomb calorimeter under specified conditions. Corrections are made for the cotton thread ignition fuse (Table A.3.4) and heat loss to the water jacket (BS 1016-105:1992).

Average weight of cotton	Fuse correction
0.01	48
0.0105	50
0.011	52
0.0115	54
0.012	56
0.0125	58
0.013	60
0.0135	62
0.014	64
0.0145	66

TABLE A.3.4 fuse correction based on average weight of cotton thread (average of ten measured threads) (FCL/SOP/03, 2001).

Endothermic reactions of N, S and mineral matter during combustion can alter the calorific value of the coal, and a Sulphur correction is made post analysis [94.2030 × S per gram of sample (KJ/Kg), where S = sulphur content (% ad basis)] (FCL/SOP/03, 2001). In a laboratory setting the atmospheric conditions are restricted, enabling material to condense after ignition which gives an elevated calorific value (Ward, 1984). A correction needs to be applied to calculate the net calorific value for a unit of coal (0.7 - 0.8g) combusted at constant atmospheric pressure where the water is not condensed but removed with the flue gases which simulates boiler conditions (BS 1016-105:1992; Equation A.3.7).

Repeatability and Reproducibility: Results obtained by the same operator using the same apparatus on the same sample should not vary by 120 J/g. Samples analysed by more than one laboratory should not vary by 300 J/g and duplicates need to be within 0.1 MJ of each other (BS 1016-105:1992).

$$CV_{net} = ((CV_{gr} \times 1000) - (212.1\ H) + 24.4\ (M + (0.1A)) + 0.7 \times O) / 1000$$

Whereby terms correspond to:

CV_{net} = Net CV at constant pressure (as received basis)

CV_{gr} = Gross CV at constant volume (as received basis)

H = Hydrogen % (as received basis)

M = Total Moisture

A = Ash % (as received)

O = Oxygen (calculated using equation 3.5)

EQUATION A.3.7 Conversion of gross calorific value to net calorific value (units in MJ/Kg) (BS 1016-105:1992).

A.3.4 Reporting analyses to different bases

At each stage the results of each experiment are reported to different bases (Table A.3.5). When the coal arrives in the laboratory it is termed 'as received'. After the coal has been air dried any analysis is then reported on a 'dry basis'. Of most use to industry is the 'dry ash free' basis which removes the effect of mineral matter on the heating behaviour of the coal (Speight, 1990). Converting to each basis can be carried out by using the Table A.3.5.

Desired basis → **Given basis ↓**	**As Received**	**Air dried (ad)**	**Dry (d)**	**Dry Ash Free (daf)**	**Dry Mineral Matter Free (dmmf)**
As received		100-Mad 100-Mar	100 100-Mar	100 100-(Mar+Aar)	100 100-(Mar+MMar)
Air dried (ad)	100-Mar 100-Mad		100 100-Mad	100 100-(Mad+Aad)	100 100-(Mad+MMad)
Dry (d)	100-Mar 100	100-Mad 100		100 100-Ad	100 100-MMad
Dry Ash Free (daf)	100-(Mar+Aar) 100	100-(Mad+Aad) 100	100-Ad 100		100-Ad 100-MMad
Dry Mineral Matter Free (dmmf)	100-(Mar+MMar) 100	100-(Mad+MMad) 100	100-MMd 100	100-MMd 100-Ad	

TABLE A.3.5 Calculating the different bases for coal analysis (Speight, 1990)

FIG A.3.1

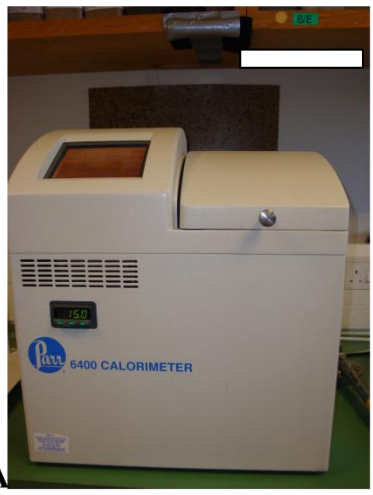

A

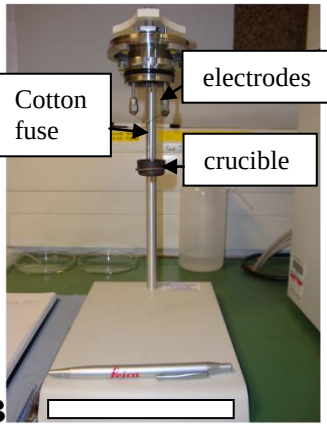

B

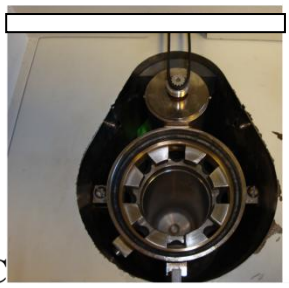

C

D

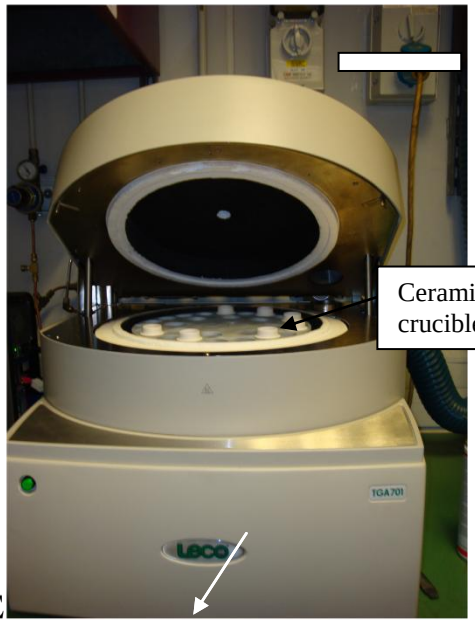

E

F

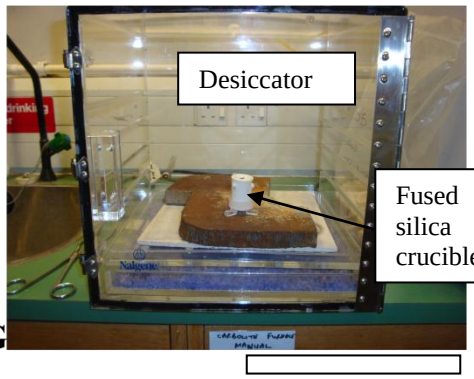

G

Scale bar corresponds to 15cm and is the same for all images (A-G)

APPENDIX 4

Sample name	Detrovitrinite	Telovitrinite	**Total Vitrinite**	**Total Liptinite**	Fusinite	Semifusinite	Inertodetrinite	Secretinite	Funginite	Macrinite	**Total inertinite (%)**	**Mineral matter**	**Total number of points**
68	49.1	11.9	61	5.6	6.9	11.1	5.1	5.9	0	3.9	32.9	0.5	875
73	63.8	10	73.9	3	8.6	4.5	5.6	1.3	0	1.8	21.8	1.3	1,136
78	50.8	8.8	59.7	2.3	12.6	11.1	5.8	2.6	0.9	2.7	35.6	2.4	1,019
78 lower	62.2	20.2	82.4	2.9	2.8	5.6	3.2	0.5	0	0.1	12.3	2.4	954
78 mid	70.7	3.2	73.9	2.9	5.3	10	5	0	0.1	2.3	22.6	0.6	1,005
78 upper	41.1	24.2	65.3	7.4	3.3	8.8	6.9	0.6	0.2	3.3	23.3	4	1,109
78 S2	52.3	10.6	62.9	3.4	16.6	6.8	3.5	0.5	1.3	4	32.9	0.8	1,274
78 S3	48.2	18.5	66.7	5.2	5	10.4	5	2.5	0	2.8	25.7	2.4	1,191
80-81	52.4	14.5	66.9	3.9	11.7	12.3	2.2	1.5	0.6	0.2	28.5	0.7	869
81	36.6	0	36.6	12.6	13.1	17.6	11.9	1.8	0.5	4.8	49.6	1.2	834
82	46.6	12.2	58.8	7.7	9.6	10.6	4.3	0.2	0	6.2	30.9	2.6	1,040
84	64.9	2.3	67.2	6.3	4.7	9.6	4.7	0	0.8	0.9	20.6	5.9	877
84-86	32.8	12.6	45.3	11.7	3.9	10.7	7.6	4.8	0.9	8.4	36.4	6.6	995
85	41.6	4.9	46.5	6.1	16.7	8.1	6.2	1.3	0	6.3	38.5	8.9	875
88	61.4	14.1	75.5	4.1	2.9	3.8	3	5	0.1	0.3	15.1	5.3	1,036
91(1)	32.4	8.5	41	12.2	5.2	10.9	2.8	2.5	0.3	6.5	28.2	18.6	925
91(2)	77.9	4.3	82.2	2.8	4.3	0	2.3	0	0	0	6.6	8.4	938
92	44.8	16.2	61	1	1	1.3	0.7	0	0	1.8	4.8	33.2	715
94	23	9.5	32.5	9.6	10.7	15	6.1	1.8	0.2	4.8	38.6	19.3	960
Stockpile fine	55.4	13.4	68.8	3.5	3.7	11.2	9	0	0.1	2	25.9	1.8	1,120
Stockpile pieces	47.3	15.4	62.7	4.1	7.6	12.2	5.8	1.1	0.4	3.2	30.3	2.9	948

TABLE A.4.1 Summary table of petrographic data for crushed general seam samples. For raw petrographic point counts see Appendix 1.

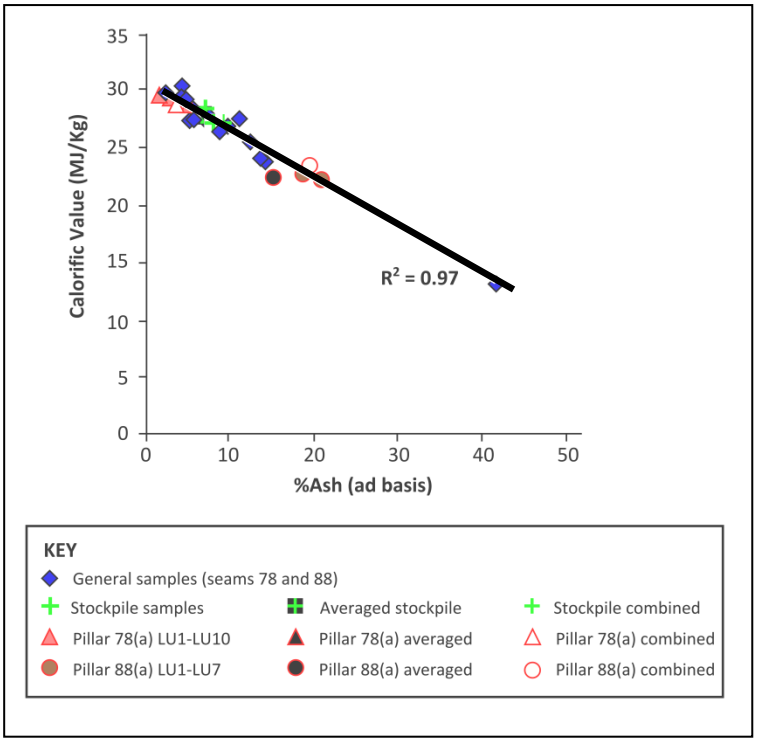

FIG. A.4.1 Relationship between %ash and calorific value for all general, stockpile and certain lithotype units from pillars 78(a) and 88(a). Ash is reported to an air dried (ad) basis and Calorific value is reported to a dry ash free basis. %Ash of general and stockpile samples was analysed at RWE Npower. Lithotype units were analysed at CAER (symbols with red outlines).

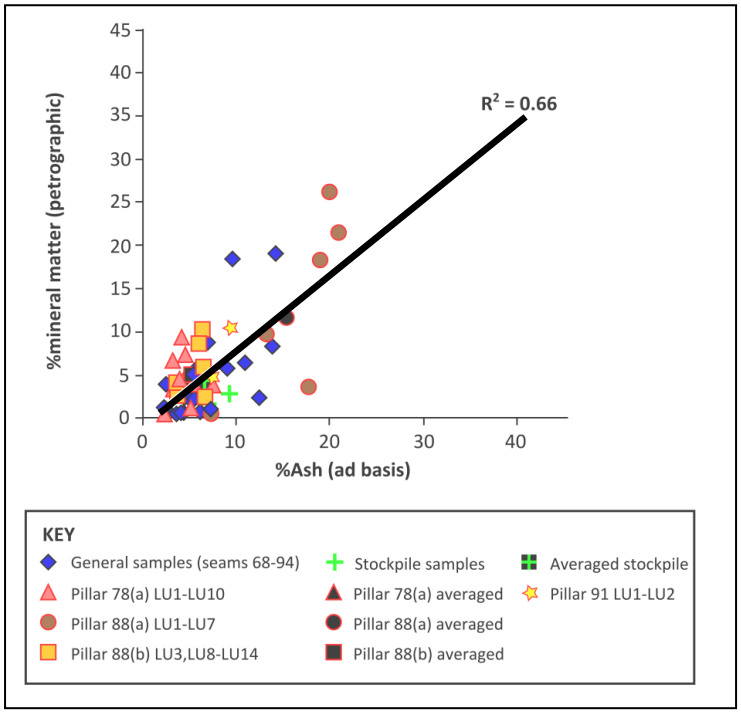

FIG. A.4.2 Relationship between %ash and %mineral matter for all samples. %Ash are reported to an ad (air dried) basis. Mineral matter point count values represent all mineral species in the coal (see Fig. 7.1 for XRD results for some samples). %Ash of general and stockpile samples was analysed at RWE Npower. Lithotype units were analysed at CAER (symbols with red outlines).

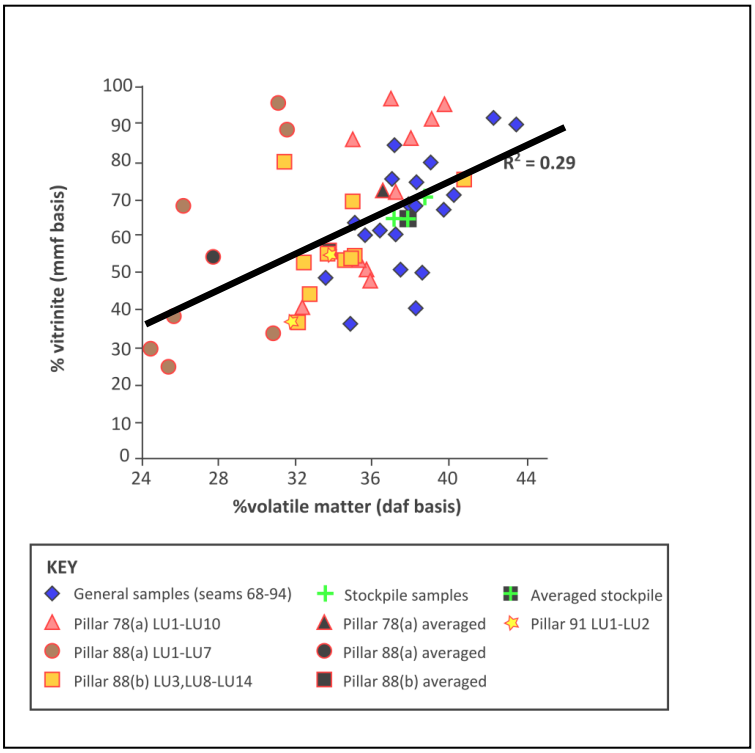

FIG. A.4.3 Relationship between vitrinite content and %volatile matter for all samples. Vitrinite values are reported to a mmf (mineral matter free) basis and %volatile matter to a daf (dry ash free) basis. Compare to Fig. 7.8. %volatile matter of general and stockpile samples was analysed at RWE Npower. Lithotype units were analysed at CAER (symbols with red outlines).

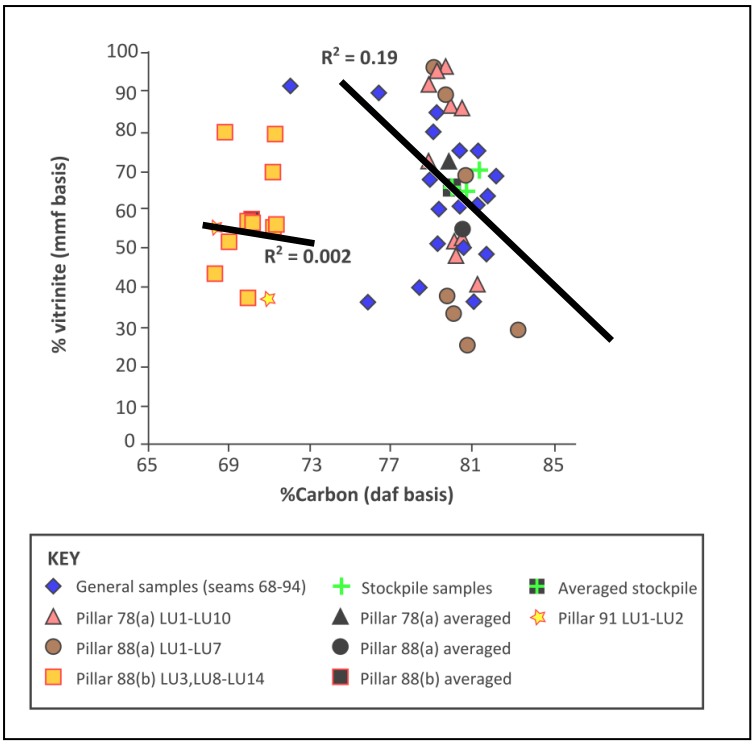

FIG. A.4.4 Relationship between vitrinite content and %Carbon for all samples. Vitrinite values are reported to a mmf (mineral matter free) basis and %Carbon to a daf (dry ash free) basis. Compare to Fig. 7.11. %Carbon of general and stockpile samples, and lithotype units from pillar 78(a) and 88(a) (symbols with black outlines) were analysed at RWE Npower. Lithotype units from pillars 88(b) and 91 were analysed at CAER (symbols with red outlines).

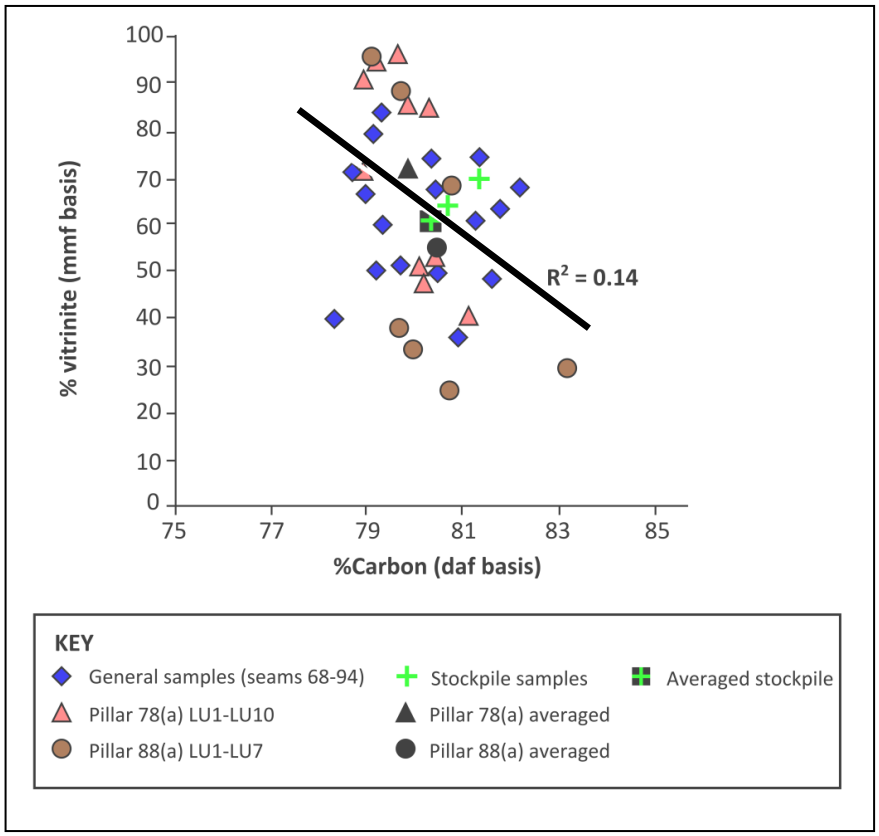

FIG. A.4.5 Relationship between vitrinite content and %Carbon for samples analysed at RWE Npower. Outlying general seam samples have also been removed [91(2) and 92]. Vitrinite values are reported to a mmf (mineral matter free) basis and %Carbon to a daf (dry ash free) basis. Compare to Fig. 7.12.

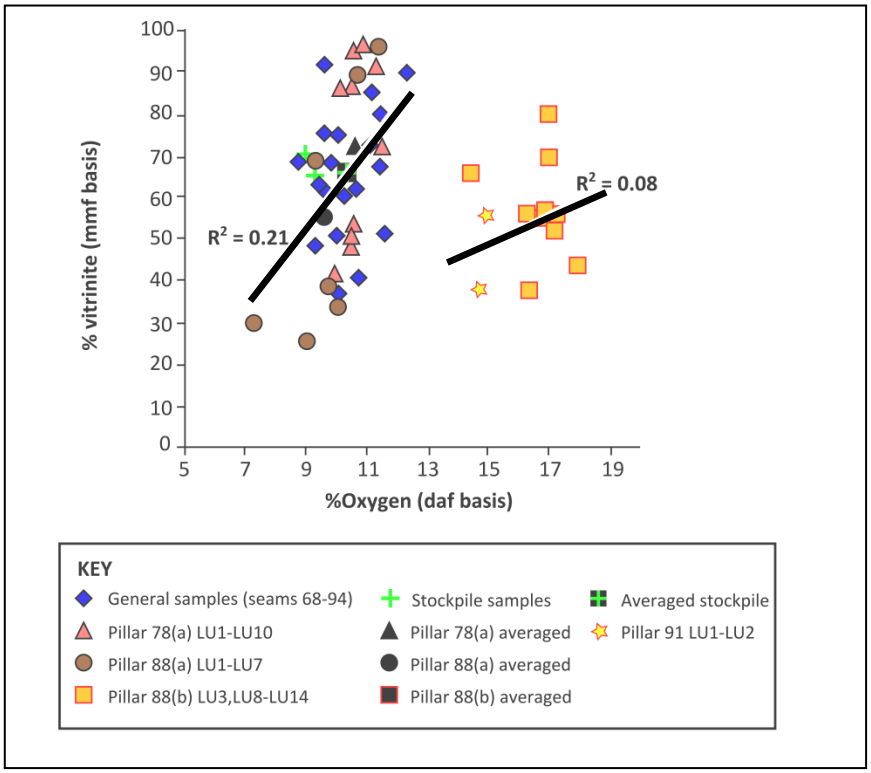

FIG. A.4.6 Relationship between vitrinite content and %Oxygen for all samples. Vitrinite values are reported to a mmf (mineral matter free) basis and %Oxygen to a daf (dry ash free) basis.

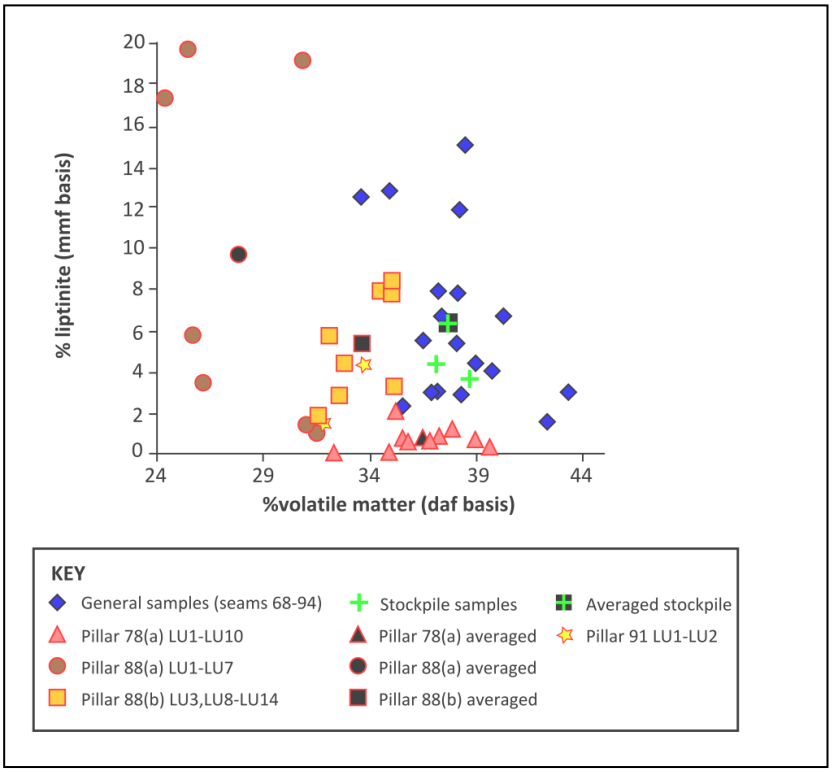

FIG. A.4.7 Relationship between liptinite content and %volatile matter for all samples. Liptinite values are reported to a mmf (mineral matter free) basis and volatile matter to a daf (dry ash free) basis. Compare to Fig. 7.8 and Fig. A.4.3. %Volatile matter of general and stockpile samples was analysed at RWE Npower. Lithotype units were analysed at CAER (symbols with red outlines).

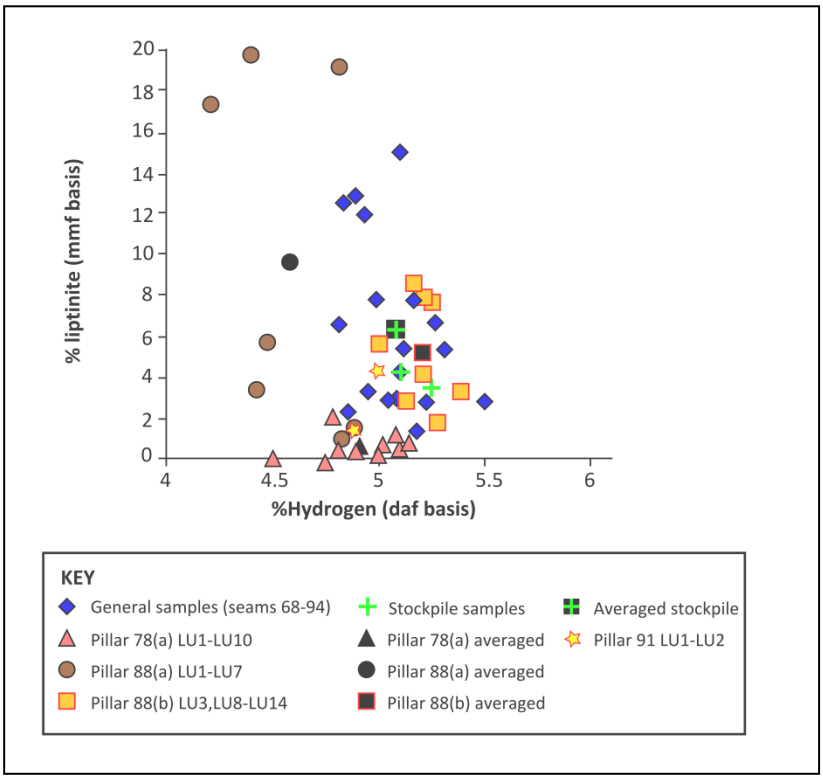

FIG. A.4.8 Relationship between liptinite content and %Hydrogen for all samples. Liptinite values are reported to a mmf (mineral matter free) basis and Hydrogen to a daf (dry ash free) basis. %Hydrogen of general and stockpile samples, and lithotype units from pillar 78(a) and 88(a) (symbols with black outlines) were analysed at RWE Npower. Lithotype units from pillars 88(b) and 91 were analysed at CAER (symbols with red outlines).

APPENDIX 5

REFER TO APPENDIX CD

APPENDIX 6

REFER TO APPENDIX CD

APPENDIX 7

REFER TO APPENDIX CD

APPENDIX 8

Oviedo ICCS&T 2011. Extended abstract

Program topic – coal combustion

The Effect of Particle Size and Petrographic Composition on Combustion Behaviour of selected Russian Coals

Hudspith. V[1], Nuamah. A[2,3], Scott. A.C.[1], Drage. T[2], Powis. J[3], Riley. G[3], Collinson. M.E[1], Lester. E[2]

[1] *Department of Earth Sciences, Royal Holloway University of London, Egham, Surrey, TW20 0EX, U.K.*

[2] *Faculty of Engineering, The University of Nottingham, Nottingham, NG7 2RD, U.K.*

[3] *Fuels and Combustion, RWEnpower, Windmill Hill Business Park, Whitehill Way, Swindon, Wiltshire, SN5 6PB*

Abstract

Two size fractions (53-75µm and 106-125µm) of pulverised fuel from five high volatile bituminous coal samples were selected to determine the effect of particle size and petrographic composition on combustion behaviour. Three Late Permian coal seams (numbered 78 (S1 and S2), 88, 91) and one stockpile (incorporating 13 seams) were sampled from two open cast mines in the Kuzbass region of Russia. In addition, sample 78 S1 represents a heat affected coal from a modern coal seam fire. The samples showed petrographic variation both between seams and size fractions. The burnout of the largest size fraction was measured using a drop tube furnace operating at 1300°C using a range of oxygen contents and residence times. The heat affected coal showed different chemical, petrographic and poorer burnout behaviour than the non heat affected coal samples.

1. Introduction

The importance of coal in the current and future global energy mix cannot be overestimated. Even though it poses a major threat to the environment if not carefully and efficiently combusted to reduce the emission of CO_2 [1], it is one of the major fuels needed to meet the energy needs of the ever increasing global population and economies [2]. The initial combustion of coal results in the generation of chars after the release of volatiles and moisture [3]. The combustion of this char depends on, the rank [4], maceral/ microlithotype associations [5], particle size, shape, structure and chemical composition [6], as well as the reflectance of vitrinite and inertinite [4, 5]. It is important to understand the extent these factors influence char combustion, which is vital in determining the carbon loss in ash and ultimately boiler design [7]. Carbon loss in ash is an important parameter because it indicates combustion efficiency and also affects the sale and use of the pulverised fuel ash [8].

The aim of this study is to carry out a series of combustion tests on a Drop-Tube Furnace (DTF), image analysis procedures and burnout to investigate the effect of particle size and petrographic composition on selected subbituminous Russian coals.

2 Experimental section

2.1 Coal preparation

The five samples were milled then sieved to 53-75µm and 106-125µm fractions and run through an airjet sieve to remove any fines. The 53-75µm fraction represents mid range commercial pulverised fuel for combustion whereas the 106-125µm fraction is more representative of the larger particles that might not have sufficient time to burnout completely. The larger size fraction may also help to highlight the impact of petrographic variations between the samples.

2.2 Drop Tube Furnace

Drop-Tube Furnace re-fire studies were undertaken at the Fuel Characterisation Laboratory Facility (CTF) at RWE Npower in Didcot. The DTF is made up of a screw feeder, feeder probe and collector probe, and a controllable gas system. Sixteen grams of each size fraction was injected into the feeder probe at a flow rate of 15g/hour. The larger samples were pyrolysed in a drop-tube furnace at 1300ºC with 1 vol% oxygen at 200ms and then refired at 5 vol% oxygen and with residence

times of 200 and 500ms. Burnout (or using the ash tracer method) was determined by ashing the coal, char and refired char samples at 815°C for two hours in a muffle furnace. Burnout is calculated using equation1 below.

$$\text{Volatile Yield } V_V \text{ or Burnout (\% daf)} = \frac{A_2 - A_1}{A_2(100 - A_1)} \times 10^4 \quad (1)$$

Whereby: A_1 = % dry ash content of coal
A_2 = % dry ash content of char.

2.2 Maceral Analysis

Pulverised fuel petrographic analysis was undertaken on polished blocks, under oil using a Leica DM 2500P reflectance microscope and a ×20 objective. Petrographic and microlithotype counts were taken using a Kötter graticule using the methodology outlined in [9, 10]. Intersections on embedding resin were not counted. Maceral groups were identified using ICCP schemes [11, 12].

A further set of polished blocks (53-75µm and 106-125µm of DTF char and original coal) were prepared using Struers liquid resin. These blocks were analysed using a Leica Ortholux POL II BK microscope with a 32x oil immersion lens attached to a PC based image analysis system using KS400 v3.1 software supplied by Imaging Associates Ltd. and a 1Mb Zeiss Axiocam Colour digital camera using a PCI interface card with thin-fibre optic cable for data and control lines at 200 Mbit/s. Standard immersion oil was used (1.518 at 23^{o}C) and the camera exposure time was approximately 250ms after calibration with a sapphire standard (0.58%). The camera captures reflected light images at 1300 x 1030 pixels which, with a total magnification of 320x, gives an image width of 221µm. Composite mosaic images (10x10 frames) were captured for each sample. The same microscope arrangement was used to capture char images.

2.3 Proximate and ultimate Analysis

Proximate and ultimate characterisation analyses were undertaken on bulk pulverised fuel samples (<200µm) at the RWE Npower Fuel Characterisation Laboratory Facility in Swindon using British standards [13-18]. Results are shown in Table 1.

3 Results and Discussion

3.1 Characterisation properties of coal

Sample Name	Ash (%)	Moisture (%)	Volatile Matter (%)	Fixed Carbon (%)	Net Calorific Value (MJ/Kg)	C (%)	H (%)	N (%)	S (%)
78 S1	21.87	16.5	42.18	35.64	13.3	68.48	2.32	2.83	0.19
78 S2	4.56	4.06	35.16	59.25	29.44	81.73	4.96	2.62	0.29
88	5.34	6.81	38.92	53.66	27.32	79.16	5.10	2.41	0.21
91	13.70	5.68	43.31	45.71	24.23	76.46	5.50	2.47	0.30
Stockpile	7.07	4.41	38.72	54.24	28.35	81.32	5.25	2.75	0.43

TABLE 1 Proximate and ultimate data for bulk unsieved pulverised coal samples. Moisture and ash are reported to air dried basis. Volatile matter, and ultimate analyses (C, H, N, S) are all reported to a dry ash free basis.

3.2 Maceral content and microlithotype associations

Petrographic composition varies between seams (Table 2), with vitrinite totals from 65% (78 S2) to 76.7% (88). Liptinite, 2.5% (stockpile) to 7.11% (88). Inertinite from 14% (88) to 30.24% (78 S2). Mineral matter, 0.34% (78 S2) to 3.48% (stockpile).

Petrographic and microlithotype variation is also seen between size fractions. Inertinite is more brittle than other maceral groups [20, 21, 22]. Liptinite tends to be more prevalent in the larger size fraction, since it is more difficult to grind than the other macerals [21]. The smaller particle size shows more liberation of the individual macerals i.e. the monomaceral vitrite is more abundant in the 53-75µm fraction in all samples (Table 3). Minerite is also more abundant in the 53-75µm fraction (78 S2, 88, 91). Conversely, liptinite is more abundant in all 106-125µm fractions (Table 2). Liptite was not observed and clarite is low in total abundance up to 7.9% (91). Bi- and tri- macerals are also more resistant to grinding than monomacerals [7]. The majority of liptinite in the 106-125µm fraction must therefore come from trimacerite microlithotype associations (up to 45.98% microlithotype totals (78 S2); Table 3). Inertinite is more abundant in the 53-75µm fraction 88 and stockpile samples. Of the inertinite maceral group, fusinite and macrinite are the only macerals more abundant in the 53-75µm fraction in four samples. Semifusinite is more abundant in the 53-75µm size fraction in two of the samples (88, 91). The majority of inertinite is

present in mixed maceral assemblages as vitrinertite (11% – 29.5%) or trimacerite (7.5% - 46%) only 1.2% - 15% of the total is the monomaceral inertite. Variation in maceral content between size fractions is a function of their maceral associations (microlithotypes) and the difference in microlithotype assemblages between the two size fractions may affect the reactivity of the pulverised fuel [7].

The heat affected coal (78 S1) is chemically (Table 1) and petrographically different from the other four samples (Table 2; Table 3). The vitrinite and inertinite macerals have qualitatively high reflectance (comparable to coal of anthracite rank) and there is no liptinite present. The clast shape is rounded with regular cracks around the perimeter, suggesting volatile loss. Vitrinite is the most abundant identifiable maceral (up to 35%), the majority of which is as the microlithotype vitrite (16% – 23.8%; Table 3) and vitrinertite (8.8% - 12.5%). Inertinite is a minor component (up to 4%) either as inertite (2.1%) or vitrinertite.

SAMPLE NAME	TOTAL VITRINITE (%)	TOTAL LIPTINITE (%)	INERTINITE (%)							UNIDENTIFIABLE MACERALS (%)	MINERAL MATTER	TOTAL NUMBER OF POINTS
			FUSINITE	SEMIFUSINITE	INERTODETRINITE	SECRETINITE	FUNGINITE	MACRINITE	TOTAL INERTINITE			
78 S1 (53-75µm)	22.89	0	0	0	1.37	0	0	2.64	4.01	70.15	2.95	948
78 S1 (106-125µm)	34.93	0	0.17	0	1.18	0	0	0.67	2.02	60.45	2.60	1,191
78 S2 (53-75µm)	71.62	3.75	3.41	0.34	11.35	0	0.68	7.26	23.04		1.59	881
78 S2 (106-125µm)	65.37	4.04	2.11	8.34	9.44	5.14	0.93	4.3	30.24		0.34	1,187
88 (53-75µm)	74.82	3.68	4.42	6.19	5.60	0	0.44	3.24	19.88		1.62	679
88 (106-125µm)	76.7	7.11	0.42	3.03	8.05	0	0.1	2.72	14.32		1.88	957
91 (53-75µm)	72.69	2.94	8.96	1.91	4.55	0.29	0	5.58	21.29		3.08	681
91 (106-125µm)	67.52	5.59	8.54	10.21	3.73	0	0	1.08	23.55		3.34	1,019
Stockpile (53-75µm)	75.49	2.49	5.51	5.6	3.46	1.33	0	3.11	19.01		3.02	1,126
Stockpile (106-125µm)	75.84	4.69	1.2	5.09	7.83	0	0	1.87	16		3.48	1,494

TABLE 2 Summary of petrographic point count data of pulverised coal 53-75µm and 106-125µm size fractions. Data are reported to a mineral included basis. Unidentifiable macerals are from the heat affected coal (78 S1) and are too altered to be identified using ICCP schemes [11, 12]

SAMPLE NAME	VITRITE (%)	LIPTIITE (%)	INERTITE (%)	CLARITE (%)	DURITE (%)	VITRINERTITE (%)	TRIMACERITE (%)	MINERITE (%)	UNIDENTIFIABLE MICROLITHOTYPES (%)
78 S1 (53-75µm)	16.1	0.0	2.1	0.0	0.0	8.8	0.0	3.3	69.7
78 S1 (106-125µm)	23.8	0.0	0.0	0.0	0.0	12.5	0.0	6.4	57.3
78 S2 (53-75µm)	27.7	0.0	5.0	2.3	0.0	29.5	30.7	4.8	
78 S2 (106-125µm)	17.3	0.0	11.8	0.9	1.0	22.9	46.0	0.0	
88 (53-75µm)	52.1	0.0	11.8	4.9	0.6	14.9	9.0	6.8	
88 (106-125µm)	34.7	0.0	2.1	4.2	1.7	18.8	33.2	5.3	
91 (53-75µm)	51.0	0.0	15.4	7.9	0.0	11.0	7.5	7.3	
91 (106-125µm)	45.8	0.0	11.5	3.2	1.3	12.6	20.1	5.6	
Stockpile (53-75µm)	50.8	0.0	8.0	3.5	0.9	19.8	10.9	6.1	
Stockpile (106-125µm)	30.2	0.0	1.2	7.6	1.4	21.1	29.2	9.5	

TABLE 3 Summary of microlithotype associations within the five samples studied. Unidentifiable microlithotypes are from the heat affected sample (78 S1) and are too altered to be identified.

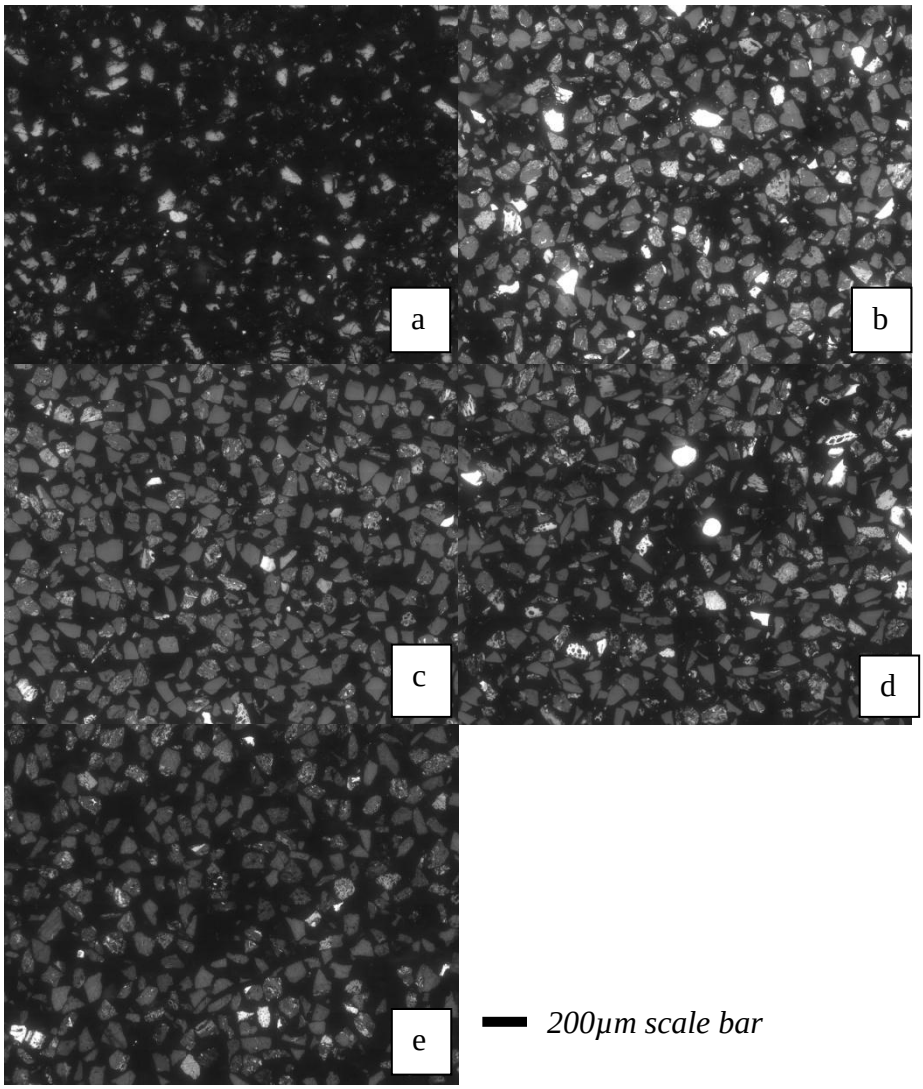

Figure 1 Mosaic images for the 5 coal samples (106-125 micron); (a) seam 78 S1(heat affected) (b) seam 78 S2 (c) seam 88 (d) seam 91, (e) Stockpile fine

3.3 Burnout behaviour

The burnout profiles in Figure 2 (below) include volatile release and char burnout for the larger size fraction. Samples with better burnout behaviour should have less combustible components remaining at earlier residence times [23]. Furthermore Cloke et al. [24] have shown that particle size can also affect burnout. Clearly seam 78 S1 shows the poorest burnout rates, with an almost linear burnout profile. Figure 3 shows that the chars structure appear to be almost solid, post pyrolysis. This must relate to the heat affected nature of the particles, slowing down the pyrolysis rate, lowering the formation of open pores within a char structure. In a diffusion controlled reaction, it is likely that burnout would be limited to the external surface, allowing slow burnout of the solid particles. This would explain the relatively slow

burnout rates. 78 S2 forms predominantly thick walled spheres (crassispheres) or solids. In addition, from Figure 3, Stockpile and coal 88 form the thinnest char structures and this is reflected in the highest burnout rates in Figure 2. However, all the samples, by 700ms total refire time achieve 70-85% burnout. The remaining char structures, at these latter stages of combustion, require further investigation in order to explain which morphologies are responsible for this residual level of carbon in ash.

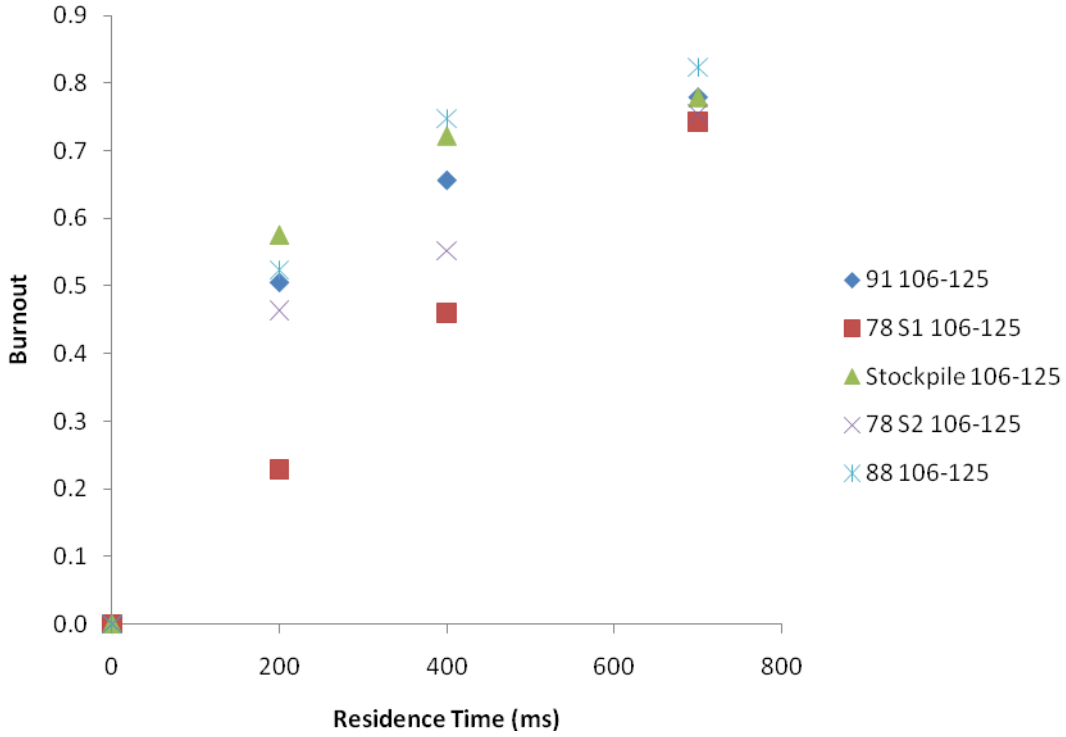

Figure 2 Burnout behaviour of refired char from the larger pulverised coal fraction (106-125µm).

From Figure 3, Coal 91 clearly has a significant number of solid chars which relate to the higher levels of inertite particles (Table 3) that are present in the original coal.

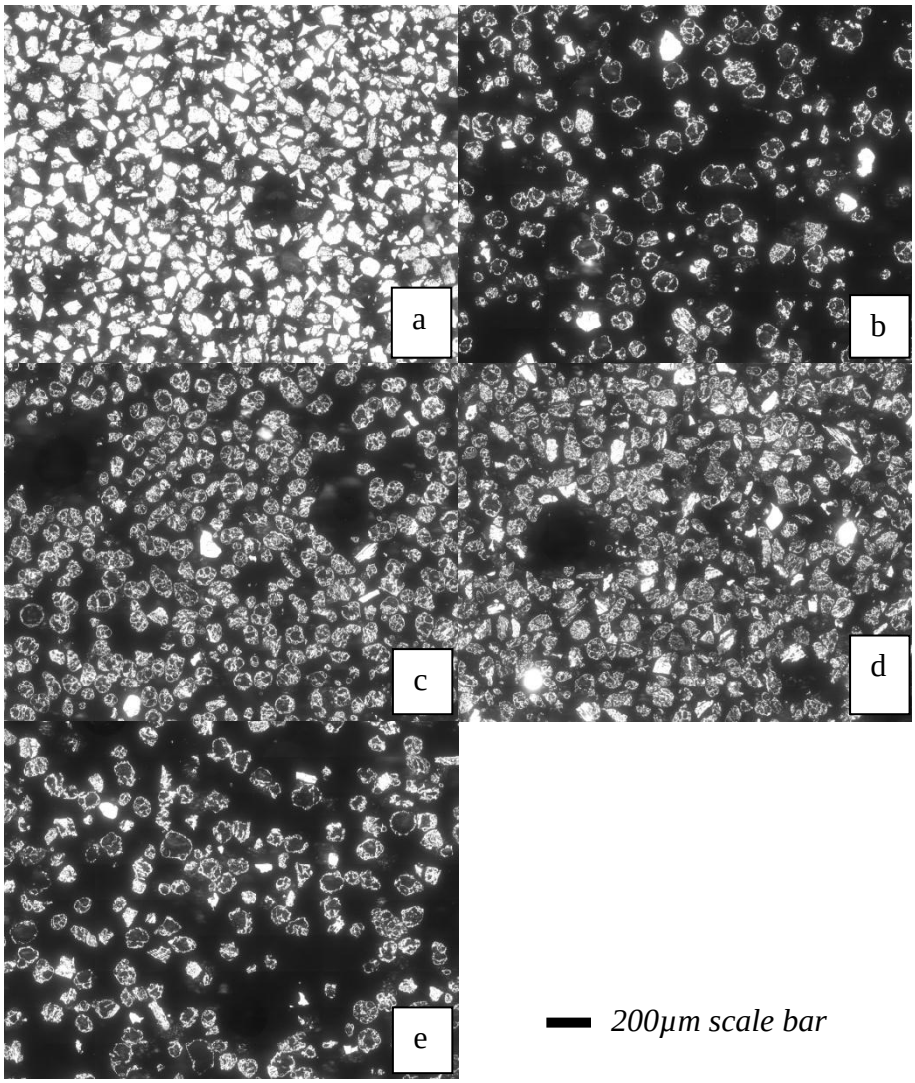

Figure 3 Char Morphology of the pyrolysis char from the larger pulverised coal fraction (106-125µm) (a) seam 78 S1(heat affected) (b) seam 78 S2 (c) seam 88 (d) seam 91, (e) Stockpile fine.

3 Conclusions

i. Petrographic variations are seen both between seams and size fractions, with vitrinite ranging from 65 – 77%, liptinite (2.5% - 7.1%) and inertinite (16 – 30%). Microlithotype associations aid in explaining these differences and are more informative than petrographic data alone.

ii. The heat affected coal (seam 78 S1) is chemically (Table 1) and petrographically different from the other four samples (Table 2; Table 3). Of the identifiable macerals counted, vitrinite is the most abundant (up to 35%), the majority of which is as the microlithotype vitrite (16% – 23.8%; Table 3) and vitrinertite (8.8% - 12.5%). Inertinite is a minor component (up to 4%) either as inertite (2.1%) or vitrinertite.

iii. Burnout profiles show that the heat affected coal 78 S1 has the poorest burnout rates. From char analysis, it produces char morphologies that are denser with low porosity. The stockpile and coal 88 have the best profiles for burnout and this is reflected in the petrographic compositions where the inertinite is relatively low (compared to the other coals) and the char structures are the thinnest.

iv. The quantity of dense chars appears to relate directly to the petographic composition of the initial coals.

Acknowledgement

We would like to thank NERC, RWE Npower for sponsorship and RWE Npower for training and technical support. We would also like to thank Neil Holloway and Sharon Gibbons for technical support at Royal Holloway.

References

[1] Hadjipaschalis I, Kourtis G, Poullikas A. Assessment of oxyfuel power generation technologies. Renewable and sustainable energy review 2009; 13: 2637-2644

[2] Wall T, Liu Y, Spero C, Elliot L, Khar S, Rathman R, Zeenathal F, Moghtaderi B, Buhre B, Sheng C, Gupta R, Yamada T, Makino K, and Yu J. An overview of oxyfuel coal combustion-state of the art research and technology development. Chemical engineering research and design 2009; 87: 1003-1016.

[3] Cloke, M., Wu, T., Barranco, R. and Lester, E. Char characterization and its application in a coal burnout model. Fuel 2003; 82: 1989-2000.

[4] Lester E, Cloke M. The characterization of coals and their respective chars formed at 1300ºC in a drop-tube furnace. Fuel 1999; 78: 1645-1658.

[5] Choudhury N, Biswas S, Sarkar P, Kumar M, Ghosal S, Mitra T, Mukherjee A, Choudhury A. Influence of rank and macerals on the burnout behaviour of pulverized Indian coal. Int. J. Coal Geol. 2008; 74: 145-153.

[6] Card, J.B.A., Jones, A.R. A drop tube furnace study of coal combustion and unburned carbon content using optical techniques. Combustion and Flame. 1995; 101: 539-547.

[7] Cloke M, Lester E, Belghazi A. Characterization of the properties of size fractions from ten world coals and their chars produced in a drop-tube furnace. Fuel. 2002; 81: 699-708.

[8] Lester, E. Characterisation of coals for combustion. PhD thesis 1994.

[9] BS 6127.4: 1990, ISO 7404-4:1988, British Standard, Petrographic analysis of bituminous coal and anthracite – Part 4: method of determining microlithotype division, carbominerite and minerite composition

[10] BS 6127.3: 1995, ISO 7404-3:1994, British Standard, Petrographic analysis of bituminous coal and anthracite – Part 3: method of determining maceral group composition of bituminous coal and anthracite.

[11] International Committee for Coal and Organic Petrology (ICCP). The new vitrinite classification (ICCP System 1994), Fuel 1998; 77: 349-358.

[12] International Committee for Coal and Organic Petrology (ICCP). The new inertinite classification (ICCP system 1994), Fuel 2001; 80: 459-471.

[13] BS 1016-105:1992, methods for analysis and testing of coal and coke, part 105: determination of gross calorific value: 1-11.

[14] BS 1016-104.3:1998, ISO 562:1998, methods for analysis and testing of coal and coke, part 104: proximate analysis, section 104.3: determination of volatile matter content, second edition, 1998-02-01, 1-6.

[15] BS 1016-104.4:1998, ISO 1171, Solid mineral fuels – determination of ash, third edition, 1997-12-15, 1-8.

[16] BS 1016-104.1:1999, ISO 11722, solid mineral fuels – Hard coals – Determination of moisture in the general analysis test sample by drying in nitrogen, first edition 1999-05-01, 1-5.

[17] BS ISO 17246:2005, Coal - Proximate analysis, International Standard, First Edition,
2005-05-01, 1-2.

[18] BS ISO 17247:2005, Coal – Ultimate analysis, International Standard, First Edition, 2005-05-01, 1-4.

[19] Cloke, M., Wu, T., Barranco, R. and Lester, E. Char characterization and its application in a coal burnout model. Fuel 2003; 82: 1989-2000.

[20] Unsworth JF, Barrat DJ, Robert PT. Coal quality and combustion performance: an international perspective. Coal science and technology series 19, Amsterdam: Elsevier; 1991. P350.

[21] Stach E. The microlithotypes of coal and their strength. In: Stach, E., et al., Stach's
Textbook of Coal Petrology, Gebr. Borntraeger, Berlin-Stuttgart; 1982, p.173-177.

[22] Taylor GH, Teichmüller M, Davis A, Diessel CFK, Littke R, Robert P. Organic Petrology, Gebrüder Bornstraeger, Berlin, Stuttgart; 1998.

[23] Bostick NH, Betterton WJ, Gluskoter HJ, Nazrul Islam M. Petrography of Permian “Gondwana” coals from boreholes in northwestern Bangladesh, based on semiautomated reflectance scanning. Org. Geochem. 1991; 17: 399-413.

[24] Cloke M, Lester E, Gibb W. Characterisation of coal with respect to carbon burnout in p.f.-fired boilers. Fuel 1997; 76: 1257-1267.

APPENDIX 9

REFER TO APPENDIX CD